Quantifying protein expression and activity complements genetics to optimize the use of targeted therapies in precision oncology

Constance Ananta Sobsey, BA, MSc
Experimental Medicine, McGill University, Montréal

May 2023

A thesis submitted to McGill University
in partial fulfillment of the requirements of
the degree of Doctor of Philosophy

Dedication

To my amazing daughter, Amalia.
Nothing could have made my days brighter like you have.

To my incredible partner, Tom, who knows that we
"*don't make fun of grad students -- they just made a terrible life choice*."
Thank you for smoothing this path.

To my treasured mentors on this path, especially
Dr. Gerald Batist
Dr. Elizabeth MacNamara
Dr. Christoph Borchers
Dr. David Wishart
You've each given me two most precious gifts:
knowledge and kindness.
I am beyond grateful.

Abstract

The analysis of tumour tissues with modern analytic technologies has shown that most cancer types are composed of multiple subpopulations with distinct molecular signatures, and that correct identification of molecular subtypes can predict response to a particular drug. As a result, targeted treatments have emerged as an important tool for disease management, resulting in some striking successes. The phosphatidylinositol-3-kinase (PI3K) pathway is one of the most commonly dysregulated pathways in cancer and the target of many new drugs. One of these, capivasertib, is a potent and selective inhibitor of AKT. In Phase I trials of capivasertib, patients in some arms were screened for activating *PIK3CA* mutations expected to render them sensitive. However, even among this genetically pre-selected cohort, the overall response rate was limited to approximately 30%. Alternative mass spectrometry (MS)-based approaches to quantify proteins and metabolites can offer a "real-time" portrait of the cellular processes that are active in a specific cancer. The purpose of our project is to link MS analyses with genetic and clinical information to create more comprehensive molecular profiles, and to assess whether these may be useful for patient selection and treatment planning.

Results Chapter 1 describes the development and validation of a new proteomics workflow encompassing both targeted and global proteomics approaches. The methods were applied to comprehensively analyze volume-limited stored tumour slices from *PIK3CA*-mutated tumours of patients in a Phase II clinical trial of capivasertib. Patients were coded as "clinical benefit" or "no clinical benefit" based on their time to progression after starting the drug. AKT expression was not associated with capivasertib treatment benefit in this cohort. However, the global proteomic analysis revealed significant protein expression differences, leading to the hypothesis that increased activation of translational control pathways may be associated with capivasertib resistance in tumours with activating PI3K mutations.

In Results Chapter 2, to verify the association between the observed proteomic profile and capivasertib response, we developed targeted quantitative proteomic assays for 50 proteins. Assay performance was fully characterized according to the guidelines of the Clinical Proteomics Tumor Analysis Consortium (CPTAC). The multiplexed panel was then applied to reproducibly determine the concentration of the proteins of interest in samples of 6 hormone receptor-positive PI3K pathway-altered breast cancer cell lines, with varying levels of sensitivity to capivasertib. As compared to the profile originally observed in the "No Clinical Benefit"

patient samples, the capivasertib-resistant cell lines showed a similar pattern of increased expression of proteins associated with translational control. The detection of a similar profile of capivasertib-resistance in two independent models using orthogonal methods provides much stronger evidence of an association. The validated assays were adapted for future use in patient samples.

In Results Chapter 3, we take a different approach to treatment optimization, assessing the feasibility of the Geneva cocktail approach for characterizing patient-specific differences in Cytochrome P450 activity that can alter the metabolism of cancer drugs. The results confirm that diet-associated differences in CYP450 activity can be measured using the assay. The ultimate aim is to enable regular monitoring of drug metabolism and strategic tailoring of medication doses to maximize effectiveness while mitigating adverse effects.

As a whole, the thesis demonstrates the utility of protein-focused MS-based approaches in combination with genetic and phenotypic data to more fully characterize the system of pathway alterations that drive oncogenesis, to inform the strategic design of combination therapies, and to contribute to more rational patient selection and dosing of drugs.

Résumé

La voie biochimique de la phosphatidylinositol-3-kinase (PI3K) est l'une des voies les plus souvent dérégulées dans le cancer et la cible de nombreux nouveaux médicaments. Le capivasertib est un inhibiteur puissant et sélectif de l'AKT. Dans les essais de phase I, les patients ont été dépistés pour les mutations PIK3CA provoquant une activation qui pourrait les rendre sensibles au capivasertib; mais le taux de réponse était limité à environ 30 % même parmi les patients génétiquement présélectionnés. Des approches alternatives basées sur la spectrométrie de masse (MS) pour quantifier les protéines et les métabolites peuvent offrir un portrait temporal des processus cellulaires qui sont actifs dans un cancer spécifique. Le but de notre projet est donc d'évaluer si les analyses basées sur la MS, liées aux informations génétiques et cliniques, peuvent fournir des profils moléculaires plus complets pour la planification du traitement.

Le chapitre 1 décrit le développement d'un modèle d'analyse protéomique englobant à la fois des approches protéomiques ciblées et globales. Les méthodes ont été appliquées pour analyser de manière exhaustive des tranches de tumeurs à volume limité de patients qui ont des mutations de PIK3CA. Ils ont tous reçu du capivasertib dans un essai clinique de phase II. Les patients ont été codés comme « bénéfice clinique » ou « aucun bénéfice clinique » en fonction de leur délai de progression après le début du traitement. L'expression de l'AKT n'était pas associée au bénéfice du traitement par capivasertib dans cette cohorte. Cependant, l'analyse protéomique globale a révélé des différences significatives dans l'expression des protéines, ce qui a conduit à l'hypothèse qu'une activation accrue des voies biochimique de contrôle de la translation pourrait être associée à une résistance au capivasertib dans les tumeurs présentant des mutations activatrices de PI3K.

Dans le chapitre 2, pour vérifier l'association entre le profil protéomique observé et la réponse capivasertib, nous avons développé 53 tests quantitatifs ciblés pour déterminer de manière reproductible la concentration des protéines d'intérêt. Les tests ont été caractérisés selon les directives du Clinical Proteomics Tumor Analysis Consortium (CPTAC), avant d'application à 6 lignées cellulaires de cancer du sein positives pour les récepteurs hormonaux, avec différents niveaux de sensibilité au capivasertib. Les lignées cellulaires résistantes au capivasertib ont montré un motif similaire d'expression accrue des protéines associées au contrôle de la translation. La détection d'un profil similaire de résistance au capivasertib dans deux modèles indépendants utilisant des méthodes orthogonales fournit une crédibilité beaucoup plus solide

d'une association. Les tests validés ont été adaptés pour une utilisation future dans des échantillons de patients.

Dans le chapitre 3, nous adoptons une approche différente de l'optimisation du traitement, en évaluant la faisabilité de l'approche « Geneva cocktail » pour caractériser les différences spécifiques au patient dans l'activité du cytochrome P450 qui peuvent modifier le métabolisme et la dose efficace des médicaments anticancéreux. Les résultats confirment que les différences associées au régime alimentaire dans l'activité du CYP450 peuvent être mesurées. L'objectif est de permettre une surveillance régulière du métabolisme des médicaments et une adaptation stratégique des doses de médicaments afin de maximiser l'efficacité tout en atténuant les effets indésirables.

Ensemble, la thèse démontre l'utilité des approches basées sur la MS pour proteomics et metabolomics en combinaison avec des données génétiques et phénotypiques pour caractériser plus complètement le système d'altérations des voies biochimique qui conduisent à l'oncogenèse, pour éclairer la conception stratégique des thérapies combinées et pour contribuer à choix de traitement plus rationnel.

Table of Contents

List of Tables

List of Figures

List of Abbreviations

ACN ..... Acetonitrile

AI ..... Aromatase Inhibitor

ATP ..... Adenosine Triphosphate

BCA ..... Bicinchoninic Acid

BSA ..... Bovine Serum Albumin

CB ..... Clinical Benefit

CPTAC ..... Clinical Proteomics Tumour Analysis Consortium

CR ..... Complete Response

CV ..... Coefficient of Variation

CYP ..... Cytochrome P450

DiMQu ..... Diet & Medication Questionnaire Score

DOC ..... Sodium Deoxycholate

DTT ..... Dithiothreitol

EIF2 ..... Eukaryotic Initiation Factor-2

EIF4 ..... Eukaryotic Translation Initiation Factor 4

END ..... Endogenous peptide

ER ..... Endoplasmic Reticulum

ER+ ..... Estrogen Receptor-positive

ESI ..... Electrospray Ionization

FA ..... Formic Acid

FBS ..... Fetal Bovine Serum

FC ..... Fold Change

FDA ..... United States Food & Drug Administration

FDR ..... False Discovery Rate

FFPE ..... Formalin-Fixed Paraffin-Embedded

GI_{50} ..... Half-Maximal Growth Inhibition Concentration

HCCA ..... α-Cyano-4-Hydroxycinnamic Acid

HCD ..... Higher-energy Collisional Dissociation

HR+ ..... Hormone Receptor-positive

IAA ..... Iodoacetamide

IC_{50} ..... Half-Maximal Inhibitory Concentration

ID ..... Identification

IHC ..... Immunohistochemistry

iMALDI .... ImmunoMALDI

IPA ..... Ingenuity Pathway Analysis

IS ..... Internal Standard

LC ..... Liquid Chromatography

LFQ ..... Label-Free Quantification

LLOD ..... Lower Limit of Detection

LLOQ ..... Lower Limit of Quantitation

LXR ..... Liver X Receptor

M/Z ..... Mass-To-Charge Ratio

MALDI ..... Matrix Assisted Laser Desorption Ionization

MeOH ..... Methanol

MR ..... Metabolic Ratio

MRM ..... Multiple Reaction Monitoring

MS ..... Mass Spectrometer or Mass Spectrometry or Mass Spectra

MS/MS ..... Tandem Mass Spectrometry

mTORC1 .. Mammalian Target Of Rapamycin Complex 1

mTORC2 .. Mammalian Target Of Rapamycin Complex 2

NaOH ..... Sodium Hydroxide

NAT ..... Natural Isotope Abundance Synthetic Peptide

NCB ..... No Clinical Benefit

NCI..... National Cancer Institute

nLC ..... Nano-LC

OE ..... Overexpressing

ORR ..... Objective Response Rate

P/S ..... Penicillin / Streptomycin

PBS ..... Phosphate-Buffered Saline

PCA..... Principal Components Analysis

PD ..... Progressive Disease

PFS..... Progression-Free Survival

PI3K Phosphatidylinositol-3-Kinase

PK ..... Pharmacokinetic

PLS-DA ... Partial Least Squares-Discriminant Analysis

PPI..... Protein-Protein Interaction

PPQ ..... Phosphatase-based Phosphopeptide Quantitation

PR..... Partial Response

PRM ..... Parallel Reaction Monitoring

Q1 / Q3..... Quadruople 1 / Quadrupole 3

QC ..... Quality Control

RECIST.... Response Evaluation Criteria in Solid Tumours

RPL ..... 60S Ribosomal Protein L

RPLC ..... Reversed Phase Liquid Chromatography

RPS ..... 40S Ribosomal Protein S

RTK..... Receptor Tyrosine Kinase

RXR ..... Retinoid X Receptor

SD ..... Stable Disease

SIS..... Stable Isotope-Labelled Standard

SPE..... Solid Phase Extraction

TCA ..... Trichloroacetic Acid

TCEP..... Tris(2-Carboxyethyl)Phosphine

TCPK ..... L-1-Tosylamido-2-Phenylethyl Chloromethyl Ketone

TFA ..... Trifluoroacetic Acid

TIC ..... Total Ion Chromatogram

TKI ..... Tyrosine Kinase Inhibitor

TLCK ..... Tosyl-L-Lysyl-Chloromethane Hydrochloride

TNBC ..... Triple Negative Breast Cancer

TOF ..... Time Of Flight

ULOQ ..... Upper Limit of Quantitation

UPLC..... Ultrahigh Pressure Liquid Chromatography

VIP ..... Variable Importance in Projection

XIC..... Extracted Ion Chromatogram

Gene & protein names

Gene	Abbreviation	Uniprot	Protein Name
AHCY	AdoHcyase	P23526	Adenosylhomocysteinase
AKT1	AKT1, pAKT1	P31749	RAC-alpha serine/threonine-protein kinase
AKT2	AKT2, pAKT2	P31751	RAC-alpha serine/threonine-protein kinase
ALB	Albumin	P02768	Albumin
AMPK	AMPK α-2	P54646	5'-AMP-activated protein kinase catalytic subunit alpha-2
APRT	APRT	P07741	Adenine phosphoribosyltransferase
ARHGAP1	p50-RhoGAP	Q07960	Rho GTPase-activating protein 1
ARPC4	ARPC4	P59998	Actin-related protein 2/3 complex subunit 4
ATF4	ATF4	P18848	Cyclic AMP-dependent transcription factor ATF-4
CCT3	TCP-1-gamma	P49368	T-complex protein 1 subunit gamma
CCT8	TCP-1-theta	P50990	T-complex protein 1 subunit theta
CDK4	CDK4	P11802	Cyclin-dependent kinase 4
CDK**6**	CDK6	Q00534	Cyclin-dependent kinase 6
CPNE1	Copine I	Q99829	Copine-1
CYP1A2	CYP1A2	P05177	Cytochrome P450 1A2
CYP3A4	CYP3A4	P08684	Cytochrome P450 3A4
DCXR	XR	Q7Z4W1	L-xylulose reductase
DECR1	DECR	Q16698	2,4-dienoyl-CoA reductase [(3E)-enoyl-CoA-producing], mitochondrial
EIF2A	eIF-2A	Q9BY44	Eukaryotic translation initiation factor 2A
EIF2AK3	PEK, PERK	Q9NZJ5	Eukaryotic translation initiation factor 2-alpha kinase 3
EIF2S1	eIF2α	P05198	Eukaryotic translation initiation factor 2 subunit 1
EIF3E	eIF3e	P60228	Eukaryotic translation initiation factor 3 subunit E
EIF4A1	eIF4A-I	P60842	Eukaryotic initiation factor 4A-I
EIF4E	eIF4E	P06730	Eukaryotic translation initiation factor 4E
EIF4EBP1	(p) 4E-BP1	Q13541	Eukaryotic translation initiation factor 4E-binding protein 1
EIF5	eIF-5	P55010	Eukaryotic translation initiation factor 5
ERBB	EGFR	P00533	Epidermal growth factor receptor
ERBB2	HER2	P04626	Receptor tyrosine-protein kinase erbB-2
ETFB	Beta-ETF	P38117	Electron transfer flavoprotein subunit beta
GSK3B	GSK-3Beta	P49841	Glycogen synthase kinase-3 beta
HADHB	TP-Beta	P55084	Trifunctional enzyme subunit beta, mitochondrial
HK1	HK I	P19367	Hexokinase-1
HNRNP-F	hnRNP F	P52597	Heterogeneous nuclear ribonucleoprotein F
HNRNP-L	hnRNP L	P14866	Heterogeneous nuclear ribonucleoprotein L

Gene	Abbreviation	Uniprot	Protein Name
IGKC	IGKC	P01834	Immunoglobulin kappa constant
IGKV4	IGKV4-1	P06312	Immunoglobulin kappa variable 4-1
ILF2	ILF2	Q12905	Interleukin enhancer-binding factor 2
ILF3	ILF3	Q12906	Interleukin enhancer-binding factor 3
KRAS	K-Ras 2	P01116	GTPase KRas
MAPK1	MAP kinase 1, ERK2	P28482	Mitogen-activated protein kinase 1
MDH2	MDH2	P40926	Malate dehydrogenase, mitochondrial
MTOR	mTOR	P42345	Serine/threonine-protein kinase mTOR
MYC	c-Myc	P01106	Myc proto-oncogene protein
PCBP1	hnRNP E1	Q15365	Poly(rC)-binding protein 1
PCBP2	hnRNP E2	Q15366	Poly(rC)-binding protein 2
PDIA6	ERp5	Q15084	Protein disulfide-isomerase A6 / Endoplasmic reticulum protein 5
PHB1	PHB1	P35232	Prohibitin 1
PHB2	PHB2	Q99623	Prohibitin-2
PIGR	PIgR	P01833	Polymeric immunoglobulin receptor
PIK3CA	PI3K p110α	P42336	Phosphatidylinositol 4,5-bisphosphate 3-kinase catalytic subunit alpha isoform
PIK3CB	PIK3C-Beta	P42338	Phosphatidylinositol 4,5-bisphosphate 3-kinase catalytic subunit beta isoform
PSMA6	PSMA6	P60900	Proteasome subunit alpha type-6
PTEN	PTEN	P60484	Phosphatidylinositol 3,4,5-trisphosphate 3-phosphatase and dual-specificity protein phosphatase PTEN
RICTOR	Rictor	Q6R327	Rapamycin-insensitive companion of mTOR
RPS6KB1	(p)S6K1	P23443	Ribosomal protein S6 kinase beta-1
SDHA	SDHA	P31040	Succinate dehydrogenase [ubiquinone] flavoprotein subunit, mitochondrial
SEPTIN2	Septin-2	Q15019	Septin-2
SGK1	SGK1	O00141	Serine/threonine-protein kinase Sgk1
SLC25A3	PTP	Q00325	Phosphate carrier protein, mitochondrial
TNF	TNFα	P01375	Tumour necrosis factor alpha
TSC1	Hamartin	Q92574	Tuberous sclerosis 1 protein
TSC2	Tuberin	P49815	Tuberous sclerosis 2 protein
TSTA3	TSTA3	Q13630	GDP-L-fucose synthase
TUFM	EF-Tu, P43	P49411	Elongation factor Tu, mitochondrial
XRCC5	XRCC5	P13010	X-ray repair cross-complementing protein 5

Acknowledgements

Supervisor

Dr. Gerald Batist

Gerry, please accept my warmest thanks for your supervision throughout this journey. I am grateful for your unwavering support, encouragement, and compassion despite the many challenges I encountered. I appreciate your intellectual partnership and the rare window into clinical practice – both have shaped my perspective and my interests. I've learned so much from you, both personally and professionally.

Committee Members

Dr. Christoph Borchers
Dr. Elizabeth MacNamara
Dr. Kostas Pantopoulos
Dr. Pierre Thibault

To my Committee members, thank you to each of you for the time invested in advising on this project. I so appreciate your engagement, and your willingness to share your ideas, your expertise, and your counsel with me. To Christoph and to Liz, my special thanks for your continued investment in me both as a researcher and as a person.

Project team & collaborators

My unending thanks to colleagues and partners, particularly those listed in the Contributions of Authors section, without whom this work would not have been possible. In particular, I owe a significant debt of gratitude to:

Dr. R. Thomas Jagoe *for a fascinating project, mentorship, and delightful teamwork.*

Dr. Antonis Koromilas *for generously offering his time, academic engagement, and unique expertise to consult on this project.*

Dr. Elza de Bruin at AstraZeneca *for her faithful and fruitful collaboration.*

Dr. Arif Awan *for his direct contributions consenting patients, annotating records, generating project ideas, and teaching me about the clinical context.*

Dr. Tahar Aboulkassim *for his patience in training me and dedication in supporting me in the cell culture suite.*

My labmates at the Segal Cancer Proteomics Centre -- especially Drs. **Georgia Mitsa, Sahar Ibrahim, Vincent Richard, Rene Zahedi, Vanessa Gaspar, Björn Fröhlich, Robert Popp, Andre LeBlanc, Noor Mady** -- *for all of the ways in which you trained me and sustained me. I could never have seen this through without your kindness, companionship, and solidarity.*

Funders

This research was made possible through funding and in-kind support from:

Fonds De Recherche Du Québec - Santé *for graduate funding (FRQS #254160)*

McGill Faculty of Medicine *for graduate funding under the Max Binz Fellowship and Charles James Patton, M.D. & Elizabeth Ross Patton Memorial Prize*

Genome Canada & **Genome BC** *for project funding under the Genomics Applied Partnership Program (#183AKT).*

AstraZeneca *for in-kind support including access to samples from the clinical trial*

Dr. Christoph Borchers & the Segal Cancer Proteomics Centre *for extensive project support*

Dr. Mark Basik & the Segal Cancer Centre *for a gift of cancer cell lines*

Additional support for the laboratories and researchers involved in this work was provided by the **Genome Canada** Genomics Technology Platform program, the **Terry Fox Research Institute**, the **Segal McGill Chair in Molecular Oncology** at McGill University, the **Warren Y. Soper Charitable Trust**, the **Alvin Segal Family Foundation** to the Jewish General Hospital, the **Peter Brojde Lung Cancer Centre**, the **Jewish General Hospital Department of Medicin**e.

Research Participants

Sincere thanks to patients and families who opt to participate in research and clinical trials. Each and every advancement is thanks to you.

Contribution to Original Knowledge

This doctoral research encompasses novel findings and the creation of new knowledge. Most significantly, the candidate identified novel putative markers of capivasertib resistance. The results provide some of the first evidence that (a) differences in translational control are associated with capivasertib resistance in a clinical trial cohort, (b) there is a profile of AKT inhibitor resistance that is detectable in patients many years before trial enrollment or exposure to the drug, and (c) a genetically pre-selected cohort of patients with *PIK3CA*-mutated cancers can be further subdivided into treatment response groups based on protein quantitation. Quantitation in cell line models verified these novel protein markers in an independent model using orthogonal methods, showing strong evidence of a meaningful association with capivasertib resistance. Despite literature suggesting either EIF4 or EIF2 were capable of driving AKT inhibitor resistance, targeted proteomics results distinguished that EIF4/mTOR signaling was the most likely mechanism in this setting.

The research findings build on the candidate's development and validation of optimized methods and innovative workflows for proteomics-driven biomarker research, in particular:

- A workflow combining targeted and untargeted proteomics approaches for more comprehensive characterization of volume-limited tumour material (Ch. 1)
- Development & validation of a multiplexed quantitative proteomics panel to reproducibly quantify 50 proteins with research applications in cancer, cardiology, and neurology (Ch. 2)
- The use of a modified biomarker verification pipeline to enable markers identified in patient samples to be verified in cell line models using fit-for-purpose multiplexed assays (Ch. 2)
- Inter- and intra-tumour protein concentration data to help assess markers' suitability for biomarker applications and clinical quantitation (Ch. 2)
- Validation of a modified Geneva cocktail method for regularly measuring cancer drug metabolism in patients (Ch. 3), incorporating a glucuronide deconjugation step for more accurate results along with single-timepoint testing and dried blood spot sampling for realistic clinical implementation

The thesis as a whole represents a relatively early example of translational research that demonstrates the value of modern fit-for-purpose proteomic technologies in precision oncology.

Format of the Thesis

This thesis is written according to the guidelines for a monograph-style thesis, as outlined by the McGill University Faculty of Graduate and Postdoctoral Studies. The traditional format facilitates presentation of the work in a logical sequence. The thesis begins with an Introduction, including a comprehensive review of the relevant literature, followed by a section on Materials and Methods. Research findings are presented in Results Chapters 1 to 3. The Discussion section analyses the outcomes, significance, and context of the findings individually and as a whole, along with future directions. The Conclusion reviews how the research objectives were addressed. The Bibliography and Appendix of supplementary materials are appended.

Subsets of this work have been published or submitted for publication, as follows:

- Published review paper describing systematic literature review of proteomics technologies for biomarker and clinical applications (Introduction):
    - **Sobsey CA**, Ibrahim S, Richard VR, Gaspar V, Mitsa G, Lacasse V, et al. Targeted and Untargeted Proteomics Approaches in Biomarker Development. *Proteomics* 2020. (1)
- Published research articles, conference proceedings, and book chapter describing the development, optimization & validation of the iMALDI methods (Results Chapter 1):
    - Froehlich B, Popp R, **Sobsey CA**, Ibrahim S, LeBlanc AM, Mohammed Y, et al. Systematic Optimization of the iMALDI Workflow for the Robust and Straightforward Quantification of Signaling Proteins in Cancer Cells. *Proteomics Clinical Appl* 2020. (2)
    - Froehlich BC, Popp R, **Sobsey CA,** Ibrahim S, LeBlanc A, Mohammed Y, et al. A multiplexed, automated immuno-matrix assisted laser desorption/ionization mass spectrometry assay for simultaneous and precise quantitation of PTEN and p110α in cell lines and tumor tissues. *Analyst* 2021. (3)
    - **Sobsey CA,** Popp R, Ibrahim S, Froehlich BC, Aguilar-Mahecha A, Basik M, et al. Abstract B21: Protein quantitation assays for Akt, PI3K p110α, and PTEN to assess PI3K pathway activity in tumor tissue. Conf proceed in *Molecular Cancer Research* 2020. (4)
    - Ibrahim S, **Sobsey CA,** Popp R, Zahedi RP, Batist G, Borchers CH. Abstract P4-10-20: Protein quantitation assays for AKT and PTEN to better understand sensitivity and

resistance of breast cancer patients to treatment with AKT inhibitor capivasertib. Conf proceed in *Cancer Research* 2020. (5)

- **Sobsey CA,** Froehlich B, Batist G, Borchers CH. Immuno-MALDI-MS for Accurate Quantitation of Targeted Peptides from Volume-Restricted Samples. In *Neuronal Cell Death*: *Methods and Protocols* 2022. (6)

- Results from analysis of baseline samples from AstraZeneca clinical trial (Chapter 1) and breast cancer cell lines (Chapter 2) were published in conference proceedings and submitted as a research article:
  - Batist G, **Sobsey CA**, Mitsa G, Borchers C. WIN Symposium 2022 - Abstract No: 1 Beyond the tip of the iceberg: Proteomic analysis in colon and breast cancer. *Journal of Immunotherapy and Precision Oncology* 2022. (7)
  - **Sobsey CA**, Froehlich BC, Mitsa G, Ibrahim S, Popp R, Zahedi RP, et al. Proteomic analysis of PIK3CA-mutated tumours identifies protein networks correlated with clinical benefit of capivasertib in genetically pre-selected patient. *Submitted* 2023.
- The development and validation of 53 quantitative proteomics assays (Results Chapter 2) is being prepared for publication as a research article in a peer-reviewed journal:
  - **Sobsey CA**, Borchers C, Batist G. CPTAC validation of multiplexed targeted proteomics assays to enable verification studies of 50 proteins associated with AKT inhibitor response. *In preparation* 2023.
- The modified Geneva cocktail approach (Results Chapter 3) was submitted for publication as a research article (first authorship shared with Noor Mady):
  - **Sobsey CA**, Mady N, Richard VR, LeBlanc AM, Zakharov T, Borchers C, Jagoe RT. Measurement of CYP1A2 and CYP3A4 activity by a simplified Geneva cocktail approach in a free-living cohort. *Submitted* to *Frontiers in Pharmacology* 2023.

The candidate also contributed to a complementary project for cancer drug monitoring whose results were published. This research is referred to, but not presented in the scope of the thesis:

- Gaspar VP, Ibrahim S, **Sobsey CA**, Richard VR, Spatz A, Zahedi RP, Borchers CH. Direct and precise measurement of bevacizumab levels in human plasma based on controlled methionine oxidation and multiple reaction monitoring. *ACS Pharmacology & Translational Science* 2020. (8)

Contribution of Authors

Please see the Contributor Roles Taxonomy (CRediT) for an explanation of terms (9).

Thesis as a whole

The candidate conceptualized the doctoral research, wrote, reviewed and edited the original thesis, and developed all visualizations (except where noted below). The candidate also contributed to funding acquisition and administration.

Others contributed to the Thesis as a Whole through:

Supervision	Dr. Gerald Batist (overall) Dr. Christoph Borchers (additional supervision for proteomics)
Funding Acquisition & Resources	Gerald Batist, Christoph Borchers (overall) Gaia Schiavon, Elza de Bruin (AstraZeneca support, Chapter 1) Mark Basik, Adriana Aguilar-Mahecha (cell lines, Chapter 2) R. Thomas Jagoe (resources, Chapter 3)
Project Administration	Gerald Batist, Christoph Borchers, Rene Zahedi, Andre LeBlanc, Lady Davis Institute, Jewish General Hospital
Training	Vincent Richard (general laboratory & technical advice) Andre LeBlanc (general laboratory & technical advice)
Review & editing	Gerald Batist (Chapter 1 &2) R. Thomas Jagoe (Chapter 3)

Results Chapter 1

The candidate conceptualized the research (experimental design), developed methodology (AKT assay optimization, proteomics workflow), performed investigation (AKT iMALDI-MS, global proteomics sample analysis), performed data curation (all data), formal analysis (all data), and validation (all data), with additional support where noted below.

Others contributed to Results Chapter 1 through:

Conceptualization	Gerald Batist, Christoph Borchers (overall) Rene Zahedi (proteomics workflow)
Methodology	Gerald Batist (overall) Christoph Borchers (proteomics) Robert Popp (iMALDI method for AKT, Bravo automation) Björn Fröhlich (iMALDI method for PTEN, p110α) Sahar Ibrahim (FFPE slide tissue extraction protocol) Rene Zahedi (global proteomics workflow)

	Elza de Bruin (Clinical Benefit criterion)
Training	Gerald Batist (observership, training on clinical context) Christoph Borchers, Rene Zahedi (training in proteomics) Robert Popp (training on iMALDI-MS, Bravo automation) Björn Fröhlich (training on iMALDI-MS, Bravo automation) Sahar Ibrahim (training on tissue extraction)
Investigation	Bjorn Frohlich (PTEN, p110a analysis) Georgia Mitsa (global proteome data acquisition & processing)
Data curation	Rene Zahedi (global proteomics data) Elza de Bruin, AstraZeneca (clinical data)
Formal Analysis	Rene Zahedi (global proteomics data)
Software	Björn Fröhlich MS-VIS (spectral processing)
Visualization	Björn Fröhlich (contributed to Figs 8, 12, 13)

Results Chapter 2

The candidate conceptualized the research in Results Chapter 2 (defining research questions, developing the ideas, selecting models and cell lines, determining experimental design), developed methodology (MRM-MS assays, PRM-MS assays, proteomics workflows for cell culture), performed investigation (all cell culture work, sample extraction, sample analysis, data analysis), performed data curation (database development), formal analysis (all data), and validation (all data), with additional support where noted below.

Others contributed to Results Chapter 2 through:

Conceptualization	Gerald Batist (overall approach, proposed models for verification)
Methodology	Gerald Batist (cell culture) Antonis Koromilas (advice on design, target & inhibitor selection) Tahar Aboulkassim (cell line protocol advice) Adriana Aguilar (cell line protocol advice) Georgia Mitsa (cell lines protocol advice, extraction protocols) Vincent Lacasse (cell line protocol advice) Yassene Mohammed (advice on timecourse data analysis)
Training	Christoph Borchers (proteomics & assay validation) Arif Awan (clinical data annotation, clinical context) Tahar Aboulkassim (cell line protocol) Sahar Ibrahim (how to review H&E slides, select core sites) Georgia Mitsa (core extraction protocol)
Investigation	Arif Awan (clinical data annotation, consenting patients) Negin Mostolizadeh (sample preparation assistance) Negar Mostolizadeh (sample preparation assistance)

Results Chapter 3

The candidate did not contribute to conceptualizing the research in Results Chapter 3. The candidate developed and validated methodology (MRM-MS assays), contributed to investigation (sample analysis, data analysis, DBS testing), completed validation (MRM-MS assays), and contributed to formal analysis (all data, together with Noor Mady).

Others contributed to Results Chapter 3 through:

Conceptualization	R. Thomas Jagoe (overall) Noor Mady (glucuronidase treatment)
Methodology	R. Thomas Jagoe (overall) Thomas Zakharov (dietary questionnaire development) Noor Mady (induction score development) Christoph Borchers, Andre LeBlanc (proteomics) Vincent Richard (DBS assay development)
Investigation	Noor Mady (patient recruitment & consenting, sample collection) Vincent Richard (sample analysis with glucuronidase treatment)
Data curation	Noor Mady (Dietary questionnaire and clinical data)
Formal analysis & Validation	Vincent Richard (glucuronidase-treated measurements, DBS assay) Noor Mady (Patient statistics, DiMQu score, literature review)
Visualization	Noor Mady (prepared Figs 45, 46)

Introduction

The emergence of targeted therapies & precision medicine in oncology

The impetus for new treatment approaches

While cancer rates and deaths have declined over recent decades, cancer is still the cause of death for 1 in 4 Canadians (10). Even as treatments improve, cancer remains a heterogenous disease and patients with "rare" cancer subtypes are seeing a smaller share of the gains. This represents a major concern because, in spite of their name, "rare" subtypes collectively account for >20% of all cancers (11). Prognosis is dramatically worse; in a European study, patients diagnosed with low-incidence cancer subtypes were almost 40% more likely to die of their disease within 5 years than their counterparts with more common ones (11). Remarkably, survival differences were much smaller in the first year after diagnosis, which is consistent with the idea that the available treatments are simply less effective for these patients (11). Improving treatments and outcomes for patients with rare cancers will require new treatment strategies and individualized insights into disease (12).

While chemotherapy and radiation continue to be the mainstays of treatment, these have left a pool of patients with 'hard-to-treat' disease (13). These approaches are also well known for their serious adverse effects including the potential for severe toxicity. In addition, patients spend extended time in hospital receiving treatments, which must be carefully monitored with additional weekly visits and are often followed by acute discomfort, resulting in important "time toxicity" (14). Chemotherapy commonly induces acquired resistance and the resulting tumour heterogeneity makes any active or recurring disease more difficult to target with any new treatment (15). Radiation is suitable only for localized tumours that are positioned to enable anatomical access without unacceptable collateral damage to adjacent structures. While additional therapeutic benefit can, in some cases, be derived by adding radiation to chemotherapy (e.g., cisplatin, gemcitabine), overall toxicity is typically increased.

Endocrine therapies have become a pillar of treatment for breast and gynecological cancers. However, these are only appropriate for hormone receptor-positive (HR+) cancers that are dependent on estrogen receptor (ER) or progesterone receptor (PR) for growth signalling. While these agents have dramatically improved cancer care overall, combination therapies are still needed to improve effectiveness, particularly in cases of cancer recurrence (16). The

example of prostate cancer, where treatment with androgen deprivation therapy sometimes reprograms the malignancy into a more aggressive subtype, clearly demonstrates the need for strategic combination therapies as a first-line approach before standard monotherapies render the disease harder-to-treat (17,18). This need as well as the limitations in existing standard-of-care treatments have both contributed to an increasing emphasis on the development of targeted therapies.

History and significance of targeted therapies

New drug development is now heavily focused on targeted cancer therapies including immunotherapies (19). As with chemotherapies, targeted therapies seek to block proliferation and metastasis, and ideally, to induce the death of cancer cells. However, targeted treatments do so by directly interfering with the proteins responsible for driving tumour oncogenicity (19). Whereas patient-specific immunotherapies require engineering of individual treatments based on unique tumour- exclusive neoantigens (20), most targeted therapies (including monoclonal antibodies and immune checkpoint inhibitors) are directed at shared pathways that are commonly exploited by cancer to drive uncontrolled proliferation and survival. This allows for their broad application to treat a group of patients, who are most often identified based on a shared biomarker.

The most salient example of this is the discovery of imatinib in the late 1990s, which revolutionized the treatment of chronic myelogenous leukemia (CML). It had been previously discovered that up to 99% of CML patients express some form of the BCR-ABL fusion protein (21). Oncogenic BCR-ABL promotes leukemogenesis by driving activation of the RAS/RAF, PI3K/AKT and other downstream pathways (22). Its inhibition with imatinib halts disease with minimal effects on normal cells (23). Though imatinib could not cure CML, its approval in 2001 radically transformed the prognosis. What was once a grim diagnosis became an indolent disease with survival exceeding 25 years (23,24). This incredible impact in turn intensified oncology's focus on the hunt for "silver bullets", accelerating the development of tyrosine kinase inhibitors (TKIs) and other targeted treatments (24,25).

Imatinib's success was followed by a stream of other small molecule drugs with exceptional clinical impact (26). Another tyrosine kinase inhibitor (TKI), erlotinib was approved for non-small cell lung cancer (NSCLC) in mid-2002 when it was shown to improve survival (27). The overall response rate (ORR) exceeded 75% for *EGFR* mutation-positive NSCLC (27).

The breakthrough ALK inhibitor, crizontinib was approved in 2011; together with its successors, it has since extended median survival of Stage 4 NSCLC from less than 1 year to more than 6 years for the 2.5% of patients with EML4-ALK fusions (28,29). Vemurafenib, the first inhibitor of the mutated serine/threonine kinase BRAF, was similarly approved for metastatic melanomas, on the basis of a landmark Phase I clinical trial that demonstrated an ORR of >80% in this large subset of patients with $BRAF^{V600E}$ mutations (30,31). These examples each demonstrated how a unique genomic change could render a specific tumour type highly responsive to single-target inhibitors.

Idelalisib followed in 2014 as the first approved Phosphoinositide 3-kinase (PI3K) inhibitor, with applications in chronic lymphocytic leukemia (CLL) (26). The number of FDA-approved targeted small molecule drugs has since proliferated to include the use of CDK4/6 inhibitors, PARP inhibitors, and several others for breast cancer (26). Multi-targeted kinase inhibitors emerged as an new tool for managing resistance to targeted inhibitors (32). In parallel, many targeted immunotherapies demonstrated strong clinical efficacy. Monoclonal antibodies targeting HER2+ in breast cancer (trastuzumab), CD20 in B-cell non-Hodgkin's lymphoma (rituximab), and PD-1 in lung cancer, melanoma and kidney cancer (immune checkpoint inhibitors like pembrolizumab) were all moved into standard-of-care (33). The effective use of each of these targeted therapies depends on identifying the specific molecular changes that are responsible for driving survival, growth, and metastasis in a given tumour.

Approaches to molecular subtyping

Molecular subtyping of tumours

The analysis of tumor tissues with modern analytic technologies has shown that multiple subpopulations can be identified by molecular signatures, with breast cancer subtypes as the archetype for this model. Around the same time that imatinib was introduced, the sequencing of the human genome and the advent of platforms like microarray began to enable more routine analyses of genetics and gene expression with better coverage and higher throughput (34). Pioneering studies conducted in 2000 by Sørlie et al. reported that analysis with 456 cDNA clones could generate a 'molecular portrait' distinctive of a given breast cancer, from which tumors could be classified into subtypes with distinct clinical outcomes (e.g., luminal A, luminal B, HER2+, and basal subtypes) (35,36).

Applying genomics-based subtypes ultimately confirmed that response to breast cancer treatment was determined by intrinsic molecular characteristics (37). Further research efforts initially aimed at identifying patients with sufficiently good prognosis to allow the safe omission of adjuvant chemotherapy (38). Since then, countless additional studies have worked to confirm, further subtype, or even converge the observed genomics-based groups (34) at both the gene and transcript level. However, molecular signatures still mostly belong to research settings. The most impactful molecular signatures so far identified generally map to subtypes that can defined by conventional immunohistochemistry (IHC). These include the analysis of estrogen receptor (ER), progesterone receptor (PR), and HER-2 in breast cancer, as well as p63 in prostate cancer and c-Kit in gastrointestinal tumours (39). Therefore, to date, treatment decisions continue to be guided largely by traditional pathology including tumor stage, tumor grade, and IHC markers (34).

Genomics technologies in current use

Most of the markers in current clinical use for patient selection are gene-based (mutations, rearrangements, amplifications, deletions) (25). By producing oncogenic fusion proteins or mutations not found in normal cells, gene rearrangements can, in some cases, act as both an extraordinarily powerful biomarker and a target of treatment. Since their development, polymerase chain reaction (PCR) assays have offered the speed, affordability, and reliability needed for clinical testing of known targeted gene mutations. Most companion diagnostics currently FDA-approved to guide NSCLC treatment (i.e., testing for mutations of EGFR, ALK, and PD-L1 in NSCLC) are based on either real-time PCR or fluorescence *in situ* hybridization (FISH) technologies. These assays now collectively earmark ~50% of new NSCLC patients for treatment with targeted therapies instead of standard chemotherapy (25).

However, recent improvements in next generation sequencing (NGS) have made it faster, more economical, and compatible with formalin-fixed paraffin-embedded (FFPE) tissue (25). While both NGS and PCR technologies are well-suited for assessing somatic mutations (e.g., pathogenic variants) and indels (e.g., insertions, deletions) that can alter the function of the expressed protein, NGS is better suited for the assessment of copy number variants (CNVs) and gene amplifications or deletions (25).

NGS is mostly implemented as hotspot testing, which simultaneously targets a few dozen to a few hundred genes by specifically sequencing the genomic regions (e.g,. exons) associated with their highest-frequency alterations (25). The depth of coverage of this technique is sufficient to measure alterations with low allele frequency or that are heavily diluted by tumour

heterogeneity or signal from non-tumour tissue (25). Observed genetic variants are interpreted through the use of public resources such as the heavily-curated COSMIC database (40). Nevertheless, variants of unknown significance are an increasingly common occurrence due to greater use of NGS. Broader genomic sequencing, including whole exome sequencing, is also possible but is rarely used (other than for research purposes) due to cost and the exponential challenges in the clinical interpretation of the data.

There are currently a handful of commercially-available clinical tools using genomics panels to supplement existing clinical tools for predicting prognosis (see Appendix 1 for detailed examples). These panels apply microarray to fresh-frozen tumour tissue or PCR assays to formalin-fixed paraffin-embedded (FFPE) tissue to generate signatures consisting of 2 to 97 genes that are correlated to recurrence, metastasis, and/or survival. Of those reviewed, only 1 – MammaPrint – was FDA-approved at the time of writing for clinical use (41). MammaPrint uses a 70-gene signature to predict the risk of recurrence (low or high) for Stage I and II breast cancers to help inform decisions on adjuvant systemic treatment. The remainder of genetic panels function as laboratory-developed tests (LDTs). While working groups continue to tousle with the challenge of establishing federal regulations suitable for assuring the technical and clinical validity of NGS, there is strong demand for these approaches from both patients and oncologists (42).

Transcriptomics technologies on the horizon

Epigenetic modifications that alter gene expression without DNA mutations contribute to the pathogenesis and molecular heterogeneity of cancers by regulating the transcriptional program (43). These can include DNA and histone modifications. For instance, abnormal methylation of CpG islands in gene promoters has been identified as a common mechanism by which cancer cells suppress expression of tumour suppressor genes (44). Epigenetics has also been tied to treatment response and resistance (45). Quantitation of mRNA therefore stands to serve as an important tool for assessing changes in gene expression in cancer. However, the complex signatures derived from the clustering of gene expression data have proven difficult to interpret and even more difficult to implement for clinical use (46). Fortunately, this is far from the only application for transcriptomic data.

RNA analysis has opened a treasure trove of additional markers not reachable by gene-based approaches. These include microRNAs (miRNAs), which have recently been shown to regulate the expression of up to 60% of all human protein-coding genes (47). miRNA expression

profiles are unique for a wide range of human diseases including different stages of tumor progression and metastasis (48). Circulating miRNAs are extremely stable in blood and serum, creating a perfect pairing with cutting-edge advancements in the use of liquid biopsies (49). Long non-coding RNAs (lncRNA), which perform signalling, regulatory, and chaperoning functions, can also be exclusively assessed at the transcriptomic level. A number of lncRNAs have been investigated as prognostic and predictive markers in breast, prostate, bladder, and kidney tumors (50-52).

PCR technology is applicable to analyze each of these types of RNA (25). However, in a clinical setting, RNA sequencing offers more extensive gene expression information with the potential to improve on NGS for the characterization of large-scale genomic rearrangements, fusion proteins, and other splice variants (25). A handful of prospective trials have now demonstrated an incremental benefit for treatment selection guided by gene expression analysis (either alone or in combination with genomics) (53-55). Although no RNA biomarkers have yet arrived in clinical practice, some recent oncology trials have begun to incorporate them (56). Nonetheless, implementation of transcriptomic biomarkers remains largely on the horizon, in part because they remain expensive and time-consuming to analyze (57).

Proteomics assays in the clinic – a rarity

While genomics defines the potential universe of gene products, transcriptomics reflects and regulates their expression. However, in the context of the central dogma, only proteomics provides direct real-time phenotypic information about the protein targets of small molecule inhibitors and immunotherapies (1,58). Protein biomarkers have been used for decades to guide cancer diagnosis, subtyping and treatment decisions in the form of single-protein antibody-based tests (e.g, HER2 in breast cancer, cytokeratin staining in melanoma, etc) (59,60).

Yet examples of true "proteomics" assays – multiplexed panels akin to the NGS approaches now common in genomics – are virtually non-existent in a clinical setting. Approved in 2009, the Multivariate Index Assay (MIA OVA1) test for ovarian cancer risk consists of 5 serum protein biomarkers, initially quantified with mass spectrometry and later with immunoassay, together with a scoring algorithm (39,61). The resulting score enables preoperative classification of an ovarian tumour as high- or low-risk of malignancy, with numerical cut-offs specific to the patient's pre- or post-menopausal status (61). This panel provides better predictive power than imaging or CA125 alone, and has proven to be a safe and

effective tool for avoiding unnecessary intervention for patients with low risk of malignancy (62-64).

MIA OVA1 remains the first and only panel of proteomic biomarkers to ever receive FDA clearance to guide cancer therapy. The extreme dearth of proteomics panels in clinical use presents a stark contrast with the essential role that individual protein markers play in the tumour pathology that routinely dominates treatment decisions. It is also at odds with the abundance of proteomic cancer biomarkers currently being published (65).

Opportunities to optimize the use of targeted therapies

Limited success of targeted therapies

In light of the promise of targeted therapies, intensive research focus has yielded a continuous stream of biological insights, targets, and agents. But aside from a few blazingly positive successes, molecularly targeted treatments have overall been plagued by a high failure rate, modest benefits, and the development of resistance (32,66,67). The ORR to new targeted treatments in unselected patient populations is generally <20%, meaning any impact is restricted to a small segment of the clinical population (32). Among responders, clinical benefit rarely exceeds 12 months (32). Significant benefits are needed to justify the associated costs (68).

Despite initial excitement about the dramatic overall response rates to TKIs and ALK inhibitors in genetically pre-selected patients, it has since become clear that the enduring responses achieved with imatinib are exceptional among targeted therapies (24). The performance of virtually any new targeted therapy is limited by tumour heterogeneity (32,69,70). In so far as inhibitor monotherapy does not cure solid tumours, eventual relapse is inevitable. Clonal evolution under pressure from the drug creates resistance, commonly through reactivation of the addictive pathway through mutations to the target or other proteins (69,70). For instance, in the case of erlotinib, 50% of treated patients eventually present with the T790M mutation that prevents the drug from binding to EGFR. Cells may also develop the capacity to transport out or degrade the drug.

Discrepancies between genomic information and the cancer phenotype also limit the utility of many existing biomarkers (69,70). For instance, despite the extraordinary response rates originally leading to erlotinib's approval in EGFR+ NSCLC, outcomes were found to vary widely and many responders quickly progressed diminishing the impact on overall survival

(24,71). Even more confusing, erlotinib was demonstrated to have a survival benefit in some EGFR wild-type patients (24,72). Osimertinib has since demonstrated higher overall response rates (up to 80%) including among T790M mutated tumours; it is now standard of care for EGFR+ NSCLC (73-75). However, erlotinib and other examples show how further research is needed to deconvolute the reasons for unexpected behaviour of some existing molecular subtypes, including the important role of intra- and inter- tumour heterogeneity (32).

Enhanced molecular subtyping with better biomarker panels & tools

Several studies have suggested that success rates of targeted therapies can be ameliorated by using panels of biomarkers to stratify patients in order to maximize predictive power (32,69,70). The application of these tools must similarly be expanded. While studies suggest that >80% of patient tumours carry "clinically actionable" genomic alterations (76), few patients receive targeted therapies outside of clinical trials (25). Molecular subtyping is similarly rarely used outside of research, except in dire clinical scenarios. There is therefore still a need for new and improved tools for molecular subtyping whose enhanced performance would justify more widespread use.

Commercially-available multiplexed panels are increasingly available, but selection of the appropriate lab-developed test among panels with few overlapping targets requires an understanding of both technical considerations and biological insights (25). The assays themselves consume large amounts of tumour material. Between the cost and the need to dedicate 10-20 slides with high tumour cellularity, genomic testing can usually only be conducted once (25). The test selection and potential for timely benefits must be therefore be clearly indicated. This is even more critical if re-biopsy is required, given the potential for associated morbidity.

Multiplexed panels must be paired with the necessary tools to empower oncologists to interpret and action results. Even at academic centres, many oncologists still feel that they lack the expertise to make treatment recommendations based on multiplexed genomic testing (77). This is partially due to widespread challenges interpreting uncommon variants (77). Some oncologists also report that they struggle with communicating the significance of genomics findings to patients (77). In fact, many oncology clinics now rely on specialty consulting services employing molecular biologists to review, analyze, and generate concise summaries of relevant clinical evidence from genomics results (78).

Early intervention with combination therapies

As described above, the use of molecularly-targeted agents is inherently limited by tumour heterogeneity and the latent potential for resistance that it implies. It has been argued that the success of imatinib in treating CML *only* prior to blastic transformation is analogous to the challenges faced in applying targeted therapies for advanced solid tumours (24). Essentially, turning to targeted drugs after a patient fails standard-of-care treatments is a recipe for failure. In spite of this, most clinical practices apply panels only when patients present with recurring or hard-to-treat disease (25) . It is imperative to identify tumour drivers and introduce targeted treatments, in the form of strategic combination therapies, at an early stage of treatment to see their full impact on disease and to achieve an enduring response.

Overcoming side effects and maximizing efficacy with precision dosing

Despite their reputation as less harmful alternatives to chemotherapy, many targeted therapies address pathways required by normal cells and therefore demonstrate a narrow therapeutic index (NTI). This is not unique, in that many medical specialties, including cardiology and psychiatry, make heavy use of essential NTI drugs. Dose optimization is generally accomplished through traditional dose titration with vigilant monitoring. This approach can be practical in such settings; if someone feels faint, it is easy enough to recognize hypotension and reduce their statin, whereas continued high blood pressure might require an increase. Cancer treatment, on the other hand, often involves a delay of many months between introducing an intervention and measuring its results. In the case of preventative agents like tamoxifen, severe consequences -- like tumour development resulting from an inadequate dose -- may not be apparent for years. Adverse effects often yield irreversible outcomes in medical oncology: a treatment “holiday” or dose reduction due to poorly-tolerated therapy can result in significant disease progression. Based on personal observations during the course of an oncology clinic observership, it appears that hospitalization as a result of adverse events is often associated with a cascade of deterioration. Even for patients presenting with treatable disease, some report that experience with or fear of side effects leads some patients to refuse further intervention.

Opportunities to optimize targeted treatments

Notwithstanding the remarkable outcomes achieved by some with excellent biomarkers, the overall success rate of newly developed targeted therapies and associated biomarkers in routine clinical applications is modest (32). Given the promise and substantial investment so far

dedicated to these agents, it is imperative to optimize their use. Improving our knowledge, not only of molecular cancer subtypes, but also of cancer biology and individual physiology can help to guide strategic use of targeted therapies in terms of who (patient selection), what (combination therapies), when (timely intervention), and how much (precision dosing).

Use case: Targeting the PI3K/AKT/mTOR pathway

Role of the PI3K/AKT/mTOR pathway in oncogenesis

The PI3K/AKT/mTOR signaling pathway is one of the most frequently dysregulated pathways in human cancers (79). As shown in Figure 1, when activated by growth factors (e.g., insulin, EGFR, VEGFR), receptor tyrosine kinases (RTKs) initiate PI3K signalling via PIK3CA, which phosphorylates phosphatidylinositol lipids in the cell membrane to generate phosphatidylinositol (3,4,5)-trisphosphate (PIP3) (80-82). If not converted back to PIP2 through negative regulation by PTEN (80), PIP3 then recruits a specific set of signaling proteins to the membrane (83). The recruited proteins are those with pleckstrin homology (PH) domains, including AKT and PI3K-dependent kinase-1 (PDK1) (83). Once translocated to the membrane, AKT is activated by phosphorylation at Thr308 (by PDK1) and Ser473 (by PDK2) (84). Activated AKT modulates multiple downstream oncogenic functions, in large part through activation of mammalian target of rapamycin (mTOR), a critical regulator of protein synthesis, cell growth, and metabolism (80,81,84,85). This is accomplished as activated AKT phosphorylates TSC2, which then ceases to inhibit mTOR (83). Upregulation of mTOR activity resulting from release of TSC and PTEN inhibition subsequently promotes cell proliferation and suppresses apoptosis (80-83,85).

Activation of the PI3K pathway stimulates cell cycle progression, stimulates protein synthesis, and inhibits apoptotic pathways, ultimately promoting proliferation and survival (79-81,85). The PI3K pathway also alters cellular metabolism through changes in glucose uptake, glycolysis, and mitochondrial function (81). This increased nutrient uptake and utilization supports the increased energy demands of cancer cells. More recently, the PI3K pathway has been shown to modulate the activity of many, if not most, immune cells to create an immunosuppressive tumor microenvironment (86). Taken together, this implicates PI3K pathway functions in almost all the hallmarks of cancer (87,88). The PI3K pathway also sits at the nexus of many other oncogenic pathways demonstrating substantial cross talk with signalling in the MAPK/ERK, JAK/STAT, and Wnt/β-catenin pathways (89-91).

PI3K pathway activation has been linked to a long list of solid tumours including gynecological, breast, bladder, head and neck, colorectal, gastric, squamous lung, esophageal, pancreatic, glioblastoma, glioma), as well as to certain melanomas and lymphomas (80,92). Genetic pathway alterations are widespread, being detected in at least 50% of breast cancers (93). Common oncogenic mutations include activating mutations in PI3K genes (e.g., PIK3CA), loss of function mutations in PTEN (a negative regulator of the pathway), and amplification of growth factor receptors, all of which result in constitutive activation (80,81).

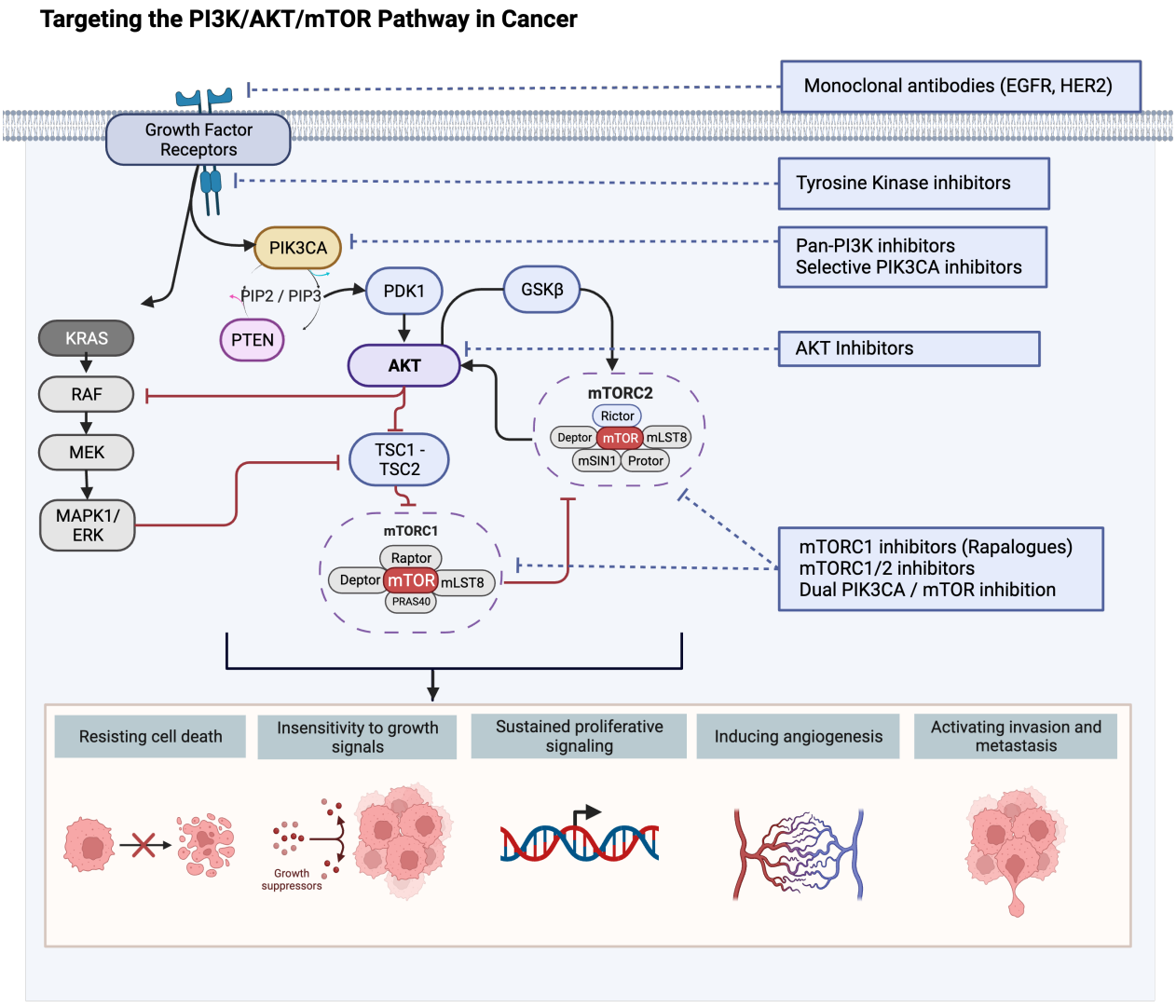

Figure 1. Targeting the PI3K/AKT/mTOR pathway in oncogenesis.

Treatment targets in the PI3K pathway

Given its central role in oncogenesis and treatment resistance, the PI3K pathway is now the target of a wide range of therapeutic agents (79,80,94,95). A plethora of literature addresses the idea that the pathway is druggable and >40 targeted agents had reached clinical development as of 2020 (80,95). Several PI3K inhibitors have now received FDA approval (96). Therapeutic strategies are directed to several different targets including RTK inhibitors, PI3K inhibitors, AKT inhibitors, and mTOR inhibitors (96). Many approved monoclonal antibody therapies target upstream growth factor receptors (96).

PI3K inhibitors

PI3K represents a large family of related isoforms, of which Class I PI3Ks are the most well-known (97). Class IA PI3Ks consist of a catalytic subunit (p110α, p110β, or p110δ) that converts PIP2 into PIP3 and a regulatory subunit (p85α, p55α, or p50α) (97) (98). Class IA PI3Ks are primarily activated by receptor tyrosine kinases (RTKs) and G-protein-coupled receptors (GPCRs) (97). The most common isoform in this class is p110α (97). Treatment strategies targeting PI3K include both pan- and selective PI3K inhibitors (80,96).

Idelalisib was the first-in-class treatment targeting the PI3K pathway, receiving FDA approval in 2014 for the treatment of chronic lymphocytic leukemia (CLL) (99). This PI3Kδ kinase inhibitor is now used in combination with rituximab for relapsed CLL and in combination with rituximab or ofatumumab for relapsed follicular B-cell non-Hodgkin lymphoma or small lymphocytic lymphoma (99). Copanlisib, a pan-PI3K inhibitor with activity against PI3K-α and PI3K-δ isoforms, received accelerated FDA approval in 2017 for treating patients with relapsed follicular lymphoma (100). Most recently, in 2019, alpelisib became the first selective PIK3CA-p110α inhibitor available for use in solid tumours. The FDA approval was based on the use of a companion diagnostic to select patients with HR+, HER2-, PIK3CA-mutated advanced or metastatic breast cancer who previously progressed on endocrine therapy (101). Alpelisib plus fulvestrant in this cohort showed a significantly improved progression-free survival (PFS) of 11.0 months versus only 7.4 months in the mutation negative cohort (as compared to ~5.7 months PFS in the placebo arm of either cohort) (101).

Despite initial excitement about PI3K inhibitors as a therapeutic strategy, their use has been limited by a broad range of serious toxicities (102), including unexpected autoimmune toxicity which can be serious and even fatal (103).

mTOR inhibitors

mTORC1 promotes cancer growth and proliferation by stimulating protein synthesis and ribosome biogenesis downstream from AKT activation (96). It regulates the translation of specific messenger RNA (mRNA) into proteins involved in cell cycle progression, cell growth, and metabolism (96,104). Interactions of mTORC1 and mTORC2 also compose a feedback loop that regulates AKT activity. mTORC1 and mTORC2 are both druggable targets (96,104); in fact, mTOR was the first protein in the pathway to be targeted with inhibitors (96). Multiple mTOR inhibitors have been developed with different mechanisms of action (96,104). Competitive ATP inhibitors bind to both mTORC1 and mTORC2, enabling dual inhibition, whereas rapologs and allosteric ATP inhibitors target mTORC1 exclusively (104). Two mTORC1 inhibitors have now received FDA approval: temsirolimus and everolimus (96).

Temsirolimus received FDA approval in 2007 after it demonstrated a survival benefit of 3.5 months for naïve patients with metastatic renal cell carcinoma as compared to a standard treatment (105). However, only a small minority (8.6%) of patients demonstrated objective responses according to RECIST criteria (105). It is delivered intravenously and is typically used only in patients with poor prognosis or with advanced disease (96). Everolimus was approved in 2016 for the treatment of various cancers, including advanced renal cell carcinoma (RCC) after failure of treatment with other agents, selected neuroendocrine tumours, and HR+, HER2- breast cancer in post-menopausal women (96). In RCC, everolimus treatment was associated with a 2-month PFS benefit over placebo (106). However, this did not translate into better overall survival in multiple cohorts (106,107). Overall response rates are typically very low (1-5%) though some responders benefit significantly (106,108). Poor response rates to everolimus in metastatic breast cancer were significantly improved when everolimus was used in combination therapies (109).

AKT inhibitors

In response to PI3K pathway activation, AKT is the effector responsible for transducing signals to promote cell growth, inhibit cell death, and regulate metabolism (89). Although direct mutations of AKT are comparatively rare in the mutational landscape, overexpression and overactivation of AKT is a key factor in cancer progression (89). Gain of function mutations are found in 2-6% of breast, esophageal, and bladder cancers, with the most common being AKT1 E17K (110-112). Amplifications appear to occur with a higher frequency of 5 to 21%, and are

detected in a number of human cancers, including gastric carcinoma, glioblastoma, head and neck squamous carcinoma, pancreatic, ovarian, prostate and breast cancer (92,111).

AKT has three isoforms, which share high sequence identity and each consist of 3 conserved domains: an N-terminal pleckstrin homology (PH) domain, a kinase domain containing the catalytic site involved in binding ATP, and a C-terminal regulatory hydrophobic motif. The kinase domain is very similar to that found in other protein kinases (e.g., PKA, PKC, p70 S6K) (87). Activation is achieved through phosphorylation at specific sites during transient localization to the cell membrane (113). Despite their similarity, each AKT isoform has a distinct, non-redundant functional characteristics and a unique role in oncogenesis (87,114-116). Increased AKT1 activity is typically associated with local proliferation, while increased AKT2 activity is associated with metastatic potential and worse prognosis (87). AKT3 has been specifically linked to particularly aggressive breast cancer subtypes (116). The functional specificity of AKT isoforms results from differing cytoskeleton interactions and cellular localization (114,117). This altered localization regulates AKT's binding partners to induce different downstream signaling cascades (114,117).

Though no AKT inhibitors have yet been approved by the FDA as standalone therapies, several have been developed and studied in preclinical and clinical trials for the treatment of solid tumours. Most of these drugs bind competitively in the ATP pocket (118). This approach targets all active forms of AKT, but also results in poor selectivity against PKA, PKB and PKC kinases (119). Some examples are listed in Table 1. At the time of writing, clinicaltrials.gov listed >100 active clinical trials related to the targeting or analysis of AKT.

Table 1. Selected examples of AKT inhibitors and their current phase of development.

Inhibitor	Mechanism of Action	Stage of Development
Ipatasertib	Selective ATP competitive	Phase III/IV
Capivasertib (AZD5363)	Pan-AKT ATP competitive	Phase III
MK2206	Allosteric	Phase II
Uprosertib	ATP competitive	Phase II
Afuresertib (GSK-2110183)	ATP competitive	Phase II
TAS-117	Allosteric	Phase II basket trial
Vevorisertib (ARQ 751)	Allosteric	Phase I
MSC2363318A	ATP competitive	Phase I
BAY 1125976	Allosteric	Phase I
Miransertib	Allosteric	Preclinical for cancer

AKT as a common mechanism of resistance to cancer therapies

The scope of use for AKT inhibitors may be wider than initially surmised. AKT lies downstream of several notable drug targets and is implicated in resistance to a wide variety of treatments. Activation of AKT is induced by treatment with traditional chemotherapy and pathway activation evades cytotoxic effects by restoring essential functions for proliferation and survival (92). In HR+ breast cancer, activation of AKT phosphorylates and inactivates estrogen receptor or decreases expression of progesterone receptor, rendering tumours less responsive to endocrine therapies (e.g., tamoxifen, aromatase inhibitors) (120).

Similar effects are observed for targeted treatments directed at proteins upstream of AKT and in adjacent pathways. In HER2-positive breast cancer, reactivation of the pathway by AKT causes resistance to upstream HER2 inhibition with trastuzumab (120). Up to 23% of HER2+ and triple-negative breast cancers harbour detectable mutations in the PI3K pathway (121). Similar reactivation mechanisms are observed in NSCLC resulting in resistance to EGFR inhibitors (122). In the case of PI3K inhibitors, AKT is the protein that is commonly reactivated to restore pathway function (123). In melanoma, AKT mediates resistance to BRAF inhibitors (e.g., vemurafenib) or MEK inhibitors (e.g., trametinib) in *PTEN*-wildtype tumours (124). The same is true for sorafenib in kidney cancer, where resistance to the dual MEK/ERK and VEGFR inhibitor is reversed by PI3K pathway inhibition (125). Combination therapy with AKT inhibitors also restores sensitivity to CDK4/6 inhibition (126). In each scenario, the genetic alterations that promote resistance converge on compensatory PI3K signalling by AKT.

Challenges in using PI3K pathway inhibitors effectively

Despite their promise, there are several issues still to be addressed in agents targeting this pathway. None of the currently developed inhibitors are specific to activating mutations. Since the PI3K pathway is also required by healthy cells for essential functions, like glucose transport, a limited therapeutic window inevitably applies; important drug-related toxicity, including hyperglycemia, limits doses (127). Mechanisms of treatment resistance are still not fully characterized, though reactivation of the PI3K pathway through alternative pathway members is one possibility (127). Most significantly, although clinical activity has been observed for single-agent AKT inhibitors, existing approaches to patient selection are sub-optimal (96,127). Studies have not yet consistently confirmed an incremental treatment benefit for these agents associated with the currently used markers (e.g., selecting for PIK3CA, AKT1 or PTEN mutations) (96). This may be in part due to an overly narrow focus on the genome to provide patient selection

markers. To help these targeted treatments reach their enormous potential benefit, we must (i) introduce, test, and validate new patient selection markers of response, (ii) identify and screen for markers of resistance, (iii) design strategic combination therapies to limit adaptive response, and (iv) optimize dose schedules or modify target specificity to prevent toxicities (127).

Approach: proteomics for translational biomarker research

Rationale - The central dogma & the genetic biomarker challenge

Genomics approaches have yielded important advancements and currently dominate the molecular subtyping landscape in terms of their adoption in clinical settings. However, genome-only approaches do come with some caveats that limit their utility for biomarker discovery and validation. First, cancer cells rapidly accumulate a multitude of mutations, of which only a portion act as central drivers of cancer progression (128,129). Even in germline cells, where mutations are much better controlled, individual genetic variations such as single nucleotide polymorphisms typically account for a modest proportion of phenotypic variability (<10%) and relatively small increments in disease risk (<1.5 fold) (130,131).

Secondly, there is limited concordance between genetics, mRNA abundance, and the expression of proteins targeted by small molecule drugs (70). The level of discordance can be substantial. Across organisms and cell types, gene expression measured by mRNA transcripts only explains approximately 30-65% of protein expression; the remainder is largely attributable to post-transcriptional and translational regulation as well as protein degradation (70). This phenomenon manifests even more dramatically in cancer cells, where regulation of cancer-driving proteins without detectable DNA mutations also occurs through epigenetic modification of expression (132,133), and the products of mutated genes may go unexpressed or be quickly degraded (134). Regulatory interactions are also modified; in a study to identify co-regulated protein networks in cancer, there was only an 8% overlap between the associations identified at the mRNA level and those seen at the protein level (135). Evaluation determined that co-regulation analyses performed on proteome profiles had substantially higher power for identifying functional protein–protein associations than the same analysis applied on transcriptome profiles (135).

Substantial research evidence demonstrates that direct measurement of the proteome has special potential for identifying and verifying active cancer-driving alterations in tumours that closely correspond to treatment sensitivity or resistance. A large-scale multi-omics study used

Reverse Phase Protein Array (RPPA) to measure expression of 230 cancer-related proteins from >650 cancer cell lines (136). Relative protein expression data was then analyzed in the context of previously-published genomic, transcriptomic, and drug-screening data (136). The overall correlation between protein expression and mRNA transcript abundance was surprisingly limited (R^2 <0.15) (136). It also varied significantly from protein to protein, with signalling phosphoproteins, including kinases, showing a greater-than-average degree of discordance between mRNA levels and protein expression (136). In cases where significant discordance was observed, protein-level data predicted drug response better than mRNA data (136).

A similar multi-omics study characterized patient NSCLC tumours in terms of their DNA (by copy number variation - CNV, SNP array), RNA (by gene expression Illumina array), and protein expression (LC-MS/MS Orbitrap-based label-free quantitation) (137). In this instance, there was little correspondence between CNV and mRNA expression (r_s <0.2) and even less to tie CNV to protein expression (r_s <0.1). Once again, proteomic signatures offered the highest impact for predicting disease course among this cohort (137).

Clinical validation studies have further confirmed that transcriptomics and proteomics have the ability to enrich molecular profiles and augment existing clinical information to guide better treatment decisions than NGS alone (53-55,138). Several examples have demonstrated that proteomics and genomics offer more predictive power together than they do apart. When used in liquid biopsies, combining data from circulating tumor DNA and protein biomarker analysis enabled earlier detection of pancreatic ductal carcinoma with higher specificity and sensitivity than either alone (139).

The reason that protein markers have such strong diagnostic and prognostic value is intuitive. Proteins are the machinery and substrates involved in performing day-to-day cellular activities. The proteome is dynamic; it varies dramatically from tissue to tissue and changes over time, reflecting the interplay of biology and the environment. Changes in protein activity are where the mechanisms of disease pathology play out. Moreover, proteins are the direct target of most drugs, particularly small molecule inhibitors.

Antibody-based protein quantitation in a clinical setting

In a clinical setting, and particularly in oncology, the vast majority of all protein quantitation is still performed using antibody-based immunoassays (1). Immunohistochemistry (IHC) is applied to generate protein expression data from tissues (59,60). While IHC is generally

qualitative or semi-quantitative, it offers valuable spatially-resolved information about protein expression in the tumour and adjacent tissue, and is a mainstay of tumour pathology for all solid tumours (60). FDA-approved companion diagnostics for cancer treatment selection employ IHC to quantify PD-L1, ALK, and HER2 protein expression in tumour tissues (25).

Enzyme-linked immunosorbent assay (ELISA) has been the "gold standard" clinical approach for quantitation of circulating protein biomarkers from body fluids for >50 years (140). A miniaturized version called reverse phase protein array (RPPA) permits large-scale multiplexing (141). Important ELISA-based assays in oncology include those for prostate-specific antigen (PSA) and carcinoembryonic antigen (CEA), which are both used for monitoring cancer treatment response. In total, fewer than 25 protein biomarkers spanning all medical applications received FDA approval between 1995 and 2010 (65).

The quantitative performance of ELISA and IHC assays varies from platform-to-platform, depending on reporters, detectors, and methodology. However, all antibody-dependent assays face the same fundamental challenges related to the quality, kinetics, and specificity of antibodies (142). Cross-reactivity is major challenge, particularly in tissue. Most antibody-based methods struggle with the discrimination of disease-related isoforms and variants that bear high similarity to the wildtype or other proteins. Together, these factors limit the accuracy and reproducibility of quantitation, with the potential to undermine clinical performance (143).

Large-scale efforts are currently underway to improve antibody availability (144). However, to date, the time, cost, and risk associated with developing new antibodies (or more often, antibody pairs) for new assays still limits the scope of proteins to which such assays can be applied (145). The limited availability of high-quality antibodies has biased scientific investigation toward heavily investigated targets: more than 75% of proteomic research still focuses on the 10% of proteins that were known before the genome was mapped (146). The expansive "neglected proteome" is a direct result of scientific concentration on proteins for which antibody-based assays were already available (146).

Mass spectrometry-based proteomics in clinical and translational research

Mass spectrometry (MS) is a relatively new technology for protein analysis in a clinical context. While clinical MS is well-established for small molecules, its application for both absolute and relative quantitation of proteins is more recent (147). Unlike antibody-based methods, MS-based proteomics offers high analytical specificity, the ability to distinguish

protein isoforms, and is well-suited for the discovery, verification, and validation of new biomarkers in the "neglected proteome" (1). Over the past few decades, its significance in life-science research has grown significantly, aided by advancements such as the identification of peptide fragment ion spectra through database searches and the introduction of high sensitivity analysis using nano-LC–MS/MS (148).

MS-based proteomics can be broadly classified into two types of approaches: untargeted proteomics (also known as global or discovery proteomics) and targeted proteomics. The aim of global proteomics is to maximize proteome coverage for biomarker discovery and biological insight (1,149). Inter-laboratory studies have shown that diligent standardization is critical for this type of workflow (150). However, even with the implementation of careful and deliberate quality control measures, these approaches are typically limited to research use only since they can only achieve relative quantitation (149). This limits comparison over time, across instruments, and across research groups, and inherently prohibits the development of meaningful references ranges for standardized clinical applications.

Targeted proteomics, on the other hand, is recognized as well-suited for biomarker validation and clinical applications thanks to its potential for reproducible quantitation (151,152). Direct multiple/selected reaction monitoring MS (MRM/SRM-MS) assays also offer shorter development times than other technologies, enabling extensive multiplexing and delivering notable advancements in speed, sensitivity, and quantitative precision (152-154). Reliable identification of a proteotypic peptide representing the protein target is confirmed by concurrent analysis of a stable isotope-labeled standard (SIS) peptide (155). The SIS peptide typically consists of a purified synthetic peptide that differs from the endogenous analyte only by the inclusion of stable isotope-labeled amino acid (R+10, K+8) and can be easily discriminated by mass-to-charge ratio. Normalization to this co-eluting internal standard compensates for ion suppression to ensure that protein concentration values can be definitively calculated for unknown samples by using a response curve of characterized reference standard (purified synthetic NAT peptide) spiked at varying concentration in samples of digested matrix (156).

Recent advancements in high mass accuracy parallel reaction monitoring (PRM)-MS exhibit similar or improved performance characteristics versus MRM-MS, with the added benefit of post-acquisition filtering of high-resolution fragment ion spectra to obtain specific ion traces with minimal noise (157-159). Targeted assays can be multiplexed to simultaneously quantify a

large number of proteins. Highly-multiplexed panels can, in some cases, quantify hundreds of targets from a single volume-limited sample with high dynamic range (154).

New technologies including ion mobility MS, MALDI-MS imaging, top-down proteomics, mass cytometry, SWATH-MS, iMALDI-MS and many others continue to extend the capabilities and applications of MS proteomics, with well-characterized benefits (1,6,59,160). However, despite these promising technological advances, successful validation and translation of proteins into clinical biomarkers remains extraordinarily rare (59). The reasons cited for this disparity include researchers' limited knowledge of analytical, diagnostic, and regulatory requirements for a clinical assay, inadequate assay performance, the need for standardization of methodology, the need for better data analysis pipelines, and the need for sufficient study samples to power meaningful conclusions (39,59).

The need for validation & fit-for-purpose assays in translational research

Years prior to OVA1's 2009 FDA clearance, a separate proteomics-based panel was developed in an attempt to improve ovarian cancer screening for patients with pelvic masses. The OvaCheck proteomics panel consisted of a computational model that analyzed mass spectra to discriminate malignancies from benign tumours (161). This widely-publicized test was marketed to gynecologists prematurely, prior to the publication of validation studies (161,162). This led to immediate intervention by the FDA, which prohibited its commercial implementation on the basis that the algorithm constituted a medical device and was subject to premarket review (161,162). Within just a couple of years of its introduction, significant scientific criticisms of the published data led to the stalling of clinical implementation and eventually to its abandonment (163). OvaCheck suffered from many serious pitfalls, including not publishing its original data, the use of "black-box" algorithms, overfitting, failure to identify the molecules corresponding to the peaks proposed to have predictive value, lack of verification/validation, and numerous other flaws in its experimental design (59,161,164,165). In spite of this, OvaCheck's discoverers claim that some of the ions originally identified as part of the proteomic signature may have subsequently been re-identified in independent studies (166).

Since then, proteomics standards have changed significantly – in no small part due to the OvaCheck debacle. In 2005, the NCI repurposed $89 million in funding earmarked for proteomics discovery work in favour of an allocation for the new Clinical Proteomic Tumor Analysis Consortium (CPTAC) (165). CPTAC was born to tackle the observed problems with standardization, validation, and translation of proteomics assays (165). Their developed

recommendations pertain to all areas of proteomic biomarker translation, including addressing variability within and across technical platforms, improved sample handling and experimental design, better strategies for biomarker candidate prioritization, better interfaces between proteomics and regulatory science, and the need for better data analysis tools (65). CPTAC has developed a clear set of guidelines to enable thorough assay characterization and validation, launching public databases to house this key information (167,168). They have also endorsed a new biomarker pipeline that emphasizes the use of biomarker verification together with fit-for-purpose assays to facilitate translation. (65)

As shown in Figure 2, the fit-for-purpose approach emphasizes selecting analytical methods and techniques based on the specific goals and requirements of each stage in the biomarker discovery and development process (1,149,156). For example, in the early stages of biomarker discovery, the emphasis may be on screening a large number of potential targets, even if the measurements are less precise or accurate (1,149). As the biomarkers progress towards clinical qualification, the focus shifts towards more targeted and quantitative methods with superior analytical performance to guarantee precise quantitation, reproducibility, and suitability for clinical applications (1,149). By recognizing that different stages of biomarker development have varying needs in terms of target coverage, precision, accuracy, sensitivity, dynamic range, and throughput, this approach aims to maximize the likelihood of successful biomarker identification, validation, and clinical utility (149). In the case of proteomics, the need for precise quantitation and reproducibility in the later stages of biomarker development favors targeted approaches such as MRM/PRM-MS, which offer more exact, more sensitive, and faster quantitation over a wider dynamic range, particularly when used with internal standards (1,149).

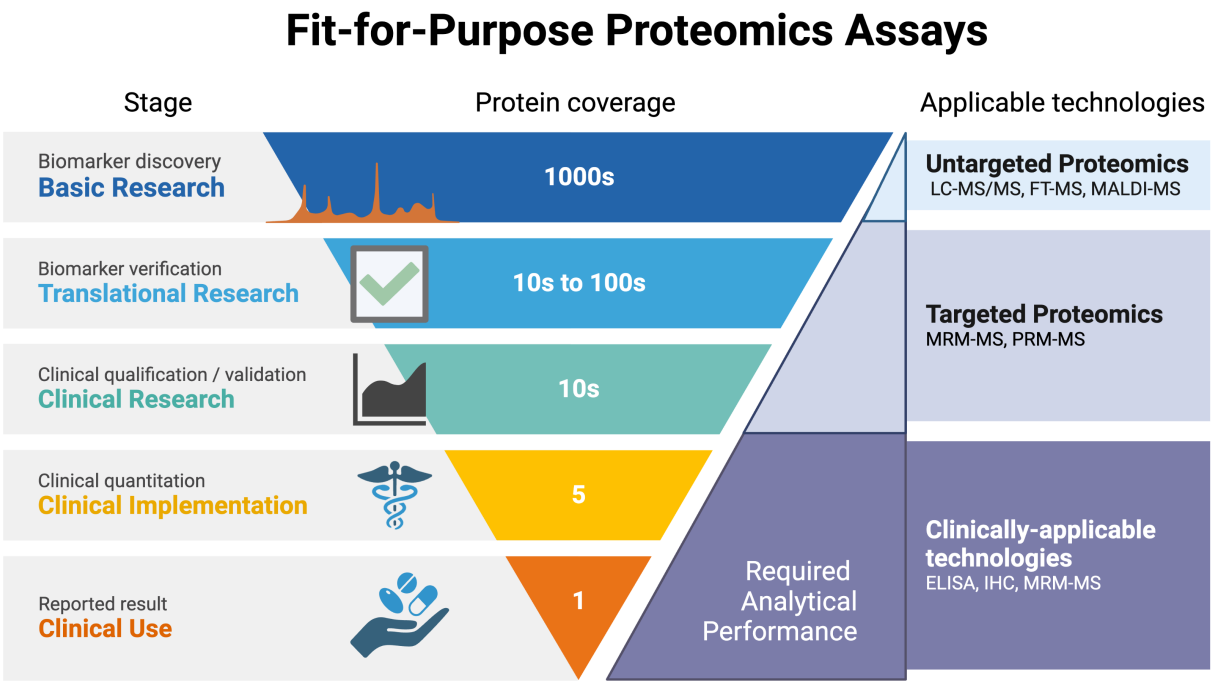

Figure 2. Fit-for-purpose proteomics technologies in the biomarker development pipeline.

Hypothesis, Objectives & Approach

Objectives. The objective of our work is to improve patient selection in precision oncology and optimize use of emerging targeted therapies with the use of more comprehensive, enriched molecular profiles. Secondly, we aim to use the insights generated by a multi-omics approach to improve our understanding of and ability to treat disease. The overarching premise is that proteomics-focused approaches are essential to supplement genetics-heavy molecular profiles and to advance precision oncology. Fit-for-purpose proteomics approaches will render the technologies suitable for translational research and eventual clinical implementation.

Hypotheses. To this end, we will test the core hypotheses that:

1. There are proteomic markers associated with treatment response to capivasertib that can be identified in the stored tumour samples of patients enrolled in a clinical trial (Results Chapter 1);

2. Any identified markers that are truly predictive of capivasertib treatment response will be verified when reproducibly quantified with targeted methods in orthogonal models and sample sets (Results Chapter 2);
3. Beyond patient selection, it is feasible to routinely measure variations in drug metabolism in a clinical setting to enable precision dosing of cancer drugs (Results Chapter 3).

Approach. To test the hypotheses, we will take the following approach:

1. Identify relevant technologies, implement & optimize them, validate their analytical performance, and assess fit-for-purpose.
2. Apply assays to quantify analytes of interest in carefully chosen well-characterized models and samples.
3. Apply rigorous statistical approaches to test the hypothesis that any of the measured analytes can be correlated to clinical variables such as treatment response or drug metabolism.
4. Wherever possible, verify markers in additional sample sets or models.

The specific experimental methodology used to test the hypotheses is described in the next chapter, titled Materials & Methods.

Materials & Methods

Phase II Clinical Trial Study (Results Chapter 1)

Patients & samples

Patient cohort. Research ethics approval for this study was granted by the Research Ethics Committee at the Jewish General Hospital in Montreal, Quebec, Canada (Project #2018-663, 17-004). Anonymized patient tumour samples were obtained from AstraZeneca's multi-centre clinical trial of AZD5363 (NCT01226316) (169). The sample set for the current study was drawn from the Part C dose-expansion cohort, which included patients with breast cancer whose tumour pathology was either estrogen-receptor positive (ER+) or human epidermal growth factor receptor 2-positive (HER2+) breast cancer, as well as patients with gynecological (ovarian, cervical, or endometrial) cancers for whom no standard therapy was effective.

For this cohort, eligibility was restricted to patients whose tumours contained known activating *PIK3CA* mutation(s), as detected by PCR-based approaches during screening (local testing). As described in Banerji et al. (169), exclusion criteria included prior treatment with PI3K inhibitors or glucose metabolism abnormalities. The enrolled patients received capivasertib 480 mg twice-daily for 4 days followed by 3 days off, repeated in 21-day cycles. Tumour volume was measured according to RECIST v1.1 criteria within 28 days of the start of treatment and at specified timepoints after the start of treatment (i.e., weeks 6, 12, 18, 24, etc.). RECIST v1.1 criteria were used to categorize target lesion response into complete response (CR), partial response (PR, ≥30% decrease in volume), stable disease (SD, volume ±<30%), or progressive disease (PD, ≥30% increase in volume) (169). Treatment was continued as tolerated, until either withdrawal of consent or evidence of disease progression.

Samples. Patient tumour samples obtained at the time of screening for genetic/histological assessment were stored at room temperature as 4 µm-thick FFPE tumour tissue slices mounted to glass slides. A subset of 2 slides per tumour for each of 24 tumour samples was selected for our study. Of these, 23 slides, representing 16 tumours, yielded sufficient material (≥25 µg total protein/slide) for the planned analyses.

Treatment response coding. For each tumour, standardized, anonymized response data were used to classify patient drug response based on progression-free survival (PFS). PFS was defined as event-free survival from the date of first capivasertib dose until the date of observed

PD (or death by any cause in the absence of progression), regardless of withdrawal from study therapy or protocol. PFS was censored at the time of latest evaluable RECIST v1.1 assessment for patients with two or more missed visits. "Clinical Benefit" (CB) was defined as PFS for a minimum of 12 weeks. "No Clinical Benefit" (NCB) was defined as less than 12 weeks of observed PFS while receiving capivasertib.

Protein extraction, digestion, & immuno-MALDI-MS

Reagents & materials. Solutions were prepared using LC-MS grade water and solvents, and analytical grade reagents.

Protein extraction. Slide-mounted slices were extracted using xylene deparaffinization followed by stepwise ethanol rehydration, high-temperature incubation in sample extraction buffer (2% sodium deoxycholate in 50 mMol Tris-HCl, pH 8, 20 minutes, 99°C) to break formalin crosslinks, sonication (25% power, 15 sec, 2 rounds), and an additional incubation (2 hours, 80°C). The concentration of total protein in each sample was then quantified using a Pierce bicinchoninic acid (BCA) protein assay kit (Thermo Scientific, Cat # 23225) with a ThermoFisher MultiSkan Go spectrophotometer.

Sample preparation for iMALDI-MS of AKT. A published workflow for quantitation of AKT by immuno-MALDI-MS was implemented with automation, as previously described (170,171). The assay is compatible with fresh frozen or formalin-fixed paraffin-embedded (FFPE) tissue samples and can be performed on as little as 100-200 ug of tissue (~10 ug of total protein per analyte). Briefly, aliquots of 40 µg of total protein were diluted to 0.1 µg/µL total protein and prepared in an automated fashion on an Agilent Bravo Liquid Handling Robot. As shown in Figure 3, the samples were further divided into aliquots of 100 µL (10 µg total protein) each for independent quantitation of surrogate peptides for AKT1 and AKT2 with and without phosphatase treatment, as in Domanski et al (172). A standard calibration curve was prepared by spiking known quantities (20, 10, 5, 2.5, 1.25, 0.63, 0.32, 0 fmol) of unlabeled standard peptide (AKT1: ^{466}RPHFPQFSYSASGTA^{480}, AKT2: ^{468}THFPQFSYSASIRE^{481}) into 10 ug of bovine serum albumin at 0.1 µg/µL.

Sample Analysis Workflow

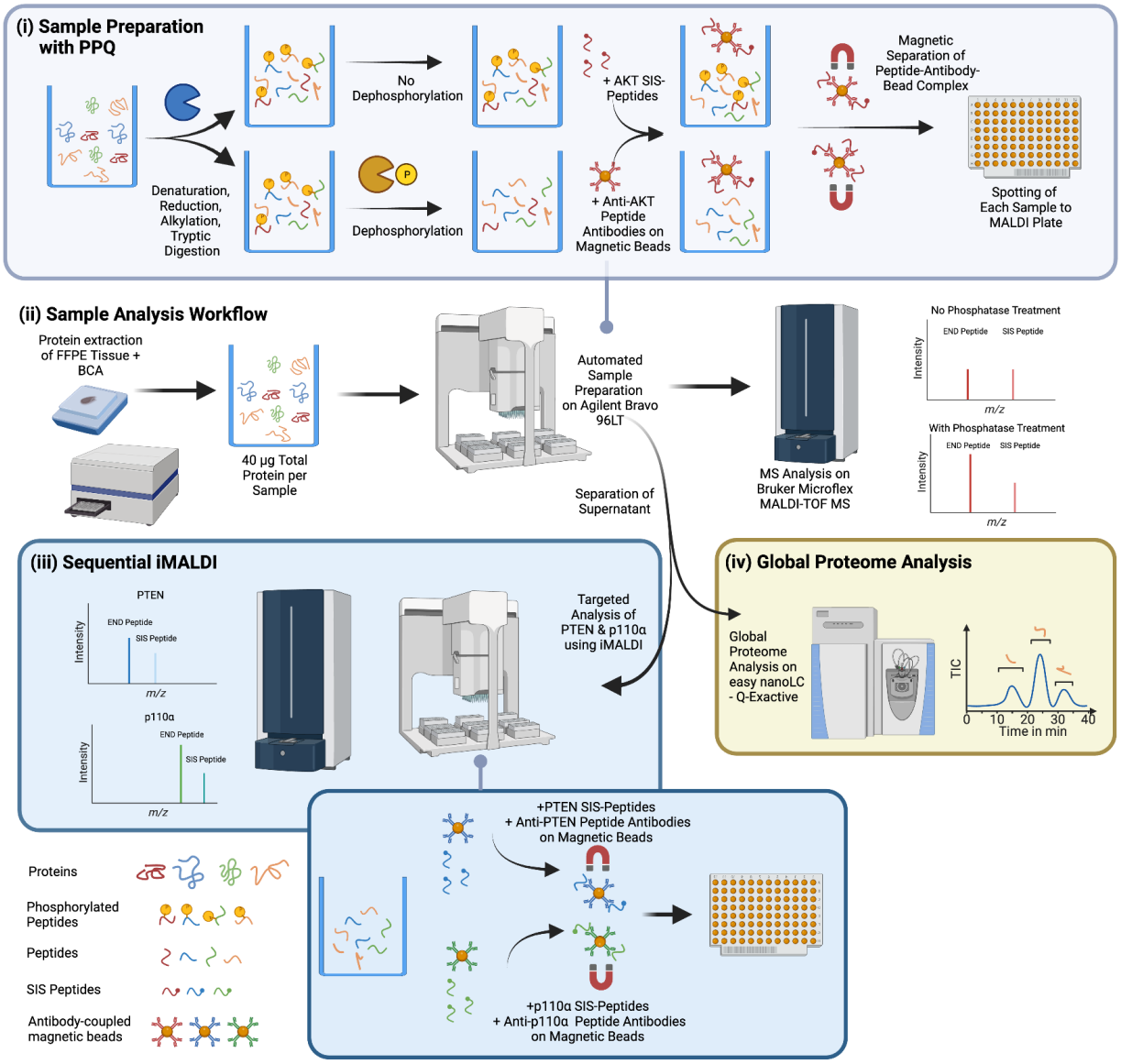

Figure 3. Proteomics workflow for slide-mounted FFPE tumour clinical trial samples.
(i) Proteins extracted from samples were digested with trypsin. Phosphorylation stoichiometry was assessed via phosphatase-based phosphopeptide quantitation (PPQ). After addition of stable isotope labeled standard (SIS) peptides, AKT1/AKT2 were enriched together with their internal standards and quantified by iMALDI-MS against an external calibration curve. (ii) Using a novel sample analysis workflow, supernatants from the AKT enrichment step were retained for subsequent analyses. (iii) PTEN + PI3K p110α were quantified from sequential iMALDI-MS of the supernatants. (iv) An aliquot of supernatant was reserved for label-free quantitation (LFQ) of the global proteome.

Tryptic digestion & dephosphorylation. Each sample or calibration standard was then denatured and reduced with 10 µL sodium deoxycholate denaturing mix (20 mM TrisHCl, pH 8.4, 0.74 mM TCEP, 10% DOC) at 60ºC for 30 minutes. Samples were then brought to room temperature before alkylation with 10 µL 0.74 mM iodoacetamide (IAA) for 30 minutes while protected from light, followed by quenching of any remaining IAA with 10 µL 0.74 mM dithiothreitol (DTT). Digestion was performed with trypsin (Worthington, TPCK Treated, 97% purity) dissolved in 1mM HCl, added at a substrate-to-enzyme ratio of 2:1, and allowed to incubate for 1 hour at 37°C. The digest was then chilled on ice and quenched with Nα-Tosyl-L-lysine chloromethyl ketone hydrochloride (TLCK) in a 2-fold molar ratio over trypsin. The dephospohorylation step was performed on selected samples by incubating with or without alkaline phosphatase (1U/µg total protein) for 2 hours at 37°C. The relevant stable isotope-labeled internal standard peptide (AKT1:^{466}RPHFPQFSYSASGTA^{480}, AKT2: ^{468}THFPQFSYSASIRE^{481}) was then added to each aliquot prior to immunoenrichment.

Immunoenrichment & spotting. Immunoenrichment was achieved by tumbling samples overnight at 4ºC with anti-peptide antibodies (Signatope GmbH) coupled to magnetic beads (ThermoFisher Protein G Dynabeads). Beads were washed with ammonium bicarbonate (5 mM), 15% ACN/phosphate-buffered saline, and 15% ACN/ammonium bicarbonate (4.25 mM), prior to spotting on a MALDI target. HCCA MALDI matrix consisting of 3 mg/mL cyano-4-hydroxycinnamic acid, 7 mM ammonium citrate, 70% ACN, 0.15% TFA was applied to the dried spot, which was then washed with 7 mM ammonium citrate. The spotted plate was stored at room temperature until analysis.

AKT MALDI-MS Acquisition & Data Analysis. Mass spectra were acquired on a Bruker Microflex™ LRF benchtop MALDI-TOF-MS. Instrument settings were optimized in the linear mode to maximize signal intensity. Data analysis was performed in Flexanalysis 3.4 using Savitsky-Golay smoothing, baseline subtraction, and automated peak picking. Concatenation of peak intensity measurements from spectra was performed with MS-VIS (mass-spectrum.com) (173). Linear range and precision were evaluated using a calibration curve of synthetic peptides spiked. The calibration curve was generated using a linear regression with a 1/x2 weighting. The performance of the optimized iMALDI-MS assays was confirmed with quality control samples (QCs) prior to analysis of the clinical samples.

Supernatant Analysis. As shown in Figure 3, the AKT-depleted supernatant from this step was retained; a portion was reserved for global proteome analysis by nano-LC-Orbitrap MS, and the remainder was enriched for PTEN and PI3K p110α using anti- PTEN and PI3K p110α anti-peptide antibodies. The PTEN and PI3K p110α antibody-coupled beads were spotted on the MALDI target and quantitated using our previously validated iMALDI method (19). The peptide used for PI3K p110α quantitation (^{503}EAGFSYSHAGLSNR^{516}) did not overlap with the sequences affected by the *PIK3CA* mutations that were detected in this patient group.

Nano-LC-Orbitrap MS analysis, protein identification and quantification

Sample preparation for Nano-LC-Orbitrap MS analysis. A 2-µL aliquot of the AKT-depleted supernatant from each sample digest's immunoenrichment, corresponding to 117.5 ng of total protein digest, was reserved from the iMALDI workflow for label-free quantitation of non-targeted peptides. Samples were prepared for LC-MS using custom StageTips, consisting of a 200 µL pipette tip loaded with Oligo R3 material and C18 disk, for desalting. Tips were activated with 100 % ACN and equilibrated with 0.1 % trifluoroacetic acid (TFA), prior to loading the supernatant samples (with flow-through reloaded 2x), which were washed with 0.1 % TFA and eluted with 70 % ACN, 0.1 % TFA. Samples were then dried under vacuum and resuspended in 6 µL of 0.1% formic acid (batch 1) or 10 µL of 0.1% formic acid (batch 2). Five (5) µL of each sample was injected in Batch 1, resulting in 107 ng of total protein digest injected on-column. Ten (10) µL of each sample was injected in Batch 2, resulting in ~117 ng of total protein digest injected on-column.

Online nano-LC. Online liquid chromatography was performed on an Easy-nLC 1200 coupled to a ThermoFisher Scientific Q-Exactive Plus MS that was operated with a Nanospray Flex ion source (all from Thermo Fisher Scientific, Waltham, MA, USA). The LC system was equipped with an AcclaimPepMap 100 C18 pre-column (Thermo Fisher Scientific, 3 µm particle size, 75 µm inner diameter × 2 cm length) and a nanoscale analytical column (Thermo Fisher Scientific, AcclaimPepMap 100 C18 main column, 2 µm particle size, 75 µm inner diameter x 25 cm length). Chromatography was performed with mobile phase A: 0.1% formic acid and mobile phase B: 84% acetonitrile, 0.1% formic acid. The 78-minute method, optimized for complex samples, uses a 300 nL/minute flow rate at 20 ºC and incorporates a 50-minute gradient (3 to 17% B for 30 minutes, 17 to 40% B for 20 minutes).

Orbitrap-MS data acquisition. Mass spectra were acquired on the Q-Exactive using a data-dependent acquisition (DDA) method, where the 15 most abundant precursor ions (charge states: 2+ to 4+) were selected for MS/MS fragmentation. Full MS scans were acquired over the mass range from m/z 350 to m/z 1500 at 70,000 resolution using automatic gain control (AGC) target value of 1×10^6 and a maximum injection time of 50 ms. MS2 spectra were acquired with an isolation width of m/z 1.2, an AGC target value of 2×10^4, and a maximum injection time of 64 ms, at a resolution of 17,500. Fragmentation was performed using higher energy collisional dissociation (HCD) with a normalized collision energy of 28. Dynamic exclusion was set at 40 seconds.

Data processing. MS raw data were processed using Proteome Discoverer™ 2.4 (PD, Thermo Scientific). Database searches were performed using SequestHT and a human Swissprot database (January 2019; 20,414 target entries), with trypsin as the enzyme and a maximum of 1 missed cleavage. Carbamidomethylation of cysteine (+57.021 Da) was set as a fixed modification and oxidation of methionine (+15.995 Da) as a variable modification. Mass tolerances were set to 10 ppm for precursor ions and 0.02 Da for product ions. Percolator algorithm was used to calculate posterior error probabilities and the data was filtered to a false discovery rate (FDR) of <1% on the peptide and protein levels. Label-free quantitation (LFQ) was performed using the Minora feature-detector node and applying low-abundance resampling imputation which replaces missing values randomly with values from the lower 5% of detected values.

Data normalization, filtering & batch concatenation. Samples were normalized based on the total summed protein intensities to correct for differences in sample loading. For each protein, the obtained abundances were also scaled to reach a fixed total value when summed by feature while maintaining the ratio observed in the samples -- this facilitates comparisons by representing different features on the same scale. Where applicable, scaled abundances of the two technical replicate measurements were averaged. Scaled abundances for proteins quantified in datasets SN1 and SN2 were then combined. Only proteins that were quantified with at least one peptide unique to that protein were included for the quantitative comparison. The scaled, normalized abundances were exported to Microsoft Excel, and further filtered by selecting protein IDs with “high” confidence (i.e., <1% chance of FDR) and at least 2 peptides unique to that protein. Features with >35% missing values across all samples were excluded in order to obtain the set of proteins with complete LFQ data for statistical analysis.

Statistical analysis & bioinformatics

Basic statistical analysis. Descriptive statistics and protein concentration data was analyzed in Microsoft Excel. Group differences were assessed using both the common t-test as well as non-parametric tests to address the possibility of non-normal distributions in the protein concentration data. Boxplots were generated with the BoxPlotR webserver (http://shiny.chemgrid.org/boxplotr/) (174).

Multivariate statistical analysis. Multivariate statistical analysis was performed using the MetaboAnalyst webserver (www.metaboanalyst.ca) (175). Features with >35% missing values across all samples were excluded from statistical analysis. Samples were re-normalized by sum following removal of incomplete variables. "Auto" data scaling, which expresses each variable measurement as the standard deviation from the variable's mean, was used to ensure equal weighting of features. Quality control (QC) analyses were performed to check the integrity of the resulting data MetaboAnalyst generated volcano plots, Principle Component Analysis, Partial Least Squares Discriminant Analysis, Variable Importance in the Projection (VIP) scores, heatmaps, and hierarchical clustering based on the normalized data.

Network & pathway mapping. StringDB was applied for network analysis, to identify clusters of related proteins, and to identify relevant publications that reference similar clusters of proteins (176). Cytoscape was used to visualize the regulation of proteins within the network (177). QIAGEN Ingenuity Pathway Analysis (QIAGEN IPA) software was used to perform pathway mapping of the remaining proteins based on the scaled LFQ data from Proteome Discoverer.

Assay development & marker verification studies (Results Chapter 2)

LC-MRM-MS assay development & validation

Peptide Selection & Synthesis. For each target protein, one or more proteotypic tryptic peptides were selected conforming to standard criteria used by Dr. Borchers' lab (178) . The initial list of candidate peptides (n=107) was refined based on: (i) the availability of previously-synthesized peptides at the Segal Cancer Proteomics Centre, (ii) peptides with published validated assays listed in the CPTAC portal that did not require enrichment or depletion steps (168), or (iii) peptides with a large number of previous observations or a high predicted suitability score in SRMAtlas (179), either of which would support the feasibility of direct

detection in our workflow. A final list of 58 peptides representing 53 proteins was chosen for assay development. Selected peptides not already available through the Segal Cancer Proteomic Centre were synthesized and purified by a commercial supplier (SynPeptide Co Ltd, Shanghai, China). Solubilized peptides were analyzed using amino acid analysis (AAA) and capillary zone electrophoresis (CZE) to confirm their concentrations and purity respectively.

Optimization. Unlabelled "NAT" peptides matching the endogenous were optimized (in batches not exceeding 50 analytes) on the Agilent 6495B triple quadrupole MS using a standard UPLC method optimized for highly-multiplexed MRM assays (more details in the sample analysis section below). Retention times were determined to create a scheduled MRM-MS method. The parameters optimized for each peptide included determining retention time, selecting the single highest-signal parent ion charge state, selecting the 5 highest-signal transitions, and identifying the optimal collision energy for each selected transition to improve signal as shown in Figure 4. Skyline software is used to facilitate the MRM assay development.

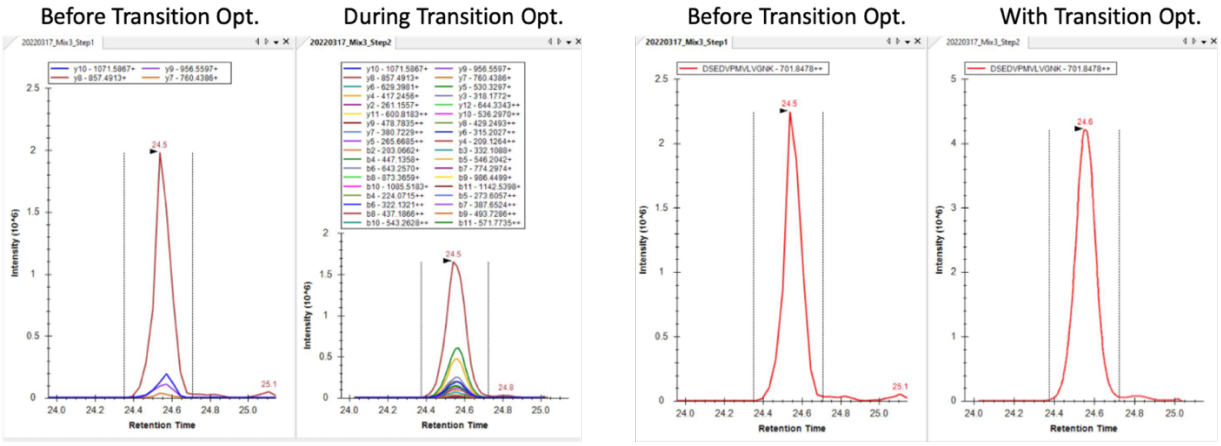

Figure 4. Transition optimization for peptide DSEDVPMVLVGNK, visualized with Skyline.

Assay performance characterization. The optimized assays were applied to 6 different breast and colorectal cancer cell lysates available in the lab to confirm detectability of the endogenous analyte prior to purchasing stable isotope-labeled peptides to develop quantitative assays. Detectable optimized peptides were further developed into validated assays through the experiments described in the CPTAC Assay Characterization Guidelines, according to a 'fit-for-purpose' approach (149,167).

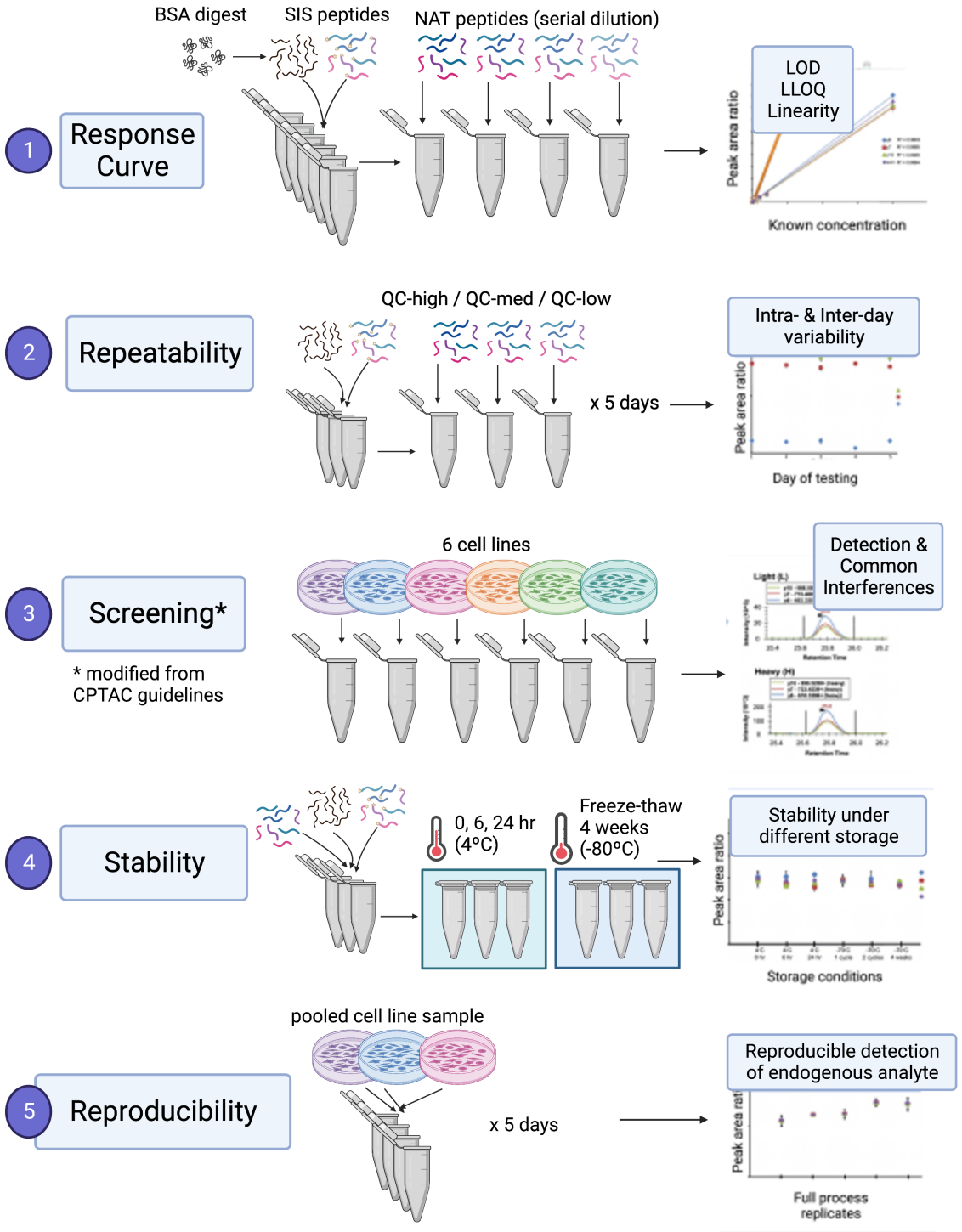

Figure 5. Overview of MRM-MS assay characterization experiments.

CPTAC validation experiments. An overview of all validation experiments is shown in Figure 5. We first determined the response curve and linearity ("CPTAC Exp. 1") by analyzing a calibration curve of synthetic peptide standards spiked into digested BSA as background matrix with internal standards for quantitation. To verify repeatability of the assays (Exp. 2), 4 quality control (QC) samples were prepared using synthetic peptide in digested matrix, at concentrations distinct from the standard curve, spanning the linear range (low:1x-15x, med low:5-300x, med: 10-600x, high: 20-1200x LLOQ). Three replicates of each QC were processed and analyzed on each of 5 different days. Stability (Exp. 4) was confirmed by assessing peak variability at timepoints under varying storage conditions (4ºC, -80ºC), as well as after freeze-thaw cycles. Reproducible quantitation of the endogenous analytes (Exp. 5) was verified by performing the complete workflow, including digestion, on 5 aliquots of a pooled cell line sample analyzed on different days. The selectivity experiment (Exp. 3) proposed by CPTAC to demonstrate parallelism in a set of biological samples (e.g., 6 tissue or cell lines of different types) was not performed due to limited availability of suitable test material at the time of assay validation. However, a basic screening for interferences was performed by comparing transition ratios in each of the cell lines tested.

Public data deposition. Assay characterization data from these experiments was publicly deposited in the CPTAC Assay Portal (https://proteomics.cancer.gov/assay-portal).

Cell lines & tissue culture

Materials & cell lines. Six (6) well-characterized HR+ positive breast cancer cell lines were selected for analysis, as shown in Table 2. Cell lines were obtained from the American Type Culture Collection (ATCC, via Cedarlane), the German Collection of Microorganisms and Cell Cultures GmbH (DSMZ), and as a gift from Dr. Mark Basik's lab at the Segal Cancer Proteomics Centre. Information about mutational status and expression of AKT1, AKT2, AKT3, PIK3CA, PIK3CB, PTEN, ERBB2 was obtained exclusively from the Cosmic Cell Lines Project (v97, released 29 Nov 2022, https://cancer.sanger.ac.uk/cell_lines) (40). Capivasertib (MedChemExpress, South Brunswick, USA) and ISRIB (Selleck Chemicals LLC, Houston, US) were dissolved in DMSO at concentrations of 30 mM and 10 mM respectively. Drugs were stored at -20ºC for a maximum of 3 months.

Table 2. Hormone receptor-positive breast cancer cell lines & culture conditions

Cell line (COSMIC Acc.#) Source	**Medium**	**Mutations & Gene Expression Changes** (OE = overexpressing) (40)				**IHC Expression** (180,181)			**Capivasertib sensitivity** (182)	**Doubling time** (183)
		ERBB2	***PIK3CA***	***AKT***	***PTEN***	**ER**	**PR**	**HER2**		
EFM-19 (COSS906851) DSMZ: ACC231	RPMI-1640 + 15% h.i. FBS + 1% P/S	OE (2.15 z-score)	mutation (H1047L)	wt	wt	+	+	-	GI_{50}: >8 µM (resistant)	50-80 hours
MCF-7 (COSS905946) Basik lab	RPMI-1640 +10% h.i. FBS + 1% P/S	wt	mutation (E545K)	wt	wt	++	+/-	-	GI_{50}: 1.3-1.6 µM (sensitive)	25-80 hours
HCC-1428 (COSS1290905) ATCC: CRL-2327	RPMI-1640 +10% h.i. FBS + 1% P/S	wt	wt	AKT1 OE (2.56 z-score)	wt	++	-	+/-	GI_{50}: 0.15 µM (sensitive)	88 hours
ZR-75-30 (COSS909907) Basik lab	RPMI-1640 +10% h.i. FBS + 1% P/S	OE (3.05 z-score)	wt	AKT1 OE (2.34 z-score)	wt	+/-	-	+++	GI_{50}: >8 µM (resistant)	80 hours
CAMA-1 (COSS946382) ATCC: HTB-21	EMEM + 10% h.i. FBS + 1% P/S	OE (2.17 z-score)	wt	AKT2 OE (2.83 z-score)	mutation (D92H +fs del.)	+	+/-	+	GI_{50}: 0.04-1 µM (sensitive)	73 hours
ZR-75-1 (not listed) Basik lab	RPMI-1640 +10% h.i. FBS + 1% P/S	wt	wt	wt	Mutation (L108R)	+/-	+/-	+/-	GI_{50}: 0.1-1.5 µM (sensitive)	54-80 hours

Cell culture maintenance. Cryopreserved cell lines were tested for mycoplasma contamination and/or treated prophylactically after long-term storage with 14-day incubation with 0.1% ciprofloxacin (Bioworld ciprofloxacin hydrochloride, 10 mg/mL, 1000X) prior to expansion (184). All cell lines were cultured in the manufacturer-recommended medium with 10% or 15% fetal bovine serum (FBS), with 1% penicillin and streptomycin (10,000 U/mL, ThermoFisher Scientific). Each cell line was maintained at 37°C in a 5% CO2 humidified incubator. The medium was exchanged every 2-5 days, as required. Cell cultures were maintained at less than 85% confluency and passaged as needed using 0.25 % trypsin + EDTA to liberate adherent cells, for no more than 8 passages. Cryopreserved samples were stored after expansion to enable subsequent rounds of analysis.

Baseline sampling for proteomics. Cell line samples were collected prior to capivasertib exposure, in at least triplicate, with replicates for a given cell line taken from at least 2 different passages. For collection, adhered cells were gently lysed using 0.25 % trypsin + EDTA, washed with sterile PBS, then pelleted and immediately stored at -80ºC until extraction.

Single-drug cytotoxicity assays. A standard cell viability assay was used to assess cell lines' sensitivity to capivasertib. Cells were seeded onto 96-well plates at least 24 hours prior to treatment. The number of cells seeded for cytotoxicity assays (~2000-10,000 cells per well) was optimized based on the observed doubling time of each individual cell line to maximize signal without reaching confluency. Drugs were prepared at varying dilutions in DMSO. On Day 0, medium was exchanged for medium with capivasertib (AZD5363) at a final concentration of 0 to 30 uM drug (0.3% DMSO).

After 72 hours of incubation with treatment, medium was replaced with 100 uL alamarBlue™ (Invitrogen) and incubated for ~30 minutes. AlamarBlue® reagent binds to redox indicators to provide a measure of proliferative activity and viability. An EnSpire® Multimode Plate Reader (PerkinElmer) was used to measure fluorescence with an excitation wavelength at 530–560 nm and an emission wavelength at 590 nm in the interior 60 wells of the plate. Single-drug cytotoxicity data was analyzed in Excel. Net growth inhibition for each drug level was calculated as: (mean DMSO reading - mean experimental reading)/(mean DMSO reading). Inhibitory concentrations (IC_{50} and IC_{15}) were determined on the basis of at least 3 fully independent replicates.

Combination cytotoxicity assays. As shown in Figure 6, a concentration matrix was used to testing combination treatment for synergistic effects. The matrix was replicated on each of 5 plates. After 72 hours of incubation with treatment, medium was replaced with 100 uL alamarBlue™ (Invitrogen) and incubated for ~30 minutes, as described above. An EnSpire® Multimode Plate Reader (PerkinElmer) was used to measure fluorescence with an excitation wavelength at 530–560 nm and an emission wavelength at 590 nm in the interior 60 wells of the plate. Multi-drug data was analyzed using SynergyFinder to compute synergy scores (185).

	1	2	3	4	5	6	7	8	9	10	11	12
A												
B	AKTi (nM)	9000	9000	9000	9000	9000	9000	9000	9000	9000	9000	
	EIF2i (nM)	9000	3000	1000	333	111	37	12	4.1	1.4	0	
C	AKTi (nM)	1500	1500	1500	1500	1500	1500	1500	1500	1500	1500	
	EIF2i (nM)	9000	3000	1000	333	111	37	12	4.1	1.4	0	
D	AKTi (nM)	250	250	250	250	250	250	250	250	250	250	
	EIF2i (nM)	9000	3000	1000	333	111	37	12	4.1	1.4	0	
E	AKTi (nM)	42	42	42	42	42	42	42	42	42	42	
	EIF2i (nM)	9000	3000	1000	333	111	37	12	4.1	1.4	0	
F	AKTi (nM)	6.9	6.9	6.9	6.9	6.9	6.9	6.9	6.9	6.9	6.9	
	EIF2i (nM)	9000	3000	1000	333	111	37	12	4.1	1.4	0	
G	AKTi (nM)	0	0	0	0	0	0	0	0	0	0	
	EIF2i (nM)	9000	3000	1000	333	111	37	12	4.1	1.4	0	
H												

Figure 6. Concentration matrix of 96-well plates used in cytotoxicity assays to test for synergistic effects of combination treatments

Time-course studies. Cell culture plates were seeded a minimum of 24 hours prior to treatment. The number of cells seeded for time-course studies (~1.0 to 2.5 M cells per 10 cm plate) was adjusted to maximize yield without reaching confluency based on the observed doubling time of each cell line. Capivasertib-containing medium was prepared for each cell line at the dose corresponding to its IC_{15} as established in the cytotoxicity assay. As shown in Figure 7, plates were incubated with the capivasertib-containing medium for 2, 4, 8, 24, 48, and where feasible, 72 hrs. Time-matched vehicle controls consisted of 0.1-0.3% DMSO, concentration-matched to the treated samples. Double-blank control plates were also included, consisting of medium alone, plated and incubated in parallel for 72 hours. Timecourse experiments were

performed for each cell line in triplicate. To account for inter-passage variability, data was analyzed as the fold-change in concentration from the double-blank plate cultured in parallel.

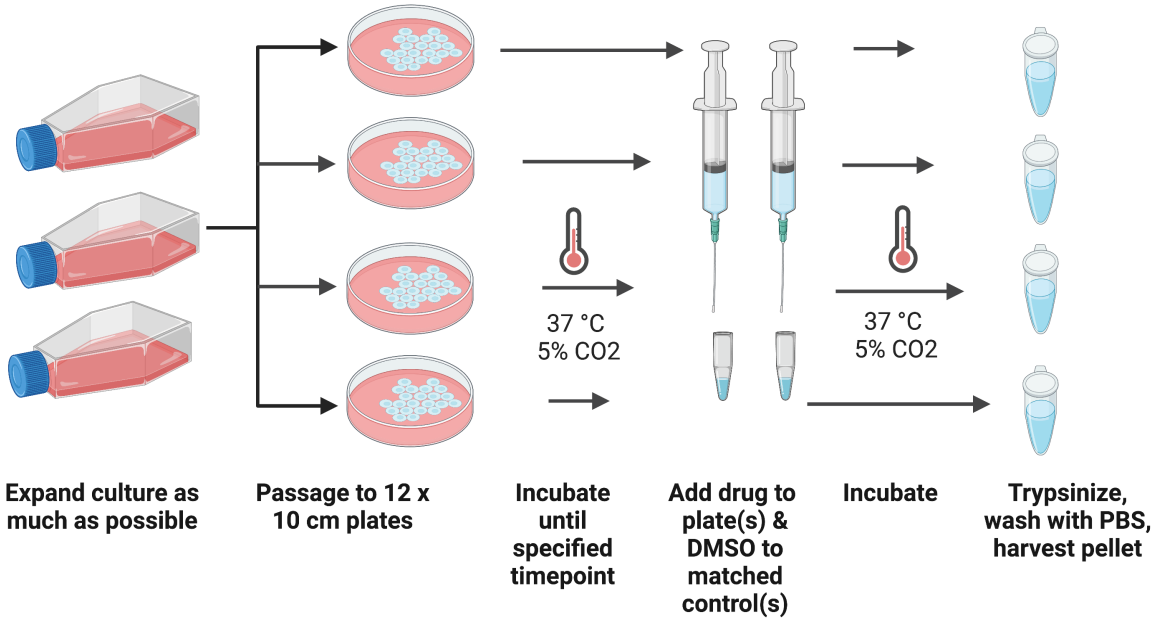

Figure 7. Experimental design of capivasertib timecourse experiments in cell lines

MRM-MS analysis of cell line samples

Protein extraction & total protein quantitation. Solutions were prepared using LC-MS grade water and solvents, and analytical grade reagents. Cell line samples were lysed, extracted, denatured, and reduced using high-temperature incubation in sample extraction buffer (2% w:v sodium deoxycholate in 50 mM Tris-HCl, pH 8.1, 10 mM TCEP, 20 minutes, 99°C), followed by sonication (20% amplitude; 30 sec; pulse, 1s/1s) and an additional incubation (2 hours, 80°C). The concentration of total protein in each sample was then quantified using a Reducing Agent Compatible Pierce bicinchoninic acid (RAC-BCA) protein assay kit (Thermo Scientific, Cat #23250) with a ThermoFisher MultiSkan Go spectrophotometer.

Tryptic digestion of cell line samples for multiplexed MRM-MS. Aliquots of 80 µg of denatured, reduced total protein were diluted to 0.4 µg/µL total protein for in-solution digestion in 25 mM ammonium bicarbonate (AmBic, pH 8). Each sample was then alkylated with 25 µL

90 mM iodoacetamide (IAA, in 25 mM AmBic) for 30 minutes while protected from light. Any remaining IAA was quenched with 20 µL 100 mM dithiothreitol (DTT, in 25 mM AmBic). Samples were diluted with 175 µL of 25 mM AmBic prior to digestion to ensure deoxycholate was not present at >1% w:v. Digestion was performed with trypsin (Worthington, TPCK Treated, 95% purity) dissolved in H2O, added at a substrate-to-enzyme ratio of 20:1, and allowed to incubate for 17±1 hours at 37°C. The digest was then chilled on ice, spiked with an equimolar mixture of 54 SIS peptides (400 fmol on-column), and quenched with acidification using formic acid at a final concentration of 1%.

Solid Phase Extraction. Samples were centrifuged to pellet precipitated deoxycholate. The supernatant was collected for Solid Phase Extraction (Oasis SPE HLB 1cc cartridges, 10 mg sorbent), which was performed according to manufacturer directions on a vacuum manifold, as follows: (i) priming with 2 x 600 µL methanol rinse, (ii) equilibration with 2 x 600 µL H2O, 0.1% FA, (iii) sample loading in 600 µL H2O, 0.1% FA, (iv) washing with 3 x 600 µL H2O, 0.1% FA, (v) elution with 400 µL 55% ACN, 0.1% FA. Eluates were then dried under vacuum (LabConco CentriVap, 4°C) and reconstituted in 40 µL H2O, 0.1% FA.

Calibration curve & quality controls. The calibration curve was prepared by spiking an equimolar mix of unlabeled standard peptides in H2O, 0.1% FA at known quantities (0, 0.41, 1.02, 2.56, 6.40, 16.0, 40.0, 100, 250, 1000 fmol on-column) into previously digested BSA (0.01 ug on-column) spiked with the SIS peptide mixture (400 fmol on-column). A previously quantified pool cell lysate sample was digested and re-quantified in parallel with each batch as a quality control.

Liquid chromatography. Samples and calibration standards were held at 4ºC in an autosampler until analysis via 10 µL injections (20 µg total protein digest on-column) on an Agilent 1290 Infinity liquid chromatography system fitted with a Zorbax Eclipse plus C18 column (RRHD, 2.1x15mm, 1.8um) at 50ºC with a flow rate of 0.4mL/min. Elution was performed over a 48-minute method including a 46-minute gradient consisting of 2% to 7% B at 2 min, to 27% B at 44 min, to 45% B at 45 min, to 80% B at 45.5 min, followed by a wash at 80% B for 2 min, and then returning to 2% B at 48 min for a 2-minute equilibration (mobile phase A: H2O, 0.1% FA, mobile phase B: ACN, 0.1% FA).

Agilent 6495-QQQ-MS data acquisition. MRM-MS analyses were performed on an in-line Agilent 6495B triple quadrupole mass spectrometer (Agilent Technologies, Santa Clara, CA).

Mass spectra were acquired in positive ion mode (ESI capillary ion spray voltage, 3500 V; source gas temperature, 150°C; sheath gas temperature, 250°C; sheath gas flow, 11 L/min). The scheduled MRM method used a cycle time of 1100 ms and a 240 sec detection window. The monitored MRM-MS transitions (5 per peptide, 1 peptide per protein), together with their optimized collision energies are provided in the Appendix 2.

Data & statistical analysis. Data from the LC-MRM-MS assays were processed in Skyline-daily software (http://skyline.ms, Ver 4.1, MacCoss Lab, University of Washington, USA) (186), which was used for peak integration, linear range determination, and quantitation against the calibration curves to yield reproducible concentration data. Multivariate statistical analysis was performed using the MetaboAnalyst webserver (www.metaboanalyst.ca) (175). Values below the LLOQ were imputed as 1/5 of the minimum value. "Auto" data scaling, which expresses each variable measurement as the standard deviation from the variable's mean, was used to ensure equal weighting of features. MetaboAnalyst generated volcano plots, Principle Component Analysis (PCA), Partial Least Squares Discriminant Analysis (PLS-DA), Variable Importance in the Projection (VIP) scores, heatmaps, and hierarchical clustering based on the normalized data.

FFPE tumour samples from patients screened for the trial at the JGH

FFPE samples. Previously-stored solid tumour blocks (n=22) were obtained with consent from patients under Research Ethics Board approval at the Jewish General Hospital (Project #2018-663, 17-004). This set was drawn from patients of the Segal Cancer Centre at the JGH, whose tumours underwent previous genetic screening in relation to the Phase II clinical trial of capivasertib. FFPE samples were selected according to the following criteria: minimum 50% tumour content, tissue volume ≥75mm^3, screened for mutations in *AKT, PI3K* and/or *PTEN* (by either real-time PCR or NGS approaches), and (for breast tumours) accompanied by a pathology report indicating hormone-receptor status. Each FFPE block was sampled as 2 x 5 µm slices from the entire block. Adjacent slices were slide-mounted and stained with hematoxylin and eosin (H&E) to enable identification of the tumour area and guide the positioning of cores. For a subset of 8 HR+ breast cancer samples, each FFPE tissue block was also sampled as ≥2 x 1 mm core punches from the tumour area and ≥1 punch from the tumour-adjacent stroma. Intra-tumour variability and inter-tumour variability for different proteins will be compared.

Patient cohort & clinical annotation. This cohort included patients with mutation-positive as well as mutation-negative tumours. A database was developed to capture key demographic and

clinical information relevant for these patients. Important variables include: sex, age, cancer type, mutations identified, hormone receptor status (breast cancers), site of screened tissue (primary tumour/metastasis), treatments received and treatment response.

PRM-MS analysis of patient FFPE tumour samples

Method adaptation to EvoSep-Q-Exactive. The developed assays were adapted for use on an EvoSep One LC system coupled to a Q-Exactive Orbitrap-MS. The EvoSep 30-SPD (30 samples per day) standard method was selected for chromatography, offering a 44-minute gradient for better separation and coverage of proteins in highly complex samples. Retention times were determined for this chromatography method by injecting synthetic peptide standards in buffer and using a "top 15" data-dependent acquisition (DDA) method with inclusion list to selectively sample and fragment the most abundant ions from the full-scan data. The method was repeated with as needed until all peptides were scheduled. Collision energies were optimized per peptide (see Appendix 2).

Protein extraction & total protein quantitation. Cores and unmounted slices (n=42) of FFPE tumour samples were extracted using a non-hazardous hot water-based deparaffinization protocol recently developed in Borchers lab (187). Samples were then homogenized and lysed by high-temperature incubation in sample extraction buffer (2% sodium deoxycholate in 50 mMol Tris-HCl, pH 8, 20 minutes, 99°C) to break formalin crosslinks, manual homogenization with disposable pestles, and an additional incubation step (2 hours, 80°C). Following centrifugation (21k x g, 4ºC, 15 minutes), the protein-containing supernatant was collected. Samples were diluted 1:1 with H_2O prior to total protein quantitation using an RAC-BCA protein assay kit as described above.

Protein Aggregate Capture digestion of extracted FFPE samples. Extracted samples were incubated with IAA (final concentration of 30 mM. 30 min, RT). Aliquots corresponding to 5 µg of denatured, reduced, alkylated total protein were then digested in an on-bead Protein Aggregation Capture (PAC) protocol suitable for robust and sensitive preparation of low-yield samples, as previously published (188). Briefly, MagReSyn® Hydroxyl magnetic beads (ReSyn Bioscience) were aliquoted at a 1:20 protein:bead ratio, and equilibrated before loading the 5 µg protein sample in 70% ACN. After 10 minutes of incubation at room temperature, the precipitated aggregated proteins immobilized to the beads were washed successively with 95% ACN (x2) and 70% ACN. Sequencing grade Trypsin (Promega, Madison, WI, USA) was then

diluted in 50 mM ammonium bicarbonate (AmBic, pH 8) at a ratio of 1:20 trypsin:protein for on-bead digestion overnight at 37ºC. The digest was then spiked with the SIS peptide mix as and acidified to 2% TFA. The supernatant containing unbound peptides was transferred to a new tube and pooled with a second wash of the beads with 1%TFA.

Calibration curve. The calibration curve was prepared by preparing a dilution series from the equimolar mix of unlabeled standard peptides in H2O, 1% FA at known quantities corresponding to 0, 0.07, 0.16, 0.41, 1.02, 2.56, 6.40, 16.0, 40.0, 200 fmol on-column) and spiking the samples into previously digested BSA (150 fmol on-column) spiked with the SIS peptide mixture (50 fmol on-column). Calibrants were also loaded onto EvoTips for injection.

Liquid chromatography. From each sample, aliquots of 1 µg digest were loaded, washed, and preserved on conditioned, equilibrated Evotips (EvoSep, Odense, Denmark) according to manufacturer directions. Evotips were stored at 4ºC until transferred to the EvoSep platform for injection. The system was fitted with an EvoSep EV1137 Performance Column (ReproSil-Pur C18, 1.5 µm beads, 15 cm X 150 µm, 1.5 µm) enclosed by an envelope-style column heater (40ºC). Separation was achieved via the EvoSep One 30 SPD standard LC method (mobile phase A: H2O, 0.1% FA, mobile phase B: ACN, 0.1% FA).

Data acquisition on the Q-Exactive Orbitrap MS. MRM-MS analyses were performed on a Q-Exactive Hybrid Quadrupole-Orbitrap-MS (Thermo Fisher Scientific). Full scan MS were acquired in positive ion mode (over the mass range from m/z 240 to m/z 1000 at 17,500 resolution using automatic gain control (AGC) target value of 1×10^6 and a maximum injection time of 50 ms. For PRM, MS2 spectra were acquired with an isolation width of 1.0 m/z, an AGC target value of 1×10^6, and a maximum injection time of 110 ms, at a resolution of 35,000. Fragmentation of targets in the inclusion list was performed using HCD with the normalized collision energy specified for each target.

Data & statistical analysis. Spectra were processed in Skyline software (http://skyline.ms, version 22.2, MacCoss Lab, University of Washington, USA) (186), which was used for peak integration, linear range determination, and quantitation of endogenous concentration values based on the calibration curves. Statistical analysis was performed using Microsoft Excel and BoxPlotR (174).

Geneva cocktail study (Results Chapter 3)

Samples & clinical variables.

Sample collection. Ethics, participant recruitment, drug administration, sample collection. The study protocol was approved by the Ethics board at the Jewish General Hospital in Montreal, Canada (Study number: CODIM-MBM-16-235). Ten (10) free-living adult participants with no acute illness were recruited to the study. Subjects with known allergies or intolerance to either caffeine or midazolam, with active cancer or on cancer treatment, suffering an acute illness in the prior 2 weeks or who started a new prescription medication in the prior 6 weeks were excluded. Participants were instructed to fast overnight for a minimum of 8 hours prior to testing. Upon arrival at the test centre, a single venous blood sample was taken from the arm at "baseline" (t=0), immediately prior to ingestion of a fixed oral dose of caffeine (100 mg) and midazolam (2 mg) to act as probes for CYP1A2 and CYP3A4 respectively. A second venous blood sample was taken 60 minutes following caffeine and midazolam dosing (t=1 hr). Collected blood samples were immediately centrifuged to obtain serum, which was frozen in cryovials (Corning Incorporated, Corning, NY) and stored at -80ºC until analysis.

Clinical data, dietary questionnaire & scoring. Participants' height and weight were measured during the visit. Biological sex and age were also recorded. Participants were further asked to complete a dietary and medical history questionnaire, as shown in Appendix 3 (189). Items in the dietary questionnaire were identified as inducers or inhibitors of CYP3A4 or CYP1A2 based on reported effects (189). Medications identified by participants were also assessed for likely inducing or inhibiting effects (189). Each predicted inducer (↑) or inhibitor (↓) of a given enzyme was assigned a "strength" (STR, low = 1, high = 2) based on the reported effects on enzyme activity. To create a weighted inducing or inhibiting score for each inventory item, the strength of a given effect was multiplied by a score assigned for "frequency of exposure" (FoE, low = 0, medium = 1, high=2, see Table 3).

Table 3. Frequency scoring of dietary, herbal and medical substance use

Frequency Reported on Questionnaire	Associated Exposure level	Score Assigned
"never or rarely" *"1-3 times per month"*	Low	0
"1-3 times per week" *"4-6 times per week"*	Medium	1
"1-2 times per day" *"3 or more times per day"*	High	2

As shown in Equation 1, for each CYP enzyme, the sum of the weighted scores for all inhibiting inventory items was deducted from the sum of the weighted scores for all inducing inventory items to generate an aggregate score reflecting total predicted activity. For example, for CYP3A4, if the subject consumed one strongly inducing drug (score 2) daily (score 2) and one mildly inducing food item (score 1) 4 times a week (score 1) as well as daily consumption of a mildly inhibiting food (score 1), their net Diet and Medication Questionnaire score was: $DiMQu_{3A4} = ((2x2)+(1x1)) – (2x1) = 3$.

Equation 1. Example calculation of DiMQu score for a given patient for CYP3A4

$$\textbf{Item X's weighted inducing score for CYP3A4}(WIS_{3A4\uparrow x}) = \text{Strength of Effect } (STR_{3A4\uparrow x}) \text{ x Patient-Reported Frequency of Exposure } (FoE_{\uparrow x})$$

$$\textbf{Item Y's weighted inhibiting score for CYP3A4}(WIS_{3A4\downarrow y}) = \text{Strength of Effect } (STR_{3A4\downarrow y}) \text{ x Reported Frequency of Exposure } (FoE_{\downarrow y})$$

$$\textbf{CYP3A4 total inducing score } (\uparrow TIS_{3A4}) = \sum(WIS_{3A4\uparrow a} + WIS_{3A4\uparrow b} \dots + WIS_{3A4\uparrow z})$$

$$\textbf{CYP3A4 total inhibiting score } (\downarrow TIS_{3A4}) = \sum(WIS_{3A4\downarrow a} + WIS_{3A4\downarrow b} \dots + WIS_{3A4\downarrow z})$$

$$\textbf{Patient} - \textbf{specific } DiMQu_{3A4} \textbf{ score} = \uparrow TIS_{3A4} - \downarrow TIS_{3A4}$$

MRM assays for selected Geneva cocktail drugs & drug metabolites

LC-MS/MS phenotyping. Phenotyping was performed as previously described using liquid chromatography tandem mass spectrometry (LC-MS/MS) to quantify caffeine and paraxanthine as markers of CYP3A4 and midazolam and OH-midazolam as metabolic markers of CYP1A2 activity (190). Briefly, we obtained high-purity commercially available standards for all 4 analytes [Midazolam, 1-OH-Midazolam, Caffeine, Paraxanthine] together with their corresponding deuterium-labeled analogues for use as internal standards [Midazolam-D4 maleate, α-Hydroxymidazolam-D4, Caffeine-(trimethyl-d9) and 1,7-Dimethylxanthine-(dimethyl-d6)] (Sigma Aldrich, St. Louis, MO). Standards were dissolved in 60% methanol and added to pooled charcoal-stripped human serum from healthy donors (BioIVT, Westbury, NY) to establish response curves to enable quantitation from participant serum.

Sample preparation. Participant serum samples were prepared by thawing on ice. Internal standards of a known concentration were added to 50 µL aliquots of each sample, following which the samples were pre-treated with 500 units of β-glucuronidase (Sigma, Cat# G7017) for 16-hr incubation at 37°C to ensure full recovery of the glucuronidated metabolic intermediate of OH-midazolam, as required for a more accurate metabolic ratio (191)**.** Proteins were then precipitated from the sample with 150 µL methanol containing stable isotope labeled internal standards (SIS) and centrifugation. Supernatants were diluted 1:1 in LC-MS grade H2O with 0.1% formic acid. Samples were then analyzed via 2 µL injections (for midazolam/OH-midazolam) or 18 µL injections (caffeine/paraxanthine) on an Agilent 1290 Infinity liquid chromatography system fitted with a Zorbax Eclipse plus column (RRHD C18, 2.1x15mm, 1.8um) at 50ºC with a flow rate of 0.6mL/min. The LC system was coupled in line to an Agilent 6495B triple quadrupole mass spectrometer (Agilent Technologies, Santa Clara, CA). Gradient-elution was performed over a 5-minute gradient from 2% - 100 % acetonitrile (Mobile phase A: H2O, 0.1% FA, mobile phase B: ACN, 0.1% FA). MS settings and MRM transitions are shown in Appendix 4. Blanks, double-blanks, and QC samples were prepared and injected in parallel with the patient samples.

Data & statistical analysis. Data from the LC-MRM-MS assays were processed in Skyline software (http://skyline.ms) (192). Peak integration and quantitation against the calibration curves was applied by Skyline to yield absolute concentration data for OH-midazolam, midazolam, paraxanthine and caffeine in ng/mL. The metabolic ratio (MR) for each pair of metabolites was determined by dividing the measured concentration of the drug metabolite (OH-

midazolam or paraxanthine) by the concentration of the associated drug (midazolam or caffeine respectively) for each sample. Descriptive statistics were applied to patient characteristics. R statistical programming language was used to create scatterplots of $DiMQu_{3A4}$ scores versus Hydroxymidazolam:Midazolam metabolic ratios (MRs) and $DiMQu_{1A2}$ scores versus Paraxanthine:Caffeine MRs. Correlations between the variables were assessed using Spearman's rank-order correlation. Correlations were reported as r_s values with a two-tailed *p*-value for determining statistical significance.

Dried blood spot analysis. Dried blood spot (DBS) analysis was performed to assess the feasibility of applying the protocol with this sample type. Both Whatman 903 and HemaSpot HF devices were tested to compare the assay's performance on these two substrates. Whatman 903 is one of the most common DBS cards currently in use and is typically sampled with a standardized punch. The HemaSpot HF device is designed to offer simplified sampling of pre-cut 'petals', reduce hematocrit effects on sample distribution, and to irreversibly seal after collection for secure shipping and storage.

Test samples were prepared from pooled participant serum samples diluted 1:1 with pooled red blood cells from anonymized specimens, which was volumetrically spotted (50 µL per spot) onto Whatman™ 903 Proteinsaver cards (Cytiva Life Sciences, Marlborough, MA) or Hemaspot HF collection devices (SpotOn Sciences, Austin, TX). For extraction, entire DBS spots were excised from Whatman 903 cards, or 2 petals were used for Hemaspot HF.

For deconjugation of hydroxymidazolam glucuronide, two workflows were tested using either: (i) on-spot deconjugation or (ii) an initial aqueous extraction followed by β-glucuronidase treatment. Briefly, for on-spot deconjugation, 500 units of β-glucuronidase in water (50 µL) was added directly to the DBS specimens and incubated for 16 hours at 37°C. Metabolites were then extracted from the DBS by addition of 200 µL of 80% methanol containing SIS and shaking with an Eppendorf Thermomixer at 2000 rpm at 37°C for 10 minutes. Samples were briefly centrifuged (2000 x g for 5 minutes), following which the supernatant was processed using the protocol described for serum samples above. For sequential extraction and deconjugation, DBS specimens were first extracted with 500 µL of water for 10 minutes using an Eppendorf Thermomixer (2000 rpm, 37°C), vacuum concentrated, and rehydrated in 50 µL of water prior to protein precipitation and processing as described above. The same MRM-MS assay was used to quantify analytes after extraction from DBS samples.

Results Chapter 1:
Analysis of PIK3CA-altered tumours reveals a proteomic profile associated with capivasertib response in Phase II clinical trial patients

Chapter Summary

Capivasertib is a potent, selective inhibitor of AKT, currently in Phase III development as a combination therapy for breast and prostate cancers. To investigate whether the proteomic profile can be used to predict treatment response to capivasertib, we analyzed baseline samples from 16 PIK3CA-mutated tumours of patients in a Phase I trial. We used two rounds of immuno-MALDI-MS to determine the concentrations of AKT1, AKT2, PTEN, and PI3K-p110α, with subsequent global proteomic analysis on the supernatants from the immuno-enrichment steps. Proteomic data were compared between patients classified as belonging to the "clinical benefit (CB)" group (≥12 weeks without progressive disease, n=7) or belonging to the "no clinical benefit (NCB)" group (progressive disease in <12 weeks, n=9) after starting capivasertib treatment as single agent.

The measured concentrations of AKT1 and AKT2 varied among PIK3CA-mutated tumours but did not differ between the CB and NCB groups. Analysis of the global proteome data, however, suggests that tumours in the CB group had lower activity of translational control pathways and associated protein networks prior to treatment with capivasertib as compared to tumours in the NCB group. Direct measurement of selected proteins may offer valuable insights for patient selection for agents targeting the PI3K-AKT-mTOR pathway, even among genetically pre-selected patients.

Context

Pre-clinical characterization of capivasertib (AZD5363)

Capivasertib is a potent and selective inhibitor of AKT with promising preclinical anti-cancer activity

The PI3K/AKT/mTOR signaling pathway has an established role in tumour cell proliferation, is mutated in more than 50% of breast cancers (93), and is the target of many new therapeutic agents (79,80,95). Although direct mutations of AKT are comparatively rare, overexpression and overactivation of AKT are key factors in cancer progression. In response to PI3K pathway activation, phospho-AKT promotes downstream oncogenic functions including cell growth, inhibition of cell death, and regulation of metabolism (89). Capivasertib (AZD5363) competitively interacts with the ATP binding site and inhibits AKT's catalytic activity with high potency and higher selectivity than previously developed compounds, resulting in the arrest of tumour cell growth (193). It has similar activity against all three AKT isoforms (AKT1, AKT2, AKT3) with an IC50 of less than 10 nmol/L in preclinical studies (194). Treatment with capivasertib was found to quickly reduce the level of phosphorylation of AKT's downstream targets. Immunoblots of GSKβ, pS6, PRAS40, and proliferation marker ki67 are frequently used as markers of capivasertib response, including in clinical studies (169,195-197). Despite its higher selectivity than previously-developed compounds, preclinical studies also showed significant inhibitory activity of capivasertib against P70S6K, PKA, ROCK2, MKK1, MSK1, MSK2, PKCγ, PKGα, PKGβ, PRKX, RSK2, and RSK3 (194).

Preclinical studies revealed promising anti-cancer activity for capivasertib, with the highest frequency of response observed in HR+ breast cancer models as compared to other cancer types tested (e.g., colorectal, lung) (194). In ER+ breast cancer cell lines, combining capivasertib with fulvestrant, anastrozole, or tamoxifen yielded results superior to any of the drugs used as monotherapy (198). This effect was even stronger in *PIK3CA*-mutated or PTEN-deficient ER+ cells (198). Similar results were obtained for capivasertib + fulvestrant in ER+ *PIK3CA*-mutated breast cancer xenografts (199). HER2+/*PIK3CA*-mutated breast cancer xenografts were also found to be capivasertib-sensitive and synergistic effects were observed when capivasertib was combined with HER2-targeted therapies (trastuzumab, lapatinib) or taxanes (docetaxel) in this setting (194). Combining capivasertib with other treatments also showed improved activity for

several other solid tumours including prostate cancer, gastric cancer, and non-small cell lung cancer in the pre-clinical setting (200-203).

Despite these promising results, sensitivity to AKT inhibition was not universal and a number of pathways were soon identified that could confer non-response or resistance in cell lines, including increased activation of BRD4/FOXO3a/CDK6 or activation of AKT's upstream receptor tyrosine kinases (RTKs) (199,204).

Existing biomarkers of capivasertib response

Early biomarkers of capivasertib activity were mostly genetics-based, except for SGK1

Biomarkers evaluated to predict capivasertib sensitivity or non-response in the preclinical setting were mostly depended on assessing tumour genetics. For instance, enhanced responses to capivasertib monotherapy were observed for: (i) breast cancer cells with *PIK3CA* or *AKT* mutations (but not MTOR mutations or TSC2 loss) (205); (ii) cell lines and xenografts with PIK3CA mutations, PTEN deficiency, or HER2 amplification (194); and (iii) patients whose *AKT1*-mutated solid tumours also contained either *PIK3CA or MTOR* mutations vs. *AKT1* mutations alone, (112). Mutations of RAS, on the other hand, were associated with poor response to capivasertib (194).

Few non-genetic markers have received much attention, with the exception of SGK1 expression. Serum- and glucocorticoid-regulated kinases (SGKs) are closely-related to AKT; SGKs are members of the same family of serine/threonine kinases, share significant sequence homology, and are similarly activated by mTORC2 in the PI3K pathway (206). Despite the heavy analogies between SGK1 and AKT's regulators, functions, and substrates, further study has revealed that SGK1 is likely responsible for independent oncogenic signalling (206,207). Moreover, capivasertib does not significantly inhibit SGK1 (194).

In the context of the positive feedback loop causing activation of RTKs (upstream of AKT and SGK1) in capivasertib resistance, SGK expression – in particular SGK1 – has proven to be a plausible mechanism of this resistance by activating downstream mTORC1 signalling independent of AKT (182,208). The significance of SGK1 as a predictive marker is uniquely supported by the observation that many breast cancer cell lines express high SGK1 levels, which are strongly correlated to capivasertib resistance (182). Knockdown of SGK1 levels restores

sensitivity (182). Blockade of PDK1 upstream of SGK1 similarly re-sensitizes cells and xenografts to PI3K inhibitors (209).

Clinical context – capivasertib trials & patient selection

Clinical trials using capivasertib as a monotherapy for PI3K-activated tumours

Pharmakokinetic studies found that capivasertib yields dose-dependent increases in plasma concentrations in the range of 80-800 mg. (169). The drug's half life was found to be 7-15 hours (169). It is mainly metabolized by the liver and is minimally excreted in urine (119). Dose-finding studies have proposed a dose of 480 mg, administered orally twice per day (b.i.d.) on an empty stomach, in either capsule or tablet form (197). At this dosage, therapeutic levels were achieved in <5 days of treatment (197,210).

The first Phase I study of capivasertib was conducted in patients with metastatic breast cancer, gynecological cancer, or other solid tumours (169). Eligibility for enrollment required, among other things, the presence of an *AKT1*, *PIK3CA*, or *PTEN* mutation, predicted to activate the PI3K pathway (169). Pharmacokinetics, tolerability, and downstream markers of response were analyzed to yield a non-continuous dosing schedule of 480 mg bid administered in a 7-day cycle of 4 days "on", followed by 3 days "off" (169). Subsequent Phase II expansion cohorts of the study enrolled patients specifically with *PIK3CA*-mutated breast and gynecological tumours (169), or with solid tumours with $AKT1^{E17K}$ mutations (112,196). When evaluated according to RECIST v1.1 criteria, the ORR in these trials was limited to 4% in $PIKCA^{mut}$ and 20 to 28.6% in the $AKT1^{E17K}$ tumours (112,169,196). Patients with multiple concurrent activating mutations of PI3K were found to achieve longer PFS (112).

The safety profile was also assessed. Serious adverse events (AEs, Grade ≥3) were common, most often hyperglycemia (~20-25%), diarrhea (~15-20%), and maculopapular rash (~10-15%) (112,169). Dose reductions due to AEs were required for 23% and 34% for patients with $PIK3CA^{mut}$ and $AKT1^{E17K}$ tumours, respectively (112,169). Overall, capivasertib was well-tolerated and both the rash and diarrhea were typically self-limiting. Hyperglycemia was treated with and responded to standard agents (e.g., metformin). However, up to 23% of patients did permanently discontinue capivasertib in these trials due to AEs (169).

Evolution of clinical trials applying capivasertib in a variety of settings

Phase I/II trial results indicated that capivasertib monotherapy shows promising clinical activity and is sufficiently well-tolerated at the selected doses. An ORR of 4-29% was observed in patients with tumours selected for specific activating PI3K pathway mutations, (169,196,211). This represents a clinically significant response rate in a population of heavily pre-treated patients with advanced solid tumours for whom no standard treatment was is effective. Since then, the number of trials applying capivasertib has multiplied. An overview of these is given in Table 4. Phase III trials are now in progress to evaluate capivasertib for activity when used in combination therapies for prostate cancer (212,213), TNBC (214,215), and HR+ breast cancer (195,216,217), while exploratory investigations continue for a range of other oncology indications. Recent results of a Phase III trial combining capivasertib and fulvestrant in HR+, HER2-, aromatase inhibitor-resistant breast cancer show a significant benefit over fulvestrant alone in patients with and without detectable PI3K pathway alterations(218).

Combination therapy is likely required to optimize efficacy for both agents, particularly in cancers with acquired resistance to hormone or HER2-directed therapies (219). In trials of patients with breast tumours with *AKT1* or other pathway alterations, combining capivasertib with fulvestrant achieved ORRs of 29-47% vs. 20% with fulvestrant alone (211,216,217). In the FAKTION trial, this combination applied in ER+, HER2- tumours of postmenopausal women who had previously progressed on an aromatase inhibitor were striking; fulvestrant + capivasertib achieved a doubling of median progression-free survival -- 10.3 months versus 4.8 months for fulvestrant alone (HR 0.58, $p<0.01$) (216). The ORR was also increased dramatically from 8% (fulvestrant group) to 29% (fulvestrant + capivasertib) (216). Patients with fulvestrant-resistant AKT-mutated tumours have also shown a higher clinical benefit rate than fulvestrant-naïve patients (211). There is also some evidence that combination therapy could improve tolerability in these patients (211).

While few of these trials include PI3K alterations as an eligibility criterion, many continue to analyze associations between capivasertib response and genetic markers. For instance, the plasmaMATCH trial found a 22% confirmed response rate to capivasertib monotherapy in patients with AKT mutations identified from circulating tumour DNA (ctDNA) (220). The PAKT trial found substantially increased median OS (19.1 months vs. 13.5 months, HR 0.70) when capivasertib was added to paclitaxel in TNBC in all comers, but median PFS was greater for patients with PI3K alterations (9.3 months vs. 3.7 months, HR 0.30) (214,221). However, the

Phase II BEECH trial (n=148) did not show a benefit for capivasertib combined with paclitaxel compared with paclitaxel alone in ER+, HER2- breast cancer, even in the subgroup with PIK3CA mutations (195).

Current challenges in optimizing capivasertib use

Despite promising early results leading to many and varied clinical trials of capivasertib, the path ahead is not so straight forward. While acknowledging that capivasertib has mostly been applied in significantly pre-treated patients, higher clinical activity might be expected for a population carefully selected for a targeted agent. Overall response rates to targeted capivasertib treatment have been somewhat disappointing, with the majority of pre-selected patients showing no confirmed response.

This may be in part due to challenges associated with the existing gene-based selection strategy. Recent studies have identified the potential for an uncoupling of AKT activity from *PIK3CA* mutations in some cancers (222,223). This includes the observation that protein levels of typical markers of pathway activity, such as pAKT, pS6, and p4EBP1, were not elevated in Luminal A (ER+) breast cancers with activating *PIK3CA* mutations (n=101) compared to those without (n=124) (224). In preclinical studies, capivasertib also inhibited the growth of cancer cell lines without PI3K pathway alterations (194). Understanding the potential reasons for this disconnect, and validating patient-selection strategies, are ongoing efforts in the therapeutic use of inhibitors of the PI3K pathway (225). Moreover, it is well known that PI3K-activation is present in most cancers, so the genetic strategy may exclude patients who could benefit. All of the genetic screening approaches in use are invariably limited by our ability to identify and characterize all possible mutations that could induce pathway activation. Additional complexity arises in interpreting genetic results in the context of other signals. For instance, preclinical studies suggested that HER2+, *PIK3CA*^{mut} breast cancer cells were selectively addicted to AKT signalling, but in HER2+, *PTEN*^{mut} cells, pathway addiction varied in an EGFR-dependent manner (226).

Table 4. *Clinical trials of capivasertib*

Cancer setting (subtype)	Phase (study size, status)	Treatment(s) tested	Eligibility	Key results	Registration # (Trial name)
Breast cancer (HR+ /HER2-)	III (n=628, recruiting)	palbociclib + fulvestrant +/- capivasertib	HR+/HER2- advanced/metastatic	-	NCT04862663 (CAPItello-292)
	III (n=834, active/closed)	fulvestrant +/- capivasertib	HR+/HER2- advanced/metastatic	↑ mdnPFS (HR 0.6) ↑ mdnOS (HR 0.6) ORR: 24-28%	NCT04305496 (CAPItello-291)
	I/II (n=148, active/closed)	Paclitaxel +/- capivasertib	ER+/HER2- advanced/metastatic	↑ mdnPFS (HR 0.80) (*PIK3CA*^{mut} HR 1.1)	NCT01625286 (BEECH)
	I (n=340, recruiting)	SERD +/- capivasertib (or other agents)	ER+/HER2- advanced/metastatic	-	NCT03616587 (SERENA-1)
	I/II (n=149, active/closed)	Fulvestrant +/- capivasertib	ER+/HER2- advanced/metastatic post-menopausal	↑ mdnPFS (HR 0.58) ↑ mdnOS (HR 0.59) ↑ mdnORR (29% vs.8%)	
Breast cancer (HR+)	II (n=48, complete)	Capivasertib	ER+ invasive	Dose of 480 mg effective in reducing downstream phosphorylation	NCT02077569 (STAKT)
Breast cancer (HER2-low)	I (n=185, recruiting)	Trastuzumab deruxtecan +/- capivasertib (or others)	HER2- / HER2-low advanced/metastatic	-	NCT04556773 (DESTINY Breast 08)
Breast cancer (TNBC)	III (n=924, recruiting)	Paclitaxel +/- capivasertib	advanced/metastatic	-	NCT03997123 (CAPItello-290)
	II (n=140, active/closed)	Paclitaxel +/- capivasertib	advanced/metastatic	↑ mdnPFS (HR 0.74) ↑ mdnOS (HR 0.70)	NCT02423603 (PAKT)

Cancer setting (subtype)	Phase (study size, status)	Treatment(s) tested	Eligibility	Key results	Registration # (Trial name)
Breast cancer (TNBC)	I/II (n=200, recruiting)	Durvalumab + paclitaxel vs. Capivasertib +/- paclitaxel	metastatic	-	NCT03742102 (BEGONIA)
Breast cancer	II (n=1150, recruiting)	A: fulvestrant vs. C: capivasertib vs. D: capivasertib + fulvestrant	advanced *AKT*^{mut} or *PTEN*^{mut} By ctDNA	ORR: 22% (C: *AKT*^{mut}) ORR: 11% (D: *AKT*^{mut}) ORR: 0% (D: *PTEN*^{mut})	NCT03182634 (plasmaMATCH)
Prostate cancer	III (n=790, recruiting)	ADT + docetaxel + steroids +/- capivasertib	metastatic castration-resistant	-	NCT05348577 (CAPItello-280)
	III (n=1000, recruiting)	ADT + abiraterone +/- capivasertib	metastatic *PTEN*-deficient hormone-sensitive	-	NCT04493853 (CAPItello-281)
Solid tumours (TNBC or Gynecologic or Peritoneal cancer)	I/II (n=159, active, closed)	Capivasertib + Olaparib	recurrent	ORR: 19%	NCT02208375
Solid tumours (ER+ Breast cancer or Prostate cancer)	I (n=12, active/closed)	Capivasertib + (fulvestrant or enzalutamide)	advanced *AKT1/2/3*^{mut}	-	NCT03310541
Solid tumours, lymphomas, multiple myeloma	II (n=6452, recruiting)	Targeted therapies matched to genetic mutations	advanced refractory *AKT*^{mut}	-	NCT02465060 (MATCH)

Cancer setting (subtype)	Phase (study size, status)	Treatment(s) tested	Eligibility	Key results	Registration # (Trial name)
Solid tumours	I (n=41, completed)	Capivasertib (dosing schedules)	advanced	ORR: 5% Tolerable safety profile	NCT01353781
	I (n=64, completed)	Capivasertib (dosing schedules) +/- Olaparib	advanced	ORR: 33% CB: 44% mdnDOR: 38.2 mo.	NCT02338622 (ComPAKT)
	I (n=33, completed)	Capivasertib (tablet or capsule)	advanced	Better absorption with tablet, fasted state	NCT01895946 (OAK)
	I (n=285, active/closed)	Capivasertib (dosing schedules)	advanced	ORR: 20% (AKT^{E17K} b.c.) ORR: 4% ($PIK3CA^{mut}$ b.c.) ↑ mdnPFS for 2x PI3K ^{mut}	NCT01226316
	I (n=23, recruiting)	Capivasertib + midazolam	advanced $PI3K^{mut}$, AKT^{mut}, *or* $PTEN^{mut}$	-	NCT04958226
	II (n=64, active/closed)	Olaparib + capivasertib	$PI3K^{mut}$	-	NCT02576444 (OLAPCO)
	I (n=40, recruiting)	Capivasertib + Olaparib + durvalumab	advanced/metastatic	Tolerated well, some excellent responses	NCT03772561 (MEDIPAC)
Cancer	II (n=35, active/closed)	Capivasertib	advanced	mdnPFS: 5.5 mo. mdnOS: 14.5 mo. ORR: 28.6%	NCT04439123 (MATCH, sub Y)

The most recent results of the CAPItello-291 Phase III trial (NCT04305496) demonstrate that treatment with capivasertib + fulvestrant extends PFS in patients with HR+/HER2- breast cancers with inadequate response to endocrine therapy (218,227). Across the overall study population, the addition of capivasertib demonstrated a 40% reduction in the risk of progression or death (218). These effects are statistically significant irrespective of tumour PIK3CA, AKT1 or PTEN status (218). In both groups, there remains a need to elucidate why some of those patients respond and others do not. The complexity of answering this question continues to grow, as do the number and sophistication of the associated trials. As capivasertib moves into earlier stages of treatment and is prescribed to a broader group of patients, enhanced patient selection approaches will be needed to identify both patients who derive even more meaningful benefits, as well as those who do not stand to benefit and should be treated otherwise.

Sub-Hypothesis, Objectives & Approach

Our hypothesis is that proteomics may offer additional insights to inform patient selection for capivasertib. In particular, we theorize that the expression or phosphorylation of AKT -- the key sentinel and effector of pathway activity -- in tumor tissues will predict sensitivity to capivasertib. We further expect that assessment of the wider global proteome will identify additional protein-based markers that are associated with capivasertib sensitivity. The ultimate objective is to use these direct measurements of the proteome (either in concert with or instead of genetic screening) to generate new biological insights and achieve better predictive power than the existing genetic selection strategies.

As shown in Figure 8, this will be accomplished through direct proteomic measurement of proteins potentially associated with capivasertib response in tumours of patients previously treated with the drug. Specifically, we aim to:

1. Implement methods to enable comprehensive characterization of the protein expression profile from volume-limited clinical samples
2. Analyze stored tumour samples from cancer patients who received capivasertib
3. Identify proteins of interest for predicting capivasertib sensitivity

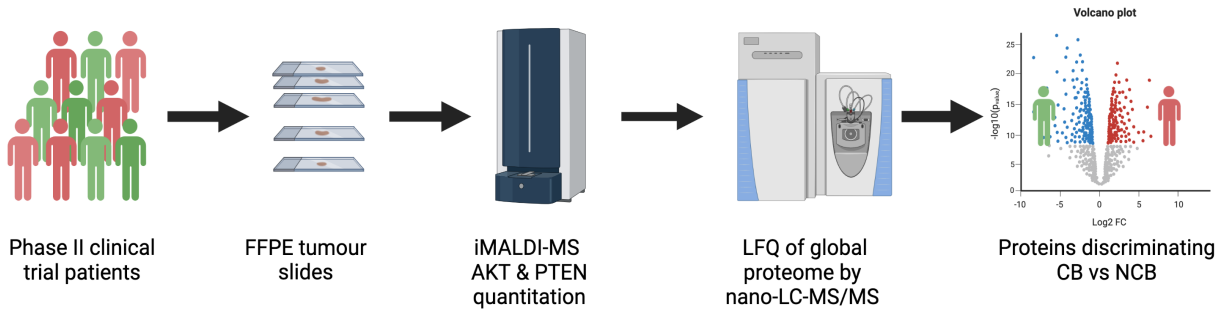

Figure 8. *A simplified schematic of experimental design for Phase I of the study.*

Clinical samples

Direct measurement of the proteome has shown unique potential for identifying and verifying active cancer-driving alterations that closely correspond to tumours' treatment sensitivity or resistance (137,228). To evaluate the utility of proteomics for predicting treatment response to capivasertib, we utilized modern mass spectrometry-based methods to directly analyse the protein content of previously-stored formalin-fixed paraffin-embedded (FFPE) tumour tissues from patients with *PIK3CA*^{mut} with ER+ or HER2+ breast or gynecological cancers, who received capivasertib in a Phase I study of capivasertib's anti-tumour activity (169). Their clinical response to capivasertib is systematically documented.

Targeted protein quantitation by iMALDI-MS

We then used an iMALDI assay to evaluate whether AKT1 or AKT2 protein concentrations in these two groups of patients could offer additional predictive power to the existing genomic strategy. Dr. Borchers' lab at University of Victoria originally developed an immuno-MALDI-MS (iMALDI) assay for precisely quantifying AKT1 and AKT2 proteins using stable isotope-labeled peptides (170). The assay is compatible with fresh frozen or formalin-fixed paraffin-embedded (FFPE) tissue samples and can be performed on as little as 100-200 µg of tissue (~10 µg of total protein per analyte). The iMALDI method involves tryptic digestion of the target protein, followed by addition of a stable isotope-labeled (SIS) peptide as an internal standard. Anti-peptide antibodies conjugated to magnetic beads are then used to affinity capture both the natural peptide and its isotopically-labeled reference standard. Beads are washed, spotted onto a MALDI plate, after which the enriched peptides are eluted from the antibodies. Peptides are then quantified with MALDI mass spectrometric analysis.

This approach to protein quantitation is compatible with automation to enhance reproducibility, throughput, and ease-of-use (171). The method does not require liquid chromatography, which was traditionally considered too complex and insufficiently robust for implementation in clinical labs (229). In fact, the mass spectrometer used in this method (Bruker Biotyper) is commonly found in hospital facilities, as they are FDA-cleared for use in microbial identification. Unlike Western Blots and IHC, the quantitative iMALDI method is not prone to inter-observer variability. The data obtained represents a real concentration value observed in the sample and can be reproduced across operators, labs, and over time. The method is also capable of better isoform discrimination than existing methods that depend exclusively on antibodies for their specificity. Given the distinct biological roles of AKT1 and AKT2, we expect that obtaining discrete data on their expression will strengthen our hypothesis testing.

To enable quantitation of the phosphorylated isoforms of AKT1 and AKT2, the method has been adapted to use a phosphatase-based phosphorylation quantitation (PPQ) approach (172). When the quantitation is performed directly, the measured quantity corresponds only to the non-phosphorylated peptide in the sample, whereas when pre-treated with phosphatase, then total AKT1 and total AKT2 concentrations can be measured. The no-phosphatase-treatment measurement is subtracted from the total AKT measurement to calculate the concentration of the phosphorylated peptide. Stoichiometry can then be estimated by dividing the calculated pAKT concentration by the corresponding total AKT concentration in a given sample.

Global proteome analysis by nano-LC-MS/MS

The supernatants from enrichment with anti-peptide antibodies will undergo subsequent global proteome analysis by nano-LC-MS/MS on the Thermo Q-Exactive. Comparison of the broader protein expression patterns between capivasertib treatment response groups will enable identification of proteins of interest that may discriminate between the groups. Extensive review of published literature has shown that while both targeted and untargeted proteomic technologies are commonly used in biomarker development, most researchers do not combine these approaches (1). Untargeted proteomic approaches are typically applied for early stages of biomarker discovery, while targeted approaches are preferred for validation and implementation using a “fit-for-purpose” approach (149). The use of both targeted and untargeted methods together in this project therefore represents a noteworthy technical approach.

Results

iMALDI-MS assay implementation

Assay optimization

The iMALDI assay for quantitation of AKT1 and AKT2 was successfully implemented at the Segal Cancer Proteomics Centre and optimized, as published (6). Signal suppression was initially observed in samples treated with 2U/ug of phosphatase. However, it was shown that 1U/ug of phosphatase did not cause signal suppression and was sufficient to fully dephosphorylate 10 fmol of synthetic pAKT1 peptide and 10 fmol of synthetic pAKT2 peptide in quality control samples. The antibody-bead conjugation protocol was modified from the published protocol to extend the incubation period to 12 hours at 4ºC, which improved signal-to-noise by 30% (t-test, p=0.008). Other minor improvements included altering the concentration of HCCA matrix applied to the samples to increase signal, and acquiring data in triplicate (3 mass spectra per spot) to improve reproducibility.

Many other modifications were tested but did not yield any significant performance improvements. Others -- including adaptation to the Bruker Ultraflex MS instrument and testing of a ReadyPrep E. coli digest as an alternative matrix – caused substantial deterioration of assay performance. Alternative anti-AKT1 and anti-AKT2 monoclonal antibodies were tested for use in the assay, in hopes that implementing the assays with mAbs would facilitate later translation for clinical use. However, the AKT1 and AKT2 mAbs tested (Signatope GmbH, Germany) all resulted in a signal reduction of >10x, making them unsuitable for use in this workflow.

Assay performance validation

Following optimization, the lower limit of quantitation (LLOQ) for AKT1 and AKT2 were found to be <0.5 fmol on-spot (28 pg/10 µg total protein), which is equal to published values (170). Intra-run coefficients of variation (CVs) between replicates at the LLOQ were <20%. The linearity of the assay was consistently high (R^2>0.95). Phosphorylation quality controls consisting of different levels of synthetic AKT1 peptide:phospho-AKT1 peptides (1:3, 1:1, 3:1) generated AKT1 and pAKT1 values within +/-20% of the known concentration. Typical calibration curves are presented in Figure 9.

Quality controls

The quantitative performance of the standards and assay was further validated through the re-analysis of known samples. FFPE samples of mouse xenograft of colorectal cancer 580 (Jewish General Hospital, Montreal, QC, Canada) that had been previously measured at the University of Victoria during assay development were remeasured. The values obtained at McGill were similar to those previously obtained during assay validation at the University of Victoria for both AKT1 (sample 1: 5.1 vs. 5.9 fmol, sample 2: 6.4 vs. 6.2 fmol) and AKT2 (sample 1: 0.8 vs. 1.2 fmol, sample 2: 1.1 vs. 1.6 fmol). Greater variability was observed in AKT2 concentrations due to the lower signal-to-noise ratio for this peptide. Phosphorylation quality controls, consisting of synthetic AKT:pAKT peptides at different ratios (1:3, 1:1, 3:1) spiked into E. coli lysate, all generated AKT values within +/-20% of the known concentration.

Clinical samples & treatment response

Slide-mounted FFPE baseline tumour samples were obtained from female patients treated in a multi-centre Phase II clinical trial of capivasertib (NCT01226316). Patients were selected for inclusion in in two expansion cohorts based on the presence of activating PIK3CA, AKT or PTEN mutations (by local testing) in their ER+ or HER+ breast or gynecological cancers, respectively (169). A total of 23 4-µm slides, representing 16 tumours with PIK3CA mutations, yielded sufficient material (≥25 µg total protein/slide) for the planned analyses. Each patient's response to capivasertib monotherapy was coded based on standardized, anonymized tumour response data. "Clinical benefit" (CB) was defined as ≥12 weeks of progression-free survival attained after starting capivasertib. "No clinical benefit" (NCB) was defined as progressive disease, as determined by RECIST v 1.1 criteria (169), observed within <12 weeks of starting capivasertib. Both groups had similar overall clinical characteristics (see Table 5). However, in the CB group, a greater proportion of samples were derived from metastatic sites, as compared to the NCB group where most samples were from primary sites.

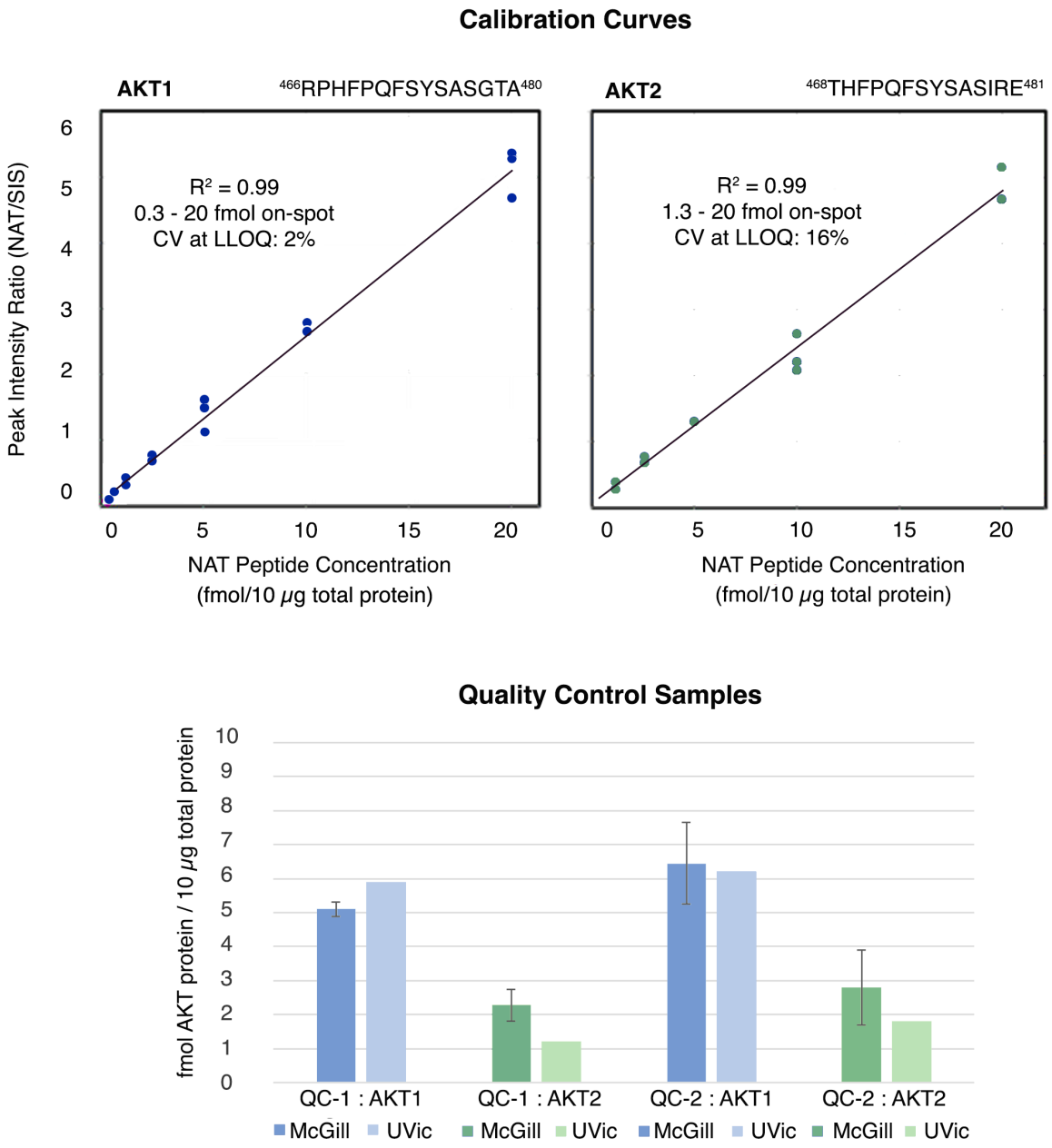

Figure 9. *iMALDI-MS assay validation data.*

Top: Calibration curves demonstrate the linear range of the assay based on the ratio of signal intensity between known quantities of unlabeled synthetic peptide (calibrants) versus a fixed quantity of SIS peptide (internal standard), each immuno-enriched from E. coli lysate digest. Three (3) samples per concentration level are plotted individually with a weighting of $1/x^2$. Bottom: Quantitation of AKT in quality control samples.

Table 5. Descriptive statistics for the clinical trial samples analyzed.

	Clinical Benefit (CB) Group (n=7)	No Clinical Benefit (NCB) Group (n=9)
Clinical Information		
Cancer Type		
Breast (n=__)	3	4
Gynecological (n=__)	4	5
Patient weight (kg)	69.9 ± 18.8	58.9 ± 10.2
Patient age (years)	63.0 ± 10.9	56.7 ± 9.4
WHO Performance Status		
PS 0 (n=__)	3	5
PS 1 (n=__)	4	4
Metastatic sites at enrollment	2.7 ± 1.0	3.4 ± 1.6
Previous lines of treatment		
≤2	1	3
≥3	4	5
Not specified	2	1
Capivasertib Response		
Adjusted progression-free survival (weeks)*	median: 21.1 (95% CI: 13.0 to 32.3)	5.6 (95% CI: 5.3 to 6.1)
Best change in tumour volume from baseline (RECIST %)**	median: -11.9 (95% CI: -52.2 to -8.1)	median: 28.6 (95% CI: 2.3 to 35.9)
Sample Characteristics		
Sample site*		
Metastatic (n=__)	5	1
Primary (n=__)	2	8
Storage time (years)	7.3 ± 0.7	7.6 ± 1.4
Tissue area (mm^2)	330.7 ± 116.8	339.5 ± 151.3
Cellularity		
Tumour cells (%)	62.9 ± 11.6	65.9 ± 22.4
Necrosis (%)	3.9 ± 3.2	5.0 ± 2.7

Values are given as mean ± standard deviation unless otherwise specified. *denotes statistical significance at $p<0.05$ (t-test unequal variance, two-tailed), ** $p<0.01$

Targeted quantitation of AKT1, AKT2, PTEN and by iMALDI-MS in clinical samples

Assay performance is sufficient for clinical applications

Twenty-two slides representing 16 patient tumours were analysed by iMALDI-MS. Among the *PIK3CA*^{mut} tumour samples that had associated AKT data (CB n=7, NCB n=5), the amount of AKT present per 10 µg total protein ranged from 0.6 to 4.5 fmol for AKT1 and 0.5 to 2.0 fmol for AKT2 (Figure 10). For tumours from which multiple slides were analyzed, the AKT concentrations showed good agreement across biological replicates, even among non-adjacent slices (R^2>0.95). Most samples did not show sufficient phosphorylation (>30%) of AKT1-Ser473 or AKT2-Ser474 to be quantified by the PPQ assay, with measurable phosphorylation observed in only 3 tumours (Figure 10). As shown in Figure 11, Sequential enrichment enabled iMALDI of quantitation of PTEN and PIK3CA p110α from limited sample quantities in 14 patient tumours (CB n=7, NCB n=7) (230). Within the patient sample set, the PTEN concentration values quantified by iMALDI correlated well with the PTEN H-score for the tumour previously determined by immunohistochemistry (R^2=0.86) (Figure 12).

Tumour concentrations of targeted proteins do not differ between CB and NCB groups

Concentrations of AKT1, AKT2, and PTEN did not differ significantly between the *PIK3CA*^{mut} tumours in the CB versus the NCB groups (t-test, Wilcoxon rank test, p>0.05) (Figure 13). For PI3K p110α, the large number of samples with concentrations below the lower limit of quantitation of the assay prevented a meaningful comparison between the groups. To evaluate whether our results could be related to the small patient cohort or to the age of the samples, we analyzed published proteomic datasets of luminal breast cancer cell lines according to their known sensitivity or resistance to capivasertib; no relationship between AKT expression and capivasertib sensitivity was observed (Appendix 5) (135).

Figure 10. *AKT1 and AKT2 concentrations measured in patient samples.*
Top: AKT1 (blue) and AKT2 (purple) concentrations measured in AstraZeneca patient samples. Lower two panels: non-phosphorylated AKT is measured before and after phosphatase treatment. Observed phosphorylation >30% is identified with a yellow highlight.

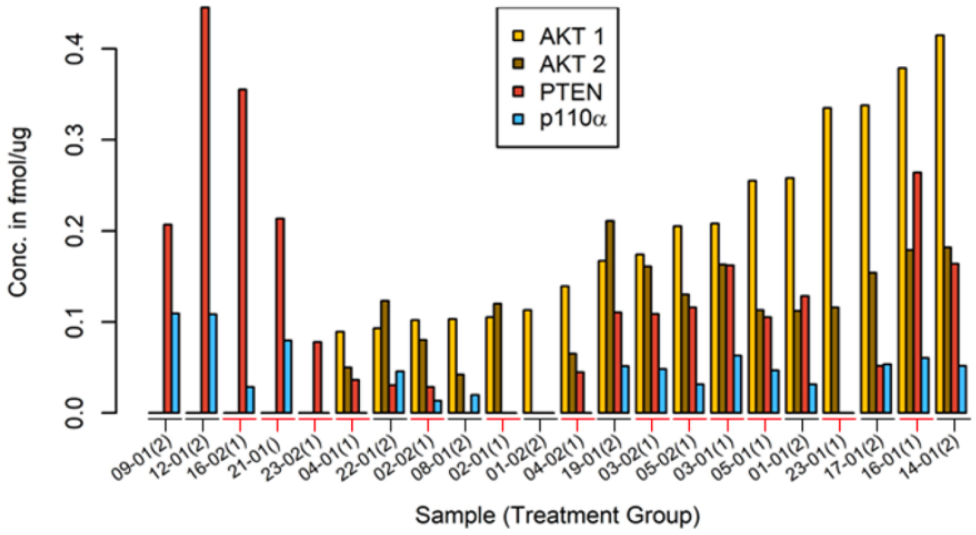

Figure 11. *PTEN and PIK3CA p110α concentrations measured in patient samples.*
Where applicable, the average of two tumour slices, analyzed as separate replicates is plotted. No correction is made to the iMALDI-measured protein concentrations to account for tumour cellularity. Figure is reproduced with permission, without modification, from the thesis of Bjoern Froelich.

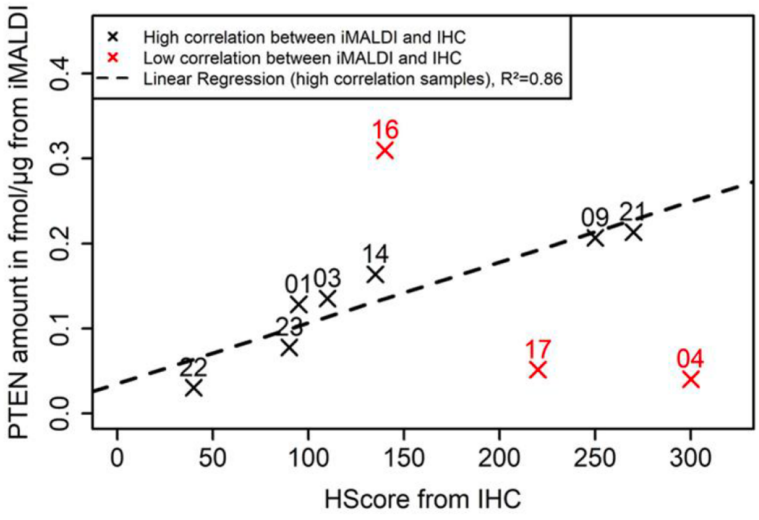

Figure 12. *PTEN concentrations measured using iMALDI-MS assays vs. PTEN IHC*
PTEN concentration measured by iMALDI-MS assay is plotted vs. IHC H-score for the same tumour. Figure is reproduced with permission, without modification, from the thesis of Bjoern Froelich.

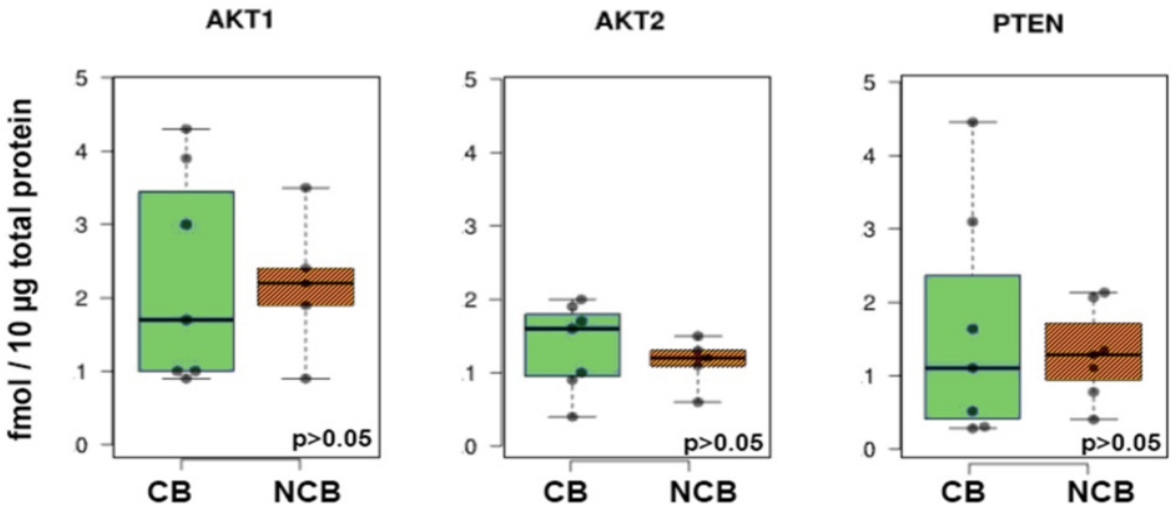

Figure 13. *Results of targeted quantitation of AKT1, AKT2 and PTEN by iMALDI-MS.* Results of targeted quantitation by iMALDI-MS. Boxplots of protein concentrations in the CB (solid green) vs NCB (striped red) groups. Each point represents one patient tumour, averaged for multiple slides. p-values are given for a two-tailed t-test.

Global proteome analysis

Using a new serialized workflow, we acquired global proteomic data using nano-LC-MS/MS for 23 distinct tumour slides from 15 patient tumours (CB n=6, NCB n=9). The workflow permitted further analysis of the previously-analyzed samples from small aliquots of AKT-depleted supernatant, each containing approximately 107 ng of digested protein. We were able to achieve label-free quantification (LFQ) of up to 1455 proteins at a false discovery rate of <1%, with a minimum of 2 specific peptides per protein. A total of 578 proteins were quantified across all samples, and were considered for further statistical analysis.

Quality control: biological relationships are preserved following data processing steps

We performed specific statistical analyses to assess the quality of our complete global proteomics workflow and data processing. First, to assess the reproducibility of the experimental workflow, we compared data from 5 tumour samples for which we analyzed multiple replicates. The replicates consisted of 2 slides per tumour, extracted and analysed separately, but in the same analytical batch. For each slide, there were 2 technical replicates corresponding to supernatant samples from the AKT1 and AKT2 immunoenrichment steps.

As shown in Figure 14 (left), related samples for tumours #2-5 cluster closely together, indicating that the data is highly reproducible, irrespective of the tumour slice used or the antibody used for enrichment. There is a greater difference between the slides from tumour #1; this may point to a difference in the original tumour material captured on the slide or a difference in what could be extracted from each slide. Since normalization, scaling, and batch integration steps were performed on the label-free quantitation data as described in the methods section, we also assessed the global proteome data for the possibility of batch effects. As shown in Figure 14 (right), no significant differences between batches were observed in PCA following data normalization. Overall, quality control (QC) analyses confirmed the integrity of the data after batch integration, normalization, and scaling of features.

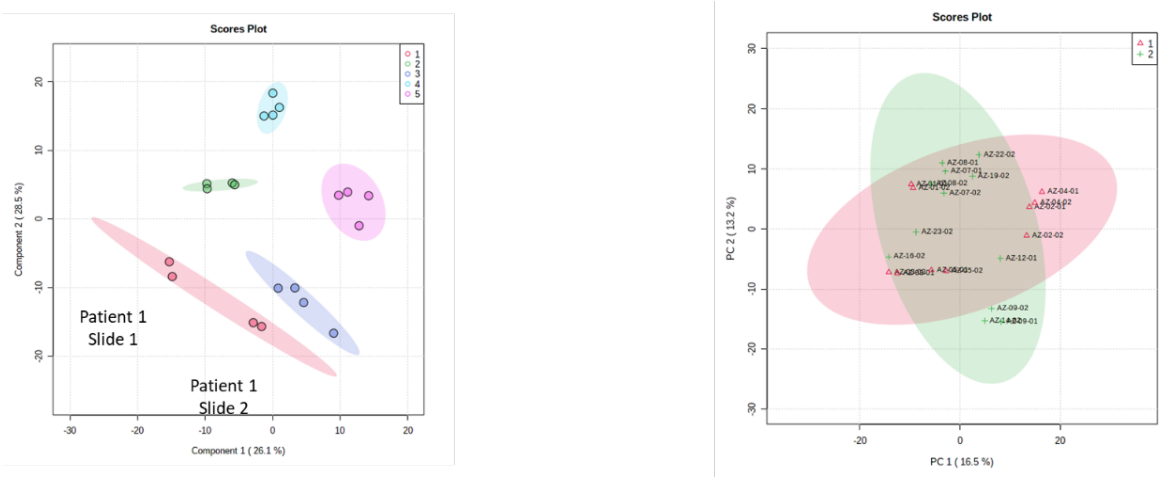

Figure 14. *Quality control of global proteome data processing steps.*
Using PCA to assess clustering of related replicates (left, each dot represents a separate replicate and each color signifies a separate patient) and (b) clustering of samples based on batch assignment (right, Batch 1 in red, Batch 2 in green). Figures generated with MetaboAnalyst webserver.

Quality control: profile of metastatic vs. primary tumours reflects known biology of metastasis

In light of the higher proportion of samples from metastatic sites in the CB group, the proteome profile of samples from metastatic versus primary origin was compared. No difference in total AKT1 concentration is observed between the groups. AKT2 was slightly higher in the metastatic tumours as compared to primary tumours, but the difference did not reach statistical significance (p=0.057, t-test, two-tailed, unequal variance) (Figure 15). As shown in Figure 16, differences in proteomic profile of the metastatic vs. primary tumours identified by PLS-DA

could be tied to known markers of metastasis, indicating that biological relationships represented in the data were preserved following batch integration and data normalization. The identified proteins are consistent with the known biology of metastasis, and do not significantly overlap the proteins of interest in the current study.

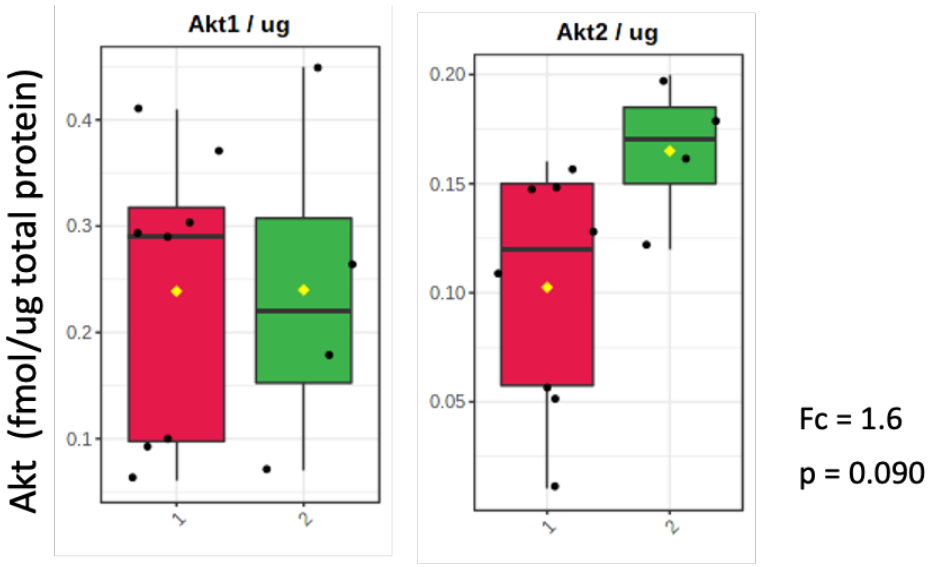

Figure 15. *AKT concentrations compared in tumour samples of primary (red) vs. metastatic (green) origin.*

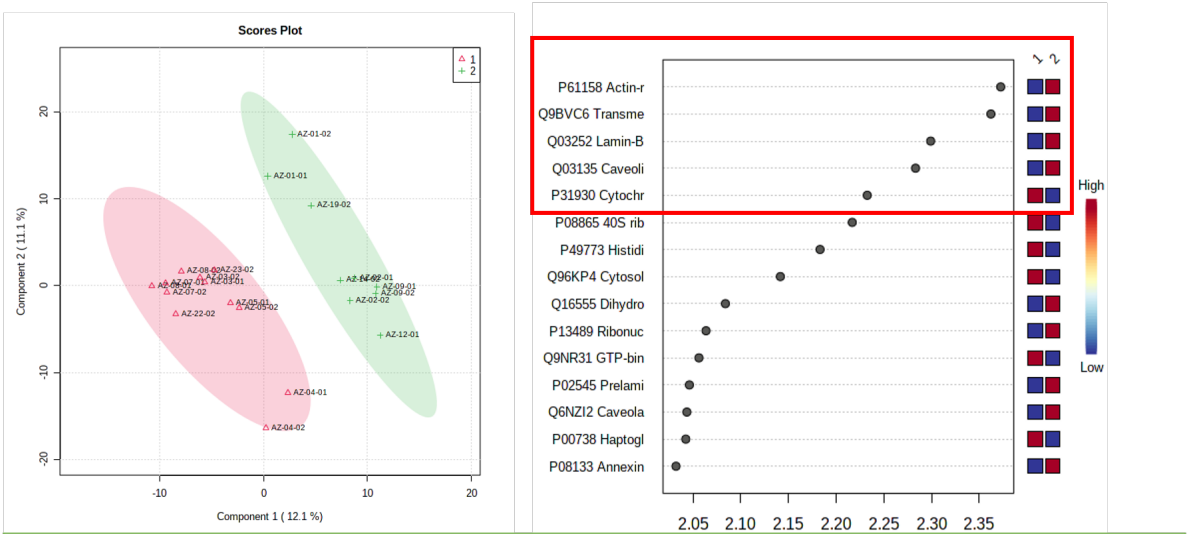

Figure 16. *Proteome profile of samples of primary (red) vs. metastatic (green) origin.* When separated by PLSDA (left), the proteins that best differentiate between patient tumours of primary (red) vs. metastatic (green) origin based on VIP score (right).

Proteomic profiles differ between the CB vs. NCB groups

Similar to the results of the quality control analyses, unsupervised statistical analysis with PCA (Figure 17) showed proximity of related sample replicates (originating from the same tumours), as indicated with a dashed yellow line. A heatmap of protein expression (Figure 18) revealed a trend toward unsupervised clustering of the CB vs. NCB groups. Supervised statistical analysis with partial least squares-discriminant analysis (PLS-DA; Figure 19) enabled a clear separation of the CB and NCB groups, with little overlap.

To identify features that correlated with clinical benefit from capivsertib treatment, we examined proteins whose abundances differed between the CB and the NCB groups. A total of 53 proteins showed fold-changes of ≥1.5 and Wilcoxon rank test p-values of ≤0.05 (Figure 20). Of these 53 proteins (listed in Table 6), the 5 proteins that were upregulated in the clinical benefit group included 4 immunoglobulins and serum albumin. Interestingly, 13 of the 48 proteins that were downregulated in the CB group were ribosomal subunit proteins. GTP-binding protein SAR1a was the only one of the 53 differentially-expressed proteins between the CB and NCB groups that overlapped with the proteins differentiating metastatic vs. primary tumours.

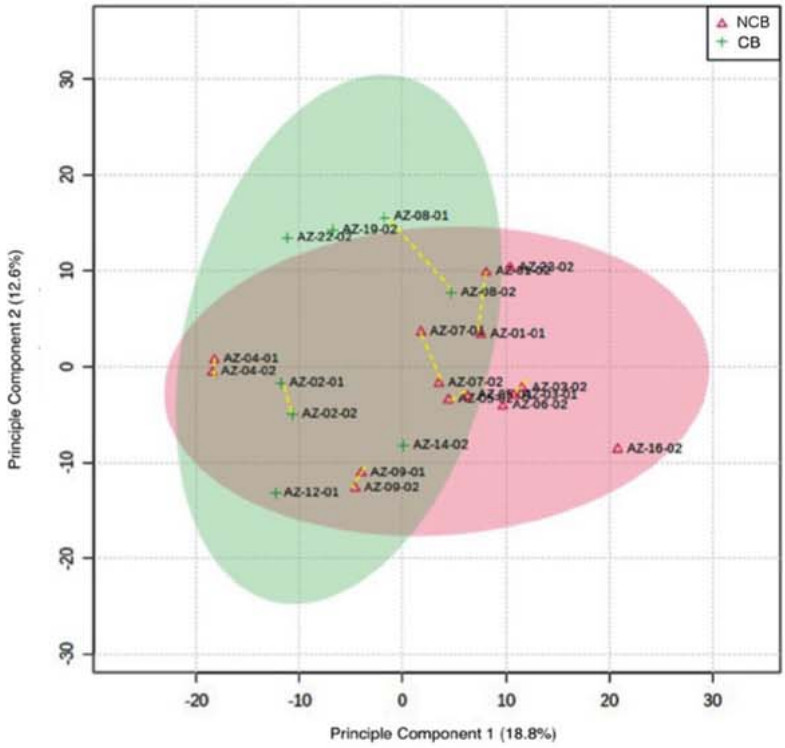

Figure 17. *Principal Components Analysis (PCA) of CB (green) and NCB (red) groups.*

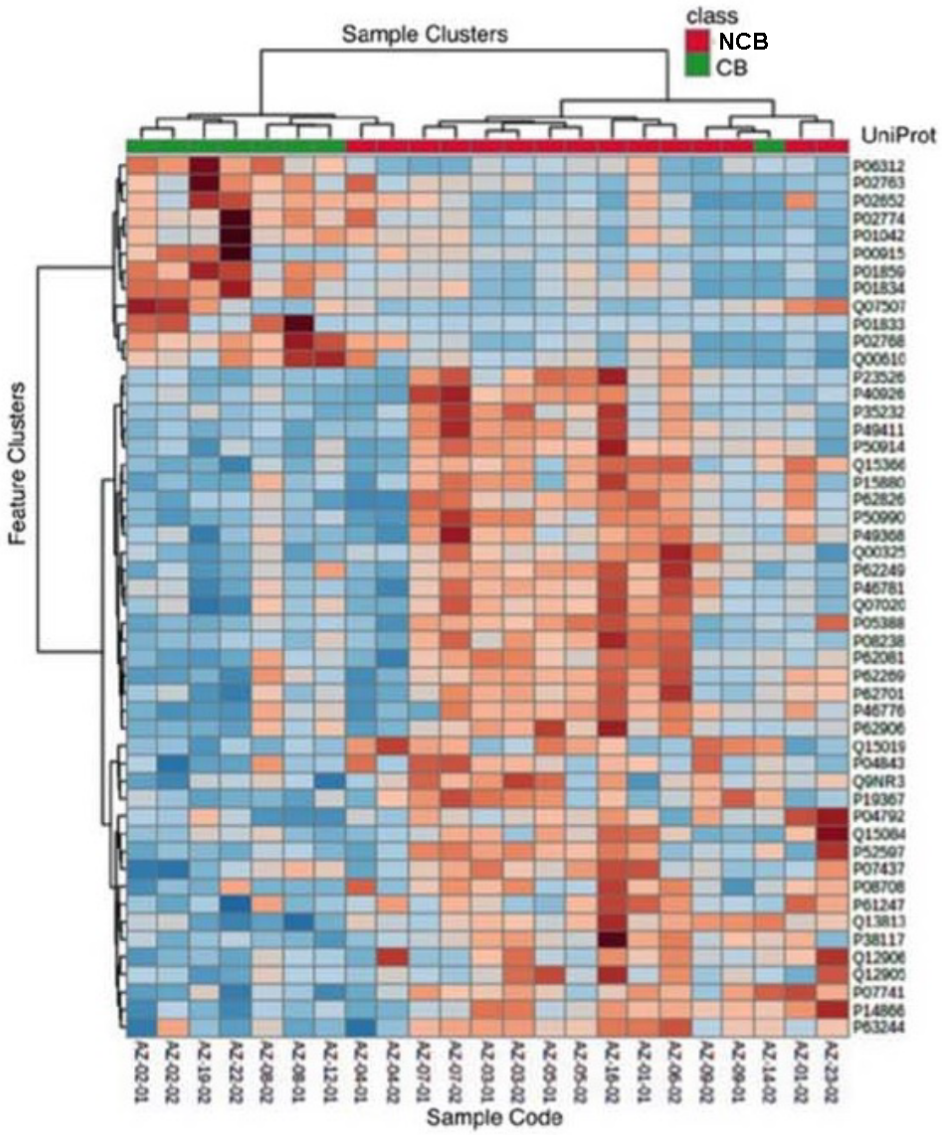

Figure 18. *Heatmap of 50 proteins with highest differential expression between groups.*
50 selected proteins with highest differential expression between groups showing their normalized LFQ abundances across both analysed batches. n=23. Arbitrary identifiers are included for the purpose of identifying replicates from the same tumour. (right) Principal Components Analysis (PCA). Proximity of sample replicates originating from the same patients is indicated with a dashed yellow line.

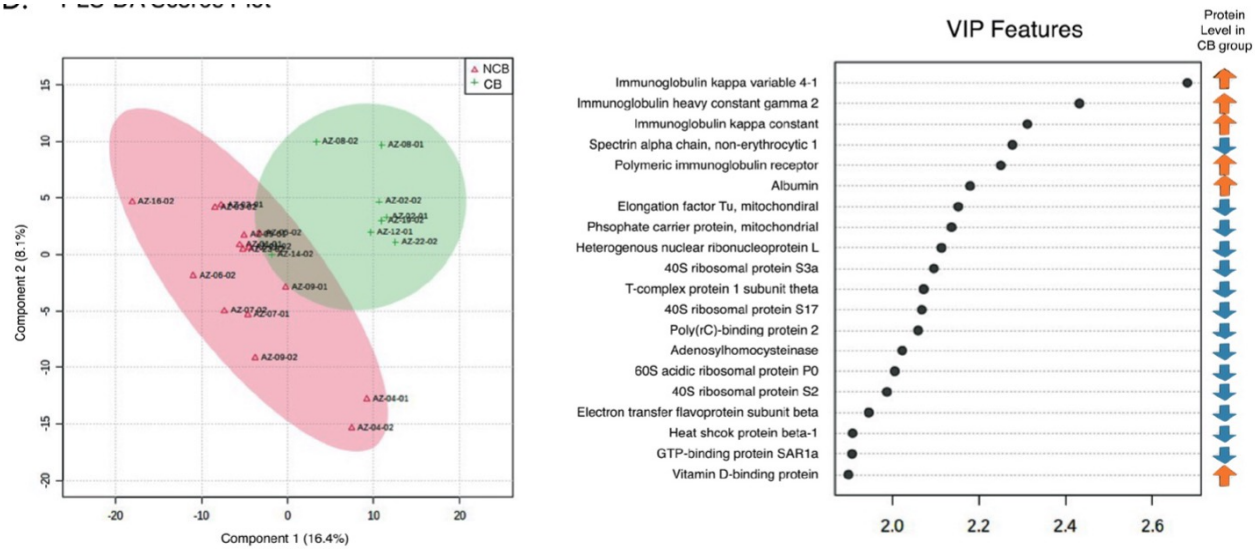

Figure 19. *Supervised statistical analysis of targeted and global proteome comparing protein expression in CB (green) vs. NCB (red) tumour tissues.*

(left) Partial Least Squares – Discriminant Analysis (PLS-DA) plot. (right) Features ranked by Variable Importance in the Projection (VIP) based on their contribution to the discrimination between the CB & NCB groups in the Partial Least Squares – Discriminant Analysis (PLS-DA). The arrows on the right of the VIP Feature list show relative expression of that protein in the NCB group vs. the CB group

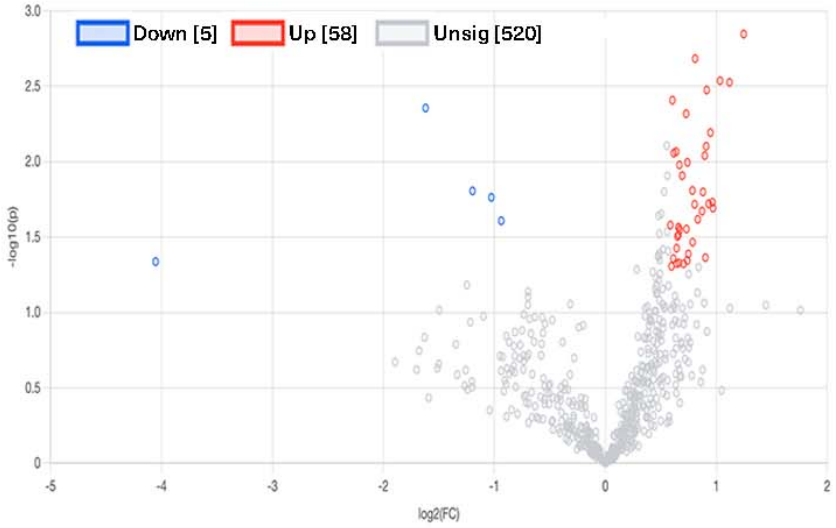

Figure 20. *Volcano plot showing the fold change (log2FC) of all protein expression features versus p-value (-log10p) in CB vs. NCB tumour tissues.*

Table 6. *Proteins differentially expressed between CB and NCB groups (FC >1.5, p<0.05)*

Protein Accession	Gene Name	FC (CB/NCB)	p-value
P23526 Adenosylhomocysteinase	**AHCY**	0.534	0.00135
P02768 Serum albumin	**ALB**	1.976	0.02088
P07741 Adenine phosphoribosyltransferase	**APRT**	0.602	0.04590
Q07960 Rho GTPase-activating protein 1	**ARHGAP1**	0.609	0.02775
P59998 Actin-related protein 2/3 complex subunit 4	**ARPC4**	0.647	0.03223
P56134 ATP synthase subunit f, mitochondrial	**ATP5MF**	0.596	0.01905
P48047 ATP synthase subunit O, mitochondrial	**ATP5PO**	0.633	0.02377
P16152 Carbonyl reductase [NADPH] 1	**CBR1**	0.548	0.02675
P49368 T-complex protein 1 subunit gamma	**CCT3**	0.637	0.00527
P50990 T-complex protein 1 subunit theta	**CCT8**	0.476	0.00129
Q99829 Copine-1	**CPNE1**	0.538	0.02061
Q7Z4W1 L-xylulose reductase	**DCXR**	0.510	0.03662
Q16698 2,4-dienoyl-CoA reductase, mitochondrial	**DECR1**	0.586	0.02935
P38117 Electron transfer flavoprotein subunit beta	**ETFB**	0.474	0.00345
P55084 Trifunctional enzyme subunit beta, mitochondrial	**HADHB**	0.507	0.04801
P19367 Hexokinase-1	**HK1**	0.509	0.01396
P52597 Heterogeneous nuclear ribonucleoprotein F	**HNRNPF**	0.520	0.00457
P14866 Heterogeneous nuclear ribonucleoprotein L	**HNRNPL**	0.595	0.00296
P08238 Heat shock protein HSP 90-beta	**HSP90AB1**	0.590	0.00552
P04792 Heat shock protein beta-1	**HSPB1**	0.533	0.01080
P01859 Immunoglobulin heavy constant gamma 2	**IGHG2**	2.339	0.01448
P01834 Immunoglobulin kappa constant	**IGKC**	2.012	0.01815
P06312 Immunoglobulin kappa variable 4-1	**IGKV4-1**	2.945	0.00499
Q12905 Interleukin enhancer-binding factor 2	**ILF2**	0.591	0.01400
Q12906 Interleukin enhancer-binding factor 3	**ILF3**	0.606	0.00687
P17931 Galectin-3	**LGALS3**	0.597	0.04662
πP40926 Malate dehydrogenase, mitochondrial	**MDH2**	0.529	0.01071

Protein Accession	Gene Name	FC (CB/NCB)	p-value
Q15365 Poly(rC)-binding protein 1	**PCBP1**	0.629	0.02384
Q15366 Poly(rC)-binding protein 2	**PCBP2**	0.500	0.00345
Q15084 Protein disulfide-isomerase A6	**PDIA6**	0.655	0.01484
P35232 Prohibitin	**PHB1**	0.562	0.00503
Q99623 Prohibitin-2	**PHB2**	0.622	0.04948
P01833 Polymeric immunoglobulin receptor	**PIGR**	15.678	0.04660
P60900 Proteasome subunit alpha type-6	**PSMA6**	0.531	0.02568
P62906 60S ribosomal protein L10a	**RPL10A**	0.608	0.02355
P62913 60S ribosomal protein L11	**RPL11**	0.660	0.04438
P50914 60S ribosomal protein L14	**RPL14**	0.583	0.01523
Q07020 60S ribosomal protein L18	**RPL18**	0.607	0.02737
P46776 60S ribosomal protein L27a	**RPL27A**	0.508	0.02702
P39023 60S ribosomal protein L3	**RPL3**	0.594	0.02538
P05388 60S acidic ribosomal protein P0	**RPLP0**	0.635	0.00178
P62249 40S ribosomal protein S16	**RPS16**	0.534	0.01384
P08708 40S ribosomal protein S17	**RPS17**	0.657	0.00425
P62269 40S ribosomal protein S18	**RPS18**	0.654	0.02504
P15880 40S ribosomal protein S2	**RPS2**	0.503	0.00412
P61247 40S ribosomal protein S3a	**RPS3A**	0.657	0.00425
P61247 40S ribosomal protein S3a	**RPS3A**	0.656	0.00728
P46781 40S ribosomal protein S9	**RPS9**	0.602	0.01431
Q9NR31 GTP-binding protein SAR1a	**SAR1A**	0.563	0.01391
P31040 Succinate dehydrogenase [ubiquinone] flavoprotein subunit, mitochondrial	**SDHA**	0.532	0.02468
Q00325 Phosphate carrier protein, mitochondrial	**SLC25A3**	0.450	0.00156
Q13630 GDP-L-fucose synthase	**TSTA3**	0.618	0.02588
P49411 Elongation factor Tu, mitochondrial	**TUFM**	0.396	0.00069
P13010 X-ray repair cross-complementing protein 5	**XRCC5**	0.647	0.02883

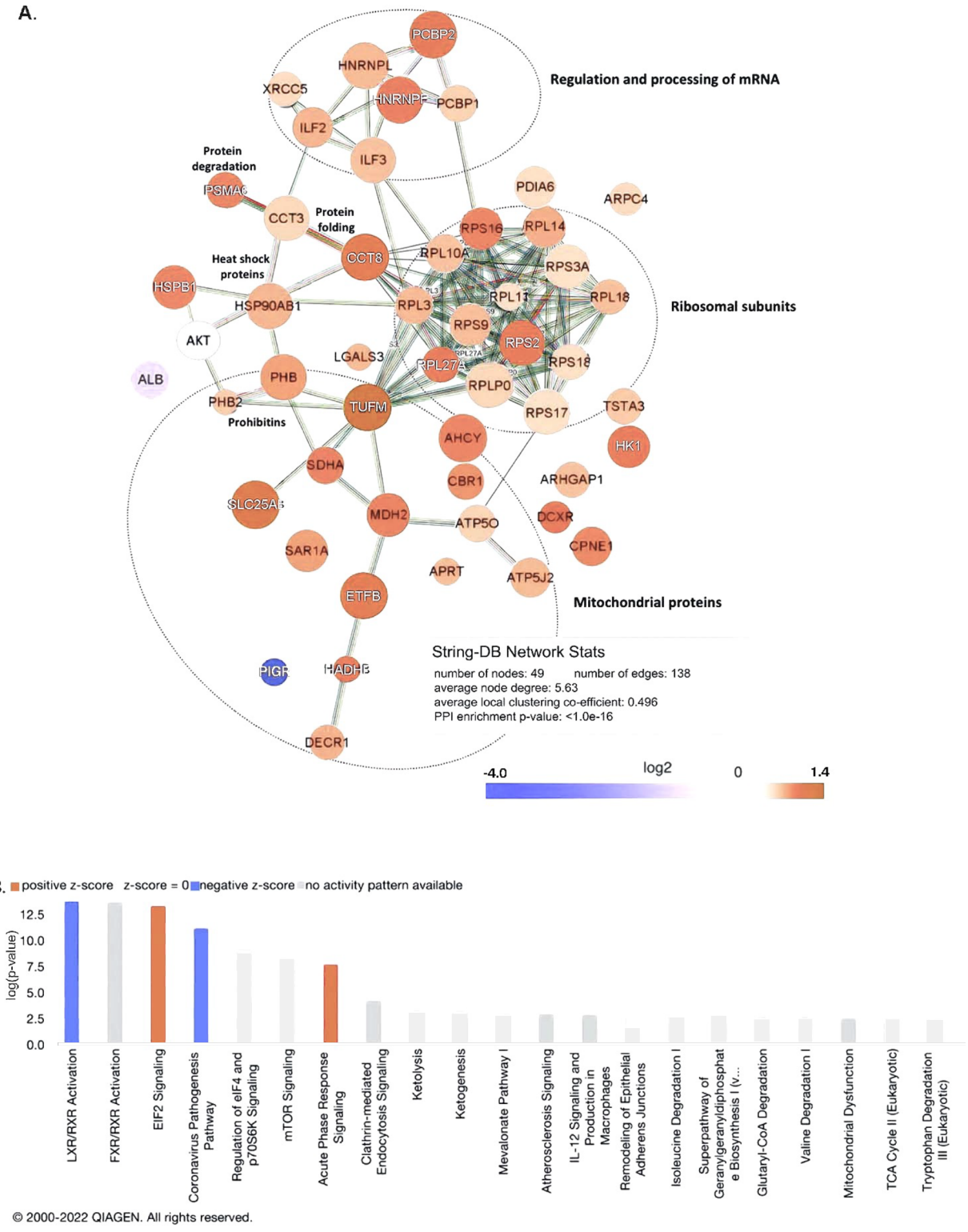

Figure 21. *Mapping of global proteomics results from CB vs NCB groups to protein networks and pathways.*

(A) Network analysis via String-DB plot of high-confidence protein/protein interactions among proteins that are significantly different between clinical benefit (CB) and no clinical benefit (NCB) group. Edges represent evidence of protein/protein interactions. Colours indicate different evidence types. Major clusters are labeled according to shared features within the cluster. Nodes are overlaid from the Cytoscape visualization, with fold-change shown by colour. Node size increases as the p-value decreases. (B) Top 20 canonical pathways that are significantly differentially activated between clinical benefit (CB) and no clinical benefit (NCB) groups, based on assessment with Fisher's Exact Test in Qiagen IPA. The height of the bar corresponds to the confidence of an association, with a threshold of $p<0.01$. IPA's Z-score indicates the direction of regulation and extreme z-scores are depicted with increased colour intensity. Orange bars represent increased activation in the NCB group whereas blue bars represent upregulated activity in the CB group. White bars indicate pathways with fewer than 4 mapped proteins or z-scores close to zero, indicating that the direction of regulation of individual pathway members does not strongly match a pre-specified pattern. Gray bars indicate pathways for which no prediction can be made due to available evidence in the database.

Proteins network analysis finds differential proteins map to shared biological functions

Protein network analysis of the 48 downregulated proteins plus AKT1, using the String-DB (176), found 138 high-confidence interactions between proteins within this group (Figure 21A). The observed PPI enrichment p-value of <1.0e-16 provides strong evidence for a meaningful biological relationship between the proteins of interest in this dataset. The network shows an enrichment of ribosomal proteins, mitochondrial proteins, and proteins involved in mRNA processing.

Differentially expressed proteins map to translational control pathways

To better understand the pathways responsible for the group differences observed, QIAGEN IPA software was used to systematically map the quantified proteins (along with their fold-changes, and p-values), to canoncial pathways. The pathway enrichment analysis showed a particularly strong involvement of EIF2 signaling ($p<1.37e20$), EIF4E /S6K and mTOR translational control pathways (Figure 21B). Table 7 illustrates the mapping of proteins to these pathways, while Table 8 provides QIAGEN-IPA's proposed upstream regulators of the observed profile.

Table 7. *Proteins mapped to top 8 differentially-regulated pathways in QIAGEN-IPA.*

***IPA* Canonical Pathways**	**Pathway proteins**	***Regulation* (NCB / CB)**	**Molecules**
LXR/RXR Activation	123	↑ 0 ↓ 12 (10%)	AGT, AHSG, ALB, AMBP, APOA2, APOH, CLU, GC, KNG1, ORM1, TF, TTR
FXR/RXR Activation	126	↑ 0 ↓ 12 (10%)	AGT, AHSG, ALB, AMBP, APOA2, APOH, CLU, GC, KNG1, ORM1, TF, TTR
EIF2 Signaling	224	↑ 14 (6%) ↓ 0	EIF4A1, RPL10A, RPL14, RPL18, RPLP0, RPS11, RPS16, RPS17, RPS18, RPS2, RPS3A, RPS4X, RPS7, RPS9
Regulation of eIF4 and p70S6K Signaling	179	↑ 10 (6%) ↓ 0	EIF4A1, RPS11, RPS16, RPS17, RPS18, RPS2, RPS3A, RPS4X, RPS7, RPS9
mTOR Signaling	212	↑ 10 (5%) ↓ 0	EIF4A1, RPS11, RPS16, RPS17, RPS18, RPS2, RPS3A, RPS4X, RPS7, RPS9
Acute Phase Response Signaling	185	↑ 0 ↓ 9 (5%)	AGT, AHSG, ALB, AMBP, APOA2, APOH, ORM1, TF, TTR
Clathrin-mediated Endocytosis Signaling	193	↑ 0 ↓ 6 (3%)	ALB, APOA2, CLTC, CLU, ORM1, TF
Coronavirus Pathogenesis Pathway	203	↑ 10 (5%) ↓ 2 (1%)	AGT, KNG1, NPM1, RPS11, RPS16, RPS17, RPS18, RPS2, RPS3A, RPS4X, RPS7, RPS9

Table 8. *Predicted upstream regulators, activation state, and associated proteins*

Regulator (*NCB/CB)*	**p-value of overlap**	**Target Molecules in Dataset**
MYCN (↑)	5.39E-15	CLU, EEF1G, EIF4A1, NME1, NPM1, PHB1, RPL18, RPLP0, RPS16, RPS17, RPS2, RPS3A, RPS4X, RPS7, RPS9, TUBB, TUFM
MYC (↑)	5.16E-14	AHCY, ALB, CCT3, CLU, EFEMP1, EIF4A1, HADHA, HADHB, HNRNPAB, HSPB1, NME1, NPM1, PHB1, PRDX3, RAB10, RPL10A, RPL14, RPL18, RPLP0, RPS11, RPS16, RPS17, RPS18, RPS2, RPS7, RPS9, TF
TCR	1.45E-09	MDH2, NME1, PHB1, RPL10A, RPLP0, RPS16, RPS17, RPS2, RPS3A, RPS4X, SDHA, SLC25A3, TUFM
MAPT	1.46E-09	ALB, CCT8, CLTC, EEF1G, HK1, NME1, PEBP1, PRDX3, RAB10, RPLP0, RPS16, SPTAN1, TUBA4A, TUBB, TUFM
YAP1	7.73E-09	RPL10A, RPL14, RPL18, RPLP0, RPS11, RPS16, RPS17, RPS18, RPS2, RPS7, RPS9, TUBB
RICTOR (↓)	9.47E-09	ATP5MF, ATP5PO, RPL10A, RPL14, RPL18, RPLP0, RPS11, RPS18, RPS2, RPS9, SDHA
APP	8.76E-08	ALB, CD59, CLTC, CLU, EEF1G, HK1, HSPB1, KNG1, NME1, PEBP1, RAN, SPTAN1, TTR, TUBA4A, TUBB, TUFM, YWHAB
TP53	1.35E-07	AHCY, ALB, ANXA2, CD59, CLTC, CLU, EIF4A1, GC, HADHA, HADHB, HSPB1, LASP1, MDH2, NME1, NPM1, ORM1, PRDX3, RAN, RPN1, RPS16, RPS18, SDHA, SERPINC1, TUBB
Lh (↑)	6.84E-07	PGRMC1, PHB1, RPL10A, RPS11, RPS16, RPS17, RPS18, RPS2, RPS7, RPS9

Interpretation

Tumour AKT concentrations do not predict capivasertib response in this cohort

We initially hypothesized that tumour's AKT1 or AKT2 protein concentrations might be directly correlated with response to an AKT inhibitor like capivasertib. AKT transcript over-expression has been observed with equal frequency in both *PIK3CA*-mutated and *PIK3CA*-wild-type tumours (231). A large transcriptomic study of 547 tumours found that AKT1 and AKT2 transcripts were over-expressed in up to 39% and 46% of HR+ human breast cancers respectively (231). The oncogenic effects of high AKT levels are linked to tumour grade and aggressiveness, and have been observed irrespective of phosphorylation status (232). In fact, over-expressed AKT1 has been reported to maintain some activity even when Ser473 phosphorylation is not present (233), though these effects typically occur only with very high levels of AKT.

Using our quantitative iMALDI-MS assay, we observed significant inter-tumour variability in the amount of AKT1 and AKT2 protein, with as much as a 4-fold difference among *PIK3CA*-mutated tumours. However, total AKT1 and AKT2 protein concentrations did not differ between the CB and NCB groups in our sample set. We did however see a possible trend toward increased AKT2 in the samples originating from metastatic sites as compared to primaries (1.7 vs. 1.2 fmol/ 10 ug total protein), though the difference did not reach statistical significance. Nonetheless, this observation is consistent with AKT2's role in promoting motility in breast cancer cells (117). It is possible that the sample set analyzed does not represent the full range of expression; even higher levels might be observed in the larger population of breast cancers and might be more closely linked to treatment response. AKT3 quantitation could also be important, given its association with difficult-to-treat disease (234).

Most of the existing literature focuses on assessment of AKT activity based on the ratio of phospho-AKT to AKT. We used mass spectrometry to quantify pAKT1 Ser473 and pAKT2 Ser474 with high isoform specificity. However, only 3 samples showed pAKT stoichiometry sufficient to be precisely quantified by the PPQ assay. Despite our expectation of high pAKT concentrations reflective of PI3K pathway activation, recent publications have reported that pAKT may be unelevated or even markedly reduced in *PIK3CA*-mutated tumours (222,235). Furthermore, experimental evidence suggests that maximal activation of AKT can occur when as little as 5% of the AKT1 pool is phosphorylated (236), so analytical approaches to measure very

low abundance phosphorylation may be necessary. There is also a significant body of literature supporting the importance of other AKT phosphorylation sites, such as Thr308 (237), whose characterization might be informative.

Since PTEN is the dominant regulator suppressing AKT phosphorylation in *PIK3CA*-mutated cells (222), we also quantified PTEN from the tumour tissues. All 3 samples with >30% pAKT1 or pAKT2 had low PTEN values (<0.36 fmol PTEN/10 µg total protein, falling in the lowest quartile of the measured values). One other sample with 22% pAKT1, which appeared elevated but fell below the LLOQ, also had low PTEN. Nonetheless, PTEN expression levels did not differ significantly between the treatment response groups.

The proteome profile associated with capivasertib treatment response

While none of the expected target proteins differed significantly between the groups, label-free quantitation data revealed that the *PIK3CA*-mutated tumours do in fact contain a series of 53 proteins that are differentially expressed between the CB and NCB groups. Many of the proteins are previously linked to cancer, prognosis, treatment response, and particularly to the modulation of AKT activation.

Only 5 of 53 differentially regulated proteins were upregulated in the clinical benefit group: serum albumin (ALB), polymeric immunoglobulin receptor (PIGR), and some immunoglobulin subunits (IGHG2, IGKC, IGKV4-1). In the StringDB/Cytoscape analysis, the immunoglobulin proteins were not mapped and albumin was not connected to the nodes of proteins downregulated in the CB group. The higher levels of serum albumin and immune-related proteins could reflect better immune infiltration and perfusion of the tumours in the CB group that might facilitate treatment.

However, systemic hypoalbuminuria has also been repeatedly linked to reduced PFS and overall survival in patients treated with TKIs (238,239). Low pre-treatment serum albumin level was found to strongly predict shorter progression-free survival (PFS) and reduced overall survival (OS) for patients with non-small cell lung cancer targeting EGFR (upstream from AKT) (238,240). A similar profile is observed in advanced thyroid cancer treated with TKIs (239). High levels of serum albumin are associated with reduced TNF-alpha and pro-inflammatory cytokine signaling, diminished gluconeogenesis, and activation of AKT to promote cell survival (241). Our CB group similarly showed higher serum albumin together with reduced levels of CPNE-1 (suggesting lower TNF-alpha signaling) and inflammatory proteins (ILF-2, ILF-3).

Immunoglobulin-related proteins with higher expression in the CB group can also be tied to AKT function. There is mixed evidence about the role of PIGR in cancer, but some evidence from hepatocellular carcinoma suggests that PIGR in extracellular vesicles promotes oncogenic AKT activity with downstream effects on GSK3B/β-catenin that are reversed by AKT inhibition (242). IGKV was one of 14 immunoglobulin genes downregulated in an AKT2 knock-out model of human lung cancer (243). IGHG2 has been linked to upstream activation of PI3K/AKT/mTOR as well as the MEK-ERK pathway through Phospholipase C signalling (244,245). AKT activation appears to play a role in regulating IgG production by cancer cells (243,246), which is associated with cisplatin resistance (246). IGKC is a well-known positive prognostic marker for metastasis-free survival and chemotherapy response that has been validated at the RNA- and protein-level (247). Though some data suggests limited prognostic utility for IGKC in HR+ breast cancers, this interpretation is likely confounded by the immuno-modulatory effects of endocrine therapies (248), which are not expected with capivasertib.

The 48 proteins that were downregulated in the CB group vs. the NCB group cluster to 3 main nodes. The first group, which is the largest, and most highly interconnected, includes 13 structural subunits of ribosomes. Specific subsets of ribosomal proteins have previously been identified as regulatory factors in breast cancer as well as pediatric acute myeloid leukemia (249-252). Additional proteins in this group such as Poly(rC)-binding proteins (PCBP1, PCBP2) and heterogeneous nuclear ribonucleoproteins (HNRNPL, HNRNPF), are involved in RNA processing as well as protein translation, localization, and degradation (253). Each of these has been implicated in cancer, with distinct functions in regulating RNA splicing and alternative splicing (254-256). A related, strongly inter-connected, node relates to regulation and processing of mRNA and DNA. Interleukin enhancer-binding factors (ILF2, ILF3) are involved in DNA repair and RNA metabolism (257). They contribute to oncogenesis as negative regulators of tumour-suppressing microRNAs and their activity is mediated by AKT-driven phosphorylation (258). Depletion of ILF3 in HCC cells has been associated with decreased AKT phosphorylation in hepatocellular carcinoma, whereas expression of ILF2 and ILF3 has been linked to PI3K/AKT and MAPK signaling in esophageal squamous cell carcinoma (259,260).

The final node consists of 11 differentially-expressed mitochondrial proteins. Of these, the prohibitins (PHB1, PHB2) have specifically been associated directly with the activation of protein kinase c activity (261). Both PHBs are directly phosphorylated by AKT, after which PHB forms a complex with RAF1 and activates the RAF1-MEK1-ERK pathway (262). This may

support higher activation of the MEK/ERK pathway, which is a known mechanism of resistance to AKT inhibitors, in the NCB group (263). PHB is also involved in a positive feedback mechanism wherein phosphorylation of PHB further increases AKT activity, perhaps further propelling over-activation. Several proteins that did not connect to the core clusters also have an important relationship to AKT's oncogenic functions; a selection of the associated evidence is provided in Appendix 6. For instance, expression of galectin-3 has been shown to activate AKT in gastric cancer, resulting in a loss of responsiveness to IFN-γ similar to that observed in the context of PI3K mutations (264).

Taken as a whole, the nodes are suggestive of strongly increased translational activity in the NCB group together with the associated energetic demands. Since many of the identified proteins have been previously linked to cancer progression, prognosis, and treatment response, there is an inherent challenge in distinguishing whether any specific association with response to AKT inhibition. However, the clustering of differential proteins to a handful of interrelated functions, and functional linkages of the proteins to AKT activity, increases the confidence of the findings in this regard.

Translational activity downstream from AKT is a potential mechanism of resistance to capivasertib

To further examine biological relationships between the differentially expressed proteins, we applied QIAGEN's Ingenuity Pathway Analysis (IPA) software to map protein expression fold-changes and p-values to canonical pathways and to statistically assess the observed patterns of regulation. IPA identified an enrichment of pathways associated with associated with hallmarks of cancer in this dataset; group differences were associated with changes in translational activity (e.g., EIF2 signaling, eIF4/p70S6K, mTOR pathway), inflammation (acute phase response signaling, LXR/RXR activation), cancer cell motility/invasion (actin cytoskeleton signaling), and altered glucose metabolism (gluconeogenesis, glycolysis). The coronavirus pathogenesis pathway is also identified and indeed inhibition of the PI3K/AKT/mTOR has been proposed for the treatment of COVID-19 because of its relationship to T-cell functions (265).

LXR/RXR activation was higher in the CB group. LXRs regulate glycolysis, lipid hemostasis, and possibly immune functions by enhancing the activity of GSK3β, which activates AKT and phosphorylates pathway proteins upstream (*RICTOR, PTEN*) and downstream (*TSC*)

from AKT (266). IPA further predicts that Rictor, a key component of mTORC2, may regulate the observed differences through higher activity in the CB group (Table 8). RXRalpha is also known to transmit cellular signals to regulate differentiation, angiogenesis, and glycolysis by phosphorylating AKT pathway, though its upregulation may be associated with tumor suppression (267).

Conversely, the EIF2 signaling pathway showed significantly higher activation in the tumours of the NCB group. eIF2α (EIF2S1) is a master regulator of translation dysregulation in cancer. It controls cell fate in response to various forms of stress, including the ER stress that occurs when unfolded proteins accumulate in the lumen (268). By modifying the efficiency of translation initiation during the unfolded protein response (UPR), PERK-phosphorylated eIF2α can both diminish translation of abundant transcripts and enhance translation of low-abundance transcripts thereby resulting in the widespread uncoupling of up to 90% transcripts from their protein products (268-270). Phospho-eIF2α has been proposed to activate AKT, by depressing mTORC1 and enhancing mTORC2 activity, to promote survival under conditions of ER or oxidative stress (271-273). However, the relationship is complex and bi-directional, with AKT regulating PERK/eIF2α as well (274,275). When phosphorylated at T799, AKT inhibits PERK in response to ER stress (275).

While there is more to be elucidated to fully understand the complex crosstalk between eIF2α and AKT, the two pathways clearly work in close partnership as a molecular switch to control cell fate decisions under cell stress conditions (271). The two proteins can compensate for one another to maintain survival under stress (271). Thus it is not surprising that EIF2 signaling has been previously implicated as a possible mechanism of resistance to AKT inhibitors (275,276). In capivasertib-sensitive breast cancer cell lines, transcription of genes associated with EIF2 signaling was significantly upregulated in response to capivasertib monotherapy (198). Inhibition of PERK/eIF2α sensitizes resistant cancers cells to AKT inhibitors (275). Increased ER stress was also shown to sensitize gastric cancer cells to AKT inhibition (277). In the NCB group tumours, the elevated baseline expression of ribosomal and translational proteins may help prevent the accumulation of mRNA transcripts that could trigger the unfolded protein response (UPR), activation of which would make them more sensitive to AKT inhibition. Meanwhile, increased AKT activation due to upstream PIK3CA mutation could help ensure continuous pro-survival signaling even under conditions of sustained EIF2 signaling. Together, this evidence supports the idea that EIF2 signaling could be a plausible molecular

context underlying resistance in the NCB group. While there is evidence for this relationship in HER2-overexpressing breast cancers (278), evidence from HR+ PIK3CA-mutated breast cancers would be novel.

Proteins belonging to other translational control pathways downstream from AKT -- mTOR and eIF4/p70S6K signaling – were also enriched among the proteins of interest. Expression is upregulated for the associated proteins in the NCB group, though IPA could not statistically confirm the direction of regulation. However, closer examination of the data shows that IPA defined its EIF2 pathway to include ribosomal proteins (RPL10A, RPL14, RPL18, RPLP0) that their EIF4 pathway does not. This omission led to statistical prioritization of EIF2 signaling in IPA, we could not find evidence in the literature of a specific association of EIF2 signaling with these RPLs; in fact, the relationship appears to be mediated by EIF4 (176).

eIF4E controls translation downstream from AKT via mTORC1. pAKT phosphorylation of TSC1/2 inhibits it, resulting in mTORC1 activation and downstream activation of eIF4E-associated translation (279). eIF4E then promotes translation of specific mRNAs (e.g., cyclins, ODC, c-Myc) (279). mTORC1-driven resistance to PI3K pathway inhibitors is now well-characterized (119,280). Persistent mTORC1 signaling in PIK3CA-mutated cell lines is associated with resistance to p110α inhibition, even when AKT phosphorylation is measurably inhibited (281). A mutation activating mTOR has even been detected and effectively targeted in at least one patient treated with AKT inhibitors (282). Previous research points to TSC1/2 or mTOR mutations as a mechanism for mTORC1-driven resistance of PI3K inhibitors However, additional genetic mechanisms likely exist.

Technical challenges and study limitations

Technical limitations in the quantitation of pAKT likely prevented optimal assessment of AKT activity in the tumours. More in-depth assessment could be achieved using alternative analytical approaches to multiplex additional targets (e.g., AKT3, AKT1 E17K, additional phosphorylation sites). An immuno-UPLC-MS/MS method was partially developed during the course of this project, which demonstrated the ability to capture peptides for AKT1 (GEYIKTWR, m/z: 351.7+++) and AKT1 E17K (G<u>K</u>YIKTWR, m/z: 351.3+++) with a single antibody (Appendix 7). Despite their similar m/z ratios, the method could distinguish the analytes, even on a short gradient, based on retention time and transition ratio. However, continued development was not merited at the time, given the absence of study samples with this

mutation and the necessity to optimize a completely new experimental workflow including digestion with a new enzyme (e.g., clostrapain). Alternative technical approaches might also support more precise measurement of pAKT and PIK3CA p110α. Nonetheless, the global proteome data was able to provide important insights into tumours' molecular activity both upstream and downstream of AKT.

Though the biological relationships observed in our data are compelling, the certainty of our findings is inherently limited by several important constraints, the greatest of which is the small number of patients in the study and the heterogeneity of a heavily-treated clinical population. "Clinical benefit" may not accurately reflect treatment efficacy, especially in the absence of a comparator group (e.g., alternative or placebo treatment) to signal the natural history of disease in this small cohort. That said, it is generally accepted as the only criterion available in this study population. Alternative definitions of "clinical benefit" (e.g. based on best response, 6 weeks PFS, 16 weeks PFS) yielded similar results with respect to the network and pathway analysis. Obtaining a sufficient number of well-characterized and high-quality patient samples with adequate material available for analysis is an ongoing challenge for translational research. The imbalance of primary versus metastatic samples in each group is another important caveat, though this is partially addressed by our statistical analysis.

Most of the samples studied were obtained from the original tumor. It is therefore possible that these samples obtained at "baseline", many years before treatment with capivasertib, did not yet show some markers that would predict treatment response. AKT activation is increasingly cited as a mechanism of resistance to chemotherapies, suggesting that important changes may arise over the course of treatment. Nonetheless, the most clinically-useful patient selection marker should ideally be detectable at an early stage of intervention with the potential to guide combination treatments.

Moreover, there remains the universal challenge of distinguishing treatment-specific markers from overall prognostic markers. A gene expression profile similar to the NCB group, including upregulation of AKT1, 30 ribosomal subunits, and EIF signalling, has been observed in gastric cancers as a signature of acquired chemoresistance to cisplatin and fluorouracil combination chemotherapy (232). This is especially difficult to parse due to the many pleiotropic proteins involved and the complexity of their behaviour in different contexts. For instance, although it is often stated that phosphorylation of AKT1 at both Thr308 and Ser473 are required for activation (283), it has been posited that increased pAKT1 Thr308 in the presence of ATP

can independently activate mTORC1/4E-BP1/S6K-driven biosynthesis, while an ATP deficit activates AMPK/FOXO/mTORC2 leading to phosphorylation of AKT at Ser478 (284). Interplay between nutritional status, cellular stress, pathway crosstalk, and feedback mechanisms affecting AKT activation likely each play a role in determining *PIK3CA*-mutated tumours' response to targeted therapy.

Nonetheless, the strong biological relationships between proteins identified in the analysis, and the agreement of this data with the literature, all provide evidence that the observed profile could be meaningfully and specifically with an increased likelihood of treatment benefit, at least in this cohort.

Results Chapter 2:
Targeted protein quantitation in breast cancer cell lines verifies an association between capivasertib response and proteins of interest

Chapter Summary

We previously analyzed PIK3CA^{mut} breast and gynecological tumours from patients enrolled in a clinical trial of capivasertib. We identified a differential proteomic profile between those patients who demonstrated a clinical benefit in response to capivasertib treatment compared to those who did not. The proteins of interest mapped to pathways involved in translational control including EIF2 and EIF4 activation. To further verify this association, we developed targeted MRM-MS assays for 50 proteins of interest (53 peptides) using synthetic proteotypic peptides and corresponding stable-isotope labelled standard peptides. Assays were optimized and characterized on a UPLC + Agilent 6495B-QQQ-MS. Each quantitative MRM-MS assays was characterized according to the guidelines of the NCI's Clinical Proteomic Tumor Analysis Consortium. Most assays were found to be fit-for-purpose in that they precisely and reproducibly quantify the analyte at the endogenous concentration in cell lines.

A standard cytotoxicity assay was used to determine capivasertib sensitivity for each of the 6 well-characterized cell lines selected for study. By applying the multiplexed panel, expression of the targeted proteins was compared between sensitive vs. resistant lines. The proteomic profile observed in the capivasertib-resistant cell lines was found to closely match the profile previously observed in the tumours of clinical trial patients. The reproducibility of the profile associated with capivasertib resistance across two orthogonal proteomics approaches and two fully independent models lends additional credibility to the proteins' relationship to capivasertib sensitivity. Changes in protein concentration after capivasertib exposure were assessed.

The assays were further developed for compatibility with clinical samples. PRM-MS assays were applied to 33 FFPE tumour blocks obtained with consent under Research Ethics Board approval at the Jewish General Hospital. The data was used to evaluate intra- vs. inter-tumour variability and the effect of different sampling approaches.

Context

Pathways of translational control in cancer

Eukaryotic initiation factors (eIFs) play a crucial role in regulating protein synthesis in eukaryotic cells. They are the primary effectors of gene expression in the cell (285). As compared to transcriptional control, translational control offers a more efficient and immediate mechanism for altering the proteome during cellular adaptation (285,286). Moreover, aberrant translation plays a crucial role in cancer (285). eIF dysregulation is commonly observed in cancer, and is implicated in oncogenesis, proliferation, metastasis, and treatment resistance (285,287). For this reason, many eIFs are now considered a promising therapeutic targets (286).

Among them, eIF4s are well-known regulators of translation initiation, which is the rate-limiting step in protein synthesis (286,288). eIF4F consists of several subunits, including eIF4E, eIF4A, and eIF4G, that are involved in recruiting the ribosome to the mRNA and unwinding the mRNA secondary structure (288). A range of anti-cancer agents has been developed to target the eIF4F complex including inhibitors of eIF4A helicase, eIF4E cap-binding, eIF4E-eIF4G association, and eIF4E expression (286). Overexpression of eIF4E is present in the majority of breast cancers and has been associated with increased cell proliferation, invasion, and metastasis (288). Moreover, the PI3K/Akt/mTOR pathway regulates eIF4 activity, leading to increased translation of specific mRNAs that promote tumor growth and survival (288).

As described in the previous chapter, the role of EIF2 signaling in cancer is more complex and is still being elucidated (286). EIF2 signaling is regulated by several kinases that respond to cellular stress, including the PERK/eIF2α pathway that is activated by endoplasmic reticulum (ER) stress (289,290). eIF4E and eIF2α are both sensitive to the cellular stress and work together to modify translation (249); mTORC1 and CK2 may help to coordinate regulation of eIF2α and eIF4E (291). In breast cancer, activation of PERK/eIF2α can contribute to the hallmarks of cancer by adapting cells for tumor growth and survival (290,292). PERK/eIF2α also appear to mediate treatment response, acting as a common mechanism of resistance (293,294). On the other hand, induction can also sensitize breast cancer cells to chemotherapy-induced cell death (294). This “double-edged sword” of PERK/eIF2α in determining treatment response is particularly significant in ER+ breast cancer where first-line antiestrogen therapies mildly induce PERK and other sensors, which interact with transcription factors like c-MYC to produce

endocrine resistance (295). However, further upregulation of PERK/eIF2α can actually drive apoptosis (295).

Biomarker verification

The results of our previous study revealed an activation of pathways associated with translational control in the tumours of heavily-treated patients who did not respond to capivasertib in a Phase II clinical trial. At least 53 putative proteomic markers of resistance to capivasertib treatment were identified from the label-free quantitation data. The differences in protein expression associated with resistance appear to be detectable from long-stored FFPE and are present at "baseline," long before exposure to the drug. The results specifically suggested a possible role for translational control pathways including EIF2 signaling pathway and/or EIF4 signaling downstream of mTORC1 in determining resistance to capivasertib. To assess the validity of this finding, we aimed to systematically assess the relationship identified proteins of interest to capivasertib in a verification study.

Traditionally, the biomarker development pipeline followed a "triangular approach" wherein the size of study cohorts increased progressively with each validation step. Often, the discovery of new putative markers is published without further study to assess the reproducibility of the findings because of the significant investment required. When further validation is attempted, research is often geared directly at clinical qualification, which requires rigorous study design, analysis, and very large numbers of biospecimens. These biomarker validation studies require extremely rigorous study design, analysis, and very large numbers of biospecimens. Despite this significant investment, extremely few validation attempts are successful. Biomarker verification has been proposed as a useful "bridge" between biomarker discovery studies and resource-intensive validation (65). The goal is to quickly (but reliably) assess a large number of targets in a new larger sample set, obtaining additional evidence to help triage leads. The verification stage can also serve to assess the suitability of a method for subsequent validation efforts.

Cell lines as a model system

Biomarker verification is typically intended to be performed in a clinical cohort very similar to the intended clinical population. However, given that capivasertib is not yet approved for clinical use, there are extremely few tumour samples available that have associated capivasertib response data. The use of an alternative model is therefore required until larger-scale

application of the drug enables access to more clinical samples. Both mouse models and cell lines are commonly used in cancer research, each with their own advantages and disadvantages (296).

Cell lines are readily available and enable cost-effective analysis. Thanks to their ability to generate large volumes of material, cell lines are well-suited to analysis of low-abundance analytes. Disadvantages include a tendency for genotypic and phenotypic drift that can limit inter-laboratory reproducibility (297). Even with optimal culture technique, the process of culturing inevitably selects for increasingly aggressive variants and is therefore unsuitable for modeling less aggressive malignancies or earlier stages of cancer development (297). This is true even of breast epithelial immortalized cell line MCF10A, which is increasingly used as a non-cancer control, but must be handled carefully to avoid increasing tumour-forming behaviour with suboptimal seeding or repeated passages (298,299).

In spite of its limitations, cell culture remains an essential tool for cancer research. As compared to mouse models, cell lines operate as a simplistic homogenous model of disease, without an immune system or anatomical effects, which may represent an advantage for mechanistic studies focused on the intra-cellular molecular landscape. To avoid potential pitfalls, best practices require limiting passage number, performing regular cell line authentication, and giving careful attention to avoiding or treating potential contaminations, especially myocoplasma infections(300,301). Employing multiple cell lines in a given study can also help ensure the robustness and validity of results.

MRM-MS assays with internal standards

In our original protocol, we obtained information about enhanced EIF2 and EIF4 pathway activity from global proteome data. Our label-free quantitation approach was able to achieve simultaneous relative quantitation of hundreds to thousands of proteins from a tiny amount of protein digest reserved from the supernatant of previously-analyzed samples. However, as discussed in the Introduction, a targeted approach is typically required as part of a fit-for-purpose approach to enable definitive quantitation of putative biomarkers for further study (1,149). The aforementioned dose-dependent nature of EIF2 signaling activity makes the precise quantitation of these proteins especially important, given the need to distinguish between slight elevations (conferring resistance) and dramatic sustained increases (resulting in apoptosis).

Multiple reaction monitoring (MRM-MS) using internal stable isotope-labeled standards is considered the gold standard in targeted protein quantitation because of its reproducibility, accuracy, and suitability for biomarker candidate verification (1,302). It is increasingly recognized for its potential for clinical applications (154,303). MRM-MS with internal standards offers exceptionally high specificity (that exceeds even iMALDI-MS or LFQ) based on matching of multiple parameters: (i) retention time, (ii) mass-to-charge of the precursor peptide, (iii) paired mass-to-charge of fragments ions, and (iv) the conserved ratio between multiple transitions. This exceeds even the specificity offered by iMALDI-MS, which collects only MS1, or LFQ approaches which may match to spectral libraries but do not contain a co-eluting standard to verify retention times or transition ratios. The ability to detect dissimilarities in the transition ratio between IS and analytes further aids in the identification and resolution of sample-specific interferences.

Like iMALDI-MS, MRM-MS traditionally uses an external calibration curve, prepared in surrogate matrix. However, direct MRM-MS offers a much higher degree of multiplexing capability, with many assays routinely quantifying hundreds of proteins per run and spanning many orders of magnitude in concentration. This is not possible with antibody-dependent methods. Precise protein quantitation can be reliably achieved by MRM assays, with coefficients of variation (CVs) typically below 20% for most peptides. MRM-MS is also highly reproducible, with good inter-laboratory comparability and stable quantitation over time. Together with its rapid development time, these qualities make MRM an optimal approach for the verification stage of biomarker research (65).

Sub-hypothesis, Objectives, Approach

We previously hypothesized that proteomics may offer additional insights to inform patient selection for capivasertib. Our initial results from patient samples suggest that specific translational control pathways, particularly EIF2 and EIF4, may regulate response to capivasertib. We hypothesize that the profile associated with capivasertib resistance in PIK3CA-mutated HR+ breast and gynecological cancers is conserved in other models. Specifically, we predict that (i) our proteins of interest will show similar expression patterns in HR+ PIK3CA-altered breast cancer cell lines that are resistant to capivasertib as compared to those that are sensitive, (ii) protein expression changes after drug exposure will reflect increased activation of these pathways in response to capivasertib exposure, (iii) strategic co-treatment with an EIF2

inhibitor will sensitize resistant cells to treatment with capivasertib. We anticipate that quantitative methods for assessing these targets can be translated for use in clinical samples.

Our verification study has the following objectives:

1. Develop and validate high-quality MRM-MS assays to reproducibly quantify the proteins of interest and associated targets from cell lines
2. Generate an appropriate series of cell culture samples with verified capivasertib sensitivity to test the hypotheses
3. Analyze cell line samples to verify the relationship between protein concentration and capivasertib sensitivity
4. Adapt the developed methods to nanoflow-PRM-MS for use with volume-limited samples and assess analytical performance
5. Analyze patient FFPE tumour cores and slices for assessing feasibility in clinical samples with respect to compatibility, sensitivity, intra- vs. inter-tumour variability

The results of this verification study will help to inform which, if any, of our putative markers merit evaluation in a large-scale clinical study toward biomarker validation.

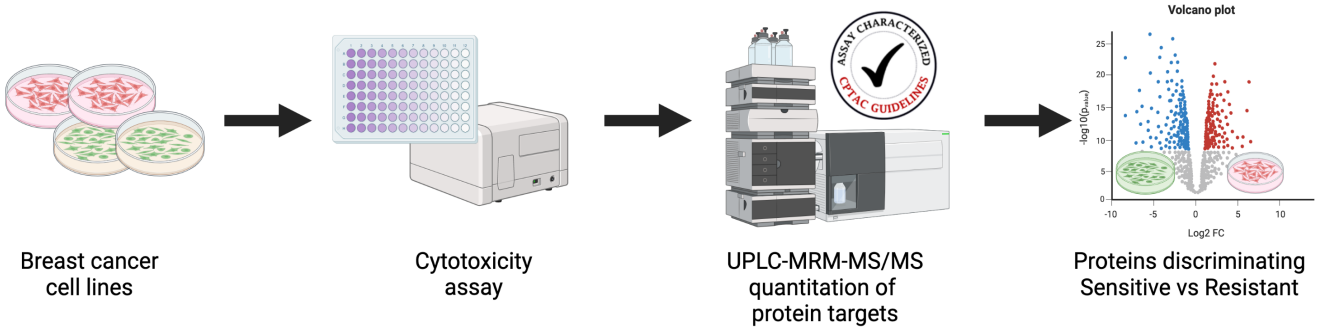

Figure 22. Experimental design for validating previously-identified targets in cell lines.

Cell line selection

To mirror the characteristics of patient samples from the previous study, we selected 6 well-characterized hormone receptor-positive (HR+) breast cancer cell lines. The COSMIC Cell Lines Project was used as a centralized, curated resource to assess the mutational profile of cell lines (40). Four cell lines with known *PIK3CA* or *AKT1* were selected to match with the clinical trial inclusion criteria. These line were predicted to show varying sensitivity to capivasertib (2

sensitive, 2 resistant), based on published and unpublished data (182). Two additional HR+ breast cancer cell lines with *PTEN* alterations (1 sensitive, 1 resistant) were selected for comparison, as our previous work did not indicate whether the profile of capivasertib is specific to *PIK3CA*-altered cell lines. Each cell line's sensitivity to capivasertib was verified following expansion using a standard cytotoxicity assay.

Protein target selection

Proteins were chosen for assay development based on (i) observed 'hits' from patient study, (ii) proteins predicted altered based on activation of EIF2 or EIF4 translational control pathways, and (iii) proteins in the PI3K pathway. Proteins of interest from the previous study were triaged based on feature reduction by selecting representative proteins were highly correlated with other biologically related features (e.g., a few ribosomal proteins). Additional targets were prioritized based on their importance to the canonical eIF or PI3K signaling pathways. In consultation with Dr. Antonis Koromilas, an expert in EIF2 signaling, we identified several desired targets for the EIF2 pathway including eIF2α, phospho-eIF2α, PERK (EIF2AK3), ATF4, and ERK (MAPK1/MAPK3). eIF-2A was also included; It is important to distinguish eIF2α (EIF2S1) from eIF-2A (EIF2A) here, as the two are commonly confused (https://www.ncbi.nlm.nih.gov › articles › PMC7139343). While eIF2α is primarily responsible for the binding of Met-tRNAi to 40S and drives large-scale changes in initiation, eIF-2A usually plays a minor role. However, eIF-2A does appear to preferentially translate a specific subset of mRNAs (e.g., those regulated by non-canonical initiation codons such as uCUG, uUUG) under conditions of eIF2α phosphorylation. From the EIF4 pathway, mTOR, eIF4A-1 and eIF4E were identified as preferred targets based on their role in cancer.

Assay development & validation

To reduce waste and limit attrition, we evaluated each potential protein target for tryptic peptide suitability, the availability of assays published in the CPTAC portal, and previous detections in PeptideAtlas to determine whether the peptide was likely to be readily detectable without enrichment or fractionation. Cell lines were screened for detection of the endogenous peptide before ordering stable isotope-labeled peptides to develop quantitative assays. Targeted multiplexed UPLC-MRM-MS assays were developed and optimized for 50 proteins of interest using synthetic proteotypic peptides for calibration and corresponding stable-isotope labelled standard peptides as internal standards for quantitation from cell lines.

Like other data-intensive 'omics disciplines, targeted proteomics has seen an increasing emphasis on standardization, which is required to support translational research (304,305). The National Cancer Institute (NCI) has established the Clinical Proteomic Tumor Analysis Consortium (CPTAC) with the aim of removing barriers to translation of proteomics into clinical biomarker studies (65). One of the main goals of CPTAC is to standardize proteomics workflows, including the development and validation of targeted proteomics assays. To this end, CPTAC has published guidelines for proteomic assay development and characterization which include recommendations for the selection of peptides, the optimization of MRM parameters, the assessment of assay performance, and the reporting of assay characterization results. While this standard does not reach the high bar of analytical validity ultimately required for clinical biomarkers (306), obtaining reliable research results is the first critical step toward eventual clinical translation. We therefore completed CPTAC validation and deposition of our assays to ensure the quality, reproducibility, and transparency of our workflows. Characterization data was publicly deposited in the CPTAC Assay Portal.

Toward translation: feasibility in clinical samples

As part of our effort to verify method suitability, we adapted our validated assays for use with clinical samples. Most existing tumour samples available for cancer research are stored in Biobanks and pathology facilities as FFPE tumour blocks. To assess feasibility of future translation, we adapted our assay for use with the lower total protein amounts typically obtained from these samples. Parallel reaction monitoring (PRM)-MS demonstrates performance characteristics that are similar or better than MRM-MS (158), and high sensitivity can be attained by pairing PRM methods with nanoflow chromatography. To prepare for clinical sample analysis, we translated our assays for use on an EvoSep One liquid chromatography system coupled to a Q-Exactive Hybrid Quadrupole-Orbitrap-MS.

The EvoSep system emphasizes a high level of standardization, together with the high throughput required for some clinical applications (307). The innovative design of this system limits sample preparation by using disposable sample loading tips to prevent contamination and carryover. Moreover, it offers the high sensitivity of nano-flow chromatography with much, much higher robustness than typical nanoflow systems (307). The Q-Exactive MS also offers the ability to acquire full-scan data simultaneously that can, for instance, be used to confirm total protein quantitation results. By adapting our assay to this platform, we aim to quantify our analytes from 1 µg of total protein digest per sample.

We applied the adapted method to analyze stored FFPE tumour samples obtained with consent from patients with advanced solid tumours genetically screened for AstraZeneca's Phase II clinical trial of capivasertib. This offers an opportunity to assess method and target suitability for future biomarker studies in terms of (i) the ability to quantify from clinically available samples, (ii) the intra- and inter-tumour variability of the analytes of interest, and (iii) any correlation of protein concentrations to annotated clinical variables.

Results

Quantitative method validation data

We initially selected 58 proteotypic peptides representing 53 target proteins for assay optimization. Of these, all but 4 peptides representing 3 proteins were found to be detectable in at least some cancer cell lines during screening (see Appendix 8). As shown in Figure 23 and Table 9, this resulted in the development of a multiplexed assay consisting of 53 peptides to represent 50 target proteins, including 31 "hits" from the previous study, 7 mTOR/eIF4 pathway proteins, 3 eIF2 signaling proteins, and 9 others associated with translation or the PI3K pathway.

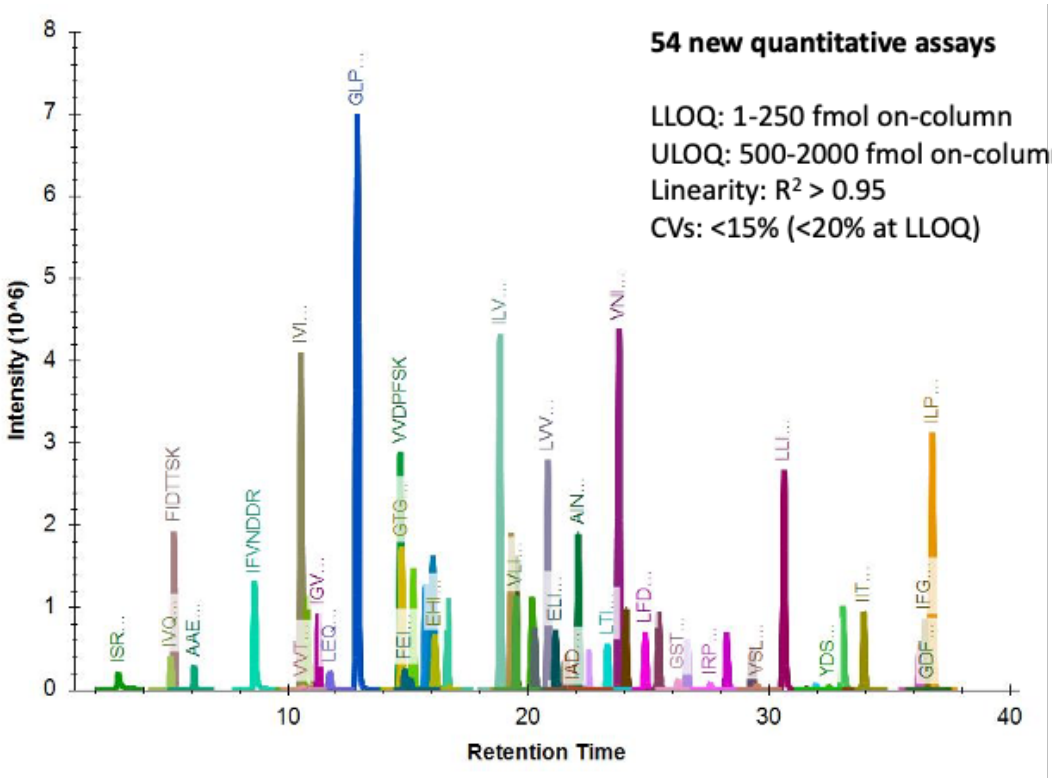

Figure 23. *Chromatographic separation of the target peptides.*

Table 9. Proteins and surrogate peptides selected as targets for assay development

Uniprot	Gene	Protein name	Selected Peptide
P31749	AKT1	RAC-alpha serine/threonine-protein kinase B	FFAGIVWQHVYEK
P31751	AKT2	RAC-beta serine/threonine-protein kinase B beta	YDSLGLLELDQR THFPQFSYSASIRE
P02768	ALB	serum albumin	LVNEVTEFAK
Q07960	ARHGAP1	Rho GTPase-activating protein 1	AINPINTFTK
P59998	ARPC4	Actin-related protein 2/3 complex subunit 4	VLIEGSINSVR
P18848	ATF4	Cyclic AMP-dependent transcription factor ATF-4	AGSSEWLAVDGLVSPSNNSK
P16152	CBR1	Carbonyl reductase [NADPH] 1	LFSGDVVLTAR
P49368	CCT3	T-complex protein 1 subunit gamma	ELGIWEPLAVK
Q99829	CPNE1	Copine-1	GTITVSAQELK
Q9NZJ5	EIF2AK3	Eukaryotic translation initiation factor 2-alpha kinase 3 (PERK)	EHIEIIAPSPQR
P05198	EIF2S1	Eukaryotic translation initiation factor 2 subunit 1 (eIF2α)	VVTDTDETELAR
P60228	EIF3E	Eukaryotic translation initiation factor 3 subunit E	YLTTAVITNK
P60842	EIF4A1	Eukaryotic initiation factor 4A-I	DQIYDIFQK
P06730	EIF4E	Eukaryotic translation initiation factor 4E	IVIGYQSHADTATK
P55010	EIF5	Eukaryotic translation initiation factor 5	VLTLSDDLER
P56537	EIF6	Eukaryotic translation initiation factor 6	HGLLVPNNTTDQELQHIR
P38117	ETFB	Electron transfer flavoprotein subunit beta	LSVISVEDPPQR
P55084	HADHB	Trifunctional enzyme subunit beta, mitochondrial	LEQDEYALR
P19367	HK1	Hexokinase-1	GDFIALDLGGSSFR
P14866	HNRNPL	Heterogeneous nuclear ribonucleoprotein L	ISRPGDSDDSR
P08238	HSP90AB1	Heat shock protein HSP 90-beta	VVNVSSIMSVR
P11021	HSPA5	Endoplasmic reticulum chaperone BiP	ELEEIVQPIISK
P04792	HSPB1	Heat shock protein beta-1	VSLDVNHFAPDELTVK
P01859	IGHG2	Immunoglobulin heavy constant gamma 2	GLPAPIEK
P06312	IGKV4-1	Immunoglobulin kappa variable 4-1	LLIYWASTR

Legend: blue = PI3K pathway, green = protein of interest from patient samples, yellow = EIF2 signaling protein, orange = EIF4 translational control protein, grey = other translation-associated protein

Uniprot	Gene	Protein name	Selected Peptide
Q12905	ILF2	Interleukin enhancer-binding factor 2	ILPTLEAVAALGNK
Q12906	ILF3	Interleukin enhancer-binding factor 3	IFVNDDR
P01116	KRAS mut	GTPase Kras	LVVVGAVGVGK
P17931	LGALS3	Galectin-3	IALDFQR
O95819	MAP4K4	Mitogen-activated protein kinase kinase kinase kinase 4	VYPLINR
P28482	MAPK1	Mitogen-activated protein kinase 1 (ERK 2)	ELIFEETAR
P27361	MAPK3	Mitogen-activated protein kinase 3 (ERK 1)	IADPEHDHTGFLTEYVATR IADPEHDHTGFLTE(pY)VATR
P40926	MDH2	Malate dehydrogenase, mitochondrial	IFGVTTLDIVR
P42345	MTOR	Serine/threonine-protein kinase mTOR	LFDAPEAPLPSR VLGLLGALDPYK
Q15365	PCBP1	Poly(rC)-binding protein 1	IITLTGPTNAIFK
Q15084	PDIA6	Protein disulfide-isomerase A6	GSTAPVGGGAFPTIVER
P35232	PHB1	Prohibitin 1	FDAGELITQR
Q99623	PHB2	Prohibitin-2	IVQAEGEAEAAK
P01833	PIGR	Polymeric immunoglobulin receptor	VYTVDLGR
P42338	PIK3CB	Phosphatidylinositol 4,5-bisphosphate 3-kinase catalytic subunit beta isoform	AAEIASSDSANVSSR EAGLDLR
P46776	RPL27A	60S ribosomal protein L27a	TGAAPIIDVVR
P39023	RPL3	60S ribosomal protein L3	FIDTTSK
P15880	RPS2	40S ribosomal protein S2	GTGIVSAPVPK
P61247	RPS3A	40S ribosomal protein S3a	VVDPFSK
P46781	RPS9	40S ribosomal protein S9	IGVLDEGK
P23443	S6K1	Ribosomal protein S6 kinase beta-1	FEISETSVNR
Q15019	SEPTIN2	Septin-2	VNIVPVIAK
Q13630	TSTA3	GDP-L-fucose synthase	ILVTGGSGLVGK
P49411	TUFM	Elongation factor Tu, mitochondrial	TIGTGLVTNTLAMTEEEK
P13010	XRCC5	X-ray repair cross-complementing protein 5	LTIGSNLSIR

Legend: blue = PI3K pathway, green = protein of interest from patient samples, yellow = EIF2 signaling protein, orange = EIF4 translational control protein, grey = other translation-associated protein

Linearity & sensitivity. Peak area ratios for each analyte and its internal standard were fitted to a linear regression model with 1/x2 weighting. The linear range was defined as the range in which the peak area ratio increases linearly with analyte concentration (R^2>95) and precision remains high (<20% CV at the LLOQ, <15% CV in the rest of the range). In blanks injected directly following the injection of the highest calibration point, carryover contributed less than 20% of signal at the lower limit of quantitation (LLOQ). No interferences were detected in the matrix blanks. As shown in Figure 24, the developed assays cover a dynamic range of more than 3 orders of magnitude. Most assays, with the exception of 4 peptides, demonstrated a linear range suitable for quantitation of the endogenous analytes.

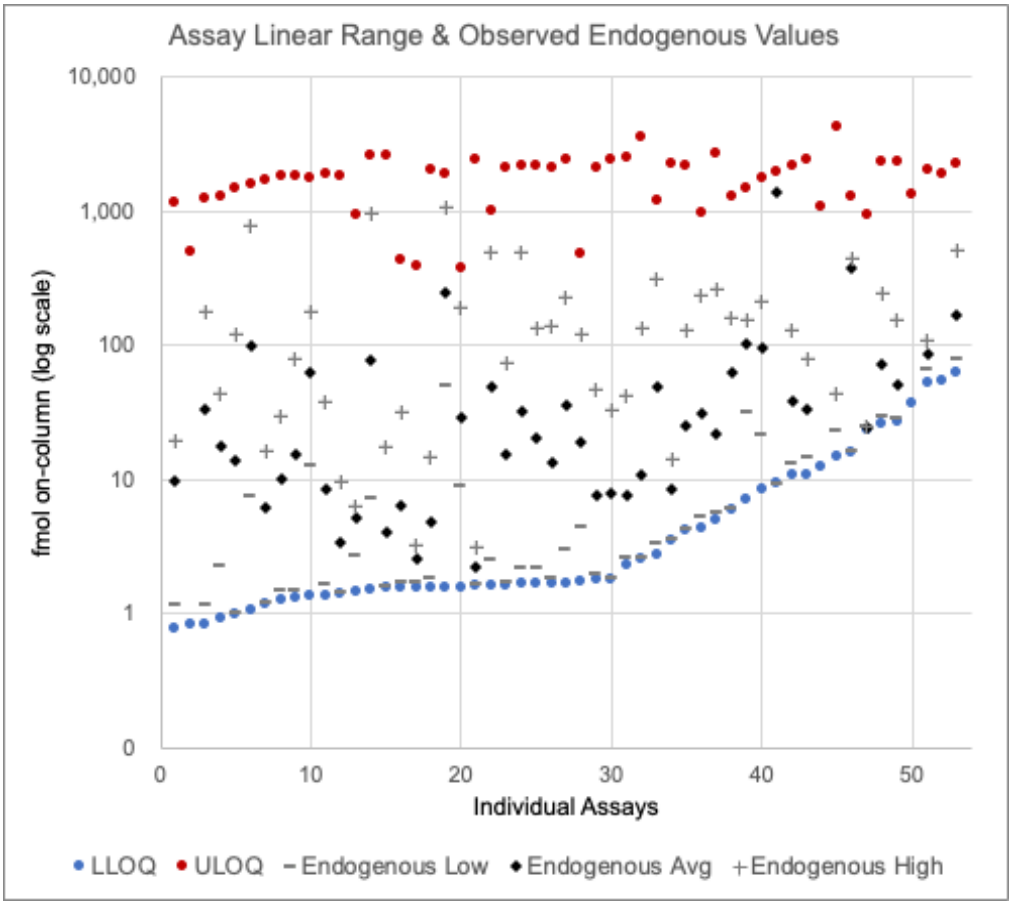

Figure 24. *Assay dynamic range & endogenous levels, sorted in order of ascending LLOQ.*

Repeatability of QC samples at 4 levels. Quality control samples of synthetic peptide in digested matrix at 4 concentrations ("low", "medium-low", "medium", "high") were processed and analyzed as 3 replicates each on each of 5 successive days. The total variability for each peptide was estimated by the sum of squares using measured concentrations. For each peptide, for each concentration level, we calculated intra-assay variability (CV between 3 replicates, averaged across the 5 days) and added this to the inter-assay variability (CV for a given replicate on 5 days, averaged across the 3 replicates). Each of this is squared, summed, and then the square root is taken to represent "total variability" for that concentration level. CPTAC requires total variability to be <20% in order to validate the assay performance at that level. For our peptides, 37 out of 54 passed for a minimum of 3 consecutive levels and 19 passed at all levels. Another 8 assays (total 45/54) demonstrated very good repeatability with total variability <25% at a minimum of 3 QC levels. Peptide assays corresponding to MAPK3 (IADPEHDHTGFLTEYVATR) and HK1 (GDFIALDLGGSSFR) were discarded due to inadequate performance (CVs >30%) at multiple levels.

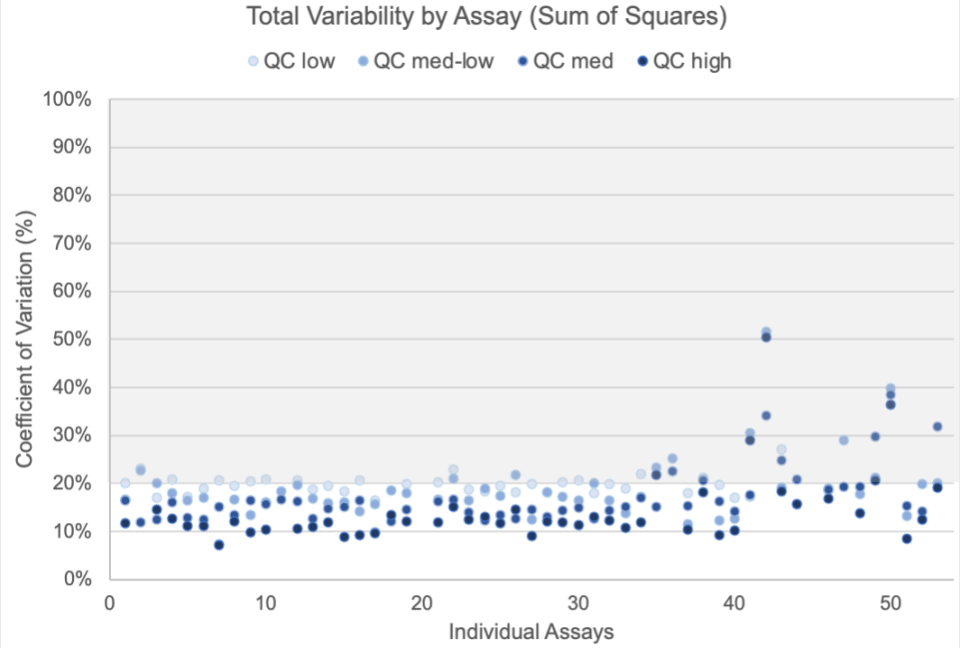

Figure 25. *Repeatability at 4 QC levels for assays sorted in order of ascending LLOQ.*

Stability. Stability (Exp. 4) was confirmed by assessing variability in the measured concentration at multiple timepoints and after one or more freeze-thaw cycles. All except 1 peptide were found to maintain stability within +/- 20% of the original concentration under all tested storage conditions. The peptide for EIF5 (HGLLVPNNTTDQELQHIR) did show a decrease in signal to 75% of the starting concentration after 4 weeks at -80ºC.

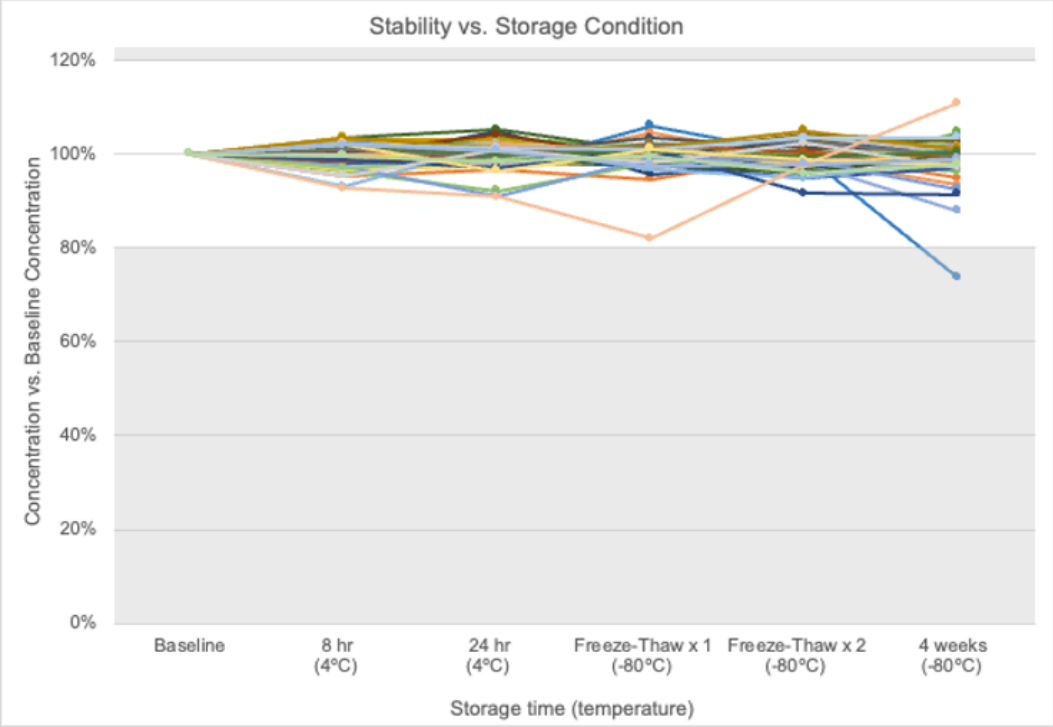

Figure 26. *Peptide stability characterized across different storage conditions.*

Reproducibility. A pooled sample of MCF-7 protein extract repeatedly subjected to the complete proteomics workflow, including the digestion step, on 5 different days to assess reproducible quantitation of the endogenous analyte. The CV calculated across the 5 measurements was <25% for 39 of 44 peptides that had endogenous concentrations above the LLOQ in the pooled sample.

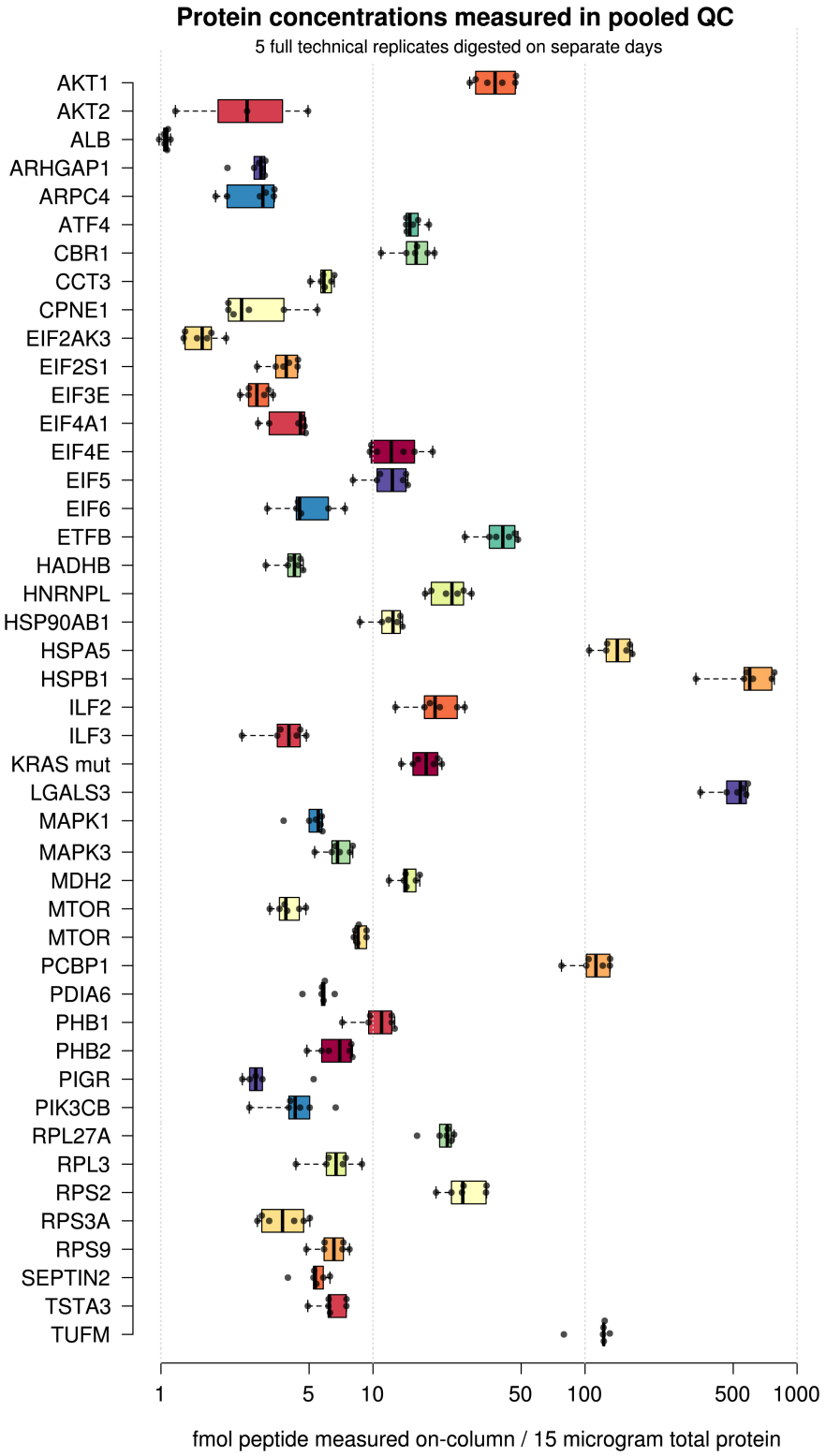

Figure 27. *Reproducibility of endogenous quantitation from pooled MCF-7 QC sample.* Prepared as 5 full-process replicates on 5 different days.

Protein concentration differences associated with capivasertib sensitivity in cell lines

Capivasertib sensitivity. Using a standard cyotoxicity assay, MCF-7 (*PIK3CA* E545K) was confirmed to be capivasertib-sensitive (IC_{50}<2 µM), while HCC1428 (*AKT1* OE), ZR-75-30 (*AKT1* OE), and EFM-19 (*PIK3CA* H1047L) were found to be capivasertib-resistant (IC_{50}>10 µM) (Figure 28). Of the *PTEN* mutant cell lines, CAMA-1 was found to be sensitive while ZR-75-30 was found to be resistant.

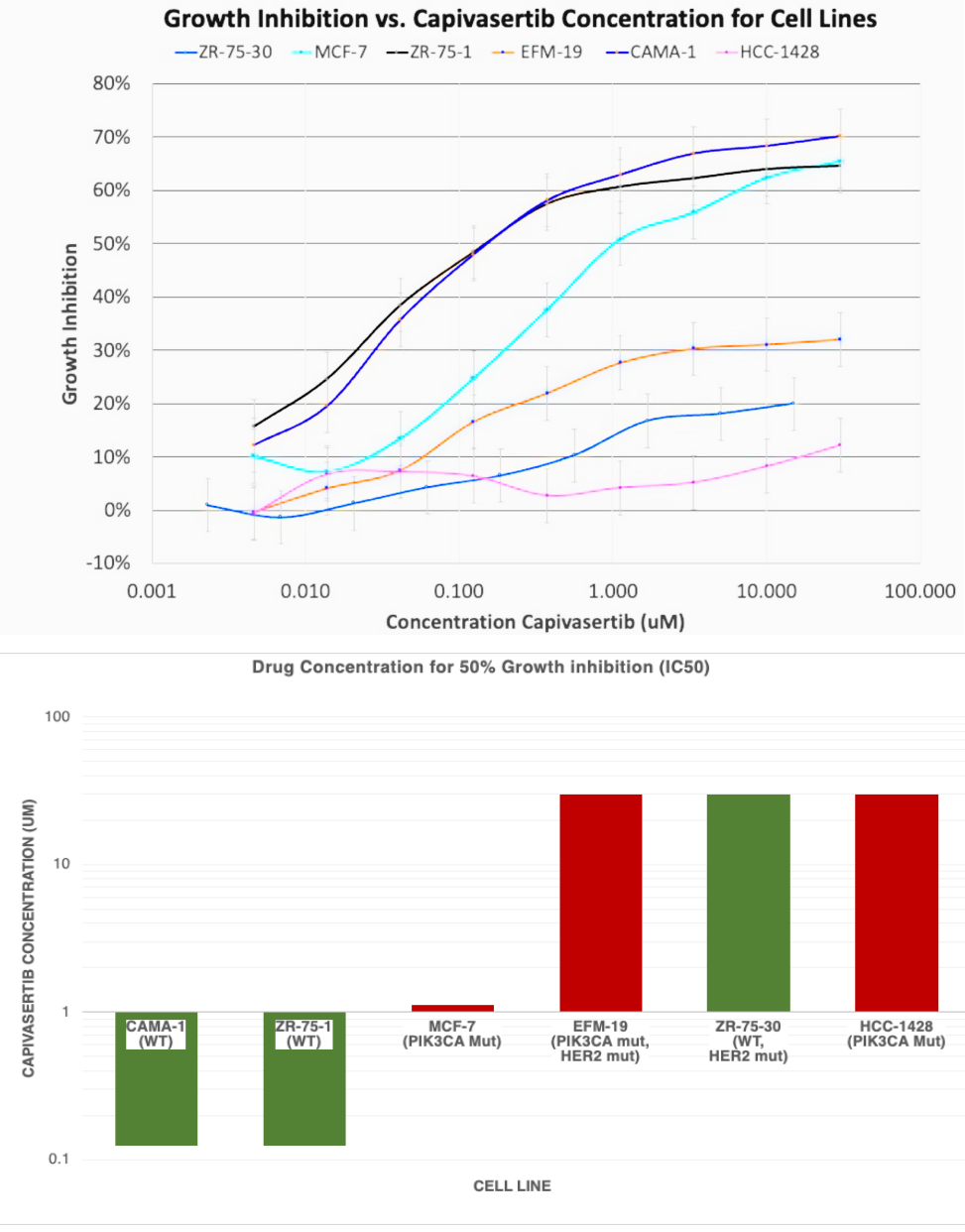

Figure 28. *Growth inhibition as a function of capivasertib dose in breast cancer cell lines.* Top: Dose-response curve for capivasertib vs. growth inhibition. Bottom: Calculated IC_{50} for the 6 breast cancer cell lines tested. WT = wild-type

Targeted analysis in cell lines reproduces the proteomic profile from patient samples.

As shown in Figure 29, hierarchical clustering separated sensitive (MCF-7, n=4) from resistant (HCC1428, n=2; ZR-75-30, n=2; EFM-19, n=5) *PIK3CA* or *AKT1*-altered cell lines on the basis of their expression of the proteins of interest. When a FDR-adjusted t-test was applied, assuming unequal variance, 3 proteins (CBR1, HSP90AB1, HSPB1) were found to be significantly downregulated in the resistant cell lines and 14 were upregulated (FC>1.5, FDR-adjusted p-value<0.05). Boxplots of concentrations observed in each group are shown in Figure 30 for a few proteins of interest. The proteomic profile observed in the capivasertib-resistant cell lines was found to closely match the profile observed in the tumours of patients in the NCB group (Table 10). Of the 22 protein concentrations that best discriminated between sensitive vs. resistant cell lines, 17 (77%) showed the same trend (high or low) as detected in the patient study.

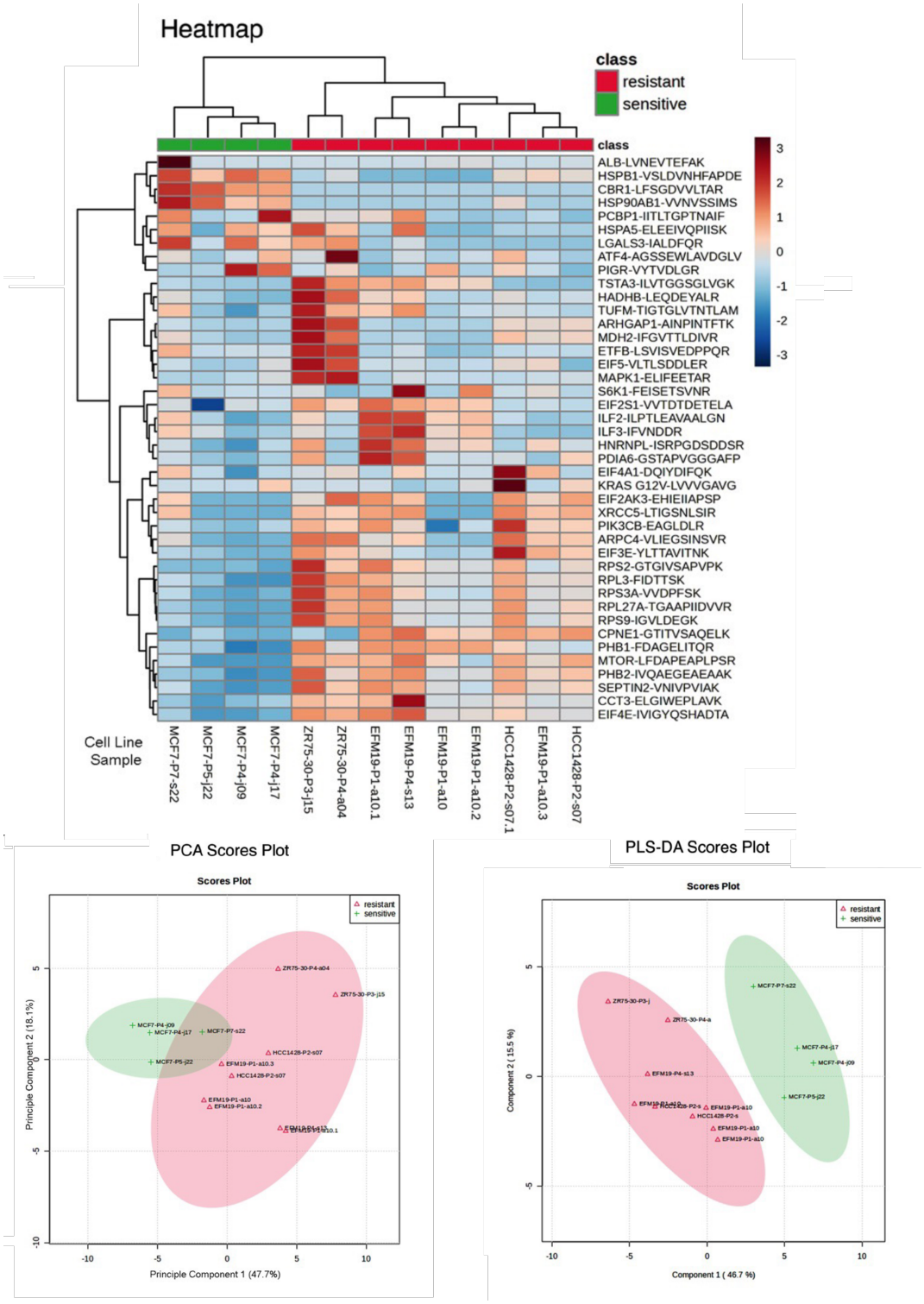

Figure 29. *Statistical analysis of targeted protein quantitation in capivasertib-sensitive (green) and capivasertib-resistant (red) HR+ PIK3CA-altered breast cancer cell lines.*
(top) Heatmap of protein concentrations quantified by MRM-MS with hierarchical clustering. (bottom left) Principal Components Analysis (PCA). (bottom right) Partial Least Squares – Discriminant Analysis (PLS-DA) plot.

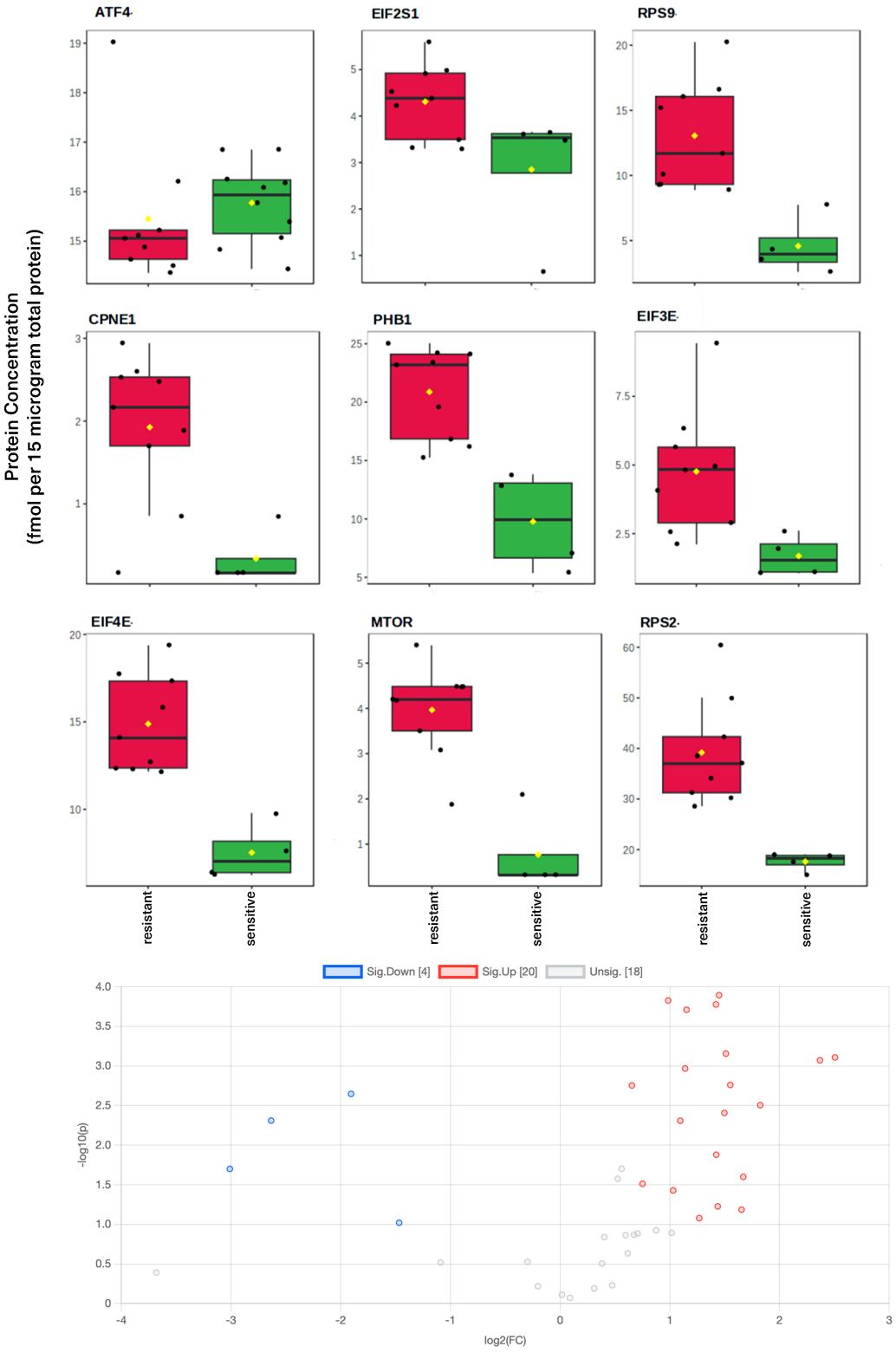

Figure 30. *Protein concentrations in capivasertib-sensitive vs. -resistant cell lines*

Table 10. *Protein expression differences in capivasertib-resistant vs. -sensitive cells compared to the profile observed in patient samples*

VIP Rank	Protein	FC (res/sen)	p-value	Expression: Resist/Sensitive	Expression: NCB vs. CB
1	CBR1	0.16	0.0049	↓	↑
2	HSP90AB1	0.12	0.0200	↓	↑
3	**PHB2**	2.73	0.0001	↑	↑
4	**MTOR**	5.16	0.0008	↑	pred. activated
5	HSPB1	0.27	0.0023	↓	↑
6	**EIF4E**	1.98	0.0001	↑	pred. activated
7	**SEPTIN2**	2.93	0.0017	↑	pred. activated
8	**PHB1**	2.14	0.0049	↑	↑
9	**RPL27A**	2.68	0.0002	↑	↑
10	**RPS2**	2.22	0.0002	↑	↑
11	**RPL3**	3.54	0.0031	↑	↑
12	**RPS9**	2.85	0.0007	↑	↑
13	**RPS3A**	2.20	0.0011	↑	↑
14	**CPNE1**	5.68	0.0008	↑	↑
15	**CCT3**	1.57	0.0018	↑	↑
16	**EIF3E**	2.82	0.0039	↑	pred. activated
17	**ARPC4**	2.68	0.0132	↑	↑
18	HNRNPL	1.47	0.0199	↑ (?)	↑
19	EIF2S1	1.51	0.1374	↑ (?)	pred. activated
20	LGALS3	0.36	0.0954	↓ (?)	↑
21	XRCC5	2.41	0.0834	↑ (?)	↑
22	EIF2AK3	2.71	0.0593	↑ (?)	pred. activated
23	**PDIA6**	1.44	0.0266	↑	↑
24	**HADHB**	2.04	0.0373	↑	↑
25	**TSTA3**	3.18	0.0252	↑	↑
26	PIK3CB	1.68	0.0308	↑	-
27	PIGR	0.47	0.3024	↓ (?)	low
28	PCBP1	0.81	0.2971	-	↑
29	TUFM	1.32	0.1445	-	↑
30	ILF2	1.63	0.1303	↑ (?)	↑
>30	ALB	0.08	0.4066	↓ (?)	low
>30	ARHGAP1	3.15	0.0652	↑ (?)	↑
>30	ATF4	1.01	0.7743	-	pred. activated
>30	EIF4A1	1.53	0.2321	↑ (?)	pred. activated
>30	EIF5	2.02	0.1280	↑ (?)	pred. activated
>30	ETFB	1.06	0.8466	-	↑
>30	HSPA5	0.87	0.6022	-	-
>30	ILF3	1.30	0.3118	-	↑
>30	MAPK1	1.60	0.1352	↑ (?)	pred. activated
>30	MDH2	1.83	0.1188	↑ (?)	↑
>30	S6K1	1.24	0.6434	-	pred. activated

Investigating the mechanism of capivasertib sensitivity in cell lines

Preliminary analysis of timecourse proteomics after capivasertib exposure. Each cell line was incubated with capivasertib at the cell line's observed IC_{15} (see Table 11) for up to 5 days. For each cell line, 2 of 3 collected timecourse replicates were analyzed using the MRM-MS method. Heatmaps of this data are shown in Figures 31 and 32. Visual inspection suggests there may be differences in the treated and control samples for MCF-7 (where many targets are decreased after drug exposure) and for HCC-1428 (where many appear increased, confirmed in Figure 33 and 34). All other cell lines show significant variability was observed between replicates.

Additional features of interest will be identified by calculating protein concentration changes on a within-replicate basis by dividing the concentration in the capivasertib-treated plate by the concentration in the matching DMSO-treated plate. As shown in Figure 35, using this approach, proteins with FC>2 at any timepoint can be flagged to see if the trend is conserved across replicates from the same cell line. Proteins that are consistently differentially modulated in a given cell line after capivasertib exposure vs. DMSO-alone will be further investigated.

Table 11. *Doses assigned to each cell line in timecourse study*

Cell line	Published sensitivity to capivasertib	Observed ICs	Concentration for timecourse
HCC-1428	HIGH SENSITIVITY (GI_{50}: 0.15 µM)	IC_{50}: >30 µM IC_{15}: 30 µM	30 µM AZD5363
MCF-7	INT SENSITIVITY (GI_{50}: 1.6, 1.3 µM)	IC_{50}: 0.95 µM IC_{15}: 0.014 µM	0.01 µM AZD5363
EFM-19	RESISTANT (GI_{50}: >8 µM)	IC_{50}: >15 µM IC_{15}: 0.125 µM	5.0 µM AZD5363
CAMA-1	HIGH SENSITIVITY (GI_{50}: 0.04, 0.08, 1 µM)	IC_{50}: 0.125 µM IC_{15}: 0.005 µM	0.005 µM AZD5363
ZR-75-1	INT SENSITIVITY (GI_{50}: 0.1, 1.5 µM)	IC_{50}: 0.125 µM IC_{15}: 0.005 µM	0.005 µM AZD5363
ZR-75-30	RESISTANT (GI_{50}: >8 µM)	IC_{50}: >15 µM IC_{15}: 1.7 µM	5.0 µM AZD5363

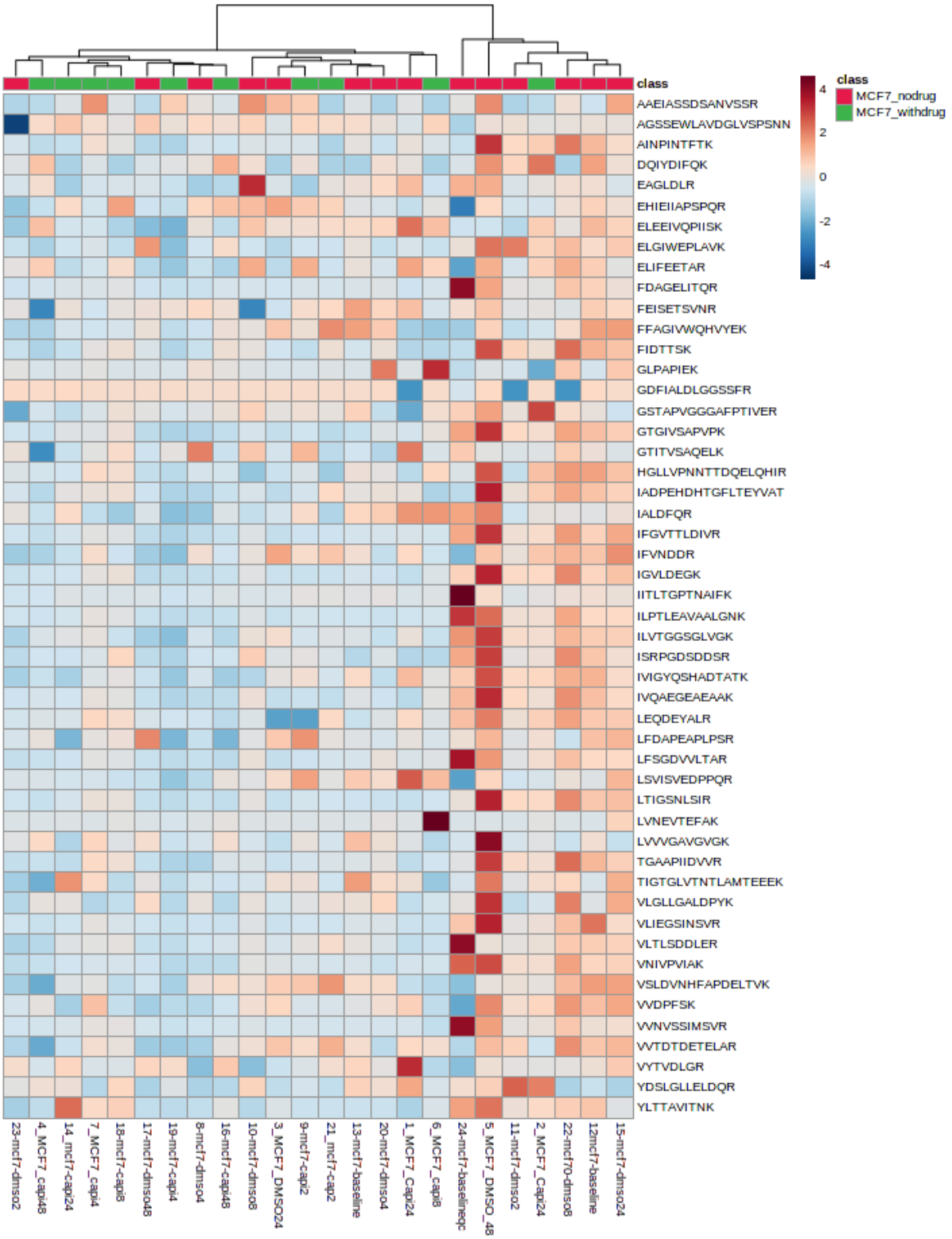

***Figure 31**. Heatmap of protein concentrations in MCF-7 after capivasertib exposure*

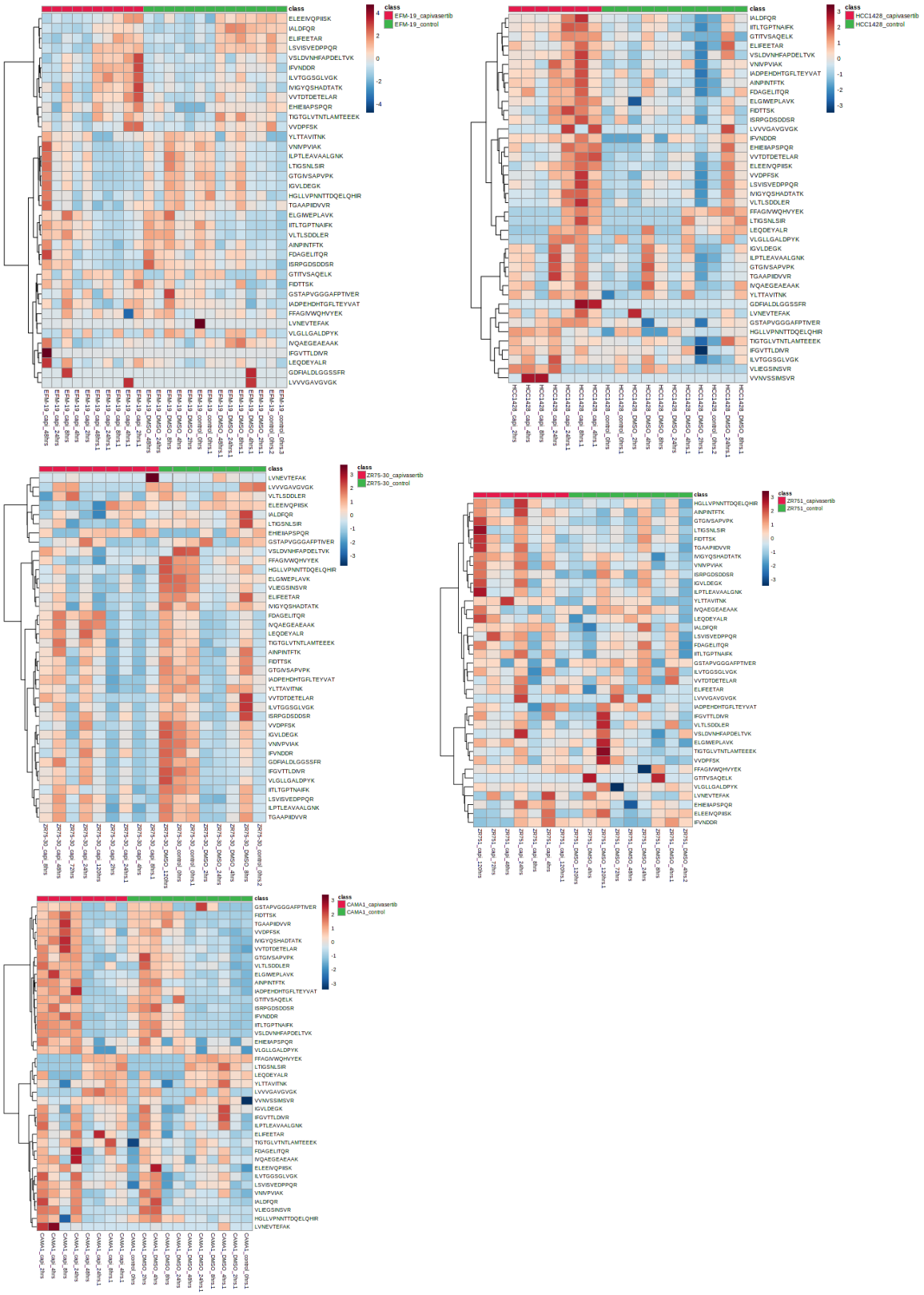

Figure 32. *Heatmaps of protein concentrations after capivasertib exposure in additional cell line*

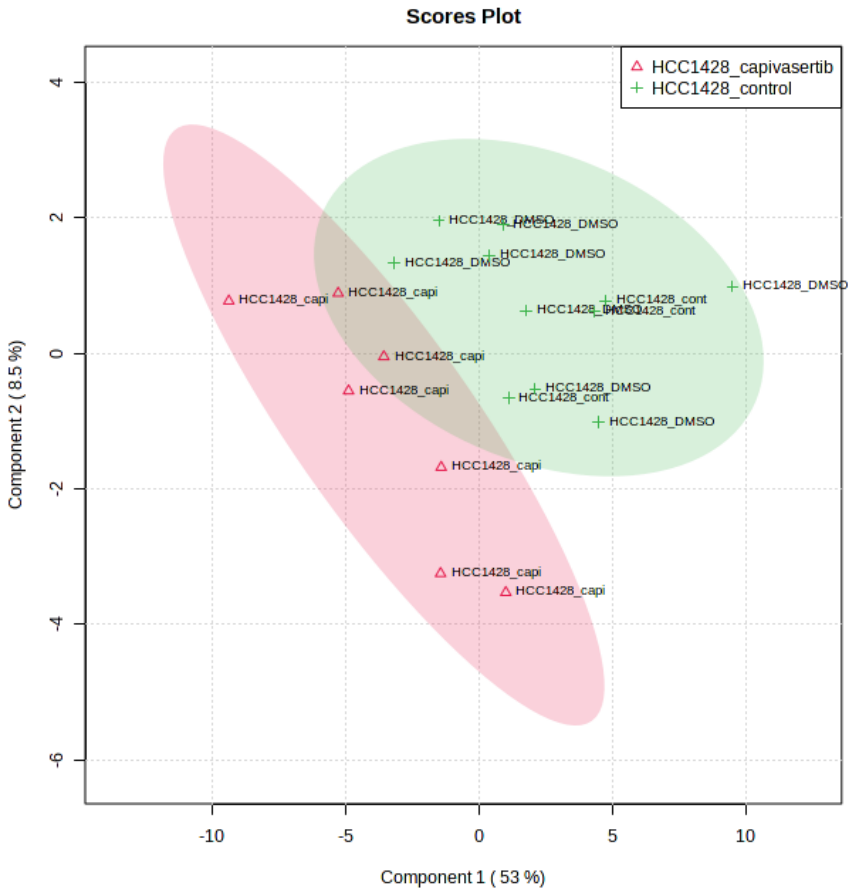

Figure 33. *PLS-DA demonstrating separation of treated vs. untreated HCC-1428*

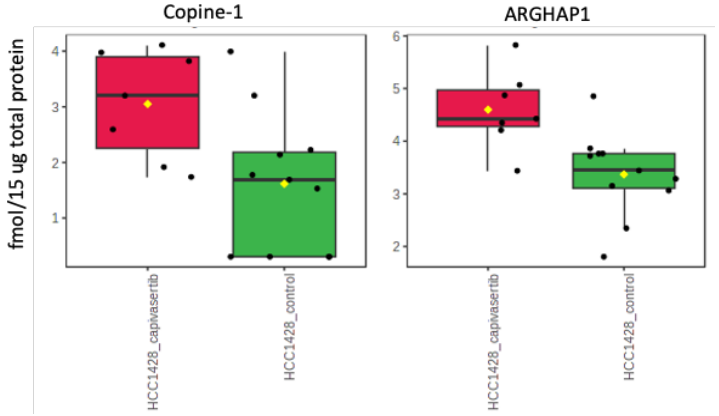

Figure 34. *Sample proteins with concentration increase in HCC-1428 after drug exposure.*

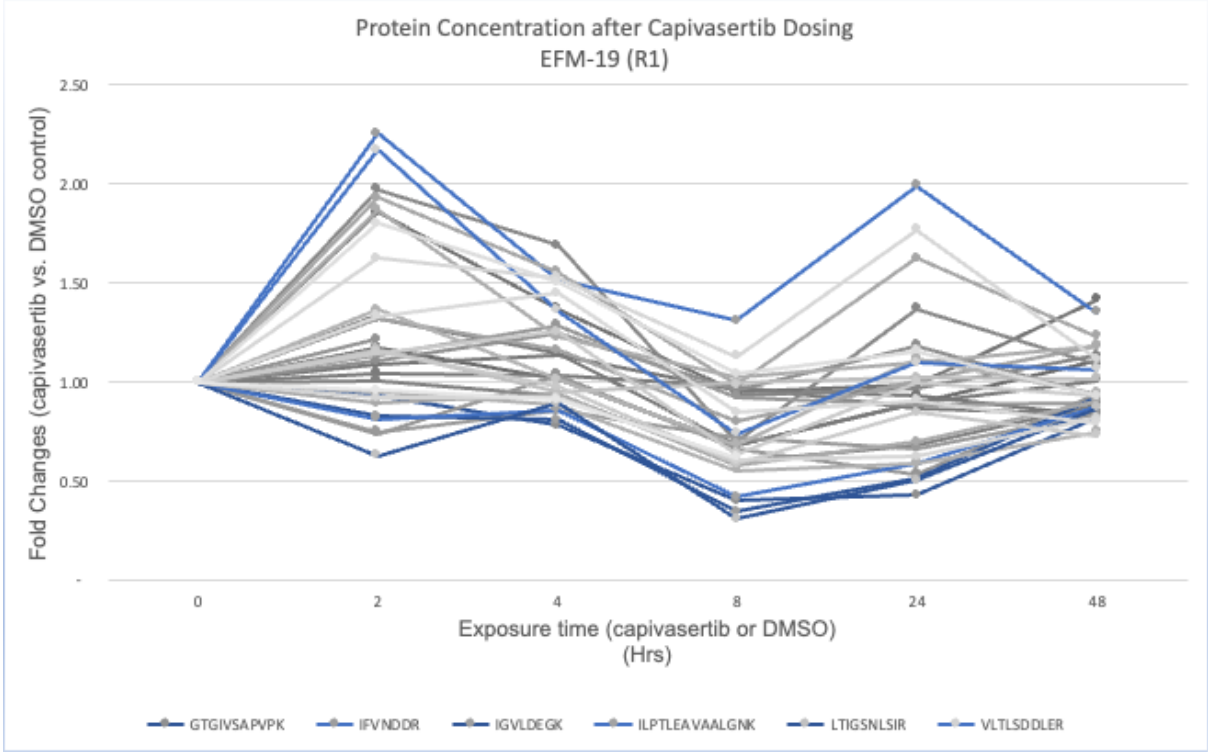

Figure 35. *Plot of protein concentration changes after capivasertib exposure in EFM-19 for use in identifying features modulated by drug exposure*

Co-treatment with EIF2 inhibitor ISRIB does not appear to increase capivasertib sensitivity.

Combination treatment of the ISRIB PERK/eIF2α inhibitor was tested using a matrix of concentrations to assess for synergistic effects. This approach was first applied to HCC-1428 using 5 independent replicates, measured by a standard Alamar blue cytotoxicity assay at 72 hours. Synfinder calculated the synergy score and provided visualization of the results, as shown in Figure 36. Across all replicates, Synfinder's average reported synergy score was -1.19 +/- 3.067, with a max reported value for any area of the plot at 12.1. These numbers represent the excess response as compared to simply an additive effect between the drugs (e.g., a score of 10 represents a response 10% greater than expected). Therefore, no synergy was detected for HCC-1428. Given the inadequate evidence from our other experiments that eIF2α is a mechanism of resistance to capivasertib in these *PIK3CA*-altered cancers, combination testing of the other resistant cell lines was postponed.

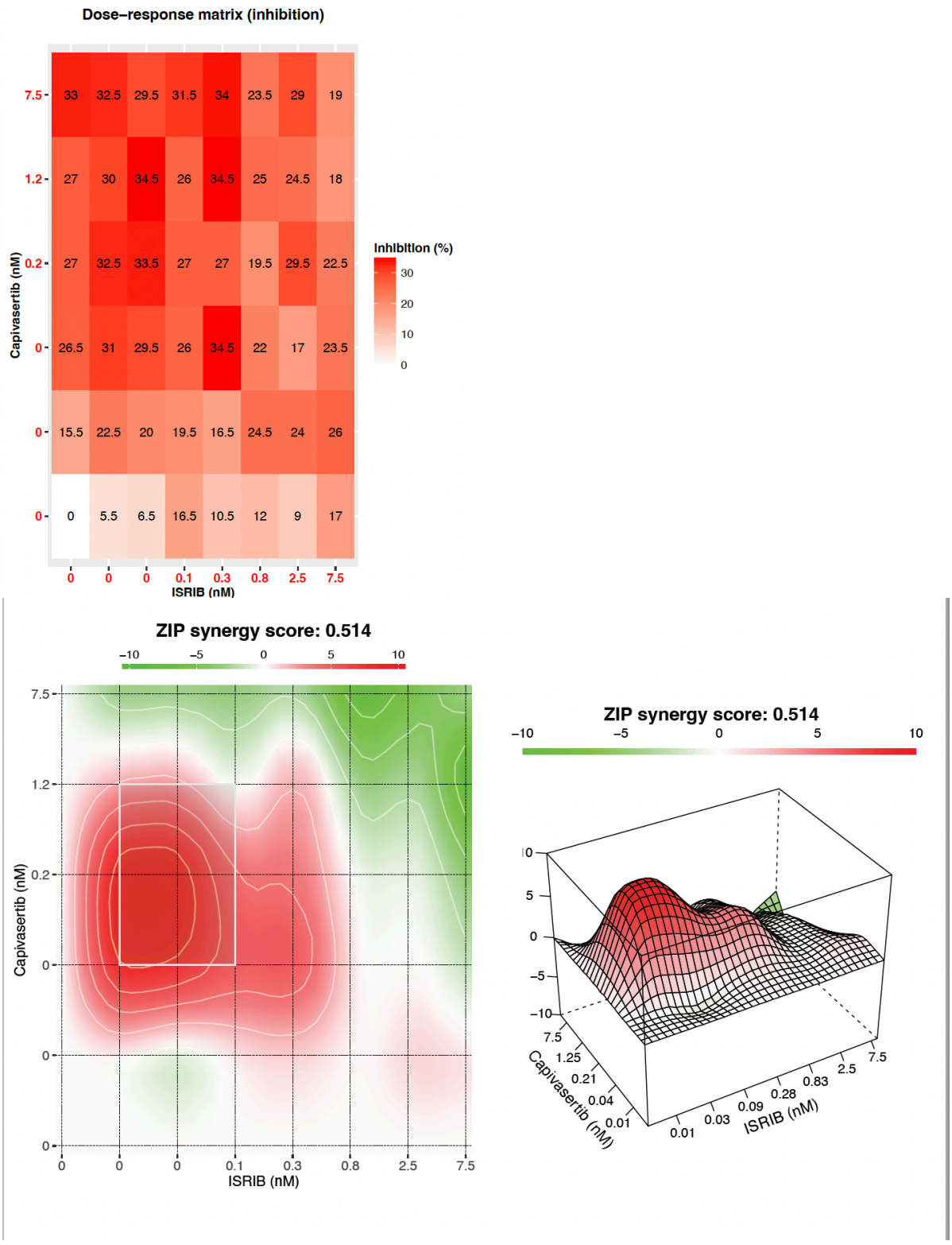

Figure 36. *Synfinder scoring of synergy between capivasertib and ISRIB*

Feasibility assessment in patient tumour samples

PRM assay development. Assays for 50 peptides were adapted to the EvoSep-Q-Exactive-MS. Assay performance characteristics, as compared to the 6495 are shown in Table 12. Samples of 3 different cell lines were initially analyzed for preliminary feasibility assessment. Of the tested PRM assays, 37 proteins demonstrated endogenous concentrations within the linear range when analyzed from 1 µg of total protein digest from cell line samples.

Table 12. *Assay performance characteristics – UPLC-MRM-MS vs. EvoSep-PRM-MS*

Parameter	UPLC-MRM-MS (Agilent 6495B)	EvoSep-PRM-MS (Q-Exactive)
Lower Limit of Quantitation (fmol on-column)	1-250	0.01-16
Upper Limit of Quantitation (fmol on-column)	500-2000	40-250
Linearity (R^2)	> 0.95	> 0.95
Typical CVs	<20%	<20%
Endogenous quantified within linear range (# of assays)	46/54	37/50
Total protein loading (µg)	25	1

Cohort. From the 40 consented patients, tumour blocks were obtained for 28. Others could not be obtained due to the material being exhausted, limitations associated with transferring the blocks from other hospital sites, or no suitable sample (e.g., fine needle biopsy only). Clinical details for the JGH patients whose samples were obtained are presented in Table 13. The characteristics of the cohort screened at the JGH appear similar to the enrolled clinical trial patients: 93% vs. 91% female, average age of 60.4 vs 63.0 at screening. Mutations were most commonly observed in breast cancer, with 44% of cases including a mutation. *PIK3CA* was the most commonly mutated gene, appearing with alterations in 25% of patient tumours. In total, 32% of tumours were found to have *PIK3CA* or *AKT* mutations. Among this cohort, all detected mutations were identified by NGS (used for 12 samples), whereas none were identified in the patients tested by real-time PCR of AKT1 and PIK3CA SNPs (n=9). Of the patients with mutation-positive tumours, 3 patients ultimately enrolled in the study.

Table 13. *Descriptive statistics for the JGH patient samples analyzed.*

	PI3K Mutation Neg (n=19)	PI3K Mutation Pos (n=9)	All (n=28)
Clinical Information			
Female (n=___)	17	9	26
Patient BMI	28.2 ± 5.2	26.7 ± 4.8	28.1 ± 5.0
Patient age (years)	60.4 ± 15.0	60.3 ± 18.3	60.4 ± 15.5
Cancer Type			
Breast (n=__)	10	8	18
Gynecological (n=__)	5	1	6
Other (n=__)	4	0	4
Mutations identified			
PIK3CA (n=__)		7	7
AKT (n=__)		2	2
PTEN (n=__)		0	0
Sample Characteristics			
Sample site			
Metastatic (n=__)	4	2	6
Primary (n=__)	13	4	17
Unknown (n=__)	2	3	5
Storage time (years)	10.5 ± 3.6	10.5 ± 5.3	10.5 ± 4.1
Cellularity (% tumour cells)	76 ± 23	78 ± 17	76 ± 21

Values are given as mean ± standard deviation unless otherwise specified.

The analyzed samples had an average tumour cellularity of 76%, similar to the FFPE tumour slices obtained from clinical trial patients in the previous chapter (63% cellularity). However, the patient samples obtained at the JGH had been stored for longer, with an average collection date >10 years before analysis. The JGH samples were also stored as blocks instead of slices.

While we initially applied xylene-based deparaffinization to extract these samples as shown in Figure 37, this was later substituted for hot water-based deparaffinization steps for ease of processing and better yield. The average yield of total protein using the hot water protocol was 69.8 +/- 12.9 µg for tumour cores and 75.4 +/- 31.9 ug for slices. Tumour cores appeared to yield slightly more protein content than cores from adjacent non-tumour areas (57.5 +/- 10.7 ug).

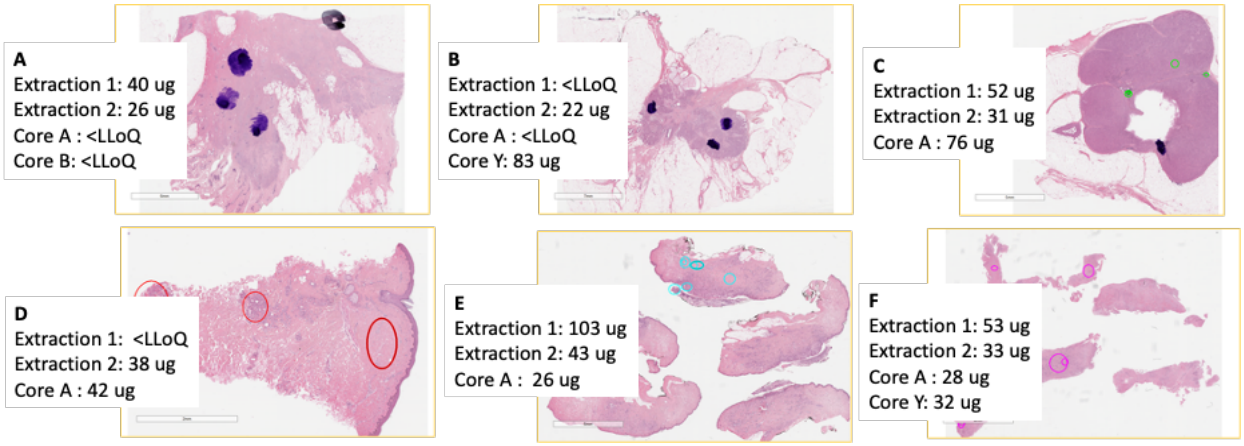

Figure 37. *Total protein yield of tumour slices & cores extracted by xylene deparaffinization*

Proteomic analysis of FFPE tumour samples from JGH patients. A total of 42 cores and unmounted slices representing 22 FFPE tumour samples were analyzed by PRM-MS on the EvoSep-Q-Exactive. For a subset of samples (n=8), we obtained both slices (n=14 total) and cores (n=12 total). Challenges with poor extraction and deparaffinization of thicker tumour slices initially hampered quantitation of AKT from JGH samples. However, quantitation in 1 mutation-negative breast cancer slice generated an AKT1 concentration of 0.42 fmol/µg total protein (Figure 38). The multiplexed PRM method was able to reproducibly quantify few of the targeted proteins from 1 µg total protein extracted from tumour FFPE. Of the 50 targeted proteins, 34 could be quantified at endogenous levels from at least 1 sample(s), but only 6 were quantified in more than half of the tested samples.

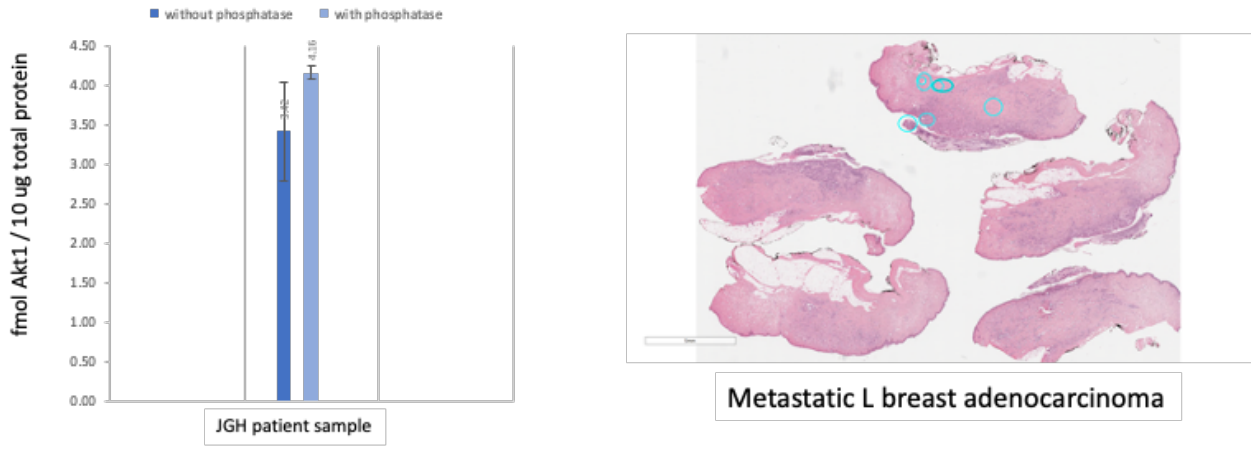

Figure 38. *AKT1 protein quantitation from a sample of metastatic left breast adenocarcinoma.*

Inter- and Intra-tumour variability of measured proteins

Measured protein concentrations were compared within and across tumour samples for the 7 proteins that were quantified from 10 or more samples. As shown in Figure 39, measurements of ILF3 and PHB1 demonstrated limited variability when measured from tumours vs. slices vs. stroma, but also showed little inter-tumour variability. EIF2S1 and EIF6 showed greater inter-tumour variability, while maintaining higher reproducibility between different samples from the same tumour block. Both LGALS3, HSPB1, and ALB were found to have very high variation between samples from the same tumour, obscuring potential comparison between tumours. ALB in particular was quantified at levels up to 100x higher in some tumour cores than from slices or tumour-adjacent cores from the same block. As shown in Table 14, there was an overall trend toward a higher concentration of the proteins when measured from tumour core extracts versus when measured from non-tumour cores or slices of the complete tissue area.

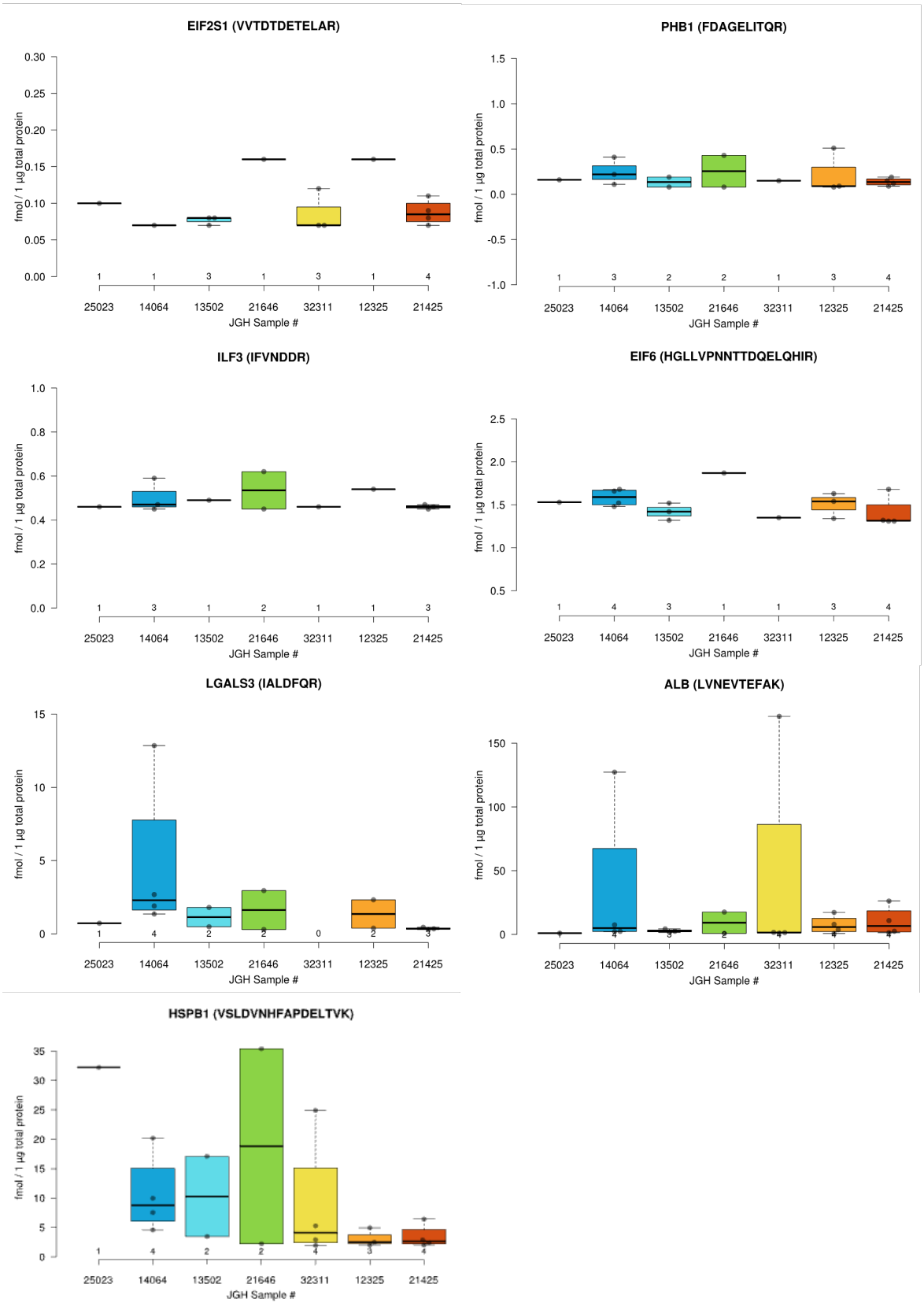

Figure 39. *Inter- and intra-tumour variability of proteins quantified from cores and slices of JGH tumour blocks.*

Table 14. *Peptide concentrations (fmol/µg total protein) in JGH patient samples.*

		PHB1	EIF6	LGALS3	ALB	HSPB1	EIF2S1	ILF3	RPL3
LLOQ	fmol on-column	0.07	1.31	0.22	0.76	1.85	0.07	0.45	0.10
ULOQ		237.97	221.10	234.94	225.43	232.77	192.29	196.18	657.15
JGH-25023	Core	0.16	1.53	0.72	1.01	32.21	0.10	0.46	-
	Slice	-	-	-	-	-	-	-	-
	Slice	-	-	-	-	-	-	-	0.87
JGH - 14064	Core	0.41	1.68	12.85	127.31	20.19	0.07	0.59	98.89
	Slice	-	1.48	1.35	2.43	4.59	-	0.45	-
	Slice	0.11	1.52	2.68	7.50	7.54	-	-	-
	Stroma	0.22	1.66	1.90	2.18	9.97	-	0.47	2.29
JGH-13502	Core	0.08	1.52	0.48	2.51	3.48	0.08	-	24.18
	Slice	-	-	-	-	-	-	-	7.47
	Slice	0.19	1.42	1.80	1.58	17.10	0.08	0.49	4.50
	Stroma	-	1.32	-	4.34	-	0.07	-	6.33
JGH - 21646	Core	0.43	1.87	2.95	17.57	35.37	0.16	0.62	9.48
	Slice	0.08	-	0.29	0.78	2.23	-	0.45	-
JGH - 29976	Slice	-	2.08	1.37	55.56	6.60	0.07	-	-
JGH-32311	Core	0.15	-	-	171.05	24.91	0.12	0.46	-
	Slice	-	1.35	-	1.58	5.28	0.07	-	-
	Slice	-	-	-	1.08	2.94	-	-	7.25
	Stroma	-	-	-	1.40	1.96	0.07	-	2.13
JGH-12325	Core	0.51	1.63	2.32	3.72	4.96	0.16	0.54	-
	Slice	-	-	-	17.28	-	-	-	-
	Slice	0.08	1.54	-	0.78	2.03	-	-	-
	Stroma	0.09	1.34	0.38	7.91	2.53	-	-	-
JGH-21425	Core	0.19	1.68	-	10.86	6.43	0.08	-	-
	Slice	0.12	1.31	0.34	2.49	2.43	0.09	0.46	-
	Slice	0.09	1.32	0.29	1.34	2.04	0.07	0.45	-
	Stroma	0.15	1.31	0.44	26.20	2.92	0.11	0.47	-
JGH-38049	Slice	0.24	1.38	-	38.07	4.99	0.085	0.46	-
Avg. Tumour core (n=7)		0.27	1.65	3.87	47.72	18.22	0.11	0.53	44.18
Avg. Non-tumour core (n=5)		0.15	1.41	0.90	8.41	4.34	0.08	0.47	3.58
Average Slice (n=15)		0.13	1.49	1.16	10.87	5.25	0.08	0.46	5.02

Interpretation

Development & validation of new MRM-MS assays

Performance of the new multiplexed MRM-MS assays was evaluated according to CPTAC guidelines. The assays have been demonstrated as fit-for-purpose under Tier II applications, with sufficient precision, stability, and reproducibility for pre-clinical research (149). Linear range and sensitivity were adequate for the majority (42/54) of the proteins of interest, 42 of which were consistently quantified at endogenous concentrations in cell line samples. Most assays (45/54) also demonstrated good to excellent precision and reproducibility when tested at levels spanning the linear range in a 5-day mini-repeatability experiment. The assays are therefore well-suited for their intended purpose of quantifying the proteins of interest from cell lines. Consultation of public resources (e.g., SRMAtlas, CPTAC Assay portal) supported identification of peptide targets with a low rate of attrition during assay development.

The newly-generated assay performance data were, in turn, submitted for public deposition in the CPTAC Assay portal. Only the linear range and mini-repeatability experiments are required for deposition into the CPTAC portal. However, the additional CPTAC experiments performed generated important data with respect to assay performance as shown in Table 15. The peptide for EIF6 with generally favourable assay characteristics was found in Experiment to have limited stability for storage beyond 4 weeks, which may be a consideration for clinical applications where samples are sometimes prepared over several weeks and then batched until analysis.

Through reproducible quantitation of the endogenous analyte, it was noted that while both peptides selected for MTOR showed similarly low variability in repeated quantitation from the endogenous sample, the inferred protein concentrations differed between the two: the concentration reported by VLGLLGALDPYK was more than double that of LFDAPEAPLPSR. Divergence between surrogate peptides from the same protein can occur due to differences in digestion efficiency, unanticipated modifications or variants, or instability of a peptide during sample preparation and digestion (308). Typically, when using multiple peptides to quantify a single protein, the assay with the better performance characteristics is selected to act as a quantifier (309). In this case, the mini-repeatability study demonstrated that LFDAPEAPLPSR more reliably quantified known quantities from quality control samples. Reassuringly, as shown in Figure 40, the two peptides are well-correlated (R^2>90%).

Table 15. *Summary of assay performance across different CPTAC experiments*

Gene name	Selected Peptide	Range	Repeatability	Stability	Reproducibility
AKT1	FFAGIVWQHVYEK	✓	X	✓	✓
AKT2	YDSLGLLELDQR	X	X	✓	-
ALB	LVNEVTEFAK	✓	✓	✓	✓
ARHGAP1	AINPINTFTK	✓	✓	✓	✓
ARPC4	VLIEGSINSVR	✓	✓	✓	✓
ATF4	AGSSEWLAVDGLVSPSNNSK	✓	<25%	✓	✓
CBR1	LFSGDVVLTAR	✓	<25%	✓	✓
CCT3	ELGIWEPLAVK	✓	<25%	✓	✓
CPNE1	GTITVSAQELK	✓	✓	✓	<30%
EIF2AK3	EHIEIIAPSPQR	✓	✓	✓	✓
EIF2S1	VVTDTDETELAR	✓	✓	✓	✓
EIF3E	YLTTAVITNK	✓	✓	✓	✓
EIF4A1	DQIYDIFQK	✓	<25%	✓	✓
EIF4E	IVIGYQSHADTATK	✓	✓	✓	<30%
EIF5	VLTLSDDLER	✓	✓	✓	✓
EIF6	HGLLVPNNTTDQELQHIR	✓	✓	<4 weeks	<30%
ETFB	LSVISVEDPPQR	✓	✓	✓	✓
HADHB	LEQDEYALR	✓	✓	✓	✓
HK1	GDFIALDLGGSSFR	X	X	✓	-
HNRNPL	ISRPGDSDDSR	✓	X	✓	✓
HSP90AB1	VVNVSSIMSVR	✓	<25%	✓	✓
HSPA5	ELEEIVQPIISK	✓	✓	✓	✓
HSPB1	VSLDVNHFAPDELTVK	✓	<25%	✓	<30%
IGHG2	GLPAPIEK	✓	✓	✓	-
IGKV4-1	LLIYWASTR	X	X	✓	-
ILF2	ILPTLEAVAALGNK	✓	✓	✓	<30%
ILF3	IFVNDDR	✓	✓	✓	✓
KRAS mut	LVVVGAVGVGK	✓	✓	✓	✓
LGALS3	IALDFQR	✓	✓	✓	✓
MAP4K4	VYPLINR	✓	✓	✓	-
MAPK1	ELIFEETAR	✓	✓	✓	✓
MAPK3	IADPEHDHTGFLTEYVATR	✓	X	✓	✓
(p)MAPK3	IADPEHDHTGFLTE(pY)VATR	✓	<25%	✓	-
MDH2	IFGVTTLDIVR	✓	X	✓	✓
MTOR	LFDAPEAPLPSR	✓	✓	✓	✓
	VLGLLGALDPYK	✓	X	✓	✓
PCBP1	IITLTGPTNAIFK	✓	<25%	✓	✓
PDIA6	GSTAPVGGGAFPTIVER	✓	✓	✓	✓
PHB1	FDAGELITQR	✓	✓	✓	✓
PHB2	IVQAEGEAEAAK	✓	✓	✓	✓
PIGR	VYTVDLGR	✓	✓	✓	✓
PIK3CB	AAEIASSDSANVSSR	X	✓	✓	-
	EAGLDLR	✓	✓	✓	<30%
RPL27A	TGAAPIIDVVR	✓	✓	✓	✓
RPL3	FIDTTSK	✓	✓	✓	✓
RPS2	GTGIVSAPVPK	✓	✓	✓	✓
RPS3A	VVDPFSK	✓	✓	✓	✓
RPS9	IGVLDEGK	✓	✓	✓	✓
S6K1	FEISETSVNR	✓	✓	✓	-
SEPTIN2	VNIVPVIAK	✓	✓	✓	✓
TSTA3	ILVTGGSGLVGK	✓	✓	✓	✓
TUFM	TIGTGLVTNTLAMTEEEK	✓	X	✓	✓
XRCC5	LTIGSNLSIR	✓	X	✓	-

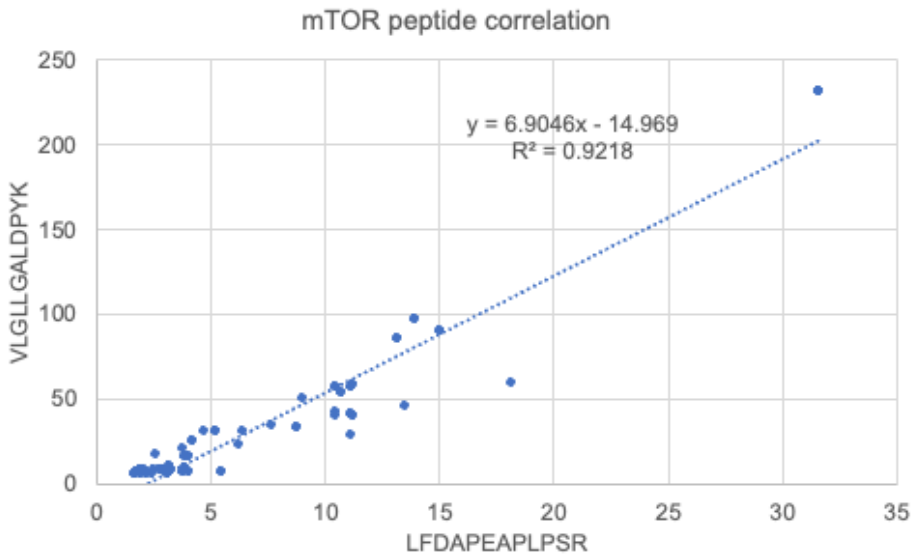

Figure 40. *Correlation of 2 mTOR peptides each measured in 80 cell line samples*

New evidence to better understand mechanism underlying capivasertib resistance

A similar proteomic profile is detected in two independent models using orthogonal methods

To further investigate the possible association of the identified proteins and pathways with capivasertib response, we then implemented the validated assays to quantify the proteins of interest (n=29) and related targets (n=16) with high precision and reproducibility from cell lysates. The multiplexed panel was applied to samples from HR+ breast cancer cell lines with known activating *PIK3CA* or *AKT1* alterations published in COSMIC. The cell lines were confirmed *in vitro* to be capivasertib-sensitive (MCF-7, n=4) or capivasertib-resistant (HCC-1428, ZR-75-30, EFM-19, n=9 total). Remarkably, the observed pattern of changes in protein expression was highly conserved between the patient tumour samples and the cell line model. Figure 41 depicts selected cancer-associated canonical pathways. The proteomic signature previously observed in the “no clinical benefit” group is depicted as orange (activation) and blue (inhibition). Overlaid in red are the differences in protein concentration subsequently confirmed with MRM-MS in capivasertib-resistant cell lines.

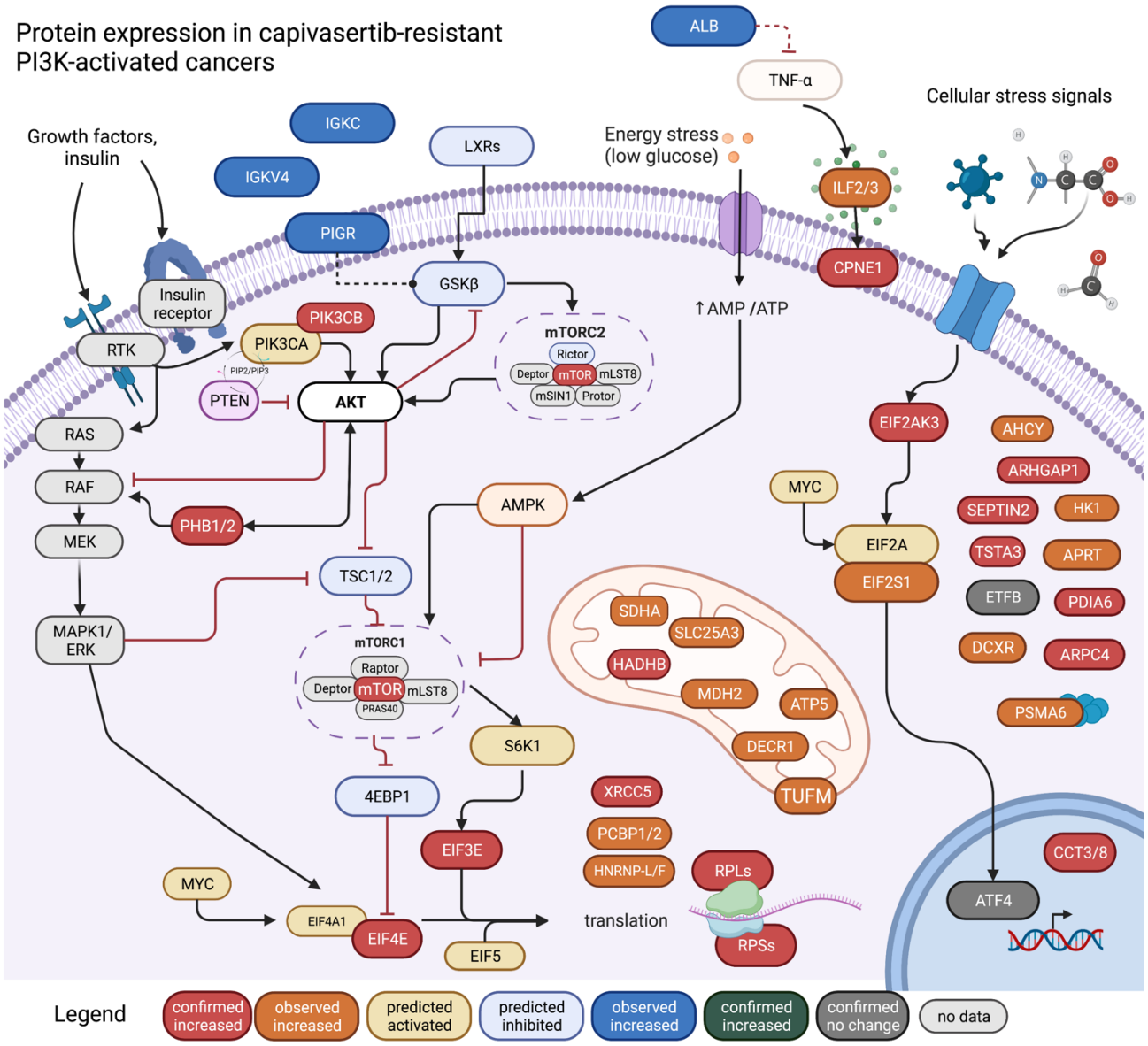

Figure 41. *Pathway schematic depicting proteins differently regulated in capivasertib-resistant cancers, as observed in both patient tumours and breast cancer cell lines.*
Proteins with expression changes confirmed (FC>1.3, p<0.1) by MRM-MS data in cell lines are shown in red (increased), dark grey (no change), and green (decreased). Proteins with expression data from label-free quantitation (LFQ) in patient tumour samples are shown in dark orange (increased) and dark blue (decreased). Light orange (activated) and light blue (inhibited) indicate proteins with predicted activity changes based on the LFQ data. Proteins with no expression data are shown in light grey.

The reproducibility of this profile across two orthogonal proteomics approaches and two fully independent models lends significant credibility to the proteins' relationship to capivasertib sensitivity. While the relationships between the analyzed proteins are complex, the sum of the evidence supports increased GSKβ/mTORC2-driven AKT activation in capivasertib-sensitive cancers versus increased downstream mTORC1-driven translation in capivasertib-resistance.

Teasing apart the roles of EIF2- and EIF4-driven translation in capivasertib resistance

Results from the targeted assay panel further provide vital evidence against attributing the observed increase in translational activity specifically to EIF2 signaling. When quantified directly, expression of ATF4 – the protein directly downstream from eIF2α and responsible for transducing EIF2-driven translation -- is near-identical between resistant and sensitive cell line samples. Previous studies suggest ATF is expressed in response to cellular stressors, and that high ATF protein levels are associated with cancer aggressiveness (310,311). Unlike many other cancer pathway proteins, ATF4 is specifically modulated through expression changes instead of through activation (e.g., by phosphorylation) (312). The absence of increased ATF4 in the resistant group therefore clearly signals that other translational control pathways are the more likely effectors of capivasertib resistance this dataset. This result is further supported by the finding that an eIF2α inhibitor did not yield synergistic effects when tested with capivasertib in a combination cytotoxicity assay applied to the capivasertib-resistant HCC-1428 cell line. ISRIB (trans-isomer, SelleckChem, S7400) is a selective eIF2α inhibitor and does not have global effects on translation, transcription, or mRNA stability in non-stressed cells (313).

Comparing the expression of EIF2-associated proteins (EIF2S1 and ATF4) after capivasertib exposure capivasertib-sensitive MCF-7 and capivasertib-resistant HCC-1428 in the timecourse samples (Figure 42), eIF2α concentration is higher at baseline in HCC-1428 and appears to climb in HCC-1428 at the 2hr and 4 hr timepoints, while MCF-7 remains flat with much lower variability. ATF4 expression is quantified in MCF-7 and may rise after drug exposure, whereas it remains <LLOQ in HCC-1428 throughout. This suggests that although eIF2α is present at higher levels in HCC-1428, contrary to our expectation, EIF2 signaling is not active to drive ATF4 expression. The large-scale endeavour of analyzing all replicates from this study continues, so additional data will help to confirm this result.

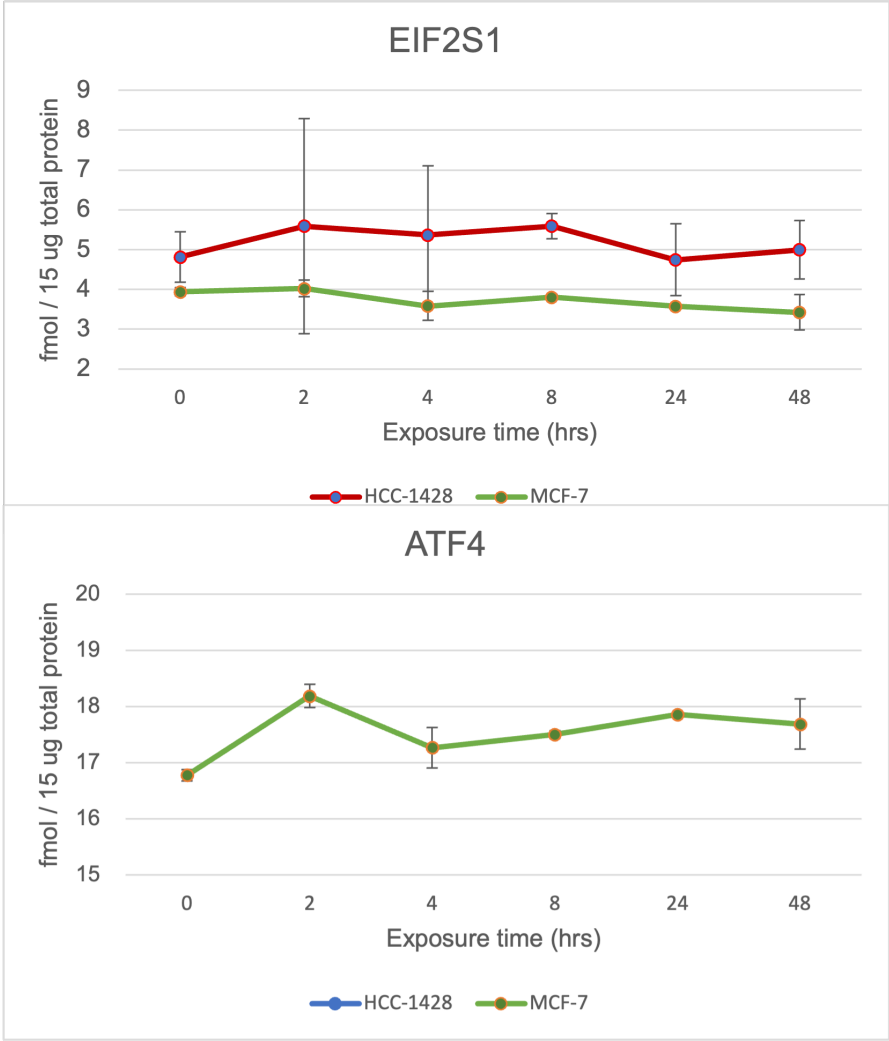

Figure 42. *eIF2a & ATF4 concentrations post-capivasertib in MCF-7 & HCC-1428*

The targeted proteomics data may also hint at a role for the MEK/ERK pathway. The prohibitins (PHB1/2), whose higher expression was confirmed in the capivasertib-resistant cells, appear to play an important role as well. PHBs are known to complex with RAF1 to activate the MEK-ERK pathway (262), which was recognized early as a potential mechanism of resistance to AKT inhibition (263). PHBs also activate a positive feedback mechanism to increase AKT activity (314). Pleiotropic PHB2 even plays a key role in ribosome biogenesis (315). Overall, the observed protein expression patterns are consistent with AKT activation in both groups -- as would be expected in PIK3CA-mutated tumours – but significant differences in downstream mTORC1-activation are evident.

Adaptation of assays for use with clinical samples

Further assay optimization is needed

While preliminary development suggested that most developed assays might be readily adapted for PRM-MS, results from the first analysis of patient samples were disappointing. This may be due in part to poor instrument performance on the day of analysis – despite performing multiple retention time checks before analyzing clinical samples, larger-than-typical retention time shifts were observed when the data were analyzed. Moreover, the peptides' LLOQs as determined from the calibration curve on the day of sample analysis were, on average, 6x higher than those observed during initial assay development.

While low-flow chromatography provides the potential for sensitivity gains, this increased sensitivity must also compensate for the lower loading volume, which is restricted to 1 µg total protein as compared to the 15-20 µg loadings used for MRM-MS of cell lines. It is established that up to 30% of protein targets may suffer from poor stability or extraction from FFPE samples (316), and this effect may be exacerbated by the very long storage of these samples. Finally, while cell lines function as a model of cancer, the process of immortalization and culturing, together with their unnaturally high purity, may result in higher expression of cancer proteins than that seen in real tumour samples. Together, these effects may help to account for the large number of samples and peptides with values below the LLOQ.

The large number of missing values, together with the small number of patients in this cohort, prohibited meaningful statistical analysis of protein concentrations with respect to the carefully-annotated clinical variables (e.g., genetics, site of sample – primary vs. metastatic, breast cancer vs. gynecological cancer, BMI and insulin resistance status). However, the high level of AKT1 measured by iMALDI-MS in a mutation-negative JGH sample suggests that indeed there are at least some instances of discordance between AKT levels and predictions based on genetics results.

Inter vs. intra-tumour heterogeneity as a considerations for biomarker development

Tumour blocks may be sectioned, cored, or micro-dissected to provide samples for analysis. While microdissection affords a high degree of control over the selected tissue, it currently remains impractical for large-scale implementation. For those assays that generated sufficient data, we sought to assess the reproducibility of quantitation from the same tumour

block when combined with different sampling approaches. Both inter- and intra-tumour variation showed significant disparities between the analytes. The results may be helpful for triaging targets for further research; suitable biomarker candidates will need to demonstrate higher inter-tumour variability over intra-tumour variability. The dramatic fluctuation in ALB and HSPB1 levels within tumour blocks will realistically prohibit interpretation of measurements, so it may be appropriate to drop these candidates from future panels.

In addition, the generally higher protein concentrations measured from tumour cores reveal that tumour cores likely offer better sampling, as they may maximize the contribution of cancer-associated proteins to the total protein content. The recently-developed hot water protocol generates good yields from most cores.

Study limitations

There is a widely-used adage that is most apt to the application of cell lines in research: "All models are wrong but some models are useful" (317). While entire theses could be written exclusively on the benefits and drawbacks of cell lines, they currently represent an irreplaceable tool in cancer research, particularly in cases where clinical samples are simply not available. Within our selections, HCC-1428 was expected to be sensitive based on published data but was confirmed resistant through cytotoxicity testing. It is unknown whether this is due to variations between stocks, acquired resistance, or contamination with a different cell line. Nonetheless, this unexpected finding caused an imbalance in the sensitive vs. resistant groups, so that MCF-7 was the only representative of capivasertib sensitivity. This creates an important bias in the statistical analysis, because although we did seek to incorporate real biological replicates of MCF-7 by using multiple different passages for our experiments, the samples are still closely related. Using MCF-7 to generate an acquired resistance model while storing proteomics samples from each passage could be a useful alternative design, which would allow any sensitive cell line to act as its own control. More generally, the cell lines do not allow for any assessment of the generalizability to PI3K-wt tumours. ZR-75-1 and MCF-7 are also typically sensitive to endocrine therapies such as fulvestrant and tamoxifen, so they do not mirror the AZ study population in this aspect. However, as capivasertib is increasingly used in combination therapies in earlier stages of treatment, this may be of interest.

With respect to protein quantitation by MRM-MS, even well-validated assays cannot claim "absolute" quantitation, since they depend on the use of synthetic peptides as opposed to the

protein standards that would be needed to control for digestion efficiency. In either case, the accuracy of quantitation of the external calibration standard (e.g., by AAA, CZE) inevitably impact the final protein measurement. The analysis of protein concentrations normalized to total protein is similarly dependent on the performance of the BCA assay. Further optimization and testing of the PRM assays will doubtlessly be required before further clinical sample analysis. Had validation experiments been performed in advance, similar to what was done for the PRM assays, the assay limitations and inconsistent performance of the EvoSep-Q-Exactive would likely have been identified sooner.

Results Chapter 3:
A simplified Geneva cocktail approach measures diet-associated CYP450 activity for optimizing cancer drug dosing

Chapter Summary

The cytochrome P450 enzyme subfamilies, including CYP3A4 and CYP1A2, play a major role in metabolism of a range of drugs including several anti-cancer treatments. Many factors including environmental exposures, diet, disease-related systemic inflammation, and certain genetic polymorphisms impact the activity of these enzymes. As a result, the net activity of each enzyme subfamily can vary widely between individuals and in the same individual over time. This variability has potential major implications for treatment efficacy and risk of drug toxicity, but there are currently no assays available to guide routine clinical decision-making.

To address this, we implemented a streamlined mass spectrometry-based method to measure activities of CYP3A4 and CYP1A2 based on single timepoint testing. The assay was also adapted for use with dried blood spots to facilitate clinical implementation. The validated assay was applied to samples from 10 participants. The participants are considered "free-living" in that they were not subject to diet, medication, or lifestyle restrictions, or exclusion on the basis of health conditions. The assay results were compared with the predicted activity of each enzyme, based on a self-report tool capturing diet and medication intake.

The results confirmed the methodology is safe and feasible to perform in free-living volunteers using midazolam and caffeine as test substrates for CYP3A4 and CYP1A2 respectively. The measured CYP3A4 activity correlated with the predicted activity score obtained from the self-report tool. The results confirm the wide variation in CYP activity between individuals and the important role of diet and other exposures in determining drug metabolism.

The finding that "everyday" exposures can be linked to CYP activity and cancer drug metabolism provides another line of evidence for the thesis' central argument that genetics-only approaches, like pharmacogenetics, must be supplemented with metabolite and protein quantitation to achieve a full molecular picture of cancer and treatment response.

Context

The therapeutic window and "precision dosing" in cancer treatment

Challenges associated with narrow therapeutic index

One common impetus for the development of new targeted therapies is to overcome limitations associated with the narrow therapeutic window of chemotherapies. Classic chemotherapies are known for their toxicity and serious adverse effects, which make achieving optimally effective doses challenging (318). However, many new agents, including targeted inhibitors, face the same challenge. DrugBank Online (go.drugbank.com, Accession Number DBCAT003972) maintains a list of drugs that are known for their narrow therapeutic index (NTI), meaning that "small differences in dose or blood concentration may lead to …serious therapeutic failures or [serious] adverse drug reactions" (319). The list of 254 NTI drugs includes 160 drugs used in cancer treatment, including hormone-based therapies (e.g., Tamoxifen), mTOR inhibitors (e.g., Temsirolimus), other kinase inhibitors (e.g., Vandetanib, Ceritinib, Idelalisib), and many immunotherapies (e.g., Trastuzumab, Durvalumab, Blinatumomab), alongside traditional taxanes (e.g., Cabazitaxel, Docetaxel, Paclitaxel) (319). Capivasertib has been associated with serious adverse effect (AEs) including grade 3 or higher hyperglycemia, rash, and gastrointestinal events. (196) In a small Phase II trial of capivasertib in patients with *AKT1 E17K* mutations (n=35), 43% of patients required at least 1 AE-related dose modification, and 31% discontinued due to AEs (196). Dose optimization is therefore crucial for the effective cancer treatment irrespective of treatment response.

Precision dosing

The concept of "precision dosing" has therefore emerged to try to maximize efficacy while mitigating toxic effects of anti-cancer agents by tailoring doses or dosing intervals for individual patients (320). In the absence of robust biomarkers, this is often achieved by developing models that link specific clinical variables (e.g., age, sex, weight, body surface area, kidney or liver function, etc) or disease severity to specific doses or dose ranges (321). However, this approach may be overly simplistic for NTI drugs due to the potential for interactions between the dose-adjusting factors and the important role of patient-specific and tumour-specific differences in pharmacokinetics (318,321). It is further complicated by intra-patient changes in pharmacokinetics over time with aging, disease progression, drug exposure/tolerance, and

environmental exposures. Sophisticated models and algorithms have been developed to try to account for the wide array of factors involved in dosing of specific drugs. However, these are often subject to limited generalizability due to bias stemming from the particularities of the population in which they are developed (322). Moreover, this approach is research-intensive, complex, and algorithms are typically not suited to routine dose adjustments. A simpler and more practical solution for NTI drugs is to implement empirical approaches – those that seek to (directly or indirectly) measure drug metabolism levels. Effective methods for measuring patients' individual NTI drug exposure can not only remove some of the "guesswork" but potentially enable finer dosing adjustments, routine safety monitoring, and "real-time" dose re-tailoring as needed over the course of treatment.

Empirical approaches to dose optimization

While there is strong interest in therapeutic drug monitoring (TDM) methods to directly quantify administered cancer drugs, the approach is limited by the need for rigorous assay development and validation for each and every new drug (320). In some cases, many assays may even be required for a single drug in order to tackle all active or toxic intermediates, some of which may be unknown due to the diversity of drug metabolism pathways. The development of non-drug-specific patient characterization approaches is therefore important, including more comprehensive patient characterization to enhance routine care and guide cancer treatment dosing (320).

One example of the latter approach is to determine cytochrome P450 enzyme activity in individual patients. Most cancer drugs are metabolized by one or more of the cytochrome P450 enyzmes (CYPs) principally those located in the mitochondria or endoplasmic reticulum of liver cells (323,324). Changes in the activity of specific CYPs may lead to rapid degradation of the drug with failure to reach a therapeutic dose of the active metabolite (323). Alternatively, low clearance of the drug may dramatically increase toxicity (323). Inter-individual differences in CYP activity are not only observed, but have been altered treatment effectiveness and overall survival for both conventional chemotherapeutics and new targeted agents such as tyrosine kinase inhibitors (TKIs) (325-327). CYP activity characterization can therefore serve as a useful marker for "precision dosing". To date, clinical testing of CYP activity prior to, or during cancer treatment is not available and there is a pressing need to address this critical knowledge gap in advancing individualized cancer drug dosing.

Factors associated with changes in CYP activity

Genetics. Research in the area of CYP-based precision dosing initially focused heavily on a pharmacogenetic approach (328). By identifying presence of known CYP gene polymorphisms with different activities, the metabolism of drugs which were substrates for a given CYP subfamily was predicted (323,329,330). This approach showed some promise as genetic polymorphisms could, in some cases, be tied to treatment response (331). All CYP enzymes present in the liver microsome are expected to be polymorphic, suggesting significant potential for important findings (332). However, many genetic variants of interest are present at low frequency, genetic sampling presents challenges for clinical implementation, and results from one cohort often cannot be generalized to another (333-335). While this is often considered to be an issue with inter-population genetic variability (336), it could also be due in part to significant interactions with other factors that affect CYP activity. A genetics-only approach does not account for the large inter- and intra-individual differences in activity of CYP enzymes, due to induction or inhibition by environmental or disease factors.

Sex. In addition to genetic factors, other patient characteristics are associated with differences in CYP activity. For instance, several studies found that females exhibit higher CYP3A4 activity compared to males, when enzyme activity is directly measured (337-339). However, the significance of these differences is unclear, studies using a midazolam probe found that despite females' higher clearance, circulating midazolam levels were similar between female and male subjects (340,341). Conversely, CYP1A2 enzyme activity may be higher in males (337-339).

Age & weight. Other patient characteristics that vary over time, such as such as age, weight, inflammation nutritional status, and disease progression, can also significantly alter the level of CYP activity present over the course of treatment (342,343). Older age has been associated with reduced CYP450 enzyme activity, as well as reduced drug clearance and changes in liver size and perfusion (344-346). Obesity and diabetes have similarly been associated with reduced CYP activity, including lower clearance by CYP3A4 and CYP1A2 (347-349).

Disease progression, nutritional status & treatment resistance. Nutritional status has an enormous impact on cancer prognosis; cachexia and muscle-wasting significantly change the body composition and metabolism (347,350). Other, subtler nutritional effects are also commonly observed. For instance, Vitamin D deficiency is a common occurrence in cancer

patients (351,352). As a strong inducer of CYP3A4, Vitamin D supplementation can influence metabolism of cancer therapies (351,353). Vitamin C deficiency can similarly decrease CYP protein expression (354) and is also commonly observed in advanced cancer patients (355). Transitory changes in inflammation can also impact CYP-driven drug metabolism and this adopts special significance in the context of immunotherapies (356,357).

Over-expression of specific CYPs has been observed in tumours and progressive CYP over-activation is now implicated as a mechanism of resistance to cancer treatments (326,329,358). For instance, upregulation of CYP3A4 expression in cancer tissue is now a known mechanism of resistance to many anti-cancer treatments including treatment with TKIs (359). In fact, CYPs themselves are now under consideration as an independent target for therapeutic intervention (326,360,361).

Diet, drug-drug interactions & exposures. Drug-drug interactions, diet, natural health products, and other exposures such as smoking are all well-known to play an important role in determining drug metabolism (319,362-365). A wide variety of foods and beverages may affect CYP activity (363,366-368), as does smoking (369,370). Natural Health Products, such as traditional Chinese herbs often favoured by patients, are often taken in large quantities and many contain compounds that can significantly inhibit CYP activity (363,371-373).

Approaches to measuring CYP activity

Given the plethora of variables contributing to CYP activity, there is a need for technologies suitable for the timely and regular reassessment of patients' contemporaneous phenotypic level of activity of important drug-metabolizing enzymes during cancer treatment.

Enzyme assays. CYP enzyme activity may be measured directly using enzyme activity assays that deliver specific "velocity values"—the number of mols of substrate converted by an enzyme over a specified time period at a controlled pH and temperature (374). Because of the dynamics of enzyme rate reactions, where the reaction slows as substrate depletes, velocity values are typically measured during the early phase of enzyme activity, where the rate reaction is approximately linear (374). To achieve this, it is critical to properly select and validated the appropriate starting concentrations of substrate (375).

One of the major limitations of this approach is that sampling of the associated enzymes from the liver is too invasive for most clinical applications. As a result, plasma is commonly

used for sampling, but may not always be a representative of enzymes' activity in the liver, where most drug metabolism occurs. It should be noted that the significance of the differences quantified in enzyme activity differences does not always accurately predict the observed level of drug clearance by an individual (340,341). This may be due to limitations with peripheral measurement of CYP activity in the blood, or even due to uncharacterized bottlenecks in a drug's metabolic pathway that limit the impact of enzyme activity on final blood levels of a drug.

Geneva cocktail approach. Several "cocktail" approaches have been applied to phenotype the concomitant activity of multiple drug-metabolizing enzymes and transporters (190,191,376). The cocktail approach involves measure the circulating plasma concentration of innocuous drugs with known routes of metabolism and their primary metabolites at one or more specified timepoint(s) after the drugs' administration. The ratio of a substrate to its metabolite acts as a probe to reflect the activity of the associated CYPs and transporters (377).

Approaches using drug probes are similarly limited by the wide variety of drug metabolism pathways in play and their incomplete characterization; clinically meaningful results will always depend on appropriate probe selection and on whether peripheral levels accurately reflect drug levels in the tissue of interest. Nonetheless, assessments based on measuring drug levels may be able to better capture at least some of the impact of rate-limiting confounders (e.g., transforming enzymes, gut absorption, etc) that could potentially uncouple blood drug levels from enzyme activity. Approaches like the Geneva cocktail can also expect to be most representative when the route of administration for the probe drug matches the drug of interest.

CYPs selected for current study and their role in anti-cancer drug metabolism

The CYP450 enzyme superfamily comprises ~60 heme enzymes that are present throughout the human body (332). The CYP enzymes are responsible for metabolizing xenobiotics as well as biosynthesis of some low-molecular weight metabolites (332). A limited subset of these are believed to metabolize >90% of drugs (323). CYP3A4/5 is estimated to be involved in the metabolism of >50% of drugs with known metabolic pathways, while CYP1A2 is involved for 4% (323,332). CYP3A4 and CYP1A1/2 are also particularly important for hepatic detoxification of systemic cancer therapies (369).

Focus on CYP3A4. CYP3A4 is highly expressed in liver and intestines and has a wide variety of drug substrates, spanning many therapeutic classes (323,328,363,378). It is commonly

considered the most important CYP enzyme for drug metabolism in humans (332). Many antineoplastic agents are metabolized by CYP3A4 including targeted inhibitors (e.g., gefitinib, erlotinib), etoposide and taxanes (323,336,379-381). The role of CYP3A4 in metabolism of testosterone and estrogen may also confer relevance for hormone-targeted cancer therapies (328). Increased CYP3A4 expression in tumours can confer resistance to many anti-cancer treatments, including treatment with TKIs (359).

Moderate variability of CYP3A4 activity is observed in liver microsomal samples, with activity and expression varying up to 60-fold; only 60% of this variability can be attributed to genetic control (332). Because of its involvement in metabolism of so many different substrates, the risk of interactions – either drug-drug interactions or with other exposures – is high. The potent inhibiting effects of grapefruit flavonoids on CYP3A4 are the reason why grapefruit juice must be avoided with so many medications.

Preclinical evidence suggests that capivasertib is both an inhibitor and substrate of CYP3A4 metabolism, as alluded to in the FAKTION study protocol (216). As a result, concomitant treatment with strong inducers or inhibitors of CYP3A4 metabolism not permitted in active trials of capivasertib (196,382). In fact, it is possible that capivasertib's effects on CYP3A4 may be part of the way that it re-sensitizes patients to some drugs (e.g., taxanes) (383).

Focus on CYP1A2. The role of CYP1A2 in cancer treatment is complex; it is heavily involved in biotransformation of drugs and drug metabolism, but it has also been linked to activation of pre-carcinogens and may in some cases play a role in cancer risk (328). CYP1A2 is primarily expressed in the liver (332). While it is involved in metabolism of comparatively fewer drugs (vs. CYP3A4), some of the substrates preferentially metabolized by CYP1A2 represent ubiquitous exposures (e.g., caffeine, acetaminophen) (332). Together with CYP3A4 and CPY1A1, CYP1A2 plays a role in metabolism of TKIs such as Erlotinib (369). Co-administration of CYP1A2-inhibiting drugs has also been shown to increase toxicity of other TKIs (384). While no specific role of CYP1A2 in capivasertib metabolism has been established, the findings with other TKIs may suggest a need for caution in this domain.

Moderate variability of CYP1A2 is observed in liver microsomal samples, represented by 40-fold differences in expression and activity (332). CYP1A2 genotype has been linked to aromatase inhibitor response in breast cancer (385). Diet also appears to play a substantial role in CYP1A2 variability with effects associated with the type of vegetables consumed or an

increase in consumption of barbequed meat (332). Common exposures such as caffeine and acetaminophen may act as competitive inhibitors, while barbequed meat and cigarette smoke constitute major inducers (386).

Sub-hypothesis, objectives & approach

CYP3A4 and CYP1A2 play a unique role in the detoxification and potentially the efficacy of systemic cancer therapies and TKIs (216,359,369,383,384). We hypothesize that: (i) a streamlined Geneva cocktail method applied in healthy free-living individuals will enable measurement of inter-individual differences in CYP3A4 and CYP1A2 activity, (ii) that the observed inter-individual differences may be linked to clinical characteristics (e.g., age, sex, BMI), and/or patterns of dietary or medication intake, as self-reported by participants. If "everyday" exposures can indeed be linked to CYP activity and cancer drug metabolism, this alone provides another line of evidence for the thesis' central argument that genetics-only approaches, like pharmacogenetics, must be supplemented with metabolite and protein quantitation to achieve a full molecular phenotype of cancer and treatment response.

In order to test the hypothesis, we will complete the following research objectives:

1. Implement & validate an LC-MS/MS-based quantitation of OH-midazolam/midazolam and paraxanthine/caffeine as probes to measure CYP3A4 and CYP1A2 activity;
2. Collect and analyze venous serum samples from 10 consenting free-living healthy volunteers before and after dosing with caffeine and midazolam, using a single 60-minute timepoint;
3. Analyze results together with data from a medication and dietary habits questionnaire completed by participants;
4. Adapt the assay for use with dried blood spots (DBS) as a practical alternative to venous sampling that would enable routine CYP activity monitoring in larger-scale clinical studies

The Geneva cocktail method. The Geneva cocktail approach has been demonstrated as an effective and practical approach for monitoring activity of various CYPs (190). The approach is also compatible with DBS sampling (387,388). Significant data specifically supports the safety

of the full 6-drug Geneva cocktail in healthy volunteers, which includes doses of caffeine, bupropion, flurbiprofen, omeprazole, dextromethorphan, midazolam, and fexofenadine (388). In this study, adverse events affected only ~1.5% of participants, were self-limiting, and were not definitively causally linked to the drug cocktail (388). However, given our long-term goal of implementing this assay in studies with cancer patients receiving active treatment, many of whom are at higher risk of adverse effects or drug-drug interactions, we opted to include a smaller number of the least harmful drugs and most important CYPs for our study.

Targeted CYP 450s. The research project was initially conceived with Dr. R. Thomas Jagoe at the Peter Brojde Lung Cancer Centre. CYP1A2, and especially CYP3A4, were selected for their relevance to metabolism of drugs used in treatment of lung cancer (369,379-381,389-391). For our purposes, CYP3A4 is of special interest based on its central role in drug metabolism, treatment resistance, and its bi-directional relationship with capivasertib. Midazolam, erythromycin, cortisol and testosterone are all commonly used as probes to measure CYP3A4 metabolism (328); midazolam has a favourably minimal side effect profile. In fact, midazolam is currently being used as part of a clinical trial (NCT04958226) to assess the effects of repeated doses of capivasertib on oral midazolam as a probe for CYP3A pharmacokinetics among patients with advanced solid tumours. Caffeine, which is commonly used as a probe for CYP1A2, was selected in part to help offset any potential drowsiness from the midazolam. CYP1A2 represents an interesting target for study given its relationship to TKI metabolism and potential to be influenced by diet and common exposures.

Practical considerations. The published methods for CYP activity assessment are frequently time-consuming for subjects and require multiple blood samples, making them difficult to use in larger clinical populations. To minimize invasiveness, we further selected a single timepoint approach, timed at 60 minutes post-dosing, which is generally considered to be sufficient (392-394). The test substrates for these CYPs (caffeine and midazolam respectively) were chosen as they are both well tolerated at the doses used and reach peak concentration at 60 minutes which is a reasonable assay time interval for clinical use. In contrast to prior studies using only healthy controls, we recruited free-living subjects to assess the feasibility of this modified protocol prior to testing in patients with cancer.

In summary, we applied a simplified version of the Geneva cocktail to assess the activity of CYP1A2 and CYP3A4 in free-living volunteers (n=10) based on a single 60-minute timepoint

serum concentration of caffeine, paraxanthine, midazolam and hydroxy-midazolam. The CYP activity measured among free-living patients was assessed for correlation with clinical variables including a score (DiMQu) of predicted CYP inhibition or induction derived from a self-reported dietary and medication use questionnaire. Given the suitability of this approach for detecting differences in CYP induction/inhibition associated with routine exposures, the method was further adapted to dried blood spot to facilitate routine sampling with the ease of use and storage required for a busy hospital setting.

Results

Method validation data

Linearity, precision, and accuracy were assessed using charcoal-stripped serum spiked with a calibration curve of caffeine/paraxanthine and midazolam/OH-midazolam reference standards, together with a fixed concentration of internal standards, as shown in Table 16 and Figure 43. Peak area ratios for each analyte and its internal standard were fitted to a linear regression model with $1/x^2$ weighting.

Table 16. *Calibration standards & spiked-serum QCs for the Geneva Cocktail Assay*

		Standard Concentration by Calibration Sample / QC (equivalent in ng/mL of serum)									
Analyte	**IS conc. (fixed)**	**A**	**B**	**C**	**D**	**E**	**F**	**G**	**QC High**	**QC Med**	**QC Low**
Caffeine	1000	5000	2000	800	320	128	51.2	20.5	2500	500	100
Paraxanthine	400	2500	1000	400	160	64.0	25.6	10.2	1250	250	50
Midazolam	2	250	100	40	16	6.4	2.6	1.0	12.5	2.5	0.5
OH-Midazolam	2	250	100	40	16	6.4	2.6	1.0	12.5	2.5	0.5

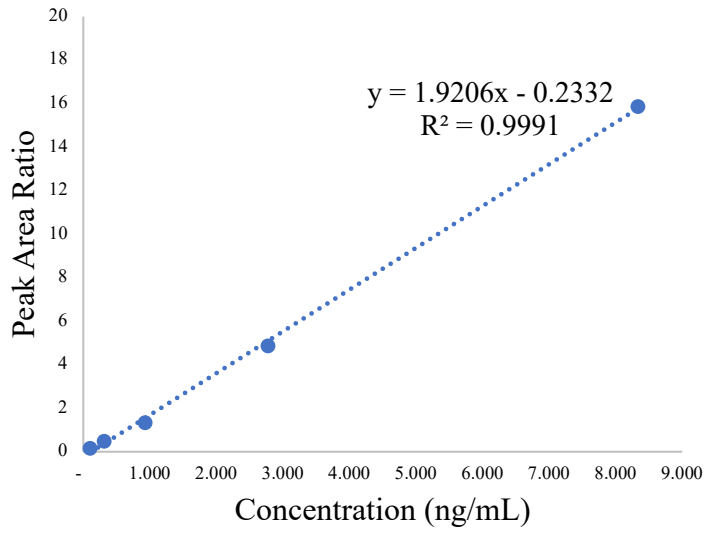

Figure 43. *Sample Standard Curve of Hydroxy-midazolam and its internal standard*

Linear Range, Precision, Accuracy, Recovery. As shown in Table 17, the linear range (R2 ≥0.99) was 1 ng/mL-250 ng/mL for midazolam and OH-midazolam, 21 ng/mL-5000 ng/mL for caffeine, and 10 ng/mL-2500 ng/mL for paraxanthine. Carryover contributed less than 20% of signal at the lower limit of quantitation (LLOQ) following injection of high calibrators, and no interferences were detected in matrix double blanks. Precision met criteria in that coefficients of variation (CVs) did not exceed 15% for calibrators and QC samples measured in triplicate. The measured concentration of calibration standards, based on the line of best fit, was accurate within +/-20% for each standard within the linear range for each analyte. Quality control samples (high/medium/low), consisting of charcoal-stripped serum spiked with known quantities of each analyte, were included with each batch and the measured concentration in these samples was also accurate within +/-20% of the known value.

Table 17. *Geneva Cocktail LC-MS/MS Assay Performance in Serum*

Analyte	Linear Range (ng/mL)	Number of points in curve	Number of QC passed	Linearity (R^2)	CV at LLOQ (%)
Caffeine	20-5000	6/6	3/3	0.9914	<15
Paraxanthine	10-5000	6/6	3/3	0.9942	<15
Midazolam	1-100	6/6	3/3	0.9990	<15
OH-Midazolam	1-200	6/6	3/3	0.9950	<15

Reproducibility & stability. The inter-run reproducibility of the assay demonstrated using quality control samples spiked at 3 levels (low, medium, high), prepared in triplicate at each level. Each set of 3 QCs (low, medium, high) was analyzed on a separate day, using an independent calibration curve and independent preparation of internal standards. Inter-day CVs were <15% for all analytes at each QC level. Since the workflow required long-term sample storage as additional patients were recruited to the study, long-term stability was also assessed. Samples re-analyzed after 90 days of storage at -80ºC showed agreement with originally-measured concentration values (mean CVs <6% for all analytes in all re-tested samples).

Recovery. The recovery for each analyte was assessed by comparing the quantitation of standards in buffer, spiked into previously-extracted charcoal-stripped serum, and spiked into charcoal-stripped serum before extraction. The recovery of standards spiked prior to extraction was measured in 3 replicates at 3 concentration levels per analyte, and was on average 95-99% for all analytes as shown in Table 18.

Table 18. *Results of recovery testing*

Analyte & sample	**Level (ng/mL) & Recovery (%)**					
Paraxanthine	high:	2000	medium:	320	low:	51.2
Buffer	102%		97%		97%	
Spiked into extract	121%		104%		107%	
Spiked & recovered	102%	±2%	94%	±2%	91%	±3%
Caffeine	high:	1000	medium:	160	low:	25.6
Buffer	97%		101%		98%	
Spiked into extract	117%		103%		102%	
Spiked & recovered	104%	±3%	91%	±1%	91%	±1%
OH-midazolam	high:	10	medium:	1.6	low:	0.26
Buffer	101%		95%		98%	
Spiked into extract	115%		93%		121%	
Spiked & recovered	97%	±6%	95%	±12%	104%	±2%
Midazolam	high:	10	medium:	1.6	low:	0.26
Buffer	103%		100%		100%	
Spiked into extract	115%		91%		98%	
Spiked & recovered	103%	±2%	84%	±1%	97%	±6%

Routine validation. The validation criteria applied to MS data prior to quantitation in patient samples is presented in Table 19. All criteria were passed on the days of patient sample analysis.

Table 19. *Validation Criteria for Geneva Cocktail Assay at JGH*

Validation check	Data reviewed	Criteria for Acceptance
Double Blank	1 replicate per run, injected 2x	Response <20% of LLoQ per analyte
Blank with IS	1 replicate per run, injected 2x	Response <20% of LLoQ per analyte
Ionization Effects	All specimens & calibrators/QCs	IS peak area variation 80-120%
Transition Ratio	Biological specimens	Consistent with calibrators/QCs
Calibration Curve	≥6 levels, bracketing curves	R^2>0.995, CV <15% (<20% at LLOQ)
Quality Controls	3xQCs (High/medium/low)	±20% of known concentration

DBS Feasibility Testing

The linear range for the assay adapted to DBS was compatible with the range observed in patient samples (Table 20). On-spot deconjugation performed as well as aqueous extraction followed by β-glucuronidase treatment, yielding similar fold increases in OH-midazolam. The observed increase in OH-midazolam was 5.2-fold (on-spot) and 6.5 –fold (aqueous extraction) for Whatman 903 cards, and 6.89-fold (on-spot) and 7.83-fold (aqueous) for HemaSpot HF (Figure 44). All analytes were successfully quantified from as little as 18.4 µL of human blood, equivalent to two petals from a HemaSpot HF DBS collection device. This indicates the suitability of DBS for proxy measurements of CYP activity with the chemical probes used.

Table 20. *Geneva Cocktail LC-MS/MS Assay Performance in DBS*

Analyte	Range observed in participants (ng/mL)	Assay linear range (ng/mL)
Caffeine	110-6300	80-4000
Paraxanthine	80-3600	40-2000
Midazolam	4-12	0.4-20
OH-Midazolam	30-100	4-200

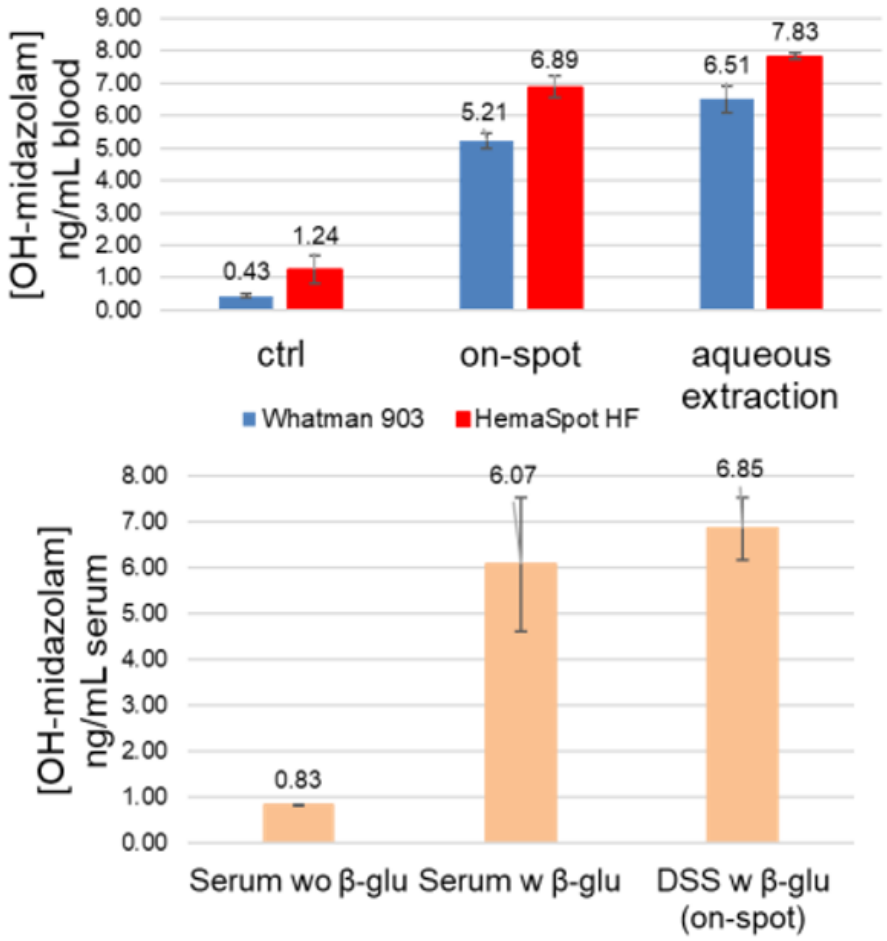

Figure 44. *Comparison of direct (on-spot) and sequential (aqueous extraction) extraction and deconjugation of OH-midazolam glucuronide*

Measurement of OH-midazolam from (a) dried blood samples and (b) and serum controls. DBS samples were either incubated directly with 500 units of β-glucuronidase overnight @ 37°C (on-spot), or extracted first using aqueous extraction followed by deconjugation. Pooled serum samples (50 µL) were incubated w/wo 500 units of β-glucuronidase for 16h @ 37°C. Dried serum spots (DSS) served as an additional control for possible effects of sample drying on the measurement of deconjugated OH-midazolam.

Participant Characteristics

A total of 10 participants (mean age 38 ± 11.8; n= 5 males) took part in the study. As shown in Table 21, none were smokers, 3 individuals reported chronic illnesses, 4 reported the use of natural health products (NHPs), and 6 reported medication use.

Table 21. *Participant Characteristics*

Characteristic	
Age (yrs)	38 (±11.8)
BMI	23.2 (±1.7)
Male	n = 5/10
Chronic illness	n = 3/10
Smokers	n = 0
Natural health product use	n = 4/10
Current medication use	n = 6/10

Predicted CYP Activation Score (DiMQu Questionnaire)

Net scores for $DiMQu_{3A4}$ and $DiMQu_{1A2}$ were calculated for each individual to provide a global prediction of the impact of their diet and medications on enzyme induction (Figure 45). No visible bar indicates a net score of zero. Positive scores were considered to be net inducing, whereas a negative score predicted inhibition. $DiMQu_{3A4}$ scores predicted either no effect or a modest net inhibiting effect of diet and medication use on CYP3A4 enzyme activity for the majority of participants, whereas $DiMQu_{1A2}$ scores predicted a net inducing effect principally driven by caffeine-containing products.

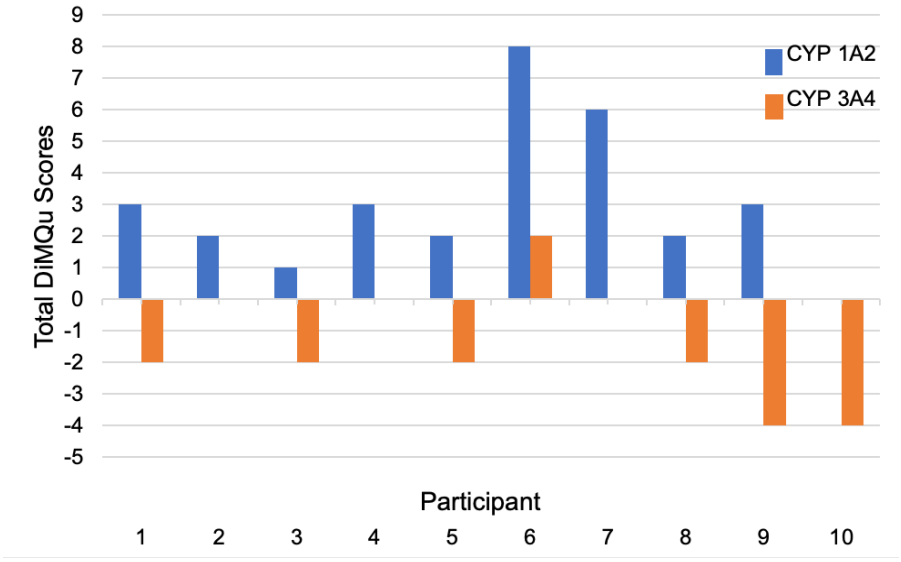

Figure 45. *Calculated DiMQu Scores for Each Participant*

CYP P450 Phenotype of Volunteers

Each participant's CYP3A4 Metabolic Ratio is presented in Table 22. As expected, all patient serum had midazolam and OH-midazolam levels below the LLOQ at baseline sampling. At the 1-hour timepoint, the mean concentration of free OH-midazolam was 6.26 ± 1.91 ng/mL whereas the mean concentration measured in the β-glucuronidase-treated samples was 54.0±14.2 ng/mL, representing a difference of more than 8-fold. CYP1A2 Metabolic Ratio for each participant is presented in Table 23. Despite instructions to fast completely prior to sampling, significant caffeine concentrations (up to 3761 ng/mL) and paraxanthine concentrations (up to 3297 ng/mL) are observed in some participants' baseline serum samples.

Table 22. *CYP3A4 Metabolic Ratio*

No reported value (-) indicates that the measured value was below the LLOQ. Total OH-midazolam is the measured concentration after glucuronidase pre-treatment of the sample. The metabolic ratio is calculated as total OH-Midazolam at 1 hr divided by Midazolam at 1 hr.

	Midazolam (ng/mL)		**OH-Midazolam (ng/mL)**			**Metabolic Ratio**
Time	0 hr	1 hr	0 hr	Free 1 hr	Total 1 hr	1 hr
Participant						
1	-	7.35	-	7.86	47.9	6.52
2	-	7.19	-	4.70	61.5	8.56
3	-	10.9	-	8.95	76.0	6.96
4	-	7.13	-	6.57	71.0	9.97
5	-	6.69	-	4.15	47.1	7.04
6	-	4.46	-	4.60	59.7	13.4
7	-	7.29	-	5.93	49.4	6.78
8	-	8.97	-	9.01	53.3	5.94
9	-	4.97	-	3.97	25.3	5.09
10	-	7.42	-	6.85	48.4	6.52

Table 23. *CYP1A2 Metabolic Ratio*

The metabolic ratio is calculated as the change (Δ) in paraxanthine at 1 hr divided by the change (Δ) in caffeine at 1 hr.

	Caffeine (ng/mL)			Paraxanthine (ng/mL)			Metabolic Ratio
Time Participant	0 hr	1 hr	Δ 1 hr	0 hr	1 hr	Δ 1 hr	1 hr
1	316.7	2246	1930	273.7	446.6	172.9	0.09
2	487.3	2888	2400	732.0	971.8	239.8	0.10
3	3761	6263	2502	3297	3227	229.3	0.09
4	1747	5705	3957	1528	1809	271.7	0.07
5	336.6	2752	2416	463.1	674.5	211.3	0.09
6	212.6	2656	2444	341.2	576.7	235.5	0.10
7	352.6	3704	3352	633.9	996.6	362.7	0.11
8	111.6	2882	2770	81.01	246.4	165.4	0.06
9	201.1	3346	3145	318.1	750.3	432.3	0.14
10	898.4	3547	2649	1294	1393	99.30	0.04

Correlation of Predicted Activation Score to Measured CYP Activity

The DiMQu induction score for CYP3A4 was strongly correlated (Rs=0.79, p<0.01)) to the metabolic ratio of OH-midazolam:midazolam only in the β-glucuronidase-treated samples. However, the DiMQu score for CYP1A2 however did not correlate to the Paraxanthine:caffeine metabolic ratio at a statistically significant level (Rs=0.54, p=0.11) (Figure 46). Participant age and participant sex were not significantly associated with the metabolic ratio phenotype for CYP3A4 or CYP1A2 (Figures 47 and 48).

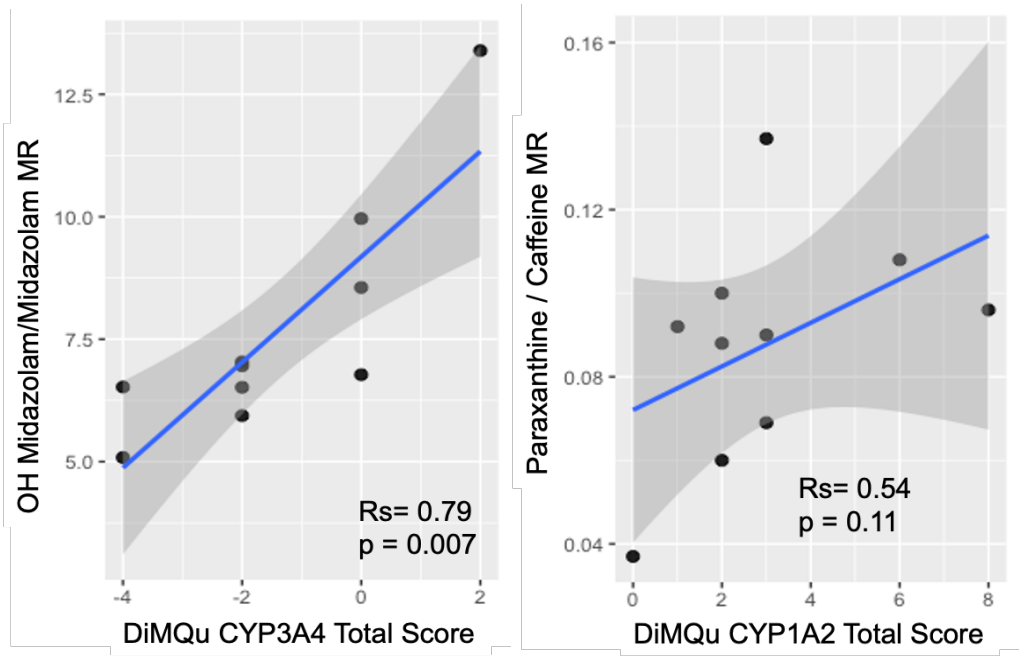

Figure 46. *Correlation of DiMQu score to metabolic ratio for CYP3A4 & CYP1A2*

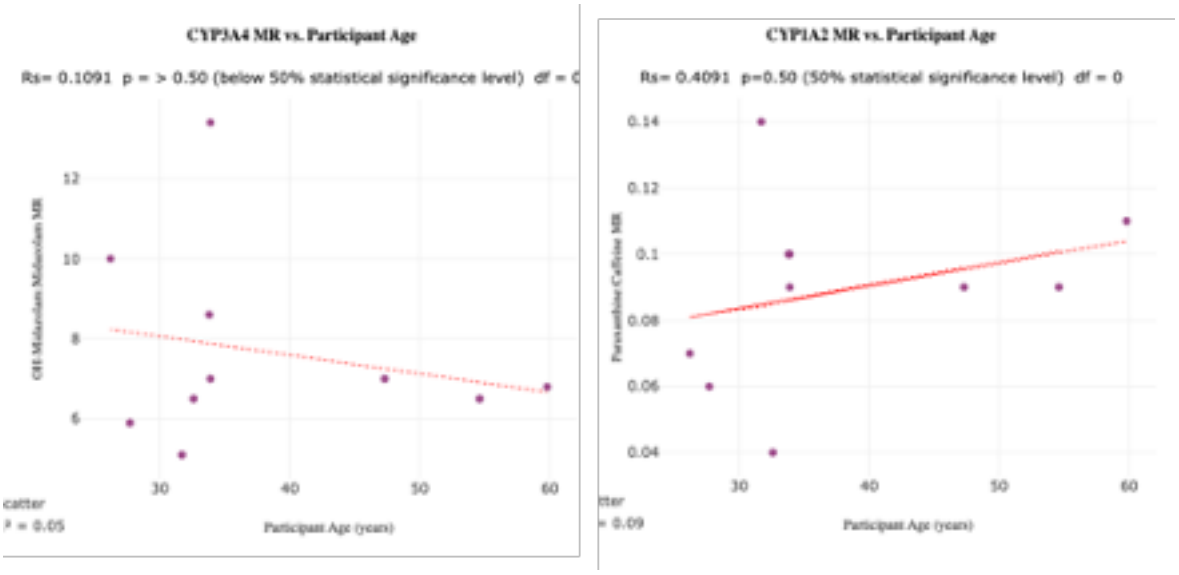

Figure 47. *Scatterplots for metabolic ratio vs. age for CYP3A4 and CYP1A2*

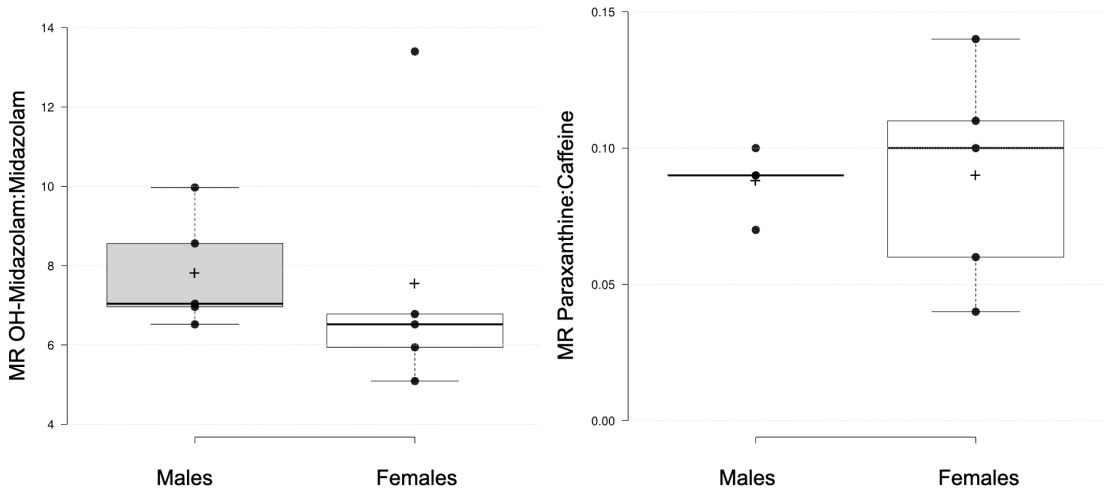

Figure 48. *Metabolic ratio vs. sex for CYP3A4 & CYP1A2*

Interpretation

Performance & utility of the approach

Assay performance

The implemented LC-MRM-MS assay demonstrates all necessary performance characteristics to be feasibly applied in a clinical study. Linear ranges were sufficient to quantify all 4 analytes in each participant serum sample and were consistent with the expected range of concentrations based on previous studies (190). Precision was consistent with FDA standards for bioanalytical method validation (395). Quality control samples prepared independently from the standard curve were consistently quantified within ±20% of the known concentration, even on independent days, suggesting high accuracy and reproducibility. Storage of collected serum samples at -80ºC over several months did not affect quantitation, which will support batched analysis for large-scale studies. Due to the presence of both caffeine and paraxanthine in the standard commercially-available pooled human serum (Bioreclamation), we instead employed charcoal-stripped serum for assay development and validation, which successfully eliminated signal from the blanks. When measured in blank samples, carryover from maximum concentration samples was limited to acceptable levels despite the wide linear range and high signal from caffeine. The method is highly robust, easy to use, and requires little instrument time

(samples run in <6 minutes). Rigorous validation criteria have been developed and implemented, which will ensure accurate quantitation of the analytes from patient samples.

Our findings will also inform future application of the Geneva cocktail method. For instance, OH-midazolam is known to be metabolized to OH-midazolam-glucuronide, but the proportion of this intermediate as compared to the more commonly-measured OH-midazolam was unknown. In comparing matched patient serum samples with and without β-glucuronidase treatment, we established that the majority of OH-midazolam (>85%) is in fact glucuronide-bound at 1 hour after midazolam dosing. Correlation between the determined CYP3A4-activity and DiMQu score was observed only when considering the ratio of total OH-midazolam:midazolam after glucuronidase-treatment (r_s=0.79, p=0.007) and not for the ratio of free-OH-midazolam-to-midazolam alone (r_s =0.06). This result suggests that including the glucuronidase deconjugation step is crucial for accurate measurement of CYP3A4 activity, though many studies applying the Geneva cocktail have not included it (190,376).

Adaptation to DBS

A method for quantitation of the 4 Geneva cocktail analytes from DBS was developed and validated, with a linear range sufficient to cover the observed concentrations in the study participants. While patient samples were not analyzed with this method yet, laboratory testing suggests that this approach is feasible, consistent with prior publications (190,376). However, our method is the first to combine DBS extraction with on-spot glucuronidase treatment, which we now know is crucial for accurate assessment of CYP3A4.

Characterizing CYP activity in free-living patients & correlation to DiMQu score

Inevitable limitations are associated with the DiMQu approach: the comprehensiveness of the dietary and medication questionnaire, non-reported exposures (e.g., to illicit substances), or inaccuracy of self-report. However, in our study, the DiMQu scoring system, developed in Dr. Thomas Jagoe's lab to quantify common food and medication exposures influencing CYP3A4 or CYP1A2 activity, appears to function as intended. A variety of DiMQu scores were observed among participants, although CYP1A2 was overwhelmingly induced while CYP3A4 was more commonly inhibited. Quantitation of phenotypic enzymatic activity by metabolic ratios was achieved for both CYP3A4 and CYP1A2 in all patients.

While the developed assay demonstrates adequate performance for the clinical study of CYP-activity based on drug and metabolite ratios, it is noted that there was no correlation between the metabolic ratio of paraxanthine to caffeine and the $DiMQu_{1A2}$ score. It is possible that the $DiMQu_{1A2}$ score was inaccurate due to limits in the comprehensiveness of the dietary and medication questionnaire, incomplete or inaccurate reporting, non-adherence to fasting instructions, or consumption of medications containing caffeine (e.g., some painkillers). It is also likely that the minimum 8-hour avoidance of caffeine in the current study protocol is insufficient given the slower clearance of caffeine and paraxanthine (376) and a longer abstinence from caffeinated products prior to the final 8hr fast would have yielded more informative results. Caffeine and paraxanthine are commonly observed in blood from even properly-fasted individuals due to ubiquitous exposure combined with the long elimination half-life of these analytes of 3-11 hours (396). Some estimates suggest it may take approximately 7 days of abstinence for habitual caffeine consumers to fully clear the drug from their blood (397).

The surprisingly high baseline caffeine and paraxanthine observed at baseline in some participants may have interfered with the measurement of CYP1A2 by altering pharmacokinetics and clearance rates; the multiple-timepoint study design (considered extraneous for some other drugs) has previously been recommended for caffeine specifically (398). This might explain why measured CYP1A2 activity did not reproduce known associations with age and sex in this cohort either, although some sources suggest that these effects may be marginal (399). Other drugs metabolized by CYP1A2, such as acetaminophen, melatonin, or phenacetin, might be better suited to reduce the risk of interference in future studies (400).

In spite of this, there does appear to be a possible trend between the $DiMQu_{CYP1A2}$ score and metabolic ratio, though it does not reach statistical significance ($p=0.11$). The $DiMQu_{CYP3A4}$ score, on the other hand, is highly correlated to the OH-Midazolam:Midazolam ratio ($p=0.007$). While it is impossible to capture all potentially relevant inputs for the dietary and medical questionnaire, this strong association provides evidence for the utility of both the DiMQu score and the phenotyping assay. While the DiMQu score cannot serve as a substitute for molecular phenotyping, it may be useful to help flag patients for whom phenotyping is required.

Study limitations

Generalization of the study results in limited by the small number of participants and the cohort's dissimilarity from the characteristics of the target patient population (i.e., cancer patients). Participants were mostly staff or graduate students at the Jewish General Hospital and none exceeded the age of 60. In comparison, the median age of onset for breast cancer patients is 62. Both obesity and smoking are known risk factors for multiple cancers. However, in our cohort all participants were non-smokers and had BMIs <26. For this reason, some expected relationships -- such as CYP1A2 induction by smoking (401) or CYP activity inhibition in obesity (402) -- could not be assessed at all in this dataset. No ethnicity or genetic data was obtained.

No clear correlation was observed between CYP activity with age or sex. The inability to detect a clear trend may be due to inter-patient phenotypic variability that is greater than the marginal effects expected to be associated with sex or age (337-339,344-346,399). As discussed in the introduction, it is also possible that drug clearance may be discordant with enzyme activity measured by enzyme assays (340,341). In general, a regression model incorporating age, sex, and DiMQu score together might be better suited to assess inter-relationships between the variables.

Discussion

Noteworthy findings & implications

Proteomics identifies potential mechanisms of resistance within a genetically pre-selected clinical trial cohort

In the first portion of this study, we performed both targeted and global proteomic characterization of *PIK3CA*-mutated breast and gynecological tumour samples from patients in a clinical trial of the AKT inhibitor capivasertib. Although AKT is the target of capivasertib, the current study did not find a difference in the expression of AKT1 or AKT2 in baseline tumour samples between the CB versus the NCB groups of samples. However, the addition of global proteomics using the iMALDI supernatants allowed further investigation of features associated with clinical benefit in response to capivasertib treatment. Statistical analysis of label-free quantitation data from 578 high-confidence proteins revealed a pattern of increased activation of translational control in the NCB group. Together with published evidence, this suggests a role for the upregulation of EIF2 pro-survival signaling and/or EIF4-driven translational initiation in resistance to AKT inhibitors.

Our workflow in this study uniquely combined proteomics technologies, making optimal use of volume-limited clinical samples and demonstrating the ability to obtain useful proteomic data from slide-mounted FFPE collected >7 years prior. While both targeted and untargeted approaches are used in biomarker development, untargeted approaches are typically used in early stages of biomarker discovery, followed by targeted approaches for validation and implementation (149,403). In contrast, we used global proteomics to expand on the results obtained from hypothesis-driven targeted proteomics.

Our data demonstrate the value of deeper molecular profiling at the protein level. The heterogeneity revealed within the genetically pre-selected cohort illustrates that a given genetic mutation does not fully predict the activation of the downstream pathway or the ability to target it with a given treatment. Network and pathway analysis pointed to greater upstream activation of AKT in the CB group, while the NCB group showed a profile of dysregulated protein biosynthesis (increased translation, mRNA processing, protein processing) and associated changes in energy balance (mitochondrial proteins). The baseline activation of EIF2 signaling detected by proteomics was found to represent a potential mechanism of resistance to AKT

inhibition, since EIF2 is known to be involved in compensatory pro-survival signaling under conditions of AKT inactivation in other models (404).

Overall, our results provide evidence that resistance to capivasertib may be mediated by EIF2 or EIF4 (mTORC1) signaling in the tumours of a small cohort of patients in a Phase II clinical trial. While our findings were well-aligned with existing literature, the low sample numbers and limitations in the study design posed important caveats to their interpretation. Small cohorts are especially problematic in the context of the highly multivariate data generated by -omics approaches (405). It was crucial to verify the proposed proteomic signatures of treatment response, particularly EIF2 and EIF4 signaling activation, in additional pre-clinical models and clinical sample sets tested for sensitivity to capivasertib. To facilitate precise and reproducible measurement in long-term, larger-scale studies, we urgently needed targeted quantitative assays for at least a subset of the proteins of interest.

Targeted assay development & validation generates fit-for-purpose proteomics assays

The successful development of quantitative MS-based proteomics approaches to confirm targets identified by global proteomics builds on a well-established idea of the "commonly applied" biomarker pipeline (296,406), though in reality only about 10% of proteomics biomarkers studies ultimately combine these technologies (1). The validated multiplexed proteomics panel developed in the second portion of the project was found to be suitable for the planned marker verification study.

Given the significant investment required for assay development and validation, sharing of assay data, protocols, methods and standards (e.g., in the form of a kit) may also help other researchers in their own verification efforts. Of the 53 validated assays, 25 peptides had existing public data and 28 were new to the CPTAC portal (167). This expanded repertoire of assays for translational control proteins may be useful for other cancer researchers, but these pathways also represent an active research area in many other disciplines. Regulation of translation plays a critical role in development, guiding embryogenesis by determining embryonic axis, body pattern and cell fate (407). In neurology, translational control, together with modulation of the PI3K and ERK pathways, are responsible for balancing long-term potentiation and long-term depression to achieve the balance required for synaptic plasticity and memory (407). The activation of EIF4 and EIF2 signaling downstream from cell growth and proliferation pathways has been tied to a wide variety of pathologies including heart disease and oxidative damage

(407). Defects in these pathways are linked to poor glycemic control resulting in metabolic diseases and severe genetic syndromes (407,408).

Marker verification & translational relevance for AKT inhibitor use

We employed an innovative study model, employing pre-existing cell lines to verify findings from clinical samples. The results from the cell line study verify that cancers genetically pre-selected for *PIK3CA* mutations can be further sub-divided into capivasertib response groups, based on differing proteomic profiles. Detection of a similar protein expression profile in breast cancer cell lines, as measured by orthogonal quantitative methods, adds significant credibility to the hypothesis that differences in translational control are strongly correlated to capivasertib response in *PIK3CA*-altered cancer tissues. Moreover, the targeted proteomics data from cell lines provided new evidence to pinpoint EIF4/mTORC1 as the driver over EIF2 signalling.

mTORC1-driven resistance to PI3K pathway inhibitors is now well-characterized (119,280). That the mTORC1-driven profile can be readily observed at the protein level using the developed assay represents a significant opportunity for translation. Previous research points to tenascin or mTOR mutations as a mechanism for mTORC1-driven resistance and this has even been detected and effectively targeted in at least one patient (282). However, additional genetic mechanisms likely exist. The proteomics panel implemented here may facilitate monitoring downstream effects to reliably detect shifts in mTORC1 activity, even in the case of unknown or uncharacterized genetic changes.

Our results provide additional evidence for an mTORC1-driven pathway of resistance from the tumours of a small cohort of patients in a Phase II clinical trial. Moreover, we present some of the first evidence that this phenomenon could be (i) associated with drug response among patients genetically pre-selected for PI3K pathway activation, (ii) present in patients in a clinical setting many years before trial enrollment, and (iii) identified on the basis of protein quantitation from tumour and cell line samples collected prior to capivasertib exposure.

The streamlined Geneva cocktail approach captures important variations in drug metabolism

This portion of the thesis diverged from the focus on capivasertib to address the broader question of how to optimize doses for a variety of cancer treatments. Our study reported one of the first uses of a simplified single-timepoint Geneva cocktail approach to phenotype the activity of CYP1A2 and CYP3A4 in healthy free-living male and female study volunteers (n=10). Our

results further demonstrated that glucuronide deconjugation is crucial for CYP3A4 phenotyping with this approach. The protocol for DBS analysis represents the first method for on-spot denconjugation of glucuronide metabolites in the context of CYP activity monitoring. The DBS method will help facilitate more routine implementation in the clinic to ultimately support dose optimization for better cancer therapies.

The DiMQu induction score created to predict enzyme activation from a dietary questionnaire appears to effectively integrate information about inducers and inhibitors, in so far as it was correlated with observed metabolic phenotype. The correlation between CYP3A4 phenotype with the induction score calculated from participants self-reported dietary and exposure questionnaire demonstrates the utility of such an approach, but more importantly, the need for this approach, given the inter-individual variation observed even among healthy volunteers. The link to diet and medication implies strong potential for intra-individual variation associated with these intakes.

Translational relevance of the implemented Geneva cocktail approach

While previous studies induced enzymatic changes with the administration of inhibitors and inducers (376), our findings highlight that common dietary exposures at "ordinary" levels of consumption can measurably impact drug metabolism. This clearly demonstrates the need for regular phenotypic assessment of changes in CYP activity that are correlated with modifiable factors such as diet and medications, which would not be captured in a pharmacogenetics approach to precision medicine. While a therapeutic drug monitoring (TDM) paradigm could also be used for phenotypic monitoring of cancer drug metabolism, and we have developed such approaches before (8), the Geneva cocktail approach has the potential to permit dose titration based on "real-time" assessment of CYP activity, *prior* to administration of a potentially toxic or ineffective dose of chemotherapy.

There is clear evidence for the impact of diverse influences on CYP activity, but extensive research will ultimately be required to develop accurate models that meaningfully incorporate genetic and non-genetic factors and accurately predict their effects (327). The interplay between contributors to CYP activity is notoriously complex (409). In the meantime, we have implemented a streamlined version of the Geneva cocktail approach for direct real-time monitoring of CYP activation that is simple, cost-effective, safe, and avoids potential challenges associated with patient privacy and genetic data. The phenotyping method has further been

successfully translated to dried blood spots for ease of implementation in a busy hospital setting and use in large-scale clinical studies. Future work should implement DBS sampling together with β-glucuronidase treatment to measure CYP activity in a broader cohort of cancer patients. Transfer of the reported assay to DBS will facilitate sample-collection and storage, while minimizing patient discomfort.

Next steps: validating & extending the work

Further investigating of mechanisms of resistance in cell culture & other pre-clinical models

Research using the developed targeted proteomics assays in breast cancer cell lines is still ongoing. Additional replicates of from the timecourse studies will be analyzed to supplement the existing data; this will provide more reliable results given the high degree of variability observed between passages of the same cell line. The remaining samples contain additional replicates prepared in parallel from matching passages. It is hoped that the full suite of data will generate or confirm additional insights concerning the markers of interest.

Moreover, we aim to apply a similar approach in a new model by repeatedly sampling a sensitive cell line (e.g., MCF-7) cultured over an extended period in the presence of capivasertib and regularly repeating cytotoxicity testing. This will allow us to test whether changes in the concentrations of putative markers may be temporally related to the development of acquired resistance, which would provide very strong evidence for a causal relationship and help to validate the proposed proteomic signature. Testing of additional combination therapies might also point to suitable co-targeting strategies to confirm and address these mechanisms of resistance.

Further research in cell lines could include studies to investigate whether the profile associated with sensitivity/resistance is conserved in different cancer types (e.g., prostate), cancer subtypes (e.g. TNBC), and those with different mutational backgrounds (e.g., without detectable PI3K pathway alterations). Additional work is also needed to determine whether the observed treatment response profile can be extended to other cancer types, mutational contexts, or combination treatments.

Other more sophisticated pre-clinical models, such as xenograft mouse models or patient-derived xenografts (PDX), are also of interest to confirm the findings. PDX models, distinctively formed by engraftment, recapitulate at least a portion of the original tumour's structure,

microenvironment, and heterogeneity (410). Like cell lines, aggressive and advanced forms of disease are over-represented in xenograft models, and immune context is missing (410). However, PDX provide for a generally better representation of clinical disease. Were it not for the resource-intensive nature of this approach, the cultivation of 3-dimensional tumour tissue could also be a useful tool for assay characterization; for example, this might facilitate experiments to determine how FFPE preservation impacts protein quantitation versus fresh-frozen tissue. Answering this question might help direct which assays to continue optimizing for use in clinical samples.

Enhancing protein quantitation methods for compatibility with clinical sample types

Analysis of stored tissues of JGH patients revealed that our EvoSep-PRM-MS method was insufficient to quantify most of the analytes in long-stored FFPE cores and slices. One important next step is therefore to further optimize the method so that more of the proteins of interest can be quantified in the linear range from this sample type. This may require the use of alternative chromatography systems (e.g., nLC) or a different mass spectrometer (e.g., TimsTOF) to enhance sensitivity. The upgraded assays should then be fully validated according to CPTAC guidelines prior to attempting further clinical sample analysis. Once the assays are well-characterized, the intra- and inter-tumour heterogeneity study can be repeated in the hopes of achieving a more informative result based on the coverage of more proteins. Given our existing findings from proteins quantified in cores versus slices, it is recommended to use exclusively cores for future sampling. Depending on the results, we can then select a subset of assays with the most suitable performance in clinical samples for further use. Further feature reduction should also be considered to eliminate redundant information from strongly correlated protein concentrations and facilitate future data analysis.

Future clinical applications

Long-term, large-scale randomized prospective studies will ultimately be required to firmly establish the utility of any identified marker for predicting treatment response in a specified setting. Capivasertib is currently being evaluated in Phase III trials as part of combination therapies in prostate cancer (411,412), triple-negative breast cancer (214,215), and HR+ breast cancer (195,216,217) Recent primary analysis of the CAPItello-291 Phase III trial (NCT04305496) demonstrates that treatment with capivasertib + fulvestrant extends PFS in

patients with HR+/HER2- breast cancers with inadequate response to endocrine therapy and prolongs overall survival(218). Evidence of treatment benefit was found in the overall population, including patients with and without identifiable AKT pathway alterations (413). As capivasertib moves into earlier stages of treatment and is prescribed to a broader group of patients, it will be necessary to validate the findings in contemporaneous tissues, as in a biopsy-driven trial (414).

Successful implementation of a practical, feasible Geneva cocktail approach at the Jewish General Hospital will enable future studies specifically aimed at: (i) assessing associations between CYP3A4 and CYP1A2 activity and cancer treatment outcomes, (ii) understanding interactions with Natural Health Products that patients commonly use in parallel with treatment regimens, and (iii) optimizing treatment doses through precision dosing. While the main goal of was to lay groundwork to enable routine monitoring, the newly emerging role of CYPs in oncogenesis also suggests a possible application the assay in precision medicine to not only dose, but actually to help select appropriate targeted treatments (415).

Synthesis & emerging themes

The distinct value of proteomics data in precision medicine

For nearly two decades, we have seen the rapid emergence of precision medicine, which at first produced evidence that specific genomic variants found in subsets of patient tumours conferred remarkable clinical sensitivity to particular targeted treatments (28,31). When the limits of this approach became evident, studies like the WINTHER trial and others demonstrated the added value of transcriptomic data (53). Pre-clinical and clinical data have since demonstrated that protein levels can diverge from transcriptomic (mRNA) data and can assist in guiding choice of therapy (137,228). The overarching hypothesis of this thesis was that proteomics approaches could supplement more these existing approaches to advance precision oncology. Our data clearly demonstrate the value of deeper molecular profiling at the protein level. We found that even in the context of an activating genetic mutation, downstream pathway activity varies sufficiently to alter treatment response.

This research also repeatedly established the importance of factors outside of the genome in modulating treatment response. The example of EIF2 signalling – in which varied cellular stress conditions rapidly induce uncoupling of the transcriptome and translatome – is one salient

example. In the context of the Geneva cocktail assay, we similarly illustrated how the activity of CYPs responsible for metabolizing the vast majority of cancer drugs (thereby regulating their effectiveness and toxicity) is modified in response to dietary exposures that do nothing to alter the genome.

Moreover, the study results demonstrate how multiple markers will likely be needed to adequately predict treatment response to many targeted agents. Beyond the notion of genetic versus protein markers, the future of precision medicine appears to depend on our ability to truly achieve "-omics-level" approaches that incorporate signals from multiple targets and multiple methodologies to elucidate tumour biology for optimizing therapy decisions. This is a crucial reason to continue prioritizing the development of true proteomics approaches for precision medicine, as opposed to solely traditional antibody-based protein quantitation that is best suited for fewer targets.

Evolving approaches to biomarker-based treatment strategies

Spotlight on resistance & rational combination therapies

With respect to companion diagnostics, one key theme emerging from this work is that identifying potential markers of resistance may prove more important for patient selection than markers of sensitivity. While many cancer cells exploit the PI3K pathway (even in the absence of detectable mutations), some are also primed to subvert AKT inhibition. This is in line with the challenges facing other targeted agents, where outcomes remain highly variable, with some patients showing dramatic responses and others showing much less efficacy. Even tumours that are initially sensitive to targeted agents inevitably develop resistance.

It is not yet clear whether this is due exclusively to direct molecular mechanisms of resistance or whether differences and changes in drug metabolism may also contribute. CYP3A4 is often over-expressed in cancer tissue and is a proposed mechanism of resistance to cancer treatments including TKIs (416-418). The recent awareness that capivasertib inhibits CYP3A4 (419), raises the question of whether capivasertib's effects on CYPs could be one mechanism by which it prevents resistance to other therapies or re-sensitizes patients to drugs to which they have previously developed resistance (358,420).

In line with the observed challenges with resistance, there is an increasing emphasis on rational, evidence-based combination therapies to improve response rates and extend treatment

longevity. There is reason to believe that combination therapy is required to optimize efficacy for capivasertib, particularly in cancers with acquired resistance to hormone or HER2-directed therapies (219). In a trial of patients with breast tumours with *AKT1* or other pathway alterations, combining capivasertib with fulvestrant gave greater ORRs up to 47% (211,216,217). The observation of a pre-treatment profile associated with future resistance in the NCB group, which may not be adequately addressed by AKT inhibition alone, suggests that adding agents targeting EIF2 or EIF4 signaling could be useful (421,422).

Expanding applications to Inform existing therapeutic regimens

Companion diagnostics are increasingly being used to facilitate new drug development and optimize clinical trials, but there is still an unmet need to optimize the use of existing treatments (423). While studies suggest that >80% of patient tumours carry "clinically actionable" genomic alterations (76), most treatment decisions are still guided by conventional pathology and clinical presentation. Few patients receive molecular subtyping or targeted therapies outside of clinical trials (25). The secondary analysis of samples from a clinical trial as in this project is one route by which proteomics can be implemented to make better use of previously-developed therapies.

In a second and more dramatic example, the Geneva cocktail assay shows how the assessment of protein activity can be made useful and practical for "routine" clinical decision-making. Eventual implementation of such an assay for routine use could have profound impacts on the practice of medical oncology. Inter-patient variation in treatment side effect profile is commonly attributed to off-target effects, but drug metabolism likely also contributes. For instance, while the pathogenesis of hand-foot syndrome (HFS) in response to some chemotherapies is not well understood, there are several lines of evidence that drug metabolism at least contributes to risk (424,425). The practicing oncologist will tell you that HFS often precedes a robust treatment response (426), which may also signal a higher effective dose in those patients. At present, oncologists are often left to guess at patient counseling and dose adjustments based on limited information (e.g., is that herbal medicine harmless? What dose should we give to someone on long-term antibiotic therapy?). Routine clinical measurement of CYP activity will help to take some of the guesswork out of medical oncology and enable evidence-based decision-making throughout treatment.

Enduring challenges in precision medicine

Emphasis on clinically-relevant standards

While this work highlights many advances in precision medicine, it also reflects several hurdles. As disruptive -omics technologies become increasingly accessible and enter the world of medicine, we must work to avoid the pitfalls of the past. Technical standardization and validation are core prerequisites in this endeavour (39,59). The tools developed by CPTAC to support method standardization, assay performance characterization, and data exchange are key to protect the future of proteomics against crucial errors (308). Guidelines for Tier 2 proteomics assays have secured the selectivity, repeatability, sensitivity, and reproducibility of biomarker candidate evaluation (149,427).

Tier 1 assays will be needed to generate medically-actionable information in a format compatible with regulatory scrutiny (149). In 2021, the Clinical Laboratory Standards Institute (CLSI) introduced the new Guideline C64 for addressing quantitative measurement of proteins and peptides by mass spectrometry. This provides a vital waypoint toward Tier 1 assays; approval under CLSI was the same path forged for initial licensure of multiplex genomic panels like OncotypeDx. There is hope that the new guidelines serve to resolve a significant regulatory gap (39,59) while assuring the safety, reliability, and credibility that proteomics technologies need to reach the clinic (163). These guidelines may eventually re-open the door to FDA approval of proteomics assays (149). However, for the moment, Tier 1 assays remain largely on the horizon.

Demand for biological insights to validate results

In addition to technical and analytical validity, there is a strong need to deliver biologically- and medically-valid results through the use of orthogonal approaches, independent cohorts, and new models. Evidence suggests that evaluating of markers in a combination of complementary models and different sample types, as we have done in this project, increases the likelihood of identifying valid markers (296). The quest for validity also comes with an increasing impetus to deliver biological insights that logically substantiate new biomarkers and treatment strategies. This lesson was highlighted for the field of translational proteomics in the aftermath of the OvaCheck debacle, where the peaks used as markers were not even identified, let alone linked meaningfully to cancer prognosis (61,163). However, there is increasing support

for the tenet of biological foundations to back molecularly-targeted approaches across multiple oncology settings (428). The work performed in this project showcases proteomics' ability to generate the desired in-depth molecular portraits that enhance our understanding of disease.

Escaping the quicksand of big data

Another aspect of validation concerns the use of appropriate data analysis pipelines, suitable statistical approaches, and translation of results. As the field of high-throughput high-coverage -omics has grown, so have the challenges of analysing, storing, standardizing and interpreting the associated data (429). There is a need for new statistical tools and standards better suited to the analysis of highly multivariate data (430) (405). Scientists, translational researchers, and clinicians all need updated training and resources on the relevant approaches well as their important limitations (430).

In almost all areas of science and medicine, we are now struggling to overcome data overload. This is especially true in the field of translational cancer research where genomics technologies are expanding faster than informatics workflows (429). Systems biology tools, like Ingenuity Pathway Analysis used in this project, are beginning to emerge to integrate previously intractable multi-omics data. However, as demonstrated here, such software is only as good as the quality of their databases. The most important data resources in cancer research, like COSMIC and CPTAC, still invest massive effort in careful manual curation. Artificial intelligence (AI) is increasingly being used to create algorithms that bring order to overwhelming datasets (430). However, the "black box" of AI approaches considerably limits how these algorithms may be applied in clinical settings. The integration and interpretation of multi-marker molecular signatures therefore remains a major challenge. In parallel to the learnings from early proteomics assays, the ability to tie a given algorithm to its biological foundations should be adopted as a reasonable check and balance.

Obtaining relevant samples

One approach to improving statistical power is to tackle larger sample sets. However, obtaining timely clinically relevant samples for molecular profiling remains a significant stumbling block. The patients with advanced and metastatic cancers receiving experimental drugs are those for whom surgery is no longer a viable therapeutic option. Therefore tumour samples from these patients are rarely contemporaneous. Biopsies pose risk to the patient and

generate limited material. In the field of tumour proteomics specifically, there is still an unmet need for standardized universal protocols to sample FFPE and methods to account for tumour heterogeneity with sampling techniques or concentration normalization strategies. While alternative sampling approaches like liquid biopsy may enable better timely and sequential sampling, they remain bounded by what can be detected at circulating levels (431). In a broader sense, biomarker studies in this population engender specific weaknesses: characterizing clinical benefit can be difficult and distinguishing specific treatment-response markers from general prognostic ones is even harder.

Translational research throughout the drug development lifecycle

The paradox of biomarker development (and pharmacovigilance, for that matter) is that despite lofty ideas about how biomarkers could expedite and improve drug approvals, most research on drugs doesn't happen until after clinical approval. During clinical development there are restrictions on information sharing, a narrow focus of study to what is commercially relevant, and limited access to both the drug itself and clinical samples. After approval is when more opportunities for characterization and publication of data arise (432).

To expand the utility of molecular subtypes, we need to incorporate molecular subtyping into all stages of the clinical research process, from early development to routine clinical care. This requires optimal selection of biomarkers and assembly into panels that address the most clinical cases. The resulting assays must be affordable, practical in terms of turnaround time and sample availability, de-risked in terms of material consumption and clinical utility, readily interpretable and clearly actionable. Such improvements will justify wider use of molecular subtyping even in "non-dire" clinical scenarios. In turn, the adoption of molecular subtyping outside of clinical trials will generate the data to inform interpretation and shape the future of clinical decision-making in more therapeutic settings.

Conclusion

Outcomes

The original objectives of this project were (i) to improve the use of existing targeted therapies through more comprehensive, enriched molecular profiles, and (ii) to use these profiles to improve our understanding of cancer. The novel findings of this research meet these objectives through the identification of novel putative proteomic markers of capivasertib resistance. In addition, the results provide some of the first evidence that there is a profile of AKT inhibitor resistance that can be detected in patients many years before trial enrollment or exposure to the drug. Our analysis tied this profile to differences in translational control downstream from mTORC1. The results demonstrate how proteomics might be useful to further segment a genetically pre-selected clinical cohort in terms of predicted treatment response. Quantitation of these novel markers by an orthogonal method in independent cell line models reinforced and clarified their association with capivasertib resistance.

The development, validation, and application of fit-for-purpose technologies throughout the project enabled effective discovery, successful validation, and will continue to facilitate further work in this area. The Geneva cocktail study further provided an example of how mass spectrometry-based -omics methods can be tailored for clinical implementation, and how protein activity measurements reflect variations in drug metabolism that could not be captured by a genome-focused approach. Together, the work demonstrates the value and feasibility of modern fit-for-purpose proteomic and mass spectrometry technologies in precision oncology for improving patient selection, guiding precision dosing, and generating novel biological insights.

Outlook & future directions: innovative models, markers & trial designs

The popular book “the Emperor of All Maladies” chronicles the recent history of incredible and rapid advances in cancer research and treatment, stemming in large part from breakthroughs since the late 1940’s (433). Discoveries over the last 70 years have transformed cancer from a hopeless mysterious illness hidden behind closed doors to a well understood and often treatable disease. However, in spite of this enormous progress, author Dr. Mukherjee rightly questions whether we can ever truly win the fight against this supremely resilient disease (433).

As we venture into the next generation of cancer research, many of the gains being made are more incremental. Many of the most recently approved cancer therapies have only modestly improved prognosis and any prolonged survival time may be spent suffering from adverse effects. In fact, when the additional time spent in hospital receiving treatment or due to drug-induced illness is taken into account, many drugs that improve overall survival actually fail to offer more "home days" for patients and their families (434). This is true for many new chemotherapies, radiotherapies, and immunotherapies, all of which must be delivered intravenously in hospital with close supervision. The oral route of administration and generally better tolerability of small molecule targeted treatments therefore represents an unparalleled opportunity to deliver meaningful outcomes for patients.

We cannot afford to ignore this potential. It is imperative that we continue to advance the molecular subtypes of disease and clinically actionable biomarkers needed to establish a role for molecularly targeted treatments in routine clinical care. This effort will benefit from enhanced models of disease, augmented biomarker strategies, and state-of-the-art clinical trial designs. New pipelines that enable discovery in real-world patient populations may help to identify more reliable biomarker candidates. Diversified disease models are also under development to better replicate the tumour microenvironment and immune functions (32). Automation and the systematic characterization of research materials are making it increasingly feasible to implement massive panels consisting of thousands of cell lines for improved validation (32).

Implementing signatures or scores derived from multiple markers is similarly expected to increase the sensitivity, specificity, and robustness of future companion diagnostics. Bringing together genomics, proteomics, and metabolomics will provide multi-layer signatures to determine treatment choice and dose. This is well demonstrated by recent advancements in proteogenomics, which is yielding fresh insights into molecular biology, illuminating new drug targets, and generating novel biomarkers for disease detection, surveillance and monitoring (160). Overcoming big data challenges will be critical to the success of these approaches.

Where trials of rare cancers or segmented populations previously depended on large-scale multi-site coordination to achieve sufficient patient numbers (12), recent innovations in clinical trial design are helping to power the next set of breakthroughs. Basket trials are transforming our ability to deploy biomarkers in clinical studies. New forms of sampling, such as liquid biopsy are also enabling more timely biomarker assessment and the greater use of markers for monitoring

(32). Early, informed dose optimization may also help potential cancer therapies move through the approval process by ensuring maximal efficacy can be obtained without encountering safety issues. The introduction of "precision dosing" studies into the drug development pipeline could help ensure that "special populations" (e.g., elderly patients, patients with co-morbidities) that are commonly excluded from trials but need NTI drugs can reliably receive evidence-informed care (321). The use of co-clinical trials where patients are treated in parallel with a personalized PDX model of their disease offer an entirely new framework for treatment selection and evaluation (32).

Targeted treatments will ultimately be key to the next big horizon in cancer: addressing the pool of patients with "hard-to-treat" disease and rare cancer subtypes who benefit less from conventional treatments. Improving treatments and outcomes for patients with rare cancers requires an emphasis on combination therapies, deep biological insights into individual disease, and guiding biomarkers (12). Given the substantial investment already committed to develop these new agents, it is well justified to continue our efforts to perfect their use. New research tools, including proteomics, will help to light the way on this journey.

Bibliography

1. Sobsey CA, Ibrahim S, Richard VR, Gaspar V, Mitsa G, Lacasse V*, et al.* Targeted and Untargeted Proteomics Approaches in Biomarker Development. *Proteomics* 2020;**20**(9):e1900029 doi 10.1002/pmic.201900029.

2. Froehlich BC, Popp R, Sobsey CA, Ibrahim S, LeBlanc AM, Mohammed Y*, et al.* Systematic optimization of the iMALDI workflow for the robust and straightforward quantification of signaling proteins in cancer cells. *PROTEOMICS–Clinical Applications* 2020;**14**(5):2000034.

3. Froehlich BC, Popp R, Sobsey CA, Ibrahim S, LeBlanc A, Mohammed Y*, et al.* A multiplexed, automated immuno-matrix assisted laser desorption/ionization mass spectrometry assay for simultaneous and precise quantitation of PTEN and p110alpha in cell lines and tumor tissues. *Analyst* 2021;**146**(21):6566-75 doi 10.1039/d1an00165e.

4. Sobsey CA, Popp R, Ibrahim S, Froehlich BC, Aguilar-Mahecha A, Basik M*, et al.* Abstract B21: Protein quantitation assays for Akt, PI3K p110α, and PTEN to assess PI3K pathway activity in tumor tissue. *Molecular Cancer Research* 2020;**18**(10_Supplement):B21-B.

5. Ibrahim S, Sobsey CA, Popp R, Zahedi RP, Batist G, Borchers CH. Abstract P4-10-20: Protein quantitation assays for AKT and PTEN to better understand sensitivity and resistance of breast cancer patients to treatment with AKT inhibitor capivasertib. *Cancer Research* 2020;**80**(4_Supplement):P4-10-20-P4-10-20.

6. Sobsey CA, Froehlich B, Batist G, Borchers CH. Immuno-MALDI-MS for Accurate Quantitation of Targeted Peptides from Volume-Restricted Samples. Neuronal Cell Death: Springer; 2022. p. 203-25.

7. Batist G, Sobsey CA, Mitsa G, Borchers C. WIN Symposium 2022 - Abstract No: 1 Beyond the tip of the iceberg: Proteomic analysis in colon and breast cancer. *J Immunother Precis Oncol* 2022;**5**(4):118-60 doi 10.36401/jipo-22-x4.

8. Gaspar VP, Ibrahim S, Sobsey CA, Richard VR, Spatz A, Zahedi RP*, et al.* Direct and Precise Measurement of Bevacizumab Levels in Human Plasma Based on Controlled Methionine Oxidation and Multiple Reaction Monitoring. *ACS Pharmacol Transl Sci* 2020;**3**(6):1304-9 doi 10.1021/acsptsci.0c00134.

9. Allen L, O'Connell A, Kiermer V. How can we ensure visibility and diversity in research contributions? How the Contributor Role Taxonomy (CRediT) is helping the shift from authorship to contributorship. *Learned Publishing* 2019;**32**(1):71-4 doi https://doi.org/10.1002/leap.1210.

10. Canadian Cancer Statistics Advisory Committee in collaboration with the Canadian Cancer Society SCatPHAoC. Canadian Cancer Statistics 2021. cancer.ca/Canadian-Cancer-Statistics-2021-EN2021 November 2021.

11. Gatta G, van der Zwan JM, Casali PG, Siesling S, Dei Tos AP, Kunkler I*, et al.* Rare cancers are not so rare: the rare cancer burden in Europe. *Eur J Cancer* 2011;**47**(17):2493-511 doi 10.1016/j.ejca.2011.08.008.

12. Ashley D, Thomas D, Gore L, Carter R, Zalcberg JR, Otmar R*, et al.* Accepting risk in the acceleration of drug development for rare cancers. *The Lancet Oncology* 2015;**16**(4):e190-e4 doi https://doi.org/10.1016/S1470-2045(14)71153-2.

13. Manegold C. Current advancements in hard-to-treat cancers. *American Journal of Cancer* 2005;**4**:105-13.

14. Gupta A, Eisenhauer EA, Booth CM. The Time Toxicity of Cancer Treatment. *J Clin Oncol* 2022;**40**(15):1611-5 doi 10.1200/JCO.21.02810.

15. Dagogo-Jack I, Shaw AT. Tumour heterogeneity and resistance to cancer therapies. *Nat Rev Clin Oncol* 2018;**15**(2):81-94 doi 10.1038/nrclinonc.2017.166.

16. Aggelis V, Johnston SRD. Advances in Endocrine-Based Therapies for Estrogen Receptor-Positive Metastatic Breast Cancer. *Drugs* 2019;**79**(17):1849-66 doi 10.1007/s40265-019-01208-8.

17. Chetta P, Zadra G. Metabolic reprogramming as an emerging mechanism of resistance to endocrine therapies in prostate cancer. *Cancer Drug Resistance* 2021;**4**(1):143.

18. Fiorica F, Buttigliero C, Grigolato D, Muraro M, Turco F, Munoz F*, et al.* Addition of New Androgen Receptor Pathway Inhibitors to Docetaxel and Androgen Deprivation Therapy in Metastatic Hormone-Sensitive Prostate Cancer: A Systematic Review and Metanalysis. *Curr Oncol* 2022;**29**(12):9511-24 doi 10.3390/curroncol29120747.

19. Baudino TA. Targeted Cancer Therapy: The Next Generation of Cancer Treatment. *Curr Drug Discov Technol* 2015;**12**(1):3-20 doi 10.2174/1570163812666150602144310.

20. Scheetz L, Park KS, Li Q, Lowenstein PR, Castro MG, Schwendeman A*, et al.* Engineering patient-specific cancer immunotherapies. *Nat Biomed Eng* 2019;**3**(10):768-82 doi 10.1038/s41551-019-0436-x.

21. Paramita DK, Hutajulu SH, Syifarahmah A, Sholika TA, Fatmawati S, Aning S*, et al.* BCR-ABL Gene Transcript Types of Patients with Chronic Myelogenous Leukemia in Yogyakarta, Indonesia. *Asian Pac J Cancer Prev* 2020;**21**(6):1545-50 doi 10.31557/APJCP.2020.21.6.1545.

22. Kharas MG, Fruman DA. ABL oncogenes and phosphoinositide 3-kinase: mechanism of activation and downstream effectors. *Cancer Res* 2005;**65**(6):2047-53 doi 10.1158/0008-5472.CAN-04-3888.

23. Iqbal N, Iqbal N. Imatinib: a breakthrough of targeted therapy in cancer. *Chemother Res Pract* 2014;**2014**:357027 doi 10.1155/2014/357027.

24. Westin JR, Kantarjian H, Kurzrock R. Treatment of chronic myelogenous leukemia as a paradigm for solid tumors: how targeted agents in newly diagnosed disease transformed

outcomes. *Am Soc Clin Oncol Educ Book* 2012(32):179-85 doi 10.14694/EdBook_AM.2012.32.60.

25. Schwartzberg L, Kim ES, Liu D, Schrag D. Precision Oncology: Who, How, What, When, and When Not? *Am Soc Clin Oncol Educ Book* 2017;**37**(37):160-9 doi 10.1200/EDBK_174176.

26. Cohen P, Cross D, Janne PA. Kinase drug discovery 20 years after imatinib: progress and future directions. *Nat Rev Drug Discov* 2021;**20**(7):551-69 doi 10.1038/s41573-021-00195-4.

27. Lim SH, Lee JY, Sun JM, Ahn JS, Park K, Ahn MJ. Comparison of clinical outcomes following gefitinib and erlotinib treatment in non-small-cell lung cancer patients harboring an epidermal growth factor receptor mutation in either exon 19 or 21. *J Thorac Oncol* 2014;**9**(4):506-11 doi 10.1097/JTO.0000000000000095.

28. Camidge DR, Bang YJ, Kwak EL, Iafrate AJ, Varella-Garcia M, Fox SB*, et al.* Activity and safety of crizotinib in patients with ALK-positive non-small-cell lung cancer: updated results from a phase 1 study. *Lancet Oncol* 2012;**13**(10):1011-9 doi 10.1016/S1470-2045(12)70344-3.

29. Pacheco JM, Gao D, Smith D, Purcell T, Hancock M, Bunn P*, et al.* Natural history and factors associated with overall survival in stage IV ALK-rearranged non–small cell lung cancer. *Journal of Thoracic Oncology* 2019;**14**(4):691-700.

30. Flaherty KT, Puzanov I, Kim KB, Ribas A, McArthur GA, Sosman JA*, et al.* Inhibition of mutated, activated BRAF in metastatic melanoma. *N Engl J Med* 2010;**363**(9):809-19 doi 10.1056/NEJMoa1002011.

31. Chapman PB, Hauschild A, Robert C, Haanen JB, Ascierto P, Larkin J*, et al.* Improved survival with vemurafenib in melanoma with BRAF V600E mutation. *N Engl J Med* 2011;**364**(26):2507-16 doi 10.1056/NEJMoa1103782.

32. Huang M, Shen A, Ding J, Geng M. Molecularly targeted cancer therapy: some lessons from the past decade. *Trends Pharmacol Sci* 2014;**35**(1):41-50 doi 10.1016/j.tips.2013.11.004.

33. Shahid K, Khalife M, Dabney R, Phan AT. Immunotherapy and targeted therapy-the new roadmap in cancer treatment. *Ann Transl Med* 2019;**7**(20):595 doi 10.21037/atm.2019.05.58.

34. Dai X, Li T, Bai Z, Yang Y, Liu X, Zhan J*, et al.* Breast cancer intrinsic subtype classification, clinical use and future trends. *Am J Cancer Res* 2015;**5**(10):2929-43.

35. Sorlie T, Perou CM, Tibshirani R, Aas T, Geisler S, Johnsen H*, et al.* Gene expression patterns of breast carcinomas distinguish tumor subclasses with clinical implications. *Proc Natl Acad Sci U S A* 2001;**98**(19):10869-74 doi 10.1073/pnas.191367098.

36. Perou CM, Sorlie T, Eisen MB, van de Rijn M, Jeffrey SS, Rees CA*, et al.* Molecular portraits of human breast tumours. *Nature* 2000;**406**(6797):747-52 doi 10.1038/35021093.

37. Prat A, Pineda E, Adamo B, Galvan P, Fernandez A, Gaba L*, et al.* Clinical implications of the intrinsic molecular subtypes of breast cancer. *Breast* 2015;**24 Suppl 2**:S26-35 doi 10.1016/j.breast.2015.07.008.

38. Weigelt B, Baehner FL, Reis-Filho JS. The contribution of gene expression profiling to breast cancer classification, prognostication and prediction: a retrospective of the last decade. *J Pathol* 2010;**220**(2):263-80 doi 10.1002/path.2648.

39. Fuzery AK, Levin J, Chan MM, Chan DW. Translation of proteomic biomarkers into FDA approved cancer diagnostics: issues and challenges. *Clin Proteomics* 2013;**10**(1):13 doi 10.1186/1559-0275-10-13.

40. Tate JG, Bamford S, Jubb HC, Sondka Z, Beare DM, Bindal N*, et al.* COSMIC: the Catalogue Of Somatic Mutations In Cancer. *Nucleic Acids Res* 2019;**47**(D1):D941-D7 doi 10.1093/nar/gky1015.

41. Schmidt C. Mammaprint Reveals Who Can Skip Chemotherapy for Breast Cancer. *J Natl Cancer Inst* 2016;**108**(8) doi 10.1093/jnci/djw197.

42. Normanno N, Apostolidis K, de Lorenzo F, Beer PA, Henderson R, Sullivan R*, et al.* Cancer Biomarkers in the era of precision oncology: Addressing the needs of patients and health systems. *Semin Cancer Biol* 2022;**84**:293-301 doi 10.1016/j.semcancer.2021.08.002.

43. Lao VV, Grady WM. Epigenetics and colorectal cancer. *Nat Rev Gastroenterol Hepatol* 2011;**8**(12):686-700 doi 10.1038/nrgastro.2011.173.

44. Jones PA. The DNA methylation paradox. *Trends Genet* 1999;**15**(1):34-7 doi 10.1016/s0168-9525(98)01636-9.

45. Karami Fath M, Azargoonjahromi A, Kiani A, Jalalifar F, Osati P, Akbari Oryani M*, et al.* The role of epigenetic modifications in drug resistance and treatment of breast cancer. *Cell Mol Biol Lett* 2022;**27**(1):52 doi 10.1186/s11658-022-00344-6.

46. Iwamoto T, Pusztai L. Predicting prognosis of breast cancer with gene signatures: are we lost in a sea of data? *Genome medicine* 2010;**2**(11):1-4.

47. Kato M, Natarajan R. MicroRNAs in diabetic nephropathy: functions, biomarkers, and therapeutic targets. *Ann N Y Acad Sci* 2015;**1353**(1):72-88 doi 10.1111/nyas.12758.

48. Lu J, Getz G, Miska EA, Alvarez-Saavedra E, Lamb J, Peck D*, et al.* MicroRNA expression profiles classify human cancers. *Nature* 2005;**435**(7043):834-8 doi 10.1038/nature03702.

49. Izzotti A, Carozzo S, Pulliero A, Zhabayeva D, Ravetti JL, Bersimbaev R. Extracellular MicroRNA in liquid biopsy: applicability in cancer diagnosis and prevention. *Am J Cancer Res* 2016;**6**(7):1461-93.

50. Kumar S, Prajapati KS, Singh AK, Kushwaha PP, Shuaib M, Gupta S. Long non-coding RNA regulating androgen receptor signaling in breast and prostate cancer. *Cancer Lett* 2021;**504**:15-22 doi 10.1016/j.canlet.2020.11.039.

51. Mirzaei S, Paskeh MDA, Hashemi F, Zabolian A, Hashemi M, Entezari M*, et al.* Long non-coding RNAs as new players in bladder cancer: Lessons from pre-clinical and clinical studies. *Life Sciences* 2022;**288**:119948.

52. Sun Z, Jing C, Xiao C, Li T. Long Non-Coding RNA Profile Study Identifies an Immune-Related lncRNA Prognostic Signature for Kidney Renal Clear Cell Carcinoma. *Front Oncol* 2020;**10**:1430 doi 10.3389/fonc.2020.01430.

53. Rodon J, Soria JC, Berger R, Miller WH, Rubin E, Kugel A*, et al.* Genomic and transcriptomic profiling expands precision cancer medicine: the WINTHER trial. *Nat Med* 2019;**25**(5):751-8 doi 10.1038/s41591-019-0424-4.

54. Weidenbusch B, Richter GHS, Kesper MS, Guggemoos M, Gall K, Prexler C*, et al.* Transcriptome based individualized therapy of refractory pediatric sarcomas: feasibility, tolerability and efficacy. *Oncotarget* 2018;**9**(29):20747-60 doi 10.18632/oncotarget.25087.

55. Worst BC, van Tilburg CM, Balasubramanian GP, Fiesel P, Witt R, Freitag A*, et al.* Next-generation personalised medicine for high-risk paediatric cancer patients - The INFORM pilot study. *Eur J Cancer* 2016;**65**:91-101 doi 10.1016/j.ejca.2016.06.009.

56. Asleh K, Lluch A, Goytain A, Barrios C, Wang XQ, Herranz J*, et al.* Correlative analysis of RNA biomarkers for adjuvant capecitabine benefit in the CIBOMA/2004-01phase III clinical trial of triple negative breast cancer patients. *Cancer Research* 2022;**82**(12_Supplement):5271-.

57. Tsimberidou AM, Fountzilas E, Bleris L, Kurzrock R. Transcriptomics and solid tumors: The next frontier in precision cancer medicine. *Semin Cancer Biol* 2022;**84**:50-9 doi 10.1016/j.semcancer.2020.09.007.

58. Panis C, Pizzatti L, Souza GF, Abdelhay E. Clinical proteomics in cancer: Where we are. *Cancer Lett* 2016;**382**(2):231-9 doi 10.1016/j.canlet.2016.08.014.

59. Boys EL, Liu J, Robinson PJ, Reddel RR. Clinical applications of mass spectrometry-based proteomics in cancer: Where are we? *Proteomics* 2023;**23**(7-8):e2200238 doi 10.1002/pmic.202200238.

60. Duraiyan J, Govindarajan R, Kaliyappan K, Palanisamy M. Applications of immunohistochemistry. *J Pharm Bioallied Sci* 2012;**4**(Suppl 2):S307-9 doi 10.4103/0975-7406.100281.

61. Zhang Z, Chan DW. The road from discovery to clinical diagnostics: lessons learned from the first FDA-cleared in vitro diagnostic multivariate index assay of proteomic biomarkers. *Cancer Epidemiol Biomarkers Prev* 2010;**19**(12):2995-9 doi 10.1158/1055-9965.EPI-10-0580.

62. Reilly GP, Gregory DA, Scotti DJ, Lederman S, Neiman WA, Sussman S*, et al.* A real-world comparison of the clinical and economic utility of OVA1 and CA125 in assessing ovarian tumor malignancy risk. *Journal of Comparative Effectiveness Research* 2023;**12**(6):e230025.

63. Dunton CJ, Eskander RN, Bullock RG, Pappas T. Low-risk multivariate index assay scores, physician referral and surgical choices in women with adnexal masses. *Current medical research and opinion* 2020;**36**(12):2079-83.

64. Ueland F, DeSimone C, Seamon L, Miller R, Goodrich S, Podzielinski I*, et al.* OVA1 has high sensitivity in identifying ovarian malignancy compared with preoperative assessment and CA-125. *Gynecologic Oncology* 2011;**120**:S73.

65. Boja ES, Rodriguez H. The path to clinical proteomics research: integration of proteomics, genomics, clinical laboratory and regulatory science. *Korean J Lab Med* 2011;**31**(2):61-71 doi 10.3343/kjlm.2011.31.2.61.

66. Zhong L, Li Y, Xiong L, Wang W, Wu M, Yuan T*, et al.* Small molecules in targeted cancer therapy: advances, challenges, and future perspectives. *Signal Transduct Target Ther* 2021;**6**(1):201 doi 10.1038/s41392-021-00572-w.

67. Jin J, Wu X, Yin J, Li M, Shen J, Li J*, et al.* Identification of Genetic Mutations in Cancer: Challenge and Opportunity in the New Era of Targeted Therapy. *Frontiers in Oncology* 2019;**9** doi 10.3389/fonc.2019.00263.

68. Bittenbring JT, Thurner L, Ahlgrimm M, Stilgenbauer S, Bewarder M, Kaddu-Mulindwa D. Cost-effectiveness of precision cancer medicine-current challenges in the use of next generation sequencing for comprehensive tumour genomic profiling and the role of clinical utility frameworks (Review). *Molecular and Clinical Oncology* 2022;**16**(1) doi https://doi.org/10.3892/mco.2021.2453.

69. Ruggles KV, Tang Z, Wang X, Grover H, Askenazi M, Teubl J*, et al.* An Analysis of the Sensitivity of Proteogenomic Mapping of Somatic Mutations and Novel Splicing Events in Cancer. *Mol Cell Proteomics* 2016;**15**(3):1060-71 doi 10.1074/mcp.M115.056226.

70. Vogel C, Marcotte EM. Insights into the regulation of protein abundance from proteomic and transcriptomic analyses. *Nature reviews genetics* 2012;**13**(4):227-32.

71. Lin JJ, Cardarella S, Lydon CA, Dahlberg SE, Jackman DM, Janne PA*, et al.* Five-Year Survival in EGFR-Mutant Metastatic Lung Adenocarcinoma Treated with EGFR-TKIs. *J Thorac Oncol* 2016;**11**(4):556-65 doi 10.1016/j.jtho.2015.12.103.

72. Piperdi B, Perez-Soler R. Role of erlotinib in the treatment of non-small cell lung cancer: clinical outcomes in wild-type epidermal growth factor receptor patients. *Drugs* 2012;**72 Suppl 1**(0 1):11-9 doi 10.2165/1163018-S0-000000000-00000.

73. Yang J, Ahn M, Kim D, Ramalingam S, Sequist L, Wc S*, et al.* Osimertinib in pretreated T790M-positive advanced non-small-cell lung cancer: AURA study phase II extension component. *Journal of Clinical Oncology* 2017:1288-96.

74. Goss G, Tsai C-M, Shepherd FA, Bazhenova L, Lee JS, Chang G-C*, et al.* Osimertinib for pretreated EGFR Thr790Met-positive advanced non-small-cell lung cancer (AURA2): a multicentre, open-label, single-arm, phase 2 study. *The lancet oncology* 2016;**17**(12):1643-52.

75. Soria J-C, Ramalingam SS. Osimertinib in EGFR Mutation-Positive Advanced NSCLC. *The New England journal of medicine* 2018;**378**(13):1262-3.

76. Johnson DB, Dahlman KH, Knol J, Gilbert J, Puzanov I, Means-Powell J*, et al.* Enabling a genetically informed approach to cancer medicine: a retrospective evaluation of the impact of comprehensive tumor profiling using a targeted next-generation sequencing panel. *Oncologist* 2014;**19**(6):616-22 doi 10.1634/theoncologist.2014-0011.

77. Gray SW, Hicks-Courant K, Cronin A, Rollins BJ, Weeks JC. Physicians' attitudes about multiplex tumor genomic testing. *Journal of Clinical Oncology* 2014;**32**(13):1317.

78. Sahajpal NS, Mondal A, Ahluwalia M, Kota V, Njau AN, Okechukwu N*, et al.* Clinical evaluation and performance of QIAGEN Clinical Insight Interpret (QCI-I) as a reporting tool for a comprehensive cancer panel (TSO 500). American Society of Clinical Oncology; 2020.

79. Fruman DA, Rommel C. PI3K and cancer: lessons, challenges and opportunities. *Nat Rev Drug Discov* 2014;**13**(2):140-56 doi 10.1038/nrd4204.

80. Khan KH, Yap TA, Yan L, Cunningham D. Targeting the PI3K-AKT-mTOR signaling network in cancer. *Chin J Cancer* 2013;**32**(5):253-65 doi 10.5732/cjc.013.10057.

81. Noorolyai S, Shajari N, Baghbani E, Sadreddini S, Baradaran B. The relation between PI3K/AKT signalling pathway and cancer. *Gene* 2019;**698**:120-8 doi 10.1016/j.gene.2019.02.076.

82. Vara JÁF, Casado E, de Castro J, Cejas P, Belda-Iniesta C, González-Barón M. PI3K/Akt signalling pathway and cancer. *Cancer treatment reviews* 2004;**30**(2):193-204.

83. Porta C, Paglino C, Mosca A. Targeting PI3K/Akt/mTOR signaling in cancer. *Frontiers in oncology* 2014;**4**:64.

84. Hay N. The Akt-mTOR tango and its relevance to cancer. *Cancer cell* 2005;**8**(3):179-83.

85. Mayer IA, Arteaga CL. The PI3K/AKT pathway as a target for cancer treatment. *Annual review of medicine* 2016;**67**:11-28.

86. O'Donnell JS, Massi D, Teng MW, Mandala M. PI3K-AKT-mTOR inhibition in cancer immunotherapy, redux. 2018. Elsevier. p 91-103.

87. Bellacosa A, Kumar CC, Di Cristofano A, Testa JR. Activation of AKT kinases in cancer: implications for therapeutic targeting. *Adv Cancer Res* 2005;**94**:29-86 doi 10.1016/S0065-230X(05)94002-5.

88. Hinz N, Jucker M. Distinct functions of AKT isoforms in breast cancer: a comprehensive review. *Cell Commun Signal* 2019;**17**(1):154 doi 10.1186/s12964-019-0450-3.

89. De Luca A, Maiello MR, D'Alessio A, Pergameno M, Normanno N. The RAS/RAF/MEK/ERK and the PI3K/AKT signalling pathways: role in cancer pathogenesis and implications for therapeutic approaches. *Expert Opin Ther Targets* 2012;**16 Suppl 2**:S17-27 doi 10.1517/14728222.2011.639361.

90. Shorning BY, Dass MS, Smalley MJ, Pearson HB. The PI3K-AKT-mTOR Pathway and Prostate Cancer: At the Crossroads of AR, MAPK, and WNT Signaling. *Int J Mol Sci* 2020;**21**(12):4507 doi 10.3390/ijms21124507.

91. Lu Y, Zhou J, Xu C, Lin H, Xiao J, Wang Z*, et al.* JAK/STAT and PI3K/AKT pathways form a mutual transactivation loop and afford resistance to oxidative stress-induced apoptosis in cardiomyocytes. *Cell Physiol Biochem* 2008;**21**(4):305-14 doi 10.1159/000129389.

92. Huang WC, Hung MC. Induction of Akt activity by chemotherapy confers acquired resistance. *J Formos Med Assoc* 2009;**108**(3):180-94 doi 10.1016/S0929-6646(09)60051-6.

93. Millis SZ, Ikeda S, Reddy S, Gatalica Z, Kurzrock R. Landscape of Phosphatidylinositol-3-Kinase Pathway Alterations Across 19 784 Diverse Solid Tumors. *JAMA Oncol* 2016;**2**(12):1565-73 doi 10.1001/jamaoncol.2016.0891.

94. Janku F, Yap TA, Meric-Bernstam F. Targeting the PI3K pathway in cancer: are we making headway? *Nature reviews Clinical oncology* 2018;**15**(5):273-91.

95. Engelman JA. Targeting PI3K signalling in cancer: opportunities, challenges and limitations. *Nat Rev Cancer* 2009;**9**(8):550-62 doi 10.1038/nrc2664.

96. Janku F. Phosphoinositide 3-kinase (PI3K) pathway inhibitors in solid tumors: From laboratory to patients. *Cancer Treat Rev* 2017;**59**:93-101 doi 10.1016/j.ctrv.2017.07.005.

97. Rathinaswamy MK, Burke JE. Class I phosphoinositide 3-kinase (PI3K) regulatory subunits and their roles in signaling and disease. *Advances in Biological Regulation* 2020;**75**:100657.

98. Wu P, Liu T, Hu Y. PI3K inhibitors for cancer therapy: what has been achieved so far? *Current medicinal chemistry* 2009;**16**(8):916-30.

99. Yang Q, Modi P, Newcomb T, Queva C, Gandhi V. Idelalisib: First-in-Class PI3K Delta Inhibitor for the Treatment of Chronic Lymphocytic Leukemia, Small Lymphocytic

Leukemia, and Follicular Lymphoma. *Clin Cancer Res* 2015;**21**(7):1537-42 doi 10.1158/1078-0432.CCR-14-2034.

100. Mensah FA, Blaize JP, Bryan LJ. Spotlight on copanlisib and its potential in the treatment of relapsed/refractory follicular lymphoma: evidence to date. *Onco Targets Ther* 2018;**11**:4817-27 doi 10.2147/OTT.S142264.

101. Wilhoit T, Patrick JM, May MB. Alpelisib: A Novel Therapy for Patients With PIK3CA-Mutated Metastatic Breast Cancer. *J Adv Pract Oncol* 2020;**11**(7):768-75 doi 10.6004/jadpro.2020.11.7.9.

102. Skånland SS, Brown JR. PI3K inhibitors in chronic lymphocytic leukemia: where do we go from here? *Haematologica* 2023;**108**(1):9-21 doi 10.3324/haematol.2022.281266.

103. Brown JR. Phosphatidylinositol 3 Kinase δ Inhibitors: Present and Future. *Cancer J* 2019;**25**(6):394-400 doi 10.1097/ppo.0000000000000414.

104. Zou Z, Tao T, Li H, Zhu X. mTOR signaling pathway and mTOR inhibitors in cancer: Progress and challenges. *Cell & Bioscience* 2020;**10**(1):1-11.

105. Kwitkowski VE, Prowell TM, Ibrahim A, Farrell AT, Justice R, Mitchell SS*, et al.* FDA approval summary: temsirolimus as treatment for advanced renal cell carcinoma. *The oncologist* 2010;**15**(4):428-35.

106. Buti S, Leonetti A, Dallatomasina A, Bersanelli M. Everolimus in the management of metastatic renal cell carcinoma: an evidence-based review of its place in therapy. *Core Evidence* 2016;**11**:23.

107. Piccart M, Hortobagyi GN, Campone M, Pritchard KI, Lebrun F, Ito Y*, et al.* Everolimus plus exemestane for hormone-receptor-positive, human epidermal growth factor receptor-2-negative advanced breast cancer: overall survival results from BOLERO-2†. *Annals of Oncology* 2014;**25**(12):2357-62 doi https://doi.org/10.1093/annonc/mdu456.

108. Choueiri TK, Escudier B, Powles T, Mainwaring PN, Rini BI, Donskov F*, et al.* Cabozantinib versus everolimus in advanced renal-cell carcinoma. *New England Journal of Medicine* 2015;**373**(19):1814-23.

109. Royce ME, Osman D. Everolimus in the treatment of metastatic breast cancer. *Breast cancer: basic and clinical research* 2015;**9**:BCBCR. S29268.

110. Cohen Y, Shalmon B, Korach J, Barshack I, Fridman E, Rechavi G. AKT1 pleckstrin homology domain E17K activating mutation in endometrial carcinoma. *Gynecologic oncology* 2010;**116**(1):88-91.

111. Kyung HY, Lauring J. Recurrent AKT mutations in human cancers: functional consequences and effects on drug sensitivity. *Oncotarget* 2016;**7**(4):4241.

112. Hyman DM, Smyth LM, Donoghue MTA, Westin SN, Bedard PL, Dean EJ*, et al.* AKT Inhibition in Solid Tumors With AKT1 Mutations. *J Clin Oncol* 2017;**35**(20):2251-9 doi 10.1200/JCO.2017.73.0143.

113. Mundi PS, Sachdev J, McCourt C, Kalinsky K. AKT in cancer: new molecular insights and advances in drug development. *British Journal of Clinical Pharmacology* 2016;**82**(4):943-56 doi https://doi.org/10.1111/bcp.13021.

114. Fortier A-M, Asselin E, Cadrin M. Functional specificity of Akt isoforms in cancer progression. 2011.

115. Gonzalez E, McGraw TE. The Akt kinases: isoform specificity in metabolism and cancer. *Cell cycle* 2009;**8**(16):2502-8.

116. Zinda MJ, Johnson MA, Paul JD, Horn C, Konicek BW, Lu ZH*, et al.* AKT-1,-2, and-3 are expressed in both normal and tumor tissues of the lung, breast, prostate, and colon. *Clinical cancer research* 2001;**7**(8):2475-9.

117. Hinz N, Jücker M. Distinct functions of AKT isoforms in breast cancer: a comprehensive review. *Cell Communication and Signaling* 2019;**17**:1-29.

118. Kostaras E, Kaserer T, Lazaro G, Heuss SF, Hussain A, Casado P*, et al.* A systematic molecular and pharmacologic evaluation of AKT inhibitors reveals new insight into their biological activity. *Br J Cancer* 2020;**123**(4):542-55 doi 10.1038/s41416-020-0889-4.

119. Andrikopoulou A, Chatzinikolaou S, Panourgias E, Kaparelou M, Liontos M, Dimopoulos MA*, et al.* "The emerging role of capivasertib in breast cancer". *Breast* 2022;**63**:157-67 doi 10.1016/j.breast.2022.03.018.

120. Tokunaga E, Kimura Y, Mashino K, Oki E, Kataoka A, Ohno S*, et al.* Activation of PI3K/Akt signaling and hormone resistance in breast cancer. *Breast Cancer* 2006;**13**(2):137-44 doi 10.2325/jbcs.13.137.

121. Nasrazadani A, Brufsky AM. Capivasertib inhibits a key pathway in metastatic breast cancer. *Lancet Oncol* 2020;**21**(3):318-9 doi 10.1016/S1470-2045(19)30857-5.

122. Jacobsen K, Bertran-Alamillo J, Molina MA, Teixido C, Karachaliou N, Pedersen MH*, et al.* Convergent Akt activation drives acquired EGFR inhibitor resistance in lung cancer. *Nat Commun* 2017;**8**(1):410 doi 10.1038/s41467-017-00450-6.

123. Clement E, Inuzuka H, Nihira NT, Wei W, Toker A. Skp2-dependent reactivation of AKT drives resistance to PI3K inhibitors. *Sci Signal* 2018;**11**(521):eaao3810 doi 10.1126/scisignal.aao3810.

124. Zuo Q, Liu J, Huang L, Qin Y, Hawley T, Seo C*, et al.* AXL/AKT axis mediated-resistance to BRAF inhibitor depends on PTEN status in melanoma. *Oncogene* 2018;**37**(24):3275-89 doi 10.1038/s41388-018-0205-4.

125. Zhang H, Wang Q, Liu J, Cao H. Inhibition of the PI3K/Akt signaling pathway reverses sorafenib-derived chemo-resistance in hepatocellular carcinoma. *Oncol Lett* 2018;**15**(6):9377-84 doi 10.3892/ol.2018.8536.

126. O'Brien NA, McDermott MSJ, Conklin D, Luo T, Ayala R, Salgar S*, et al.* Targeting activated PI3K/mTOR signaling overcomes acquired resistance to CDK4/6-based

therapies in preclinical models of hormone receptor-positive breast cancer. *Breast Cancer Res* 2020;**22**(1):89 doi 10.1186/s13058-020-01320-8.

127. Hanker AB, Kaklamani V, Arteaga CL. Challenges for the Clinical Development of PI3K Inhibitors: Strategies to Improve Their Impact in Solid Tumors. *Cancer Discov* 2019;**9**(4):482-91 doi 10.1158/2159-8290.CD-18-1175.

128. Onesti CE, Vicier C, Andre F. What to expect from high throughput genomics in metastatic breast cancers? *Breast* 2015;**24 Suppl 2**:S19-22 doi 10.1016/j.breast.2015.07.006.

129. Mardis ER. The translation of cancer genomics: time for a revolution in clinical cancer care. *Genome Med* 2014;**6**(3):22 doi 10.1186/gm539.

130. Manolio TA, Collins FS, Cox NJ, Goldstein DB, Hindorff LA, Hunter DJ*, et al.* Finding the missing heritability of complex diseases. *Nature* 2009;**461**(7265):747-53 doi 10.1038/nature08494.

131. Hirschhorn JN, Daly MJ. Genome-wide association studies for common diseases and complex traits. *Nat Rev Genet* 2005;**6**(2):95-108 doi 10.1038/nrg1521.

132. Feinberg AP. Phenotypic plasticity and the epigenetics of human disease. *Nature* 2007;**447**(7143):433-40 doi 10.1038/nature05919.

133. Reimand J, Wagih O, Bader GD. The mutational landscape of phosphorylation signaling in cancer. *Sci Rep* 2013;**3**:2651 doi 10.1038/srep02651.

134. Gonzalez-Angulo AM, Ferrer-Lozano J, Stemke-Hale K, Sahin A, Liu S, Barrera JA*, et al.* PI3K pathway mutations and PTEN levels in primary and metastatic breast cancer. *Mol Cancer Ther* 2011;**10**(6):1093-101 doi 10.1158/1535-7163.MCT-10-1089.

135. Lapek JD, Jr., Greninger P, Morris R, Amzallag A, Pruteanu-Malinici I, Benes CH*, et al.* Detection of dysregulated protein-association networks by high-throughput proteomics predicts cancer vulnerabilities. *Nat Biotechnol* 2017;**35**(10):983-9 doi 10.1038/nbt.3955.

136. Li J, Zhao W, Akbani R, Liu W, Ju Z, Ling S*, et al.* Characterization of Human Cancer Cell Lines by Reverse-phase Protein Arrays. *Cancer Cell* 2017;**31**(2):225-39 doi 10.1016/j.ccell.2017.01.005.

137. Li L, Wei Y, To C, Zhu CQ, Tong J, Pham NA*, et al.* Integrated omic analysis of lung cancer reveals metabolism proteome signatures with prognostic impact. *Nat Commun* 2014;**5**:5469 doi 10.1038/ncomms6469.

138. Blume-Jensen P, Berman DM, Rimm DL, Shipitsin M, Putzi M, Nifong TP*, et al.* Development and clinical validation of an in situ biopsy-based multimarker assay for risk stratification in prostate cancer. *Clin Cancer Res* 2015;**21**(11):2591-600 doi 10.1158/1078-0432.CCR-14-2603.

139. Cohen JD, Javed AA, Thoburn C, Wong F, Tie J, Gibbs P*, et al.* Combined circulating tumor DNA and protein biomarker-based liquid biopsy for the earlier detection of

pancreatic cancers. *Proc Natl Acad Sci U S A* 2017;**114**(38):10202-7 doi 10.1073/pnas.1704961114.

140. Badve S, Kumar GL. Predictive biomarkers in oncology: applications in precision medicine. Springer; 2018.

141. Akbani R, Becker K-F, Carragher N, Goldstein T, de Koning L, Korf U*, et al.* Realizing the Promise of Reverse Phase Protein Arrays for Clinical, Translational, and Basic Research: A Workshop Report: The RPPA (Reverse Phase Protein Array) Society. *Molecular & Cellular Proteomics* 2014;**13**(7):1625-43 doi https://doi.org/10.1074/mcp.O113.034918.

142. Voskuil JL. The challenges with the validation of research antibodies. *F1000Res* 2017;**6**:161 doi 10.12688/f1000research.10851.1.

143. Andersson S, Sundberg M, Pristovsek N, Ibrahim A, Jonsson P, Katona B*, et al.* Insufficient antibody validation challenges oestrogen receptor beta research. *Nat Commun* 2017;**8**:15840 doi 10.1038/ncomms15840.

144. Uhlen M, Fagerberg L, Hallstrom BM, Lindskog C, Oksvold P, Mardinoglu A*, et al.* Proteomics. Tissue-based map of the human proteome. *Science* 2015;**347**(6220):1260419 doi 10.1126/science.1260419.

145. Algenäs C, Agaton C, Fagerberg L, Asplund A, Björling L, Björling E*, et al.* Antibody performance in western blot applications is context-dependent. *Biotechnol J* 2014;**9**(3):435-45 doi 10.1002/biot.201300341.

146. Edwards AM, Isserlin R, Bader GD, Frye SV, Willson TM, Yu FH. Too many roads not taken. *Nature* 2011;**470**(7333):163-5 doi 10.1038/470163a.

147. Ong SE, Mann M. Mass spectrometry-based proteomics turns quantitative. *Nat Chem Biol* 2005;**1**(5):252-62 doi 10.1038/nchembio736.

148. Deterding LJ, Parker CE, Perkins JR, Arthur Moseley M, Jorgenson JW, Tomer KB. Nanoscale separations. *Journal of Chromatography A* 1991;**554**(1-2):329-38 doi 10.1016/s0021-9673(01)88460-0.

149. Carr SA, Abbatiello SE, Ackermann BL, Borchers C, Domon B, Deutsch EW*, et al.* Targeted peptide measurements in biology and medicine: best practices for mass spectrometry-based assay development using a fit-for-purpose approach. *Mol Cell Proteomics* 2014;**13**(3):907-17 doi 10.1074/mcp.M113.036095.

150. Omenn GS, States DJ, Adamski M, Blackwell TW, Menon R, Hermjakob H*, et al.* Overview of the HUPO Plasma Proteome Project: results from the pilot phase with 35 collaborating laboratories and multiple analytical groups, generating a core dataset of 3020 proteins and a publicly-available database. *Proteomics* 2005;**5**(13):3226-45 doi 10.1002/pmic.200500358.

151. Method of the Year 2012. *Nat Methods* 2013;**10**(1):1 doi 10.1038/nmeth.2329.

152. Gillette MA, Carr SA. Quantitative analysis of peptides and proteins in biomedicine by targeted mass spectrometry. *Nat Methods* 2013;**10**(1):28-34 doi 10.1038/nmeth.2309.

153. Addona TA, Abbatiello SE, Schilling B, Skates SJ, Mani DR, Bunk DM*, et al.* Multi-site assessment of the precision and reproducibility of multiple reaction monitoring-based measurements of proteins in plasma. *Nat Biotechnol* 2009;**27**(7):633-41 doi 10.1038/nbt.1546.

154. Percy AJ, Chambers AG, Yang J, Hardie DB, Borchers CH. Advances in multiplexed MRM-based protein biomarker quantitation toward clinical utility. *Biochim Biophys Acta* 2014;**1844**(5):917-26 doi 10.1016/j.bbapap.2013.06.008.

155. Liebler DC, Zimmerman LJ. Targeted quantitation of proteins by mass spectrometry. *Biochemistry* 2013;**52**(22):3797-806 doi 10.1021/bi400110b.

156. Lee JW, Devanarayan V, Barrett YC, Weiner R, Allinson J, Fountain S*, et al.* Fit-for-purpose method development and validation for successful biomarker measurement. *Pharm Res* 2006;**23**(2):312-28 doi 10.1007/s11095-005-9045-3.

157. Gallien S, Duriez E, Crone C, Kellmann M, Moehring T, Domon B. Targeted proteomic quantification on quadrupole-orbitrap mass spectrometer. *Mol Cell Proteomics* 2012;**11**(12):1709-23 doi 10.1074/mcp.O112.019802.

158. Ronsein GE, Pamir N, von Haller PD, Kim DS, Oda MN, Jarvik GP*, et al.* Parallel reaction monitoring (PRM) and selected reaction monitoring (SRM) exhibit comparable linearity, dynamic range and precision for targeted quantitative HDL proteomics. *J Proteomics* 2015;**113**:388-99 doi 10.1016/j.jprot.2014.10.017.

159. Peterson AC, Russell JD, Bailey DJ, Westphall MS, Coon JJ. Parallel reaction monitoring for high resolution and high mass accuracy quantitative, targeted proteomics. *Mol Cell Proteomics* 2012;**11**(11):1475-88 doi 10.1074/mcp.O112.020131.

160. Nice EC. The status of proteomics as we enter the 2020s: Towards personalised/precision medicine. *Anal Biochem* 2022;**644**:113840 doi 10.1016/j.ab.2020.113840.

161. Omenn GS, Nass SJ, Micheel CM. Evolution of translational omics: lessons learned and the path forward. 2012.

162. Check E. Running before we can walk? *Nature* 2004;**429**(6991):496-7 doi 10.1038/429496a.

163. Wagner L. A test before its time? FDA stalls distribution process of proteomic test. *J Natl Cancer Inst* 2004;**96**(7):500-1 doi 10.1093/jnci/96.7.500.

164. Check E. Proteomics and cancer: running before we can walk? *Nature* 2004;**429**(6991):496-7 doi 10.1038/429496a.

165. Baggerly K. Experimental Design, Randomization, and Validation. *Clinical Chemistry* 2018;**64**(10):1534-5 doi 10.1373/clinchem.2017.273334.

166. Liotta LA, Petricoin EF. Mass spectrometry-based protein biomarker discovery: solving the remaining challenges to reach the promise of clinical benefit. *Clin Chem* 2010;**56**(10):1641-2 doi 10.1373/clinchem.2010.146142.

167. Whiteaker JR, Halusa GN, Hoofnagle AN, Sharma V, MacLean B, Yan P*, et al.* CPTAC Assay Portal: a repository of targeted proteomic assays. *Nat Methods* 2014;**11**(7):703-4 doi 10.1038/nmeth.3002.

168. Whiteaker JR, Halusa GN, Hoofnagle AN, Sharma V, MacLean B, Yan P*, et al.* Using the CPTAC Assay Portal to Identify and Implement Highly Characterized Targeted Proteomics Assays. *Methods Mol Biol* 2016;**1410**:223-36 doi 10.1007/978-1-4939-3524-6_13.

169. Banerji U, Dean EJ, Pérez-Fidalgo JA, Batist G, Bedard PL, You B*, et al.* A Phase I Open-Label Study to Identify a Dosing Regimen of the Pan-AKT Inhibitor AZD5363 for Evaluation in Solid Tumors and in PIK3CA-Mutated Breast and Gynecologic Cancers. *Clin Cancer Res* 2018;**24**(9):2050-9 doi 10.1158/1078-0432.Ccr-17-2260.

170. Popp R, Li H, LeBlanc A, Mohammed Y, Aguilar-Mahecha A, Chambers AG*, et al.* Immuno-Matrix-Assisted Laser Desorption/Ionization Assays for Quantifying AKT1 and AKT2 in Breast and Colorectal Cancer Cell Lines and Tumors. *Anal Chem* 2017;**89**(19):10592-600 doi 10.1021/acs.analchem.7b02934.

171. Froehlich BC, Popp R, Sobsey CA, Ibrahim S, LeBlanc AM, Mohammed Y*, et al.* Systematic Optimization of the iMALDI Workflow for the Robust and Straightforward Quantification of Signaling Proteins in Cancer Cells. *Proteomics Clin Appl* 2020;**14**(5):e2000034 doi 10.1002/prca.202000034.

172. Domanski D, Murphy LC, Borchers CH. Assay development for the determination of phosphorylation stoichiometry using multiple reaction monitoring methods with and without phosphatase treatment: application to breast cancer signaling pathways. *Anal Chem* 2010;**82**(13):5610-20 doi 10.1021/ac1005553.

173. Froehlich BC, Gill HK, Joshi A, Goodlett DR. MS visualization and interpretation software (MS-VIS), a tool for visualizing mass spectra and analysing mass lists. *Rapid Commun Mass Spectrom* 2022;**36**(8):e9253 doi 10.1002/rcm.9253.

174. Spitzer M, Wildenhain J, Rappsilber J, Tyers M. BoxPlotR: a web tool for generation of box plots. *Nat Methods* 2014;**11**(2):121-2 doi 10.1038/nmeth.2811.

175. Pang Z, Chong J, Zhou G, de Lima Morais DA, Chang L, Barrette M*, et al.* MetaboAnalyst 5.0: narrowing the gap between raw spectra and functional insights. *Nucleic acids research* 2021;**49**(W1):W388-W96.

176. Szklarczyk D, Gable AL, Nastou KC, Lyon D, Kirsch R, Pyysalo S*, et al.* The STRING database in 2021: customizable protein–protein networks, and functional characterization of user-uploaded gene/measurement sets. *Nucleic acids research* 2021;**49**(D1):D605-D12.

177. Doncheva NT, Morris JH, Gorodkin J, Jensen LJ. Cytoscape StringApp: Network Analysis and Visualization of Proteomics Data. *J Proteome Res* 2019;**18**(2):623-32 doi 10.1021/acs.jproteome.8b00702.

178. Mohammed Y, Domanski D, Jackson AM, Smith DS, Deelder AM, Palmblad M*, et al.* PeptidePicker: a scientific workflow with web interface for selecting appropriate peptides for targeted proteomics experiments. *J Proteomics* 2014;**106**:151-61 doi 10.1016/j.jprot.2014.04.018.

179. Deutsch EW. The PeptideAtlas Project. In: Hubbard SJ, Jones AR, editors. Proteome Bioinformatics. Totowa, NJ: Humana Press; 2010. p. 285-96.

180. Smith SE, Mellor P, Ward AK, Kendall S, McDonald M, Vizeacoumar FS*, et al.* Molecular characterization of breast cancer cell lines through multiple omic approaches. *Breast Cancer Res* 2017;**19**(1):65 doi 10.1186/s13058-017-0855-0.

181. Dai X, Cheng H, Bai Z, Li J. Breast Cancer Cell Line Classification and Its Relevance with Breast Tumor Subtyping. *J Cancer* 2017;**8**(16):3131-41 doi 10.7150/jca.18457.

182. Sommer EM, Dry H, Cross D, Guichard S, Davies BR, Alessi DR. Elevated SGK1 predicts resistance of breast cancer cells to Akt inhibitors. *Biochem J* 2013;**452**(3):499-508 doi 10.1042/BJ20130342.

183. Bairoch A. The cellosaurus, a cell-line knowledge resource. *Journal of biomolecular techniques: JBT* 2018;**29**(2):25.

184. Schmitt K, Daubener W, Bitter-Suermann D, Hadding U. A safe and efficient method for elimination of cell culture mycoplasmas using ciprofloxacin. *J Immunol Methods* 1988;**109**(1):17-25 doi 10.1016/0022-1759(88)90437-1.

185. Ianevski A, Giri AK, Aittokallio T. SynergyFinder 3.0: an interactive analysis and consensus interpretation of multi-drug synergies across multiple samples. *Nucleic Acids Res* 2022;**50**(W1):W739-W43 doi 10.1093/nar/gkac382.

186. Pino LK, Searle BC, Bollinger JG, Nunn B, MacLean B, MacCoss MJ. The Skyline ecosystem: Informatics for quantitative mass spectrometry proteomics. *Mass Spectrom Rev* 2020;**39**(3):229-44 doi 10.1002/mas.21540.

187. Mitsa G, Guo Q, Goncalves C, Preston SE, Lacasse V, Aguilar-Mahecha A*, et al.* A Non-Hazardous Deparaffinization Protocol Enables Quantitative Proteomics of Core Needle Biopsy-Sized Formalin-Fixed and Paraffin-Embedded (FFPE) Tissue Specimens. *International Journal of Molecular Sciences* 2022;**23**(8):4443.

188. Batth TS, Tollenaere MX, Rüther P, Gonzalez-Franquesa A, Prabhakar BS, Bekker-Jensen S*, et al.* Protein Aggregation Capture on Microparticles Enables Multipurpose Proteomics Sample Preparation*. *Molecular & Cellular Proteomics* 2019;**18**(5):1027-35 doi https://doi.org/10.1074/mcp.TIR118.001270.

189. Mady N. A validation study measuring the cytochrome P450 enzyme subfamily 3A4 activity in free-living adults. https://escholarship.mcgill.ca/concern/theses/9p290f986: McGill University; 2020.

190. Bosilkovska M, Deglon J, Samer C, Walder B, Desmeules J, Staub C*, et al.* Simultaneous LC-MS/MS quantification of P-glycoprotein and cytochrome P450 probe substrates and their metabolites in DBS and plasma. *Bioanalysis* 2014;**6**(2):151-64 doi 10.4155/bio.13.289.

191. Derungs A, Donzelli M, Berger B, Noppen C, Krahenbuhl S, Haschke M. Effects of Cytochrome P450 Inhibition and Induction on the Phenotyping Metrics of the Basel Cocktail: A Randomized Crossover Study. *Clin Pharmacokinet* 2016;**55**(1):79-91 doi 10.1007/s40262-015-0294-y.

192. Adams KJ, Pratt B, Bose N, Dubois LG, St. John-Williams L, Perrott KM*, et al.* Skyline for small molecules: a unifying software package for quantitative metabolomics. *Journal of proteome research* 2020;**19**(4):1447-58.

193. Nitulescu GM, Margina D, Juzenas P, Peng Q, Olaru OT, Saloustros E*, et al.* Akt inhibitors in cancer treatment: The long journey from drug discovery to clinical use (Review). *Int J Oncol* 2016;**48**(3):869-85 doi 10.3892/ijo.2015.3306.

194. Davies BR, Greenwood H, Dudley P, Crafter C, Yu D-H, Zhang J*, et al.* Preclinical Pharmacology of AZD5363, an Inhibitor of AKT: Pharmacodynamics, Antitumor Activity, and Correlation of Monotherapy Activity with Genetic BackgroundAZD5363, an Oral Inhibitor of AKT. *Molecular cancer therapeutics* 2012;**11**(4):873-87.

195. Turner NC, Alarcon E, Armstrong AC, Philco M, Lopez Chuken YA, Sablin MP*, et al.* BEECH: a dose-finding run-in followed by a randomised phase II study assessing the efficacy of AKT inhibitor capivasertib (AZD5363) combined with paclitaxel in patients with estrogen receptor-positive advanced or metastatic breast cancer, and in a PIK3CA mutant sub-population. *Ann Oncol* 2019;**30**(5):774-80 doi 10.1093/annonc/mdz086.

196. Kalinsky K, Hong F, McCourt CK, Sachdev JC, Mitchell EP, Zwiebel JA*, et al.* Effect of Capivasertib in Patients With an AKT1 E17K-Mutated Tumor: NCI-MATCH Subprotocol EAY131-Y Nonrandomized Trial. *JAMA Oncol* 2021;**7**(2):271-8 doi 10.1001/jamaoncol.2020.6741.

197. Robertson JFR, Coleman RE, Cheung KL, Evans A, Holcombe C, Skene A*, et al.* Proliferation and AKT Activity Biomarker Analyses after Capivasertib (AZD5363) Treatment of Patients with ER(+) Invasive Breast Cancer (STAKT). *Clin Cancer Res* 2020;**26**(7):1574-85 doi 10.1158/1078-0432.CCR-19-3053.

198. Ribas R, Pancholi S, Guest SK, Marangoni E, Gao Q, Thuleau A*, et al.* AKT Antagonist AZD5363 Influences Estrogen Receptor Function in Endocrine-Resistant Breast Cancer and Synergizes with Fulvestrant (ICI182780) In Vivo. *Mol Cancer Ther* 2015;**14**(9):2035-48 doi 10.1158/1535-7163.MCT-15-0143.

199. Fox EM, Kuba MG, Miller TW, Davies BR, Arteaga CL. Autocrine IGF-I/insulin receptor axis compensates for inhibition of AKT in ER-positive breast cancer cells with resistance to estrogen deprivation. *Breast Cancer Res* 2013;**15**(4):R55 doi 10.1186/bcr3449.

200. Toren P, Kim S, Cordonnier T, Crafter C, Davies BR, Fazli L*, et al.* Combination AZD5363 with enzalutamide significantly delays enzalutamide-resistant prostate cancer in preclinical models. *European urology* 2015;**67**(6):986-90.

201. Li J, Davies BR, Han S, Zhou M, Bai Y, Zhang J*, et al.* The AKT inhibitor AZD5363 is selectively active in PI3KCA mutant gastric cancer, and sensitizes a patient-derived gastric cancer xenograft model with PTEN loss to Taxotere. *Journal of translational medicine* 2013;**11**(1):1-10.

202. Puglisi M, Thavasu P, Stewart A, de Bono JS, O'Brien ME, Popat S*, et al.* AKT inhibition synergistically enhances growth-inhibitory effects of gefitinib and increases apoptosis in non-small cell lung cancer cell lines. *Lung Cancer* 2014;**85**(2):141-6 doi 10.1016/j.lungcan.2014.05.008.

203. Thomas C, Lamoureux F, Crafter C, Davies BR, Beraldi E, Fazli L*, et al.* Synergistic Targeting of PI3K/AKT Pathway and Androgen Receptor Axis Significantly Delays Castration-Resistant Prostate Cancer Progression In VivoTargeting AKT Pathway and AR Axis in Prostate Cancer. *Molecular cancer therapeutics* 2013;**12**(11):2342-55.

204. Liu J, Duan Z, Guo W, Zeng L, Wu Y, Chen Y*, et al.* Targeting the BRD4/FOXO3a/CDK6 axis sensitizes AKT inhibition in luminal breast cancer. *Nat Commun* 2018;**9**(1):5200 doi 10.1038/s41467-018-07258-y.

205. Gris-Oliver A, Palafox M, Monserrat L, Brasó-Maristany F, Òdena A, Sánchez-Guixé M*, et al.* Genetic Alterations in the PI3K/AKT Pathway and Baseline AKT Activity Define AKT Inhibitor Sensitivity in Breast Cancer Patient-derived XenograftsBiomarkers of Sensitivity to AKT Inhibition in Breast Cancer. *Clinical Cancer Research* 2020;**26**(14):3720-31.

206. Di Cristofano A. Chapter Two - SGK1: The Dark Side of PI3K Signaling. In: Jenny A, editor. Current Topics in Developmental Biology. Volume 123: Academic Press; 2017. p. 49-71.

207. Cicenas J, Meskinyte-Kausiliene E, Jukna V, Rimkus A, Simkus J, Soderholm D. SGK1 in Cancer: Biomarker and Drug Target. *Cancers (Basel)* 2022;**14**(10):2385 doi 10.3390/cancers14102385.

208. Gao J, Sidiropoulou E, Walker I, Krupka JA, Mizielinski K, Usheva Z*, et al.* SGK1 mutations in DLBCL generate hyperstable protein neoisoforms that promote AKT independence. *Blood* 2021;**138**(11):959-64.

209. Castel P, Ellis H, Bago R, Toska E, Razavi P, Carmona FJ*, et al.* PDK1-SGK1 Signaling Sustains AKT-Independent mTORC1 Activation and Confers Resistance to PI3Kalpha Inhibition. *Cancer Cell* 2016;**30**(2):229-42 doi 10.1016/j.ccell.2016.06.004.

210. Dean E, Banerji U, Schellens JHM, Krebs MG, Jimenez B, van Brummelen E*, et al.* A Phase 1, open-label, multicentre study to compare the capsule and tablet formulations of AZD5363 and explore the effect of food on the pharmacokinetic exposure, safety and tolerability of AZD5363 in patients with advanced solid malignancies: OAK. *Cancer Chemother Pharmacol* 2018;**81**(5):873-83 doi 10.1007/s00280-018-3558-z.

211. Smyth LM, Tamura K, Oliveira M, Ciruelos EM, Mayer IA, Sablin MP*, et al.* Capivasertib, an AKT Kinase Inhibitor, as Monotherapy or in Combination with Fulvestrant in Patients with AKT1 (E17K)-Mutant, ER-Positive Metastatic Breast Cancer. *Clin Cancer Res* 2020;**26**(15):3947-57 doi 10.1158/1078-0432.CCR-19-3953.

212. Crabb SJ, Ye D-W, Uemura H, Morris T, Gresty C, Logan J*, et al.* CAPItello-280: A phase III study of capivasertib and docetaxel versus placebo and docetaxel in metastatic castration-resistant prostate cancer. American Society of Clinical Oncology; 2023.

213. Fizazi K, George DJ, De Santis M, Clarke N, Fay AP, Uemura H*, et al.* A phase III trial of capivasertib and abiraterone versus placebo and abiraterone in patients with de novo metastatic hormone-sensitive prostate cancer characterized by PTEN deficiency (CAPItello-281). American Society of Clinical Oncology; 2021.

214. Schmid P, Abraham J, Chan S, Wheatley D, Brunt AM, Nemsadze G*, et al.* Capivasertib Plus Paclitaxel Versus Placebo Plus Paclitaxel As First-Line Therapy for Metastatic Triple-Negative Breast Cancer: The PAKT Trial. *J Clin Oncol* 2020;**38**(5):423-33 doi 10.1200/JCO.19.00368.

215. Westin SN, Labrie M, Litton JK, Blucher A, Fang Y, Vellano CP*, et al.* Phase Ib Dose Expansion and Translational Analyses of Olaparib in Combination with Capivasertib in Recurrent Endometrial, Triple-Negative Breast, and Ovarian Cancer. *Clin Cancer Res* 2021;**27**(23):6354-65 doi 10.1158/1078-0432.CCR-21-1656.

216. Jones RH, Casbard A, Carucci M, Cox C, Butler R, Alchami F*, et al.* Fulvestrant plus capivasertib versus placebo after relapse or progression on an aromatase inhibitor in metastatic, oestrogen receptor-positive breast cancer (FAKTION): a multicentre, randomised, controlled, phase 2 trial. *Lancet Oncol* 2020;**21**(3):345-57 doi 10.1016/S1470-2045(19)30817-4.

217. Smyth LM, Batist G, Meric-Bernstam F, Kabos P, Spanggaard I, Lluch A*, et al.* Selective AKT kinase inhibitor capivasertib in combination with fulvestrant in PTEN-mutant ER-positive metastatic breast cancer. *NPJ Breast Cancer* 2021;**7**(1):44 doi 10.1038/s41523-021-00251-7.

218. Turner NC, Oliveira M, Howell SJ, Dalenc F, Cortes J, Gomez Moreno HL*, et al.* Capivasertib in Hormone Receptor–Positive Advanced Breast Cancer. *New England Journal of Medicine* 2023;**388**(22):2058-70.

219. Fujimoto Y, Morita TY, Ohashi A, Haeno H, Hakozaki Y, Fujii M*, et al.* Combination treatment with a PI3K/Akt/mTOR pathway inhibitor overcomes resistance to anti-HER2 therapy in PIK3CA-mutant HER2-positive breast cancer cells. *Sci Rep* 2020;**10**(1):21762 doi 10.1038/s41598-020-78646-y.

220. Roylance R, Kilburn L, Kernaghan S, Wardley AM, Macpherson I, Baird RD*, et al.* Abstract P1-19-11: Results from plasmaMATCH trial treatment cohort C: A phase II trial of capivasertib plus fulvestrant in ER positive breast cancer patients with an AKT1 mutation identified via ctDNA screening (CRUK/15/010). *Cancer Research* 2020;**80**(4_Supplement):P1-19-1-P1--1.

221. Schmid P, Abraham J, Chan S, Brunt AM, Nemsadze G, Baird RD*, et al.* Abstract PD1-11: mature survival update of the double-blind placebo-controlled randomised phase II PAKT trial of first-line capivasertib plus paclitaxel for metastatic triple-negative breast cancer. *Cancer Research* 2021;**81**(4_Supplement):PD1-11-PD1-.

222. Vasudevan KM, Barbie DA, Davies MA, Rabinovsky R, McNear CJ, Kim JJ*, et al.* AKT-independent signaling downstream of oncogenic PIK3CA mutations in human cancer. *Cancer Cell* 2009;**16**(1):21-32 doi 10.1016/j.ccr.2009.04.012.

223. Faes S, Dormond O. PI3K and AKT: Unfaithful Partners in Cancer. *Int J Mol Sci* 2015;**16**(9):21138-52 doi 10.3390/ijms160921138.

224. Cancer Genome Atlas N. Comprehensive molecular portraits of human breast tumours. *Nature* 2012;**490**(7418):61-70 doi 10.1038/nature11412.

225. Paplomata E, O'Regan R. The PI3K/AKT/mTOR pathway in breast cancer: targets, trials and biomarkers. *Ther Adv Med Oncol* 2014;**6**(4):154-66 doi 10.1177/1758834014530023.

226. She QB, Chandarlapaty S, Ye Q, Lobo J, Haskell KM, Leander KR*, et al.* Breast tumor cells with PI3K mutation or HER2 amplification are selectively addicted to Akt signaling. *PLoS One* 2008;**3**(8):e3065 doi 10.1371/journal.pone.0003065.

227. Rugo HS, Schiavon G, Grinsted LM, De Bruin EC, Catanese MT, Hamilton E. Abstract OT2-14-01: CAPItello-292: A phase Ib/III study of capivasertib, palbociclib and fulvestrant, versus placebo, palbociclib and fulvestrant, for endocrine therapy-resistant HR+/HER2− advanced breast cancer. *Cancer Research* 2022;**82**(4_Supplement):OT2-14-01-OT2-14-01.

228. Roumeliotis TI, Williams SP, Goncalves E, Alsinet C, Del Castillo Velasco-Herrera M, Aben N*, et al.* Genomic Determinants of Protein Abundance Variation in Colorectal Cancer Cells. *Cell Rep* 2017;**20**(9):2201-14 doi 10.1016/j.celrep.2017.08.010.

229. Vogeser M, Seger C. Pitfalls associated with the use of liquid chromatography-tandem mass spectrometry in the clinical laboratory. *Clin Chem* 2010;**56**(8):1234-44 doi 10.1373/clinchem.2009.138602.

230. Sobsey CA, Popp R, Ibrahim S, Froehlich BC, Aguilar-Mahecha A, Basik M*, et al.* Protein quantitation assays for Akt, PI3K p110 alpha, and PTEN to assess PI3K pathway activity in tumor tissue. 2020. AMER ASSOC CANCER RESEARCH 615 CHESTNUT ST, 17TH FLOOR, PHILADELPHIA, PA …. p 51-2.

231. Cizkova M, Vacher S, Meseure D, Trassard M, Susini A, Mlcuchova D*, et al.* PIK3R1 underexpression is an independent prognostic marker in breast cancer. *BMC Cancer* 2013;**13**:545 doi 10.1186/1471-2407-13-545.

232. Kim SH, Seung BJ, Cho SH, Lim HY, Bae MK, Sur JH. Dysregulation of PI3K/Akt/PTEN Pathway in Canine Mammary Tumor. *Animals (Basel)* 2021;**11**(7) doi 10.3390/ani11072079.

233. Guertin DA, Stevens DM, Thoreen CC, Burds AA, Kalaany NY, Moffat J*, et al.* Ablation in mice of the mTORC components raptor, rictor, or mLST8 reveals that mTORC2 is required for signaling to Akt-FOXO and PKCalpha, but not S6K1. *Dev Cell* 2006;**11**(6):859-71 doi 10.1016/j.devcel.2006.10.007.

234. O'Hurley G, Daly E, O'Grady A, Cummins R, Quinn C, Flanagan L*, et al.* Investigation of molecular alterations of AKT-3 in triple-negative breast cancer. *Histopathology* 2014;**64**(5):660-70 doi 10.1111/his.12313.

235. Stemke-Hale K, Gonzalez-Angulo AM, Lluch A, Neve RM, Kuo WL, Davies M*, et al.* An integrative genomic and proteomic analysis of PIK3CA, PTEN, and AKT mutations in breast cancer. *Cancer Res* 2008;**68**(15):6084-91 doi 10.1158/0008-5472.CAN-07-6854.

236. Hoehn KL, Hohnen-Behrens C, Cederberg A, Wu LE, Turner N, Yuasa T*, et al.* IRS1-independent defects define major nodes of insulin resistance. *Cell Metab* 2008;**7**(5):421-33 doi 10.1016/j.cmet.2008.04.005.

237. Vincent EE, Elder DJ, Thomas EC, Phillips L, Morgan C, Pawade J*, et al.* Akt phosphorylation on Thr308 but not on Ser473 correlates with Akt protein kinase activity in human non-small cell lung cancer. *Br J Cancer* 2011;**104**(11):1755-61 doi 10.1038/bjc.2011.132.

238. Fiala O, Pesek M, Finek J, Racek J, Minarik M, Benesova L*, et al.* Serum albumin is a strong predictor of survival in patients with advanced-stage non-small cell lung cancer treated with erlotinib. *Neoplasma* 2016;**63**(3):471-6 doi 10.4149/318_151001N512.

239. Dalmiglio C, Brilli L, Campanile M, Ciuoli C, Cartocci A, Castagna MG. CONUT Score: A New Tool for Predicting Prognosis in Patients with Advanced Thyroid Cancer Treated with TKI. *Cancers (Basel)* 2022;**14**(3):724 doi 10.3390/cancers14030724.

240. Park MJ, Lee J, Hong JY, Choi MK, Yi JH, Lee SJ*, et al.* Prognostic model to predict outcomes in nonsmall cell lung cancer patients treated with gefitinib as a salvage treatment. *Cancer* 2009;**115**(7):1518-30 doi 10.1002/cncr.24151.

241. Jones DT, Ganeshaguru K, Anderson RJ, Jackson TR, Bruckdorfer KR, Low SY*, et al.* Albumin activates the AKT signaling pathway and protects B-chronic lymphocytic leukemia cells from chlorambucil- and radiation-induced apoptosis. *Blood* 2003;**101**(8):3174-80 doi 10.1182/blood-2002-07-2143.

242. Tey SK, Wong SWK, Chan JYT, Mao X, Ng TH, Yeung CLS*, et al.* Patient pIgR-enriched extracellular vesicles drive cancer stemness, tumorigenesis and metastasis in hepatocellular carcinoma. *J Hepatol* 2022;**76**(4):883-95 doi 10.1016/j.jhep.2021.12.005.

243. Franks SE, Briah R, Jones RA, Moorehead RA. Unique roles of Akt1 and Akt2 in IGF-IR mediated lung tumorigenesis. *Oncotarget* 2016;**7**(3):3297-316 doi 10.18632/oncotarget.6489.

244. Mandal S, Bandyopadhyay S, Tyagi K, Roy A. Recent advances in understanding the molecular role of phosphoinositide-specific phospholipase C gamma 1 as an emerging onco-driver and novel therapeutic target in human carcinogenesis. *Biochim Biophys Acta Rev Cancer* 2021;**1876**(2):188619 doi 10.1016/j.bbcan.2021.188619.

245. Bhargava M, Viken KJ, Barkes B, Griffin TJ, Gillespie M, Jagtap PD*, et al.* Novel protein pathways in development and progression of pulmonary sarcoidosis. *Sci Rep* 2020;**10**(1):13282 doi 10.1038/s41598-020-69281-8.

246. Wang LM, Gan YH. Cancer-derived IgG involved in cisplatin resistance through PTP-BAS/Src/PDK1/AKT signaling pathway. *Oral Dis* 2021;**27**(3):464-74 doi 10.1111/odi.13583.

247. Schmidt M, Hellwig B, Hammad S, Othman A, Lohr M, Chen Z*, et al.* A comprehensive analysis of human gene expression profiles identifies stromal immunoglobulin kappa C as a compatible prognostic marker in human solid tumors. *Clin Cancer Res* 2012;**18**(9):2695-703 doi 10.1158/1078-0432.CCR-11-2210.

248. Schmidt M, Edlund K, Hengstler JG, Heimes AS, Almstedt K, Lebrecht A*, et al.* Prognostic Impact of Immunoglobulin Kappa C (IGKC) in Early Breast Cancer. *Cancers (Basel)* 2021;**13**(14):3626 doi 10.3390/cancers13143626.

249. Buoso E, Masi M, Long A, Chiappini C, Travelli C, Govoni S*, et al.* Ribosomes as a nexus between translation and cancer progression: Focus on ribosomal Receptor for Activated C Kinase 1 (RACK1) in breast cancer. *Br J Pharmacol* 2022;**179**(12):2813-28 doi 10.1111/bph.15218.

250. Zhang H, Cheng L, Liu C. Regulatory Networks of Prognostic mRNAs in Pediatric Acute Myeloid Leukemia. *J Healthc Eng* 2022;**2022**:2691997 doi 10.1155/2022/2691997.

251. Lin Z, Peng R, Sun Y, Zhang L, Zhang Z. Identification of ribosomal protein family in triple-negative breast cancer by bioinformatics analysis. *Biosci Rep* 2021;**41**(1) doi 10.1042/BSR20200869.

252. Fang E, Zhang X. Identification of breast cancer hub genes and analysis of prognostic values using integrated bioinformatics analysis. *Cancer Biomark* 2017;**21**(1):373-81 doi 10.3233/CBM-170550.

253. Geuens T, Bouhy D, Timmerman V. The hnRNP family: insights into their role in health and disease. *Human genetics* 2016;**135**:851-67.

254. Guo J, Jia R. Splicing factor poly (rC)-binding protein 1 is a novel and distinctive tumor suppressor. *Journal of cellular physiology* 2019;**234**(1):33-41.

255. Fei T, Chen Y, Xiao T, Li W, Cato L, Zhang P*, et al.* Genome-wide CRISPR screen identifies HNRNPL as a prostate cancer dependency regulating RNA splicing. *Proceedings of the National Academy of Sciences* 2017;**114**(26):E5207-E15.

256. Sciarrillo R, Wojtuszkiewicz A, Assaraf YG, Jansen G, Kaspers GJL, Giovannetti E*, et al.* The role of alternative splicing in cancer: From oncogenesis to drug resistance. *Drug Resist Updat* 2020;**53**:100728 doi 10.1016/j.drup.2020.100728.

257. Jin Z, Xu L, Zhang L, Zhao M, Li D, Ye L*, et al.* Interleukin enhancer binding factor 2 is a prognostic biomarker for breast cancer that also predicts neoadjuvant chemotherapy responses. *Am J Transl Res* 2018;**10**(6):1677-89.

258. Pei Y, Zhu P, Dang Y, Wu J, Yang X, Wan B*, et al.* Nuclear export of NF90 to stabilize IL-2 mRNA is mediated by AKT-dependent phosphorylation at Ser647 in response to CD28 costimulation. *J Immunol* 2008;**180**(1):222-9 doi 10.4049/jimmunol.180.1.222.

259. Higuchi T, Todaka H, Sugiyama Y, Ono M, Tamaki N, Hatano E*, et al.* Suppression of MicroRNA-7 (miR-7) Biogenesis by Nuclear Factor 90-Nuclear Factor 45 Complex (NF90-NF45) Controls Cell Proliferation in Hepatocellular Carcinoma. *J Biol Chem* 2016;**291**(40):21074-84 doi 10.1074/jbc.M116.748210.

260. Zang B, Wang W, Wang Y, Li P, Xia T, Liu X*, et al.* Metabolomic Characterization Reveals ILF2 and ILF3 Affected Metabolic Adaptions in Esophageal Squamous Cell Carcinoma. *Front Mol Biosci* 2021;**8**:721990 doi 10.3389/fmolb.2021.721990.

261. Mishra S, Ande SR, Nyomba BL. The role of prohibitin in cell signaling. *FEBS J* 2010;**277**(19):3937-46 doi 10.1111/j.1742-4658.2010.07809.x.

262. Bavelloni A, Piazzi M, Faenza I, Raffini M, D'Angelo A, Cattini L*, et al.* Prohibitin 2 represents a novel nuclear AKT substrate during all-trans retinoic acid-induced differentiation of acute promyelocytic leukemia cells. *FASEB J* 2014;**28**(5):2009-19 doi 10.1096/fj.13-244368.

263. McCubrey JA, Steelman LS, Chappell WH, Abrams SL, Franklin RA, Montalto G*, et al.* Ras/Raf/MEK/ERK and PI3K/PTEN/Akt/mTOR cascade inhibitors: how mutations can result in therapy resistance and how to overcome resistance. *Oncotarget* 2012;**3**(10):1068.

264. Tseng PC, Chen CL, Shan YS, Lin CF. An increase in galectin-3 causes cellular unresponsiveness to IFN-gamma-induced signal transduction and growth inhibition in gastric cancer cells. *Oncotarget* 2016;**7**(12):15150-60 doi 10.18632/oncotarget.7750.

265. Abu-Eid R, Ward FJ. Targeting the PI3K/Akt/mTOR pathway: A therapeutic strategy in COVID-19 patients. *Immunol Lett* 2021;**240**:1-8 doi 10.1016/j.imlet.2021.09.005.

266. Dianat-Moghadam H, Khalili M, Keshavarz M, Azizi M, Hamishehkar H, Rahbarghazi R*, et al.* Modulation of LXR signaling altered the dynamic activity of human colon adenocarcinoma cancer stem cells in vitro. *Cancer Cell Int* 2021;**21**(1):100 doi 10.1186/s12935-021-01803-4.

267. Zhang R, Li H, Zhang S, Zhang Y, Wang N, Zhou H*, et al.* RXRalpha provokes tumor suppression through p53/p21/p16 and PI3K-AKT signaling pathways during stem cell differentiation and in cancer cells. *Cell Death Dis* 2018;**9**(5):532 doi 10.1038/s41419-018-0610-1.

268. Holcik M. Could the eIF2alpha-Independent Translation Be the Achilles Heel of Cancer? *Front Oncol* 2015;**5**:264 doi 10.3389/fonc.2015.00264.

269. Tebaldi T, Re A, Viero G, Pegoretti I, Passerini A, Blanzieri E*, et al.* Widespread uncoupling between transcriptome and translatome variations after a stimulus in mammalian cells. *BMC Genomics* 2012;**13**:220 doi 10.1186/1471-2164-13-220.

270. Koromilas AE. Roles of the translation initiation factor eIF2alpha serine 51 phosphorylation in cancer formation and treatment. *Biochim Biophys Acta* 2015;**1849**(7):871-80 doi 10.1016/j.bbagrm.2014.12.007.

271. Rajesh K, Krishnamoorthy J, Kazimierczak U, Tenkerian C, Papadakis AI, Wang S*, et al.* Phosphorylation of the translation initiation factor eIF2alpha at serine 51 determines the cell fate decisions of Akt in response to oxidative stress. *Cell Death Dis* 2015;**6**(1):e1591 doi 10.1038/cddis.2014.554.

272. Kazemi S, Mounir Z, Baltzis D, Raven JF, Wang S, Krishnamoorthy JL*, et al.* A novel function of eIF2alpha kinases as inducers of the phosphoinositide-3 kinase signaling pathway. *Mol Biol Cell* 2007;**18**(9):3635-44 doi 10.1091/mbc.e07-01-0053.

273. Yang Y, Li XJ, Chen Z, Zhu XX, Wang J, Zhang LB*, et al.* Wogonin induced calreticulin/annexin A1 exposure dictates the immunogenicity of cancer cells in a PERK/AKT dependent manner. *PLoS One* 2012;**7**(12):e50811 doi 10.1371/journal.pone.0050811.

274. Blaustein M, Perez-Munizaga D, Sanchez MA, Urrutia C, Grande A, Risso G*, et al.* Modulation of the Akt pathway reveals a novel link with PERK/eIF2alpha, which is relevant during hypoxia. *PLoS One* 2013;**8**(7):e69668 doi 10.1371/journal.pone.0069668.

275. Mounir Z, Krishnamoorthy JL, Wang S, Papadopoulou B, Campbell S, Muller WJ*, et al.* Akt determines cell fate through inhibition of the PERK-eIF2alpha phosphorylation pathway. *Sci Signal* 2011;**4**(192):ra62 doi 10.1126/scisignal.2001630.

276. Koromilas AE, Mounir Z. Control of oncogenesis by eIF2alpha phosphorylation: implications in PTEN and PI3K-Akt signaling and tumor treatment. *Future Oncol* 2013;**9**(7):1005-15 doi 10.2217/fon.13.49.

277. Chen X, Dai X, Zou P, Chen W, Rajamanickam V, Feng C*, et al.* Curcuminoid EF24 enhances the anti-tumour activity of Akt inhibitor MK-2206 through ROS-mediated

endoplasmic reticulum stress and mitochondrial dysfunction in gastric cancer. *Br J Pharmacol* 2017;**174**(10):1131-46 doi 10.1111/bph.13765.

278. Booth L, Roberts JL, Tavallai M, Chuckalovcak J, Stringer DK, Koromilas AE*, et al.* [Pemetrexed + Sorafenib] lethality is increased by inhibition of ERBB1/2/3-PI3K-NFkappaB compensatory survival signaling. *Oncotarget* 2016;**7**(17):23608-32 doi 10.18632/oncotarget.8281.

279. Topisirovic I, Sonenberg N. mRNA translation and energy metabolism in cancer: the role of the MAPK and mTORC1 pathways. *Cold Spring Harb Symp Quant Biol* 2011;**76**:355-67 doi 10.1101/sqb.2011.76.010785.

280. Dunn S, Eberlein C, Yu J, Gris-Oliver A, Ong SH, Yelland U*, et al.* AKT-mTORC1 reactivation is the dominant resistance driver for PI3Kβ/AKT inhibitors in PTEN-null breast cancer and can be overcome by combining with Mcl-1 inhibitors. *Oncogene* 2022;**41**(46):5046-60.

281. Elkabets M, Vora S, Juric D, Morse N, Mino-Kenudson M, Muranen T*, et al.* mTORC1 inhibition is required for sensitivity to PI3K p110alpha inhibitors in PIK3CA-mutant breast cancer. *Sci Transl Med* 2013;**5**(196):196ra99 doi 10.1126/scitranslmed.3005747.

282. Coleman N, Subbiah V, Pant S, Patel K, Roy-Chowdhuri S, Yedururi S*, et al.* Emergence of mTOR mutation as an acquired resistance mechanism to AKT inhibition, and subsequent response to mTORC1/2 inhibition. *NPJ Precision Oncology* 2021;**5**(1):99.

283. Manning BD, Cantley LC. AKT/PKB signaling: navigating downstream. *Cell* 2007;**129**(7):1261-74 doi 10.1016/j.cell.2007.06.009.

284. Vadlakonda L, Dash A, Pasupuleti M, Anil Kumar K, Reddanna P. The Paradox of Akt-mTOR Interactions. *Front Oncol* 2013;**3**:165 doi 10.3389/fonc.2013.00165.

285. Robichaud N, Sonenberg N. Translational control and the cancer cell response to stress. *Curr Opin Cell Biol* 2017;**45**:102-9 doi 10.1016/j.ceb.2017.05.007.

286. Hao P, Yu J, Ward R, Liu Y, Hao Q, An S*, et al.* Eukaryotic translation initiation factors as promising targets in cancer therapy. *Cell Commun Signal* 2020;**18**(1):175 doi 10.1186/s12964-020-00607-9.

287. Malka-Mahieu H, Newman M, Desaubry L, Robert C, Vagner S. Molecular Pathways: The eIF4F Translation Initiation Complex-New Opportunities for Cancer Treatment. *Clin Cancer Res* 2017;**23**(1):21-5 doi 10.1158/1078-0432.CCR-14-2362.

288. Siddiqui N, Sonenberg N. Signalling to eIF4E in cancer. *Biochem Soc Trans* 2015;**43**(5):763-72 doi 10.1042/BST20150126.

289. Lu S, Yang LX, Cao ZJ, Zhao JS, You J, Feng YX. Transcriptional Control of Metastasis by Integrated Stress Response Signaling. *Front Oncol* 2021;**11**:770843 doi 10.3389/fonc.2021.770843.

290. Urra H, Dufey E, Avril T, Chevet E, Hetz C. Endoplasmic Reticulum Stress and the Hallmarks of Cancer. *Trends Cancer* 2016;**2**(5):252-62 doi 10.1016/j.trecan.2016.03.007.

291. Gandin V, Masvidal L, Cargnello M, Gyenis L, McLaughlan S, Cai Y*, et al.* mTORC1 and CK2 coordinate ternary and eIF4F complex assembly. *Nature communications* 2016;**7**(1):11127.

292. Fels DR, Koumenis C. The PERK/eIF2alpha/ATF4 module of the UPR in hypoxia resistance and tumor growth. *Cancer Biol Ther* 2006;**5**(7):723-8 doi 10.4161/cbt.5.7.2967.

293. Shi Z, Yu X, Yuan M, Lv W, Feng T, Bai R*, et al.* Activation of the PERK-ATF4 pathway promotes chemo-resistance in colon cancer cells. *Sci Rep* 2019;**9**(1):3210 doi 10.1038/s41598-019-39547-x.

294. Alasiri G, Jiramongkol Y, Zona S, Fan LY-N, Mahmud Z, Gong G*, et al.* Regulation of PERK expression by FOXO3: a vulnerability of drug-resistant cancer cells. *Oncogene* 2019;**38**(36):6382-98.

295. Fan P, Jordan VC. Estrogen Receptor and the Unfolded Protein Response: Double-Edged Swords in Therapy for Estrogen Receptor-Positive Breast Cancer. *Target Oncol* 2022;**17**(2):111-24 doi 10.1007/s11523-022-00870-5.

296. Drabovich AP, Martinez-Morillo E, Diamandis EP. Toward an integrated pipeline for protein biomarker development. *Biochim Biophys Acta* 2015;**1854**(6):677-86 doi 10.1016/j.bbapap.2014.09.006.

297. Burdall SE, Hanby AM, Lansdown MR, Speirs V. Breast cancer cell lines: friend or foe? *Breast Cancer Res* 2003;**5**(2):89-95 doi 10.1186/bcr577.

298. Sarrio D, Rodriguez-Pinilla SM, Hardisson D, Cano A, Moreno-Bueno G, Palacios J. Epithelial-mesenchymal transition in breast cancer relates to the basal-like phenotype. *Cancer Res* 2008;**68**(4):989-97 doi 10.1158/0008-5472.CAN-07-2017.

299. Lane MA, Romagnoli L, Cruise B, Cohn GM. Spontaneous conversion to estrogen receptor expression by the human breast epithelial cell line, MCF-10A. *Oncol Rep* 1999;**6**(3):507-11 doi 10.3892/or.6.3.507.

300. Freedman LP, Gibson MC, Ethier SP, Soule HR, Neve RM, Reid YA. Reproducibility: changing the policies and culture of cell line authentication. *Nat Methods* 2015;**12**(6):493-7 doi 10.1038/nmeth.3403.

301. Marx V. Cell-line authentication demystified. *Nat Methods* 2014;**11**(5):483-8 doi 10.1038/nmeth.2932.

302. Ong S, Mann M. Mass Spectrometry-based proteomics turns quantitative. *Nat Chem Biol* 2005;**1**(5):252-62.

303. Marx V. Targeted proteomics. *Nat Methods* 2013;**10**(1):19-22 doi 10.1038/nmeth.2285.

304. Abbatiello S, Ackermann BL, Borchers C, Bradshaw RA, Carr SA, Chalkley R*, et al.* New Guidelines for Publication of Manuscripts Describing Development and Application of Targeted Mass Spectrometry Measurements of Peptides and Proteins. *Molecular & Cellular Proteomics* 2017;**16**(3):327-8 doi https://doi.org/10.1074/mcp.E117.067801.

305. Freedman LP, Inglese J. The increasing urgency for standards in basic biologic research. *Cancer Res* 2014;**74**(15):4024-9 doi 10.1158/0008-5472.CAN-14-0925.

306. Hayes DF. Biomarker validation and testing. *Mol Oncol* 2015;**9**(5):960-6 doi 10.1016/j.molonc.2014.10.004.

307. Bache N, Geyer PE, Bekker-Jensen DB, Hoerning O, Falkenby L, Treit PV*, et al.* A novel LC system embeds analytes in pre-formed gradients for rapid, ultra-robust proteomics. *Molecular & Cellular Proteomics* 2018;**17**(11):2284-96.

308. van den Broek I, Romijn FP, Smit NP, van der Laarse A, Drijfhout JW, van der Burgt YE*, et al.* Quantifying protein measurands by peptide measurements: where do errors arise? *Journal of proteome research* 2015;**14**(2):928-42.

309. van den Broek I, Mastali M, Mouapi K, Bystrom C, Bairey Merz CN, Van Eyk JE. Quality Control and Outlier Detection of Targeted Mass Spectrometry Data from Multiplex Protein Panels. *J Proteome Res* 2020;**19**(6):2278-93 doi 10.1021/acs.jproteome.9b00854.

310. Wang M, Lu Y, Wang H, Wu Y, Xu X, Li Y. High ATF4 Expression Is Associated With Poor Prognosis, Amino Acid Metabolism, and Autophagy in Gastric Cancer. *Front Oncol* 2021;**11**:740120 doi 10.3389/fonc.2021.740120.

311. Du J, Liu H, Mao X, Qin Y, Fan C. ATF4 promotes lung cancer cell proliferation and invasion partially through regulating Wnt/beta-catenin signaling. *Int J Med Sci* 2021;**18**(6):1442-8 doi 10.7150/ijms.43167.

312. Wortel IMN, van der Meer LT, Kilberg MS, van Leeuwen FN. Surviving Stress: Modulation of ATF4-Mediated Stress Responses in Normal and Malignant Cells. *Trends Endocrinol Metab* 2017;**28**(11):794-806 doi 10.1016/j.tem.2017.07.003.

313. Sidrauski C, Acosta-Alvear D, Khoutorsky A, Vedantham P, Hearn BR, Li H*, et al.* Pharmacological brake-release of mRNA translation enhances cognitive memory. *Elife* 2013;**2**:e00498 doi 10.7554/eLife.00498.

314. Bao F, Hao P, An S, Yang Y, Liu Y, Hao Q*, et al.* Akt scaffold proteins: the key to controlling specificity of Akt signaling. *American Journal of Physiology-Cell Physiology* 2021;**321**(3):C429-C42 doi 10.1152/ajpcell.00146.2020.

315. Zhou Z, Ai H, Li K, Yao X, Zhu W, Liu L*, et al.* Prohibitin 2 localizes in nucleolus to regulate ribosomal RNA transcription and facilitate cell proliferation in RD cells. *Sci Rep* 2018;**8**(1):1479 doi 10.1038/s41598-018-19917-7.

316. Amarnani A, Capri JR, Souda P, Elashoff DA, Lopez IA, Whitelegge JP*, et al.* Quantitative Proteomics Using Formalin-fixed, Paraffin-embedded Biopsy Tissues in Inflammatory Disease. *J Proteomics Bioinform* 2019;**12**(7):104-12 doi 10.35248/0974-276x.12.19.503.

317. Box GE. Robustness in Statistics: Proceedings of a Workshop. Academic Press, New York; 1979.

318. Malhotra V, Perry MC. Classical chemotherapy: mechanisms, toxicities and the therapeutc window. *Cancer biology & therapy* 2003;**2**(sup1):1-3.

319. Wishart DS, Feunang YD, Guo AC, Lo EJ, Marcu A, Grant JR*, et al.* DrugBank 5.0: a major update to the DrugBank database for 2018. *Nucleic Acids Res* 2018;**46**(D1):D1074-D82 doi 10.1093/nar/gkx1037.

320. Darwich AS, Polasek TM, Aronson JK, Ogungbenro K, Wright DFB, Achour B*, et al.* Model-Informed Precision Dosing: Background, Requirements, Validation, Implementation, and Forward Trajectory of Individualizing Drug Therapy. *Annu Rev Pharmacol Toxicol* 2021;**61**:225-45 doi 10.1146/annurev-pharmtox-033020-113257.

321. Polasek TM, Shakib S, Rostami-Hodjegan A. Precision dosing in clinical medicine: present and future. *Expert Rev Clin Pharmacol* 2018;**11**(8):743-6 doi 10.1080/17512433.2018.1501271.

322. Asiimwe IG, Zhang EJ, Osanlou R, Jorgensen AL, Pirmohamed M. Warfarin dosing algorithms: A systematic review. *British journal of clinical pharmacology* 2021;**87**(4):1717-29.

323. Fujita K. Cytochrome P450 and anticancer drugs. *Curr Drug Metab* 2006;**7**(1):23-37 doi 10.2174/138920006774832587.

324. Zhao M, Ma J, Li M, Zhang Y, Jiang B, Zhao X*, et al.* Cytochrome P450 Enzymes and Drug Metabolism in Humans. *Int J Mol Sci* 2021;**22**(23):12808 doi 10.3390/ijms222312808.

325. Petros WP, Hopkins PJ, Spruill S, Broadwater G, Vredenburgh JJ, Colvin OM*, et al.* Associations between drug metabolism genotype, chemotherapy pharmacokinetics, and overall survival in patients with breast cancer. *J Clin Oncol* 2005;**23**(25):6117-25 doi 10.1200/JCO.2005.06.075.

326. Michael M, Doherty MM. Tumoral drug metabolism: overview and its implications for cancer therapy. *J Clin Oncol* 2005;**23**(1):205-29 doi 10.1200/JCO.2005.02.120.

327. Daali Y, Rostami-Hodjegan A, Samer CF. Editorial: Precision Medicine: Impact of Cytochromes P450 and Transporters Genetic Polymorphisms, Drug-Drug Interactions, Disease on Safety and Efficacy of Drugs. *Front Pharmacol* 2021;**12**:834717 doi 10.3389/fphar.2021.834717.

328. Bozina N, Bradamante V, Lovric M. Genetic polymorphism of metabolic enzymes P450 (CYP) as a susceptibility factor for drug response, toxicity, and cancer risk. *Arhiv za higijenu rada i toksikologiju* 2009;**60**(2):217.

329. Rochat B. Role of cytochrome P450 activity in the fate of anticancer agents and in drug resistance: focus on tamoxifen, paclitaxel and imatinib metabolism. *Clin Pharmacokinet* 2005;**44**(4):349-66 doi 10.2165/00003088-200544040-00002.

330. Shastry BS. Pharmacogenetics and the concept of individualized medicine. *Pharmacogenomics J* 2006;**6**(1):16-21 doi 10.1038/sj.tpj.6500338.

331. Seredina TA, Goreva OB, Talaban VO, Grishanova AY, Lyakhovich VV. Association of cytochrome P450 genetic polymorphisms with neoadjuvant chemotherapy efficacy in breast cancer patients. *BMC Med Genet* 2012;**13**(1):45 doi 10.1186/1471-2350-13-45.

332. Anzenbacher P, Anzenbacherová E. Cytochromes P450 and metabolism of xenobiotics. *Cell Mol Life Sci* 2001;**58**(5-6):737-47 doi 10.1007/pl00000897.

333. Cronin-Fenton DP, Damkier P. Chapter Three - Tamoxifen and CYP2D6: A Controversy in Pharmacogenetics. In: Brøsen K, Damkier P, editors. Advances in Pharmacology. Volume 83: Academic Press; 2018. p. 65-91.

334. Bienfait K, Chhibber A, Marshall JC, Armstrong M, Cox C, Shaw PM*, et al.* Current challenges and opportunities for pharmacogenomics: perspective of the Industry Pharmacogenomics Working Group (I-PWG). *Hum Genet* 2022;**141**(6):1165-73 doi 10.1007/s00439-021-02282-3.

335. Sukri A, Salleh MZ, Masimirembwa C, Teh LK. A systematic review on the cost effectiveness of pharmacogenomics in developing countries: implementation challenges. *Pharmacogenomics J* 2022;**22**(3):147-59 doi 10.1038/s41397-022-00272-w.

336. McGraw J, Waller D. Cytochrome P450 variations in different ethnic populations. *Expert Opin Drug Metab Toxicol* 2012;**8**(3):371-82 doi 10.1517/17425255.2012.657626.

337. Anderson GD. Gender differences in pharmacological response. *International review of neurobiology* 2008;**83**:1-10.

338. Scandlyn MJ, Stuart EC, Rosengren RJ. Sex-specific differences in CYP450 isoforms in humans. *Expert Opin Drug Metab Toxicol* 2008;**4**(4):413-24 doi 10.1517/17425255.4.4.413.

339. Soldin OP, Chung SH, Mattison DR. Sex differences in drug disposition. *J Biomed Biotechnol* 2011;**2011**:187103 doi 10.1155/2011/187103.

340. Chen M, Ma L, Drusano GL, Bertino JS, Jr., Nafziger AN. Sex differences in CYP3A activity using intravenous and oral midazolam. *Clin Pharmacol Ther* 2006;**80**(5):531-8 doi 10.1016/j.clpt.2006.08.014.

341. Hu Z-Y, Zhao Y-S. Sex-dependent differences in cytochrome P450 3A activity as assessed by midazolam disposition in humans: a meta-analysis. *Drug metabolism and disposition* 2010;**38**(5):817-23.

342. Kinirons MT, O'Mahony MS. Drug metabolism and ageing. *Br J Clin Pharmacol* 2004;**57**(5):540-4 doi 10.1111/j.1365-2125.2004.02096.x.

343. Scripture CD, Sparreboom A, Figg WD. Modulation of cytochrome P450 activity: implications for cancer therapy. *Lancet Oncol* 2005;**6**(10):780-9 doi 10.1016/S1470-2045(05)70388-0.

344. Tranvag EJ, Norheim OF, Ottersen T. Clinical decision making in cancer care: a review of current and future roles of patient age. *BMC Cancer* 2018;**18**(1):546 doi 10.1186/s12885-018-4456-9.

345. Nightingale G, Schwartz R, Kachur E, Dixon BN, Cote C, Barlow A*, et al.* Clinical pharmacology of oncology agents in older adults: a comprehensive review of how chronologic and functional age can influence treatment-related effects. *Journal of geriatric oncology* 2019;**10**(1):4-30.

346. Schmucker DL. Liver function and phase I drug metabolism in the elderly: a paradox. *Drugs Aging* 2001;**18**(11):837-51 doi 10.2165/00002512-200118110-00005.

347. Lammers LA, Achterbergh R, Romijn JA, Mathot RAA. Nutritional Status Differentially Alters Cytochrome P450 3A4 (CYP3A4) and Uridine 5'-Diphospho-Glucuronosyltransferase (UGT) Mediated Drug Metabolism: Effect of Short-Term Fasting and High Fat Diet on Midazolam Metabolism. *Eur J Drug Metab Pharmacokinet* 2018;**43**(6):751-67 doi 10.1007/s13318-018-0487-5.

348. Dostalek M, Court MH, Yan B, Akhlaghi F. Significantly reduced cytochrome P450 3A4 expression and activity in liver from humans with diabetes mellitus. *British journal of pharmacology* 2011;**163**(5):937-47.

349. Brill MJ, Diepstraten J, van Rongen A, van Kralingen S, van den Anker JN, Knibbe CA. Impact of obesity on drug metabolism and elimination in adults and children. *Clin Pharmacokinet* 2012;**51**(5):277-304 doi 10.2165/11599410-000000000-00000.

350. Fearon K, Arends J, Baracos V. Understanding the mechanisms and treatment options in cancer cachexia. *Nat Rev Clin Oncol* 2013;**10**(2):90-9 doi 10.1038/nrclinonc.2012.209.

351. Wang Z, Schuetz EG, Xu Y, Thummel KE. Interplay between vitamin D and the drug metabolizing enzyme CYP3A4. *The Journal of steroid biochemistry and molecular biology* 2013;**136**:54-8.

352. Hoffer LJ, Robitaille L, Swinton N, Agulnik J, Cohen V, Small D*, et al.* Appropriate vitamin D loading regimen for patients with advanced lung cancer. *Nutrition journal* 2015;**15**(1):1-12.

353. Schwartz JB. Effects of vitamin D supplementation in atorvastatin-treated patients: a new drug interaction with an unexpected consequence. *Clin Pharmacol Ther* 2009;**85**(2):198-203 doi 10.1038/clpt.2008.165.

354. Kobayashi M, Hoshinaga Y, Miura N, Tokuda Y, Shigeoka S, Murai A*, et al.* Ascorbic acid deficiency decreases hepatic cytochrome P-450, especially CYP2B1/2B2, and simultaneously induces heme oxygenase-1 gene expression in scurvy-prone ODS rats. *Bioscience, Biotechnology, and Biochemistry* 2014;**78**(6):1060-6.

355. Mayland CR, Bennett MI, Allan K. Vitamin C deficiency in cancer patients. *Palliat Med* 2005;**19**(1):17-20 doi 10.1191/0269216305pm970oa.

356. Harvey RD, Morgan ET. Cancer, inflammation, and therapy: effects on cytochrome p450-mediated drug metabolism and implications for novel immunotherapeutic agents. *Clin Pharmacol Ther* 2014;**96**(4):449-57 doi 10.1038/clpt.2014.143.

357. Lenoir C, Daali Y, Rollason V, Curtin F, Gloor Y, Bosilkovska M*, et al.* Impact of Acute Inflammation on Cytochromes P450 Activity Assessed by the Geneva Cocktail. *Clin Pharmacol Ther* 2021;**109**(6):1668-76 doi 10.1002/cpt.2146.

358. van Eijk M, Boosman RJ, Schinkel AH, Huitema ADR, Beijnen JH. Cytochrome P450 3A4, 3A5, and 2C8 expression in breast, prostate, lung, endometrial, and ovarian tumors: relevance for resistance to taxanes. *Cancer Chemother Pharmacol* 2019;**84**(3):487-99 doi 10.1007/s00280-019-03905-3.

359. Zhong L, Li Y, Xiong L, Wang W, Wu M, Yuan T*, et al.* Small molecules in targeted cancer therapy: Advances, challenges, and future perspectives. *Signal Transduct Target Ther* 2021;**6**(1):201.

360. Bruno RD, Njar VC. Targeting cytochrome P450 enzymes: a new approach in anti-cancer drug development. *Bioorg Med Chem* 2007;**15**(15):5047-60 doi 10.1016/j.bmc.2007.05.046.

361. Jiang F, Chen L, Yang Y-C, Wang X-m, Wang R-Y, Li L*, et al.* CYP3A5 functions as a tumor suppressor in hepatocellular carcinoma by regulating mTORC2/Akt signaling. *Cancer research* 2015;**75**(7):1470-81.

362. McGraw J, Gerhardt A, Morris TC. Opportunities and obstacles in genotypic prediction of cytochrome P450 phenotypes. *Expert Opin Drug Metab Toxicol* 2018;**14**(7):659-61 doi 10.1080/17425255.2018.1484451.

363. Samer CF, Lorenzini KI, Rollason V, Daali Y, Desmeules JA. Applications of CYP450 testing in the clinical setting. *Molecular Diagnosis & Therapy* 2013;**17**(3):165-84 doi 10.1007/s40291-013-0028-5.

364. Anderson KE, Kappas A. Dietary regulation of cytochrome P450. *Annual review of nutrition* 1991;**11**(1):141-67 doi 10.1146/annurev.nu.11.070191.001041.

365. Delgoda R, Westlake AC. Herbal interactions involving cytochrome p450 enzymes: a mini review. *Toxicol Rev* 2004;**23**(4):239-49 doi 10.2165/00139709-200423040-00004.

366. Pelkonen O, Maenpaa J, Taavitsainen P, Rautio A, Raunio H. Inhibition and induction of human cytochrome P450 (CYP) enzymes. *Xenobiotica* 1998;**28**(12):1203-53 doi 10.1080/004982598238886.

367. Dresser GK. Dietary effects on drug metabolism and transport: Effect of peppermint oil, St. John's Wort, and fruit juices on cytochrome P450 3A4, P-glycoprotein, and organic anion transporting polypeptides in vitro and in humans. 2005.

368. Harris RZ, Jang GR, Tsunoda S. Dietary effects on drug metabolism and transport. *Clin Pharmacokinet* 2003;**42**(13):1071-88 doi 10.2165/00003088-200342130-00001.

369. O'Malley M, King AN, Conte M, Ellingrod VL, Ramnath N. Effects of cigarette smoking on metabolism and effectiveness of systemic therapy for lung cancer. *J Thorac Oncol* 2014;**9**(7):917-26 doi 10.1097/JTO.0000000000000191.

370. Faber MS, Fuhr U. Time response of cytochrome P450 1A2 activity on cessation of heavy smoking. *Clin Pharmacol Ther* 2004;**76**(2):178-84 doi 10.1016/j.clpt.2004.04.003.

371. Zhao Y, Liang A, Zhang Y, Li C, Yi Y, Nilsen OG. Impact of Tetrahydropalmatine on the Pharmacokinetics of Probe Drugs for CYP1A2, 2D6 and 3A Isoenzymes in Beagle Dogs. *Phytother Res* 2016;**30**(6):906-14 doi 10.1002/ptr.5608.

372. Zhao Y, Hellum BH, Liang A, Nilsen OG. Inhibitory Mechanisms of Human CYPs by Three Alkaloids Isolated from Traditional Chinese Herbs. *Phytother Res* 2015;**29**(6):825-34 doi 10.1002/ptr.5285.

373. Chow HH, Hakim IA, Vining DR, Crowell JA, Cordova CA, Chew WM*, et al.* Effects of repeated green tea catechin administration on human cytochrome P450 activity. *Cancer Epidemiol Biomarkers Prev* 2006;**15**(12):2473-6 doi 10.1158/1055-9965.EPI-06-0365.

374. Bisswanger H. Enzyme assays. *Perspectives in Science* 2014;**1**(1-6):41-55.

375. Brooks HB, Geeganage S, Kahl SD, Montrose C, Sittampalam S, Smith MC*, et al.* Basics of enzymatic assays for HTS. *Assay Guidance Manual [Internet]* 2012.

376. Bosilkovska M, Samer CF, Deglon J, Rebsamen M, Staub C, Dayer P*, et al.* Geneva cocktail for cytochrome p450 and P-glycoprotein activity assessment using dried blood spots. *Clin Pharmacol Ther* 2014;**96**(3):349-59 doi 10.1038/clpt.2014.83.

377. Tornio A, Filppula AM, Niemi M, Backman JT. Clinical Studies on Drug-Drug Interactions Involving Metabolism and Transport: Methodology, Pitfalls, and Interpretation. *Clin Pharmacol Ther* 2019;**105**(6):1345-61 doi 10.1002/cpt.1435.

378. Robertson D, Williams GH. Clinical and translational science: principles of human research. Academic Press; 2009.

379. Maemondo M, Inoue A, Kobayashi K, Sugawara S, Oizumi S, Isobe H*, et al.* Gefitinib or chemotherapy for non-small-cell lung cancer with mutated EGFR. *N Engl J Med* 2010;**362**(25):2380-8 doi 10.1056/NEJMoa0909530.

380. Lynch TJ, Bondarenko I, Luft A, Serwatowski P, Barlesi F, Chacko R*, et al.* Ipilimumab in combination with paclitaxel and carboplatin as first-line treatment in stage IIIB/IV non–small-cell lung cancer: results from a randomized, double-blind, multicenter phase II study. *Journal of clinical oncology* 2012;**30**(17):2046-54.

381. Turrisi AT, 3rd, Kim K, Blum R, Sause WT, Livingston RB, Komaki R*, et al.* Twice-daily compared with once-daily thoracic radiotherapy in limited small-cell lung cancer treated concurrently with cisplatin and etoposide. *N Engl J Med* 1999;**340**(4):265-71 doi 10.1056/NEJM199901283400403.

382. Shore N, Mellado B, Shah S, Hauke R, Costin D, Adra N*, et al.* A Phase I Study of Capivasertib in Combination With Abiraterone Acetate in Patients With Metastatic Castration-Resistant Prostate Cancer. *Clin Genitourin Cancer* 2023;**21**(2):278-85 doi 10.1016/j.clgc.2022.11.017.

383. van Eijk M, Boosman RJ, Schinkel AH, Huitema AD, Beijnen JH. Cytochrome P450 3A4, 3A5, and 2C8 expression in breast, prostate, lung, endometrial, and ovarian tumors: relevance for resistance to taxanes. *Cancer Chemother Pharmacol* 2019;**84**:487-99.

384. Citarella F, Russano M, Galletti A, Vincenzi B, Tonini G, Santini D. Novel drugs, familiar interactions: ciprofloxacin may increase exposure to the RET inhibitor pralsetinib. *Ann Oncol* 2021;**32**(6):811-3 doi 10.1016/j.annonc.2021.02.023.

385. Simonsson M, Veerla S, Markkula A, Rose C, Ingvar C, Jernstrom H. CYP1A2--a novel genetic marker for early aromatase inhibitor response in the treatment of breast cancer patients. *BMC Cancer* 2016;**16**:256 doi 10.1186/s12885-016-2284-3.

386. Glue P, Clement RP. Cytochrome P450 enzymes and drug metabolism--basic concepts and methods of assessment. *Cellular and Molecular Neurobiology* 1999;**19**(3):309-23 doi 10.1023/a:1006993631057.

387. Bosilkovska M, Samer C, Déglon J, Thomas A, Walder B, Desmeules J*, et al.* Evaluation of mutual drug–drug interaction within Geneva cocktail for cytochrome P450 phenotyping using innovative dried blood sampling method. *Basic & clinical pharmacology & toxicology* 2016;**119**(3):284-90.

388. Rollason V, Mouterde M, Daali Y, Cizkova M, Priehodova E, Kulichova I*, et al.* Safety of the Geneva Cocktail, a Cytochrome P450 and P-Glycoprotein Phenotyping Cocktail, in Healthy Volunteers from Three Different Geographic Origins. *Drug Saf* 2020;**43**(11):1181-9 doi 10.1007/s40264-020-00983-8.

389. Tian D, Hu Z. CYP3A4-mediated pharmacokinetic interactions in cancer therapy. *Curr Drug Metab* 2014;**15**(8):808-17 doi 10.2174/1389200216666150223152627.

390. Subhani S, Jamil K. Molecular docking of chemotherapeutic agents to CYP3A4 in non-small cell lung cancer. *Biomed Pharmacother* 2015;**73**:65-74 doi 10.1016/j.biopha.2015.05.018.

391. Fujita K-i. Cytochrome P450 and anticancer drugs. *Current drug metabolism* 2006;**7**(1):23-37.

392. Streetman DS, Bertino Jr JS, Nafziger AN. Phenotyping of drug-metabolizing enzymes in adults: a review of in-vivo cytochrome P450 phenotyping probes. *Pharmacogenetics and Genomics* 2000;**10**(3):187-216.

393. Thummel KE, Shen DD, Podoll TD, Kunze KL, Trager WF, Bacchi CE*, et al.* Use of midazolam as a human cytochrome P450 3A probe: II. Characterization of inter-and intraindividual hepatic CYP3A variability after liver transplantation. *Journal of Pharmacology and Experimental Therapeutics* 1994;**271**(1):557-66.

394. Notarianni L, Oliver S, Dobrocky P, Bennett P, Silverman B. Caffeine as a metabolic probe: a comparison of the metabolic ratios used to assess CYP1A2 activity. *British journal of clinical pharmacology* 1995;**39**(1):65-9.

395. Bansal S, DeStefano A. Key elements of bioanalytical method validation for small molecules. *The AAPS journal* 2007;**9**:E109-E14.

396. Lelo A, Birkett DJ, Robson RA, Miners JO. Comparative pharmacokinetics of caffeine and its primary demethylated metabolites paraxanthine, theobromine and theophylline in man. *Br J Clin Pharmacol* 1986;**22**(2):177-82 doi 10.1111/j.1365-2125.1986.tb05246.x.

397. Burg AW. Physiological disposition of caffeine. *Drug Metab Rev* 1975;**4**(2):199-228 doi 10.3109/03602537508993756.

398. Coelho EB, Cusinato DAC, Ximenez JP, Lanchote VL, Struchiner CJ, Suarez-Kurtz G. Limited Sampling Modeling for Estimation of Phenotypic Metrics for CYP Enzymes and the ABCB1 Transporter Using a Cocktail Approach. *Front Pharmacol* 2020;**11**:22 doi 10.3389/fphar.2020.00022.

399. Gunes A, Ozbey G, Vural EH, Uluoglu C, Scordo MG, Zengil H*, et al.* Influence of genetic polymorphisms, smoking, gender and age on CYP1A2 activity in a Turkish population. *Pharmacogenomics* 2009;**10**(5):769-78 doi 10.2217/pgs.09.22.

400. Spaggiari D, Mehl F, Desfontaine V, Grand-Guillaume Perrenoud A, Fekete S, Rudaz S*, et al.* Comparison of liquid chromatography and supercritical fluid chromatography coupled to compact single quadrupole mass spectrometer for targeted in vitro metabolism assay. *J Chromatogr A* 2014;**1371**:244-56 doi 10.1016/j.chroma.2014.10.055.

401. Anderson GD, Chan L-N. Pharmacokinetic drug interactions with tobacco, cannabinoids and smoking cessation products. *Clinical pharmacokinetics* 2016;**55**:1353-68 doi 10.1007/s40262-016-0400-9.

402. Zarezadeh M, Saedisomeolia A, Shekarabi M, Khorshidi M, Emami MR, Muller DJ. The effect of obesity, macronutrients, fasting and nutritional status on drug-metabolizing cytochrome P450s: a systematic review of current evidence on human studies. *Eur J Nutr* 2021;**60**(6):2905-21 doi 10.1007/s00394-020-02421-y.

403. Whiteaker JR, Zhang H, Zhao L, Wang P, Kelly-Spratt KS, Ivey RG*, et al.* Integrated pipeline for mass spectrometry-based discovery and confirmation of biomarkers demonstrated in a mouse model of breast cancer. *J Proteome Res* 2007;**6**(10):3962-75 doi 10.1021/pr070202v.

404. Tenkerian C, Krishnamoorthy J, Mounir Z, Kazimierczak U, Khoutorsky A, Staschke KA*, et al.* mTORC2 Balances AKT Activation and eIF2alpha Serine 51 Phosphorylation to Promote Survival under Stress. *Mol Cancer Res* 2015;**13**(10):1377-88 doi 10.1158/1541-7786.MCR-15-0184-T.

405. Broadhurst DI, Kell DB. Statistical strategies for avoiding false discoveries in metabolomics and related experiments. *Metabolomics* 2006;**2**:171-96.

406. Kitteringham NR, Jenkins RE, Lane CS, Elliott VL, Park BK. Multiple reaction monitoring for quantitative biomarker analysis in proteomics and metabolomics. *J Chromatogr B Analyt Technol Biomed Life Sci* 2009;**877**(13):1229-39 doi 10.1016/j.jchromb.2008.11.013.

407. Sonenberg N, Hinnebusch AG. New modes of translational control in development, behavior, and disease. *Mol Cell* 2007;**28**(5):721-9 doi 10.1016/j.molcel.2007.11.018.

408. Calkhoven CF, Muller C, Leutz A. Translational control of gene expression and disease. *Trends Mol Med* 2002;**8**(12):577-83 doi 10.1016/s1471-4914(02)02424-3.

409. Storelli F, Samer C, Reny JL, Desmeules J, Daali Y. Complex Drug-Drug-Gene-Disease Interactions Involving Cytochromes P450: Systematic Review of Published Case Reports and Clinical Perspectives. *Clin Pharmacokinet* 2018;**57**(10):1267-93 doi 10.1007/s40262-018-0650-9.

410. Abdolahi S, Ghazvinian Z, Muhammadnejad S, Saleh M, Asadzadeh Aghdaei H, Baghaei K. Patient-derived xenograft (PDX) models, applications and challenges in cancer research. *Journal of Translational Medicine* 2022;**20**(1):206 doi 10.1186/s12967-022-03405-8.

411. Kolinsky MP, Rescigno P, Bianchini D, Zafeiriou Z, Mehra N, Mateo J*, et al.* A phase I dose-escalation study of enzalutamide in combination with the AKT inhibitor AZD5363 (capivasertib) in patients with metastatic castration-resistant prostate cancer. *Ann Oncol* 2020;**31**(5):619-25 doi 10.1016/j.annonc.2020.01.074.

412. Crabb SJ, Griffiths G, Marwood E, Dunkley D, Downs N, Martin K*, et al.* Pan-AKT Inhibitor Capivasertib With Docetaxel and Prednisolone in Metastatic Castration-Resistant Prostate Cancer: A Randomized, Placebo-Controlled Phase II Trial (ProCAID). *J Clin Oncol* 2021;**39**(3):190-201 doi 10.1200/JCO.20.01576.

413. Turner N, Oliveira M, Howell SJ, Dalenc F, Cortés J, Gomez H*, et al.* Abstract GS3-04: GS3-04 Capivasertib and fulvestrant for patients with aromatase inhibitor-resistant hormone receptor-positive/human epidermal growth factor receptor 2-negative advanced breast cancer: results from the Phase III CAPItello-291 trial. *Cancer Research* 2023;**83**(5_Supplement):GS3-04-GS3-.

414. Gambaro K, Marques M, McNamara S, Couetoux du Tertre M, Diaz Z, Hoffert C*, et al.* Copy number and transcriptome alterations associated with metastatic lesion response to treatment in colorectal cancer. *Clin Transl Med* 2021;**11**(4):e401 doi 10.1002/ctm2.401.

415. Rodriguez-Antona C, Gomez A, Karlgren M, Sim SC, Ingelman-Sundberg M. Molecular genetics and epigenetics of the cytochrome P450 gene family and its relevance for cancer risk and treatment. *Hum Genet* 2010;**127**(1):1-17 doi 10.1007/s00439-009-0748-0.

416. Zhong L, Li Y, Xiong L, Wang W, Wu M, Yuan T*, et al.* Small molecules in targeted cancer therapy: advances, challenges, and future perspectives. *Signal Transduct Target Ther* 2021;**6**(1):201 doi 10.1038/s41392-021-00572-w.

417. Miyoshi Y, Ando A, Takamura Y, Taguchi T, Tamaki Y, Noguchi S. Prediction of response to docetaxel by CYP3A4 mRNA expression in breast cancer tissues. *Int J Cancer* 2002;**97**(1):129-32 doi 10.1002/ijc.1568.

418. Floriano-Sanchez E, Rodriguez NC, Bandala C, Coballase-Urrutia E, Lopez-Cruz J. CYP3A4 expression in breast cancer and its association with risk factors in Mexican women. *Asian Pac J Cancer Prev* 2014;**15**(8):3805-9 doi 10.7314/apjcp.2014.15.8.3805.

419. Jones RH, Carucci M, Casbard AC, Butler R, Alchami F, Bale CJ*, et al.* Capivasertib (AZD5363) plus fulvestrant versus placebo plus fulvestrant after relapse or progression on an aromatase inhibitor in metastatic ER-positive breast cancer (FAKTION): A randomized, double-blind, placebo-controlled, phase II trial. *Journal of Clinical Oncology* 2019;**37**(15_suppl):1005- doi 10.1200/JCO.2019.37.15_suppl.1005.

420. Jiang F, Chen L, Yang YC, Wang XM, Wang RY, Li L*, et al.* CYP3A5 Functions as a Tumor Suppressor in Hepatocellular Carcinoma by Regulating mTORC2/Akt Signaling. *Cancer Res* 2015;**75**(7):1470-81 doi 10.1158/0008-5472.CAN-14-1589.

421. Kentsis A, Volpon L, Topisirovic I, Soll CE, Culjkovic B, Shao L*, et al.* Further evidence that ribavirin interacts with eIF4E. *RNA* 2005;**11**(12):1762-6 doi 10.1261/rna.2238705.

422. Borden KL, Culjkovic-Kraljacic B. Ribavirin as an anti-cancer therapy: acute myeloid leukemia and beyond? *Leuk Lymphoma* 2010;**51**(10):1805-15 doi 10.3109/10428194.2010.496506.

423. Gerhards NM, Rottenberg S. New tools for old drugs: Functional genetic screens to optimize current chemotherapy. *Drug Resist Updat* 2018;**36**:30-46 doi 10.1016/j.drup.2018.01.001.

424. Lou Y, Wang Q, Zheng J, Hu H, Liu L, Hong D*, et al.* Possible Pathways of Capecitabine-Induced Hand-Foot Syndrome. *Chem Res Toxicol* 2016;**29**(10):1591-601 doi 10.1021/acs.chemrestox.6b00215.

425. Nikolaou V, Syrigos K, Saif MW. Incidence and implications of chemotherapy related hand-foot syndrome. *Expert Opin Drug Saf* 2016;**15**(12):1625-33 doi 10.1080/14740338.2016.1238067.

426. Azuma Y, Hata K, Sai K, Udagawa R, Hirakawa A, Tohkin M*, et al.* Significant association between hand-foot syndrome and efficacy of capecitabine in patients with metastatic breast cancer. *Biological and Pharmaceutical Bulletin* 2012;**35**(5):717-24.

427. Diederiks N, Ravensbergen CJ, Treep M, van Wezel M, Kuruc M, Renee Ruhaak L*, et al.* Development of Tier 2 LC-MRM-MS protein quantification methods for liquid biopsies. *J Mass Spectrom Adv Clin Lab* 2023;**27**:49-55 doi 10.1016/j.jmsacl.2022.12.007.

428. Adelstein DJ. Clinical trial design in head and neck cancer: what has the oncologist learned? *The Lancet Oncology* 2012;**13**(7):e318-e23.

429. Noor AM, Holmberg L, Gillett C, Grigoriadis A. Big Data: the challenge for small research groups in the era of cancer genomics. *British Journal of Cancer* 2015;**113**(10):1405-12 doi 10.1038/bjc.2015.341.

430. Ngiam KY, Khor W. Big data and machine learning algorithms for health-care delivery. *The Lancet Oncology* 2019;**20**(5):e262-e73.

431. Bettegowda C, Sausen M, Leary RJ, Kinde I, Wang Y, Agrawal N*, et al.* Detection of circulating tumor DNA in early- and late-stage human malignancies. *Sci Transl Med* 2014;**6**(224):224ra24 doi 10.1126/scitranslmed.3007094.

432. Suvarna V. Phase IV of drug development. *Perspectives in clinical research* 2010;**1**(2):57.

433. Mukherjee S. The emperor of all maladies: a biography of cancer. Simon and Schuster; 2011.

434. Gupta A, O'Callaghan CJ, Zhu L, Jonker DJ, Wong RPW, Colwell B*, et al.* Evaluating the Time Toxicity of Cancer Treatment in the CCTG CO.17 Trial. *JCO Oncol Pract* 2023:OP2200737 doi 10.1200/OP.22.00737.

435. Chen Q, Lu M, Monks BR, Birnbaum MJ. Insulin Is Required to Maintain Albumin Expression by Inhibiting Forkhead Box O1 Protein. *J Biol Chem* 2016;**291**(5):2371-8 doi 10.1074/jbc.M115.677351.

436. Fiala O, Pesek M, Finek J, Racek J, Minarik M, Benesova L*, et al.* Serum albumin is a strong predictor of survival in patients with advanced-stage non-small cell lung cancer treated with erlotinib. *Neoplasma* 2016;**63**(3):471-6.

437. Jae Park M, Lee J, Hong JY, Choi MK, Yi JH, Lee SJ*, et al.* Prognostic model to predict outcomes in nonsmall cell lung cancer patients treated with gefitinib as a salvage

treatment. *Cancer: Interdisciplinary International Journal of the American Cancer Society* 2009;**115**(7):1518-30.

438. Li X, Chen W, Yang C, Huang Y, Jia J, Xu R*, et al.* IGHG1 upregulation promoted gastric cancer malignancy via AKT/GSK-3beta/beta-Catenin pathway. *Cancer Cell Int* 2021;**21**(1):397 doi 10.1186/s12935-021-02098-1.

439. Vishnubalaji R, Alajez NM. Transcriptional landscape associated with TNBC resistance to neoadjuvant chemotherapy revealed by single-cell RNA-seq. *Mol Ther Oncolytics* 2021;**23**:151-62 doi 10.1016/j.omto.2021.09.002.

440. Wang LM, Gan YH. Cancer-derived IgG involved in cisplatin resistance through PTP-BAS/Src/PDK1/AKT signaling pathway. *Oral Diseases* 2021;**27**(3):464-74.

441. Schmidt M, Hellwig B, Hammad S, Othman A, Lohr M, Chen Z*, et al.* A Comprehensive Analysis of Human Gene Expression Profiles Identifies Stromal Immunoglobulin κ C as a Compatible Prognostic Marker in Human Solid TumorsIGKC Predicts Prognosis. *Clinical Cancer Research* 2012;**18**(9):2695-703.

442. Zhu J, Wang M, Hu D. Identification of Prognostic Immune-Related Genes by Integrating mRNA Expression and Methylation in Lung Adenocarcinoma. *Int J Genomics* 2020;**2020**:9548632 doi 10.1155/2020/9548632.

443. Singh N, Sahu DK, Tripathi RK, Mishra A, Shyam H, Shankar P*, et al.* Differentially expressed full-length, fusion and novel isoforms transcripts-based signature of well-differentiated keratinized oral squamous cell carcinoma. *Oncotarget* 2020;**11**(34):3227-43 doi 10.18632/oncotarget.27693.

444. Franks SE, Briah R, Jones RA, Moorehead RA. Unique roles of Akt1 and Akt2 in IGF-IR mediated lung tumorigenesis. *Oncotarget* 2016;**7**(3):3297.

445. Li JP, Liu Y, Yin YH. ARHGAP1 overexpression inhibits proliferation, migration and invasion of C-33A and SiHa cell lines. *Onco Targets Ther* 2017;**10**:691-701 doi 10.2147/OTT.S112223.

446. Park N, Yoo JC, Ryu J, Hong SG, Hwang EM, Park JY. Copine1 enhances neuronal differentiation of the hippocampal progenitor HiB5 cells. *Mol Cells* 2012;**34**(6):549-54 doi 10.1007/s10059-012-0235-7.

447. Park N, Yoo JC, Lee YS, Choi HY, Hong SG, Hwang EM*, et al.* Copine1 C2 domains have a critical calcium-independent role in the neuronal differentiation of hippocampal progenitor HiB5 cells. *Biochem Biophys Res Commun* 2014;**454**(1):228-33 doi 10.1016/j.bbrc.2014.10.075.

448. Nowinski SM, Solmonson A, Rundhaug JE, Rho O, Cho J, Lago CU*, et al.* Mitochondrial uncoupling links lipid catabolism to Akt inhibition and resistance to tumorigenesis. *Nat Commun* 2015;**6**(1):8137 doi 10.1038/ncomms9137.

449. Pei Y, Zhu P, Dang Y, Wu J, Yang X, Wan B*, et al.* Nuclear export of NF90 to stabilize IL-2 mRNA is mediated by AKT-dependent phosphorylation at Ser647 in response to CD28 costimulation. *The Journal of Immunology* 2008;**180**(1):222-9.

450. Jia W, Kong L, Kidoya H, Naito H, Muramatsu F, Hayashi Y*, et al.* Indispensable role of Galectin-3 in promoting quiescence of hematopoietic stem cells. *Nat Commun* 2021;**12**(1):2118 doi 10.1038/s41467-021-22346-2.

451. Ilmer M, Mazurek N, Gilcrease MZ, Byrd JC, Woodward WA, Buchholz TA*, et al.* Low expression of galectin-3 is associated with poor survival in node-positive breast cancers and mesenchymal phenotype in breast cancer stem cells. *Breast Cancer Res* 2016;**18**(1):97 doi 10.1186/s13058-016-0757-6.

452. Xu F, Hua Q, Zhang A, Di Z, Wang Y, Zhao L*, et al.* LncRNA AC020978 facilitates non-small cell lung cancer progression by interacting with malate dehydrogenase 2 and activating the AKT pathway. *Cancer Sci* 2021;**112**(11):4501-14 doi 10.1111/cas.15116.

453. Zhuang Y, Xiang J, Bao W, Sun Y, Wang L, Tan M*, et al.* MDH2 Stimulated by Estrogen-GPR30 Pathway Down-Regulated PTEN Expression Promoting the Proliferation and Invasion of Cells in Endometrial Cancer. *Transl Oncol* 2017;**10**(2):203-10 doi 10.1016/j.tranon.2017.01.009.

454. Eletto D, Eletto D, Dersh D, Gidalevitz T, Argon Y. Protein disulfide isomerase A6 controls the decay of IRE1alpha signaling via disulfide-dependent association. *Mol Cell* 2014;**53**(4):562-76 doi 10.1016/j.molcel.2014.01.004.

455. Bavelloni A, Piazzi M, Faenza I, Raffini M, D'Angelo A, Cattini L*, et al.* Prohibitin 2 represents a novel nuclear AKT substrate during all-trans retinoic acid–induced differentiation of acute promyelocytic leukemia cells. *The FASEB Journal* 2014;**28**(5):2009-19.

456. Zhang H, Cheng L, Liu C. Regulatory networks of prognostic mRNAs in pediatric acute myeloid leukemia. *Journal of Healthcare Engineering* 2022;**2022**.

457. Lin Z, Peng R, Sun Y, Zhang L, Zhang Z. Identification of ribosomal protein family in triple-negative breast cancer by bioinformatics analysis. *Bioscience Reports* 2021;**41**(1).

458. Fang E, Zhang X. Identification of breast cancer hub genes and analysis of prognostic values using integrated bioinformatics analysis. *Cancer Biomarkers* 2018;**21**(2):373-81.

Appendices

1. Introduction: Multi-gene signatures for clinical stratification of breast cancer patients

Examples of commercially-available prognostic multi-gene panels for clinical stratification of breast cancer patients

	MammaPrint	Veridex 76-gene	MapQuant Dx	MapQuant Dx simplified	Oncotype DX	Theros
Technique	DNA microarray	DNA microarray	DNA microarray	qRT-PCR	qRT-PCR	qRT-PCR
Provider	Agendia	Currently not commercially available	Ipsogen	Ipsogen	Genomic Health	bioTheranostics
Assay type	70-gene signature	76-gene signature	97-gene signature	8-gene signature	21-gene recurrence score 16 cancer-related and 5 reference genes	2-gene ratio of HOXB13 to IL17R (H/l)/molecular grade index
Tissue type	Fresh or frozen	Fresh or Frozen	Fresh or Frozen	FFPE	FFPE	FFPE
Discovery set	78 ER±, N0, < 5 cm diameter cancers, age < 55 years	115 ER±, N0 cancers	64 ER+ cancers		447 ER+ samples, including samples from the tamoxifen only group of NSABP B-20 trial	60 ER+ tumors, tamoxifen-only treated patients, 20 micro-dissected FFPE samples
Initial validation set	295 ER±, N±, < 5 cm diameter cancer, age < 52 years	171 ER±, N0 cancers	597 ER± cancers, of which 125 profiled in-house		668 ER+ samples from NSABP B-14trial[90](tamoxifen-treated)	20 ER+ FFPE samples
Outcome	Distant metastasis at 5 years	Distant metastasis at 5 years	Good (GG II) or poor (GG I III) prognosis		Disease-free relapse at 10 years	Relapse-free & overall survival

	MammaPrint	Veridex 76-gene	MapQuant Dx	MapQuant Dx simplified	Oncotype DX	Theros
Clinical application	To aid in prognostic prediction in patients < 61 year of age with stage I or II, N0 disease with a tumor size of ≤ 5 cm	To prognose N0 patients	restratify grade 2 tumors into low-risk grade 1 or high-risk grade 3 tumors, specifically for invasive, primary, ER+ grade 2 tumors		predict the risk of recurrence in patients with ER+, N0 disease treated with tamoxifen; identify patients with a low risk of recurrence who may not need adjuvant chemotherapy	stratify ER+ patients into groups with a predicted low-risk or high-risk of recurrence and a predicted good or poor response to endocrine therapy
Results presentation	Dichotomous; good or poor prognosis	Dichotomous; good or poor prognosis	Dichotomous, GGII or GG I III		Continuous variable; recurrence score	Continuous variable; risk of recurrence score
Additional information provided	mRNA levels of ER, PR, and HER2 (Targetprint); Intrinsic subtypes (Blueprint)	-	-	-	mRNA levels of ER, PR, and HER2	Molecular grade index
Prognostic value in other populations	Up to 3 positive nodes, and HER2+ disease	ER+, N0 patients treated with tamoxifen	ER+, receiving aromatase inhibitors	ER+, receiving aromatase inhibitors	ER+ and 1-3 N+, ER+ postmenopausal receiving aromatase inhibitors	-
Predictive value	Chemotherapy response (poor prognosis group)	Chemotherapy response (poor prognosis group)	Chemotherapy response (GG I III)	Chemotherapy response (GG I III)	Chemotherapy response (high recurrence score)	Chemotherapy response (high risk of recurrence score)
Level of evidence	II	III	III	III	I	III
FDA approval	Yes	No	No	No	No	No

	MammaPrint	**Veridex 76-gene**	**MapQuant Dx**	**MapQuant Dx simplified**	**Oncotype DX**	**Theros**
Availability	Europe and USA		Europe	Europe	Europe and USA	USA
NOTES	*In cases where clinicopathological measures disagree with MammaPrint, the latter predicts outcome with higher accuracy*	*Outperforms the St Gallen's and NCI guidelines in identifying patients with good prognosis who could forgo chemotherapy*	*based on the premise that histological grade is a strong prognostic factor in ER positive tumors. stratify grade II cancers into grade I-like (with a low frequency of distant relapses) and grade III-like (having a clinical behavior similar to that of grade III) cancers*		*Prognoses risk of distant relapse at 10 years for ER+, node-breast cancer, predictive value among ER+ treated with AI; and ER+ with ≤3 nodes +; test in ASCO guidelines for making therapeutic decisions in early ER+ node-breast tumors*	

2. Methods: MS settings for multiplexed MRM and PRM assays

MRM-MS Transition List

Compound Name	Precursor Ion	Product Ion	RT (min)	Collision Energy
AAEIASSDSANVSSR.heavy	737.85	272.14	5.55	33
AAEIASSDSANVSSR.heavy	737.85	359.19	5.55	17
AAEIASSDSANVSSR.heavy	737.85	932.43	5.55	25
AAEIASSDSANVSSR.heavy	737.85	1019.46	5.55	25
AAEIASSDSANVSSR.heavy	737.85	1090.5	5.55	25
AAEIASSDSANVSSR.light	732.85	272.14	5.55	33
AAEIASSDSANVSSR.light	732.85	349.18	5.55	17
AAEIASSDSANVSSR.light	732.85	922.42	5.55	25
AAEIASSDSANVSSR.light	732.85	1009.45	5.55	25
AAEIASSDSANVSSR.light	732.85	1080.49	5.55	25
AGSSEWLAVDGLVSPSNNSK.heavy	676.0038	741.3617	31.37	13
AGSSEWLAVDGLVSPSNNSK.heavy	676.0038	654.3297	31.37	13
AGSSEWLAVDGLVSPSNNSK.heavy	676.0038	371.1845	31.37	13
AGSSEWLAVDGLVSPSNNSK.heavy	676.0038	327.6685	31.37	16
AGSSEWLAVDGLVSPSNNSK.heavy	676.0038	1186.574	31.37	13
AGSSEWLAVDGLVSPSNNSK.light	673.3324	1186.574	31.37	13
AGSSEWLAVDGLVSPSNNSK.light	673.3324	733.3475	31.37	13
AGSSEWLAVDGLVSPSNNSK.light	673.3324	646.3155	31.37	13
AGSSEWLAVDGLVSPSNNSK.light	673.3324	367.1774	31.37	13
AGSSEWLAVDGLVSPSNNSK.light	673.3324	323.6614	31.37	16
AINPINTFTK.heavy	563.821	942.5135	20.9	13
AINPINTFTK.heavy	563.821	828.4705	20.9	16
AINPINTFTK.heavy	563.821	471.7604	20.9	13
AINPINTFTK.heavy	563.821	414.7389	20.9	19
AINPINTFTK.heavy	563.821	299.1714	20.9	13
AINPINTFTK.light	559.8139	934.4993	20.9	13
AINPINTFTK.light	559.8139	820.4563	20.9	16
AINPINTFTK.light	559.8139	467.7533	20.9	13
AINPINTFTK.light	559.8139	410.7318	20.9	19
AINPINTFTK.light	559.8139	299.1714	20.9	13
DQIYDIFQK.heavy	589.3026	934.5124	27.23	16
DQIYDIFQK.heavy	589.3026	821.4283	27.23	16

Compound Name	Precursor Ion	Product Ion	RT (min)	Collision Energy
DQIYDIFQK.heavy	589.3026	658.365	27.23	19
DQIYDIFQK.heavy	589.3026	357.1769	27.23	13
DQIYDIFQK.heavy	589.3026	244.0928	27.23	19
DQIYDIFQK.light	585.2955	926.4982	27.23	16
DQIYDIFQK.light	585.2955	813.4141	27.23	16
DQIYDIFQK.light	585.2955	650.3508	27.23	19
DQIYDIFQK.light	585.2955	357.1769	27.23	13
DQIYDIFQK.light	585.2955	244.0928	27.23	19
EAGLDLR.heavy	392.2154	263.6248	9.36	10
EAGLDLR.heavy	392.2154	292.1355	9.36	7
EAGLDLR.heavy	392.2154	298.1713	9.36	19
EAGLDLR.heavy	392.2154	413.1982	9.36	7
EAGLDLR.heavy	392.2154	583.3038	9.36	10
EAGLDLR.light	387.2112	258.6506	9.36	10
EAGLDLR.light	387.2112	287.1514	9.36	7
EAGLDLR.light	387.2112	288.223	9.36	19
EAGLDLR.light	387.2112	403.21	9.36	7
EAGLDLR.light	387.2112	573.3255	9.36	10
EHIEIIAPSPQR.heavy	467.2571	806.4407	15.52	7
EHIEIIAPSPQR.heavy	467.2571	735.4036	15.52	10
EHIEIIAPSPQR.heavy	467.2571	622.3195	15.52	13
EHIEIIAPSPQR.heavy	467.2571	594.3234	15.52	10
EHIEIIAPSPQR.heavy	467.2571	297.6653	15.52	7
EHIEIIAPSPQR.light	463.921	806.4407	15.52	7
EHIEIIAPSPQR.light	463.921	735.4036	15.52	10
EHIEIIAPSPQR.light	463.921	622.3195	15.52	13
EHIEIIAPSPQR.light	463.921	584.3151	15.52	10
EHIEIIAPSPQR.light	463.921	292.6612	15.52	7
ELEEIVQPIISK.heavy	703.405	1034.634	28.35	22
ELEEIVQPIISK.heavy	703.405	792.5069	28.35	19
ELEEIVQPIISK.heavy	703.405	693.4385	28.35	16
ELEEIVQPIISK.heavy	703.405	565.3799	28.35	25
ELEEIVQPIISK.heavy	703.405	242.159	28.35	19
ELEEIVQPIISK.light	699.398	1026.619	28.35	22
ELEEIVQPIISK.light	699.398	784.4927	28.35	19
ELEEIVQPIISK.light	699.398	685.4243	28.35	16
ELEEIVQPIISK.light	699.398	557.3657	28.35	25

Compound Name	Precursor Ion	Product Ion	RT (min)	Collision Energy
ELEEIVQPIISK.light	699.398	234.1448	28.35	19
ELGIWEPLAVK.heavy	631.8654	1020.597	35.16	19
ELGIWEPLAVK.heavy	631.8654	850.4913	35.16	19
ELGIWEPLAVK.heavy	631.8654	664.412	35.16	16
ELGIWEPLAVK.heavy	631.8654	535.3694	35.16	25
ELGIWEPLAVK.heavy	631.8654	300.1554	35.16	19
ELGIWEPLAVK.light	627.8583	1012.583	35.16	19
ELGIWEPLAVK.light	627.8583	842.4771	35.16	19
ELGIWEPLAVK.light	627.8583	656.3978	35.16	16
ELGIWEPLAVK.light	627.8583	527.3552	35.16	25
ELGIWEPLAVK.light	627.8583	300.1554	35.16	19
ELIFEETAR.heavy	559.2918	875.4497	19.9	16
ELIFEETAR.heavy	559.2918	762.3656	19.9	16
ELIFEETAR.heavy	559.2918	615.2972	19.9	13
ELIFEETAR.heavy	559.2918	486.2546	19.9	22
ELIFEETAR.heavy	559.2918	243.1339	19.9	16
ELIFEETAR.light	554.2877	865.4414	19.9	16
ELIFEETAR.light	554.2877	752.3573	19.9	16
ELIFEETAR.light	554.2877	605.2889	19.9	13
ELIFEETAR.light	554.2877	476.2463	19.9	22
ELIFEETAR.light	554.2877	243.1339	19.9	16
FDAGELITQR.heavy	580.3027	897.5028	21.69	22
FDAGELITQR.heavy	580.3027	640.4016	21.69	19
FDAGELITQR.heavy	580.3027	527.3175	21.69	19
FDAGELITQR.heavy	580.3027	414.2335	21.69	16
FDAGELITQR.heavy	580.3027	263.1026	21.69	19
FDAGELITQR.light	575.2986	887.4945	21.69	22
FDAGELITQR.light	575.2986	630.3933	21.69	19
FDAGELITQR.light	575.2986	517.3093	21.69	19
FDAGELITQR.light	575.2986	404.2252	21.69	16
FDAGELITQR.light	575.2986	263.1026	21.69	19
FEISETSVNR.heavy	596.2976	277.1183	14.09	18
FEISETSVNR.heavy	596.2976	586.3183	14.09	27
FEISETSVNR.heavy	596.2976	715.3609	14.09	18
FEISETSVNR.heavy	596.2976	802.3929	14.09	21
FEISETSVNR.heavy	596.2976	915.477	14.09	18
FEISETSVNR.light	591.2935	277.1183	14.09	18

Compound Name	Precursor Ion	Product Ion	RT (min)	Collision Energy
FEISETSVNR.light	591.2935	576.31	14.09	27
FEISETSVNR.light	591.2935	705.3526	14.09	18
FEISETSVNR.light	591.2935	792.3846	14.09	21
FEISETSVNR.light	591.2935	905.4687	14.09	18
FFAGIVWQHVYEK.heavy	544.62	295.14	32.73	13
FFAGIVWQHVYEK.heavy	544.62	548.79	32.73	17
FFAGIVWQHVYEK.heavy	544.62	633.84	32.73	13
FFAGIVWQHVYEK.heavy	544.62	669.36	32.73	13
FFAGIVWQHVYEK.heavy	544.62	742.89	32.73	13
FFAGIVWQHVYEK.light	541.95	295.14	32.73	13
FFAGIVWQHVYEK.light	541.95	544.78	32.73	17
FFAGIVWQHVYEK.light	541.95	629.83	32.73	13
FFAGIVWQHVYEK.light	541.95	665.35	32.73	13
FFAGIVWQHVYEK.light	541.95	738.89	32.73	13
FIDTTSK.heavy	410.2205	672.3654	4.65	13
FIDTTSK.heavy	410.2205	559.2813	4.65	10
FIDTTSK.heavy	410.2205	444.2544	4.65	16
FIDTTSK.heavy	410.2205	261.1598	4.65	7
FIDTTSK.heavy	410.2205	242.159	4.65	22
FIDTTSK.light	406.2134	664.3512	4.65	13
FIDTTSK.light	406.2134	551.2671	4.65	10
FIDTTSK.light	406.2134	436.2402	4.65	16
FIDTTSK.light	406.2134	261.1598	4.65	7
FIDTTSK.light	406.2134	234.1448	4.65	22
GDFIALDLGGSSFR.heavy	732.8715	1032.535	35.74	22
GDFIALDLGGSSFR.heavy	732.8715	961.4977	35.74	22
GDFIALDLGGSSFR.heavy	732.8715	848.4136	35.74	25
GDFIALDLGGSSFR.heavy	732.8715	620.3026	35.74	19
GDFIALDLGGSSFR.heavy	732.8715	320.1241	35.74	28
GDFIALDLGGSSFR.light	727.8673	1022.527	35.74	22
GDFIALDLGGSSFR.light	727.8673	951.4894	35.74	22
GDFIALDLGGSSFR.light	727.8673	838.4054	35.74	25
GDFIALDLGGSSFR.light	727.8673	610.2944	35.74	19
GDFIALDLGGSSFR.light	727.8673	320.1241	35.74	28
GLPAPIEK.heavy	416.7546	662.3963	11.74	10
GLPAPIEK.heavy	416.7546	565.3435	11.74	16
GLPAPIEK.heavy	416.7546	494.3064	11.74	16

Compound Name	Precursor Ion	Product Ion	RT (min)	Collision Energy
GLPAPIEK.heavy	416.7546	331.7018	11.74	7
GLPAPIEK.heavy	416.7546	284.1696	11.74	22
GLPAPIEK.light	412.7475	654.3821	11.74	10
GLPAPIEK.light	412.7475	557.3293	11.74	16
GLPAPIEK.light	412.7475	486.2922	11.74	16
GLPAPIEK.light	412.7475	327.6947	11.74	7
GLPAPIEK.light	412.7475	276.1554	11.74	22
GSTAPVGGGAFPTIVER.heavy	542.6222	724.4227	25.49	13
GSTAPVGGGAFPTIVER.heavy	542.6222	655.3606	25.49	10
GSTAPVGGGAFPTIVER.heavy	542.6222	627.37	25.49	25
GSTAPVGGGAFPTIVER.heavy	542.6222	362.715	25.49	10
GSTAPVGGGAFPTIVER.heavy	542.6222	317.1456	25.49	7
GSTAPVGGGAFPTIVER.light	539.2861	714.4145	25.49	13
GSTAPVGGGAFPTIVER.light	539.2861	650.3564	25.49	10
GSTAPVGGGAFPTIVER.light	539.2861	617.3617	25.49	25
GSTAPVGGGAFPTIVER.light	539.2861	357.7109	25.49	10
GSTAPVGGGAFPTIVER.light	539.2861	317.1456	25.49	7
GTGIVSAPVPK.heavy	517.3102	875.544	13.58	16
GTGIVSAPVPK.heavy	517.3102	705.4385	13.58	13
GTGIVSAPVPK.heavy	517.3102	606.3701	13.58	13
GTGIVSAPVPK.heavy	517.3102	329.1819	13.58	10
GTGIVSAPVPK.heavy	517.3102	252.1798	13.58	28
GTGIVSAPVPK.light	513.3031	867.5298	13.58	16
GTGIVSAPVPK.light	513.3031	697.4243	13.58	13
GTGIVSAPVPK.light	513.3031	598.3559	13.58	13
GTGIVSAPVPK.light	513.3031	329.1819	13.58	10
GTGIVSAPVPK.light	513.3031	244.1656	13.58	28
GTITVSAQELK.heavy	577.829	883.4975	14.79	16
GTITVSAQELK.heavy	577.829	782.4498	14.79	16
GTITVSAQELK.heavy	577.829	683.3814	14.79	13
GTITVSAQELK.heavy	577.829	596.3494	14.79	16
GTITVSAQELK.heavy	577.829	373.2082	14.79	13
GTITVSAQELK.light	573.8219	875.4833	14.79	16
GTITVSAQELK.light	573.8219	774.4356	14.79	16
GTITVSAQELK.light	573.8219	675.3672	14.79	13
GTITVSAQELK.light	573.8219	588.3352	14.79	16
GTITVSAQELK.light	573.8219	373.2082	14.79	13

Compound Name	Precursor Ion	Product Ion	RT (min)	Collision Energy
HGLLVPNNTTDQELQHIR.heavy	524.5284	682.8433	19.85	10
HGLLVPNNTTDQELQHIR.heavy	524.5284	625.8218	19.85	10
HGLLVPNNTTDQELQHIR.heavy	524.5284	575.298	19.85	10
HGLLVPNNTTDQELQHIR.heavy	524.5284	520.3242	19.85	10
HGLLVPNNTTDQELQHIR.heavy	524.5284	421.2558	19.85	16
HGLLVPNNTTDQELQHIR.light	522.0264	677.8391	19.85	10
HGLLVPNNTTDQELQHIR.light	522.0264	620.8177	19.85	10
HGLLVPNNTTDQELQHIR.light	522.0264	570.2938	19.85	10
HGLLVPNNTTDQELQHIR.light	522.0264	520.3242	19.85	10
HGLLVPNNTTDQELQHIR.light	522.0264	421.2558	19.85	16
IADPEHDHTGFLTEY[+79.966331]VATR.heavy	566.258	357.212	21.85	20
IADPEHDHTGFLTEY[+79.966331]VATR.heavy	566.258	465.2038	21.85	11
IADPEHDHTGFLTEY[+79.966331]VATR.heavy	566.258	610.7702	21.85	14
IADPEHDHTGFLTEY[+79.966331]VATR.heavy	566.258	667.3122	21.85	11
IADPEHDHTGFLTEY[+79.966331]VATR.heavy	566.258	699.3101	21.85	20
IADPEHDHTGFLTEY[+79.966331]VATR.light	563.7559	347.2037	21.85	20
IADPEHDHTGFLTEY[+79.966331]VATR.light	563.7559	460.1997	21.85	11
IADPEHDHTGFLTEY[+79.966331]VATR.light	563.7559	610.7702	21.85	14
IADPEHDHTGFLTEY[+79.966331]VATR.light	563.7559	667.3122	21.85	11
IADPEHDHTGFLTEY[+79.966331]VATR.light	563.7559	689.3018	21.85	20
IADPEHDHTGFLTEYVATR.heavy	546.2664	863.889	23.61	7
IADPEHDHTGFLTEYVATR.heavy	546.2664	782.3573	23.61	10
IADPEHDHTGFLTEYVATR.heavy	546.2664	619.3438	23.61	4
IADPEHDHTGFLTEYVATR.heavy	546.2664	456.2804	23.61	13
IADPEHDHTGFLTEYVATR.heavy	546.2664	357.212	23.61	10
IADPEHDHTGFLTEYVATR.light	543.7644	863.889	23.61	7
IADPEHDHTGFLTEYVATR.light	543.7644	782.3573	23.61	10
IADPEHDHTGFLTEYVATR.light	543.7644	609.3355	23.61	4
IADPEHDHTGFLTEYVATR.light	543.7644	446.2722	23.61	13
IADPEHDHTGFLTEYVATR.light	543.7644	347.2037	23.61	10
IALDFQR.heavy	436.7468	759.4023	18.25	16
IALDFQR.heavy	436.7468	688.3652	18.25	10
IALDFQR.heavy	436.7468	575.2812	18.25	13
IALDFQR.heavy	436.7468	460.2542	18.25	22
IALDFQR.heavy	436.7468	344.6862	18.25	10
IALDFQR.light	431.7427	749.3941	18.25	16
IALDFQR.light	431.7427	678.357	18.25	10
IALDFQR.light	431.7427	565.2729	18.25	13

Compound Name	Precursor Ion	Product Ion	RT (min)	Collision Energy
IALDFQR.light	431.7427	450.2459	18.25	22
IALDFQR.light	431.7427	339.6821	18.25	10
IFGVTTLDIVR.heavy	622.3678	983.5759	35.46	19
IFGVTTLDIVR.heavy	622.3678	827.4861	35.46	19
IFGVTTLDIVR.heavy	622.3678	726.4384	35.46	22
IFGVTTLDIVR.heavy	622.3678	318.1812	35.46	25
IFGVTTLDIVR.heavy	622.3678	261.1598	35.46	19
IFGVTTLDIVR.light	617.3637	973.5677	35.46	19
IFGVTTLDIVR.light	617.3637	817.4778	35.46	19
IFGVTTLDIVR.light	617.3637	716.4301	35.46	22
IFGVTTLDIVR.light	617.3637	318.1812	35.46	25
IFGVTTLDIVR.light	617.3637	261.1598	35.46	19
IFVNDDR.heavy	444.7261	775.3609	7.49	16
IFVNDDR.heavy	444.7261	628.2924	7.49	13
IFVNDDR.heavy	444.7261	529.224	7.49	13
IFVNDDR.heavy	444.7261	388.1841	7.49	10
IFVNDDR.heavy	444.7261	300.1542	7.49	22
IFVNDDR.light	439.722	765.3526	7.49	16
IFVNDDR.light	439.722	618.2842	7.49	13
IFVNDDR.light	439.722	519.2158	7.49	13
IFVNDDR.light	439.722	383.1799	7.49	10
IFVNDDR.light	439.722	290.1459	7.49	22
IGVLDEGK.heavy	419.7416	725.3919	9.85	13
IGVLDEGK.heavy	419.7416	668.3705	9.85	13
IGVLDEGK.heavy	419.7416	569.3021	9.85	13
IGVLDEGK.heavy	419.7416	456.218	9.85	19
IGVLDEGK.heavy	419.7416	270.1812	9.85	10
IGVLDEGK.light	415.7345	717.3777	9.85	13
IGVLDEGK.light	415.7345	660.3563	9.85	13
IGVLDEGK.light	415.7345	561.2879	9.85	13
IGVLDEGK.light	415.7345	448.2038	9.85	19
IGVLDEGK.light	415.7345	270.1812	9.85	10
IITLTGPTNAIFK.heavy	698.9181	1170.661	32.96	19
IITLTGPTNAIFK.heavy	698.9181	956.5291	32.96	22
IITLTGPTNAIFK.heavy	698.9181	855.4814	32.96	22
IITLTGPTNAIFK.heavy	698.9181	328.2231	32.96	19
IITLTGPTNAIFK.heavy	698.9181	227.1754	32.96	19

Compound Name	Precursor Ion	Product Ion	RT (min)	Collision Energy
IITLTGPTNAIFK.light	694.911	1162.647	32.96	19
IITLTGPTNAIFK.light	694.911	948.5149	32.96	22
IITLTGPTNAIFK.light	694.911	847.4672	32.96	22
IITLTGPTNAIFK.light	694.911	328.2231	32.96	19
IITLTGPTNAIFK.light	694.911	227.1754	32.96	19
ILPTLEAVAALGNK.heavy	709.4289	1191.682	36.44	22
ILPTLEAVAALGNK.heavy	709.4289	880.4978	36.44	28
ILPTLEAVAALGNK.heavy	709.4289	596.3448	36.44	16
ILPTLEAVAALGNK.heavy	709.4289	581.3497	36.44	28
ILPTLEAVAALGNK.heavy	709.4289	227.1754	36.44	16
ILPTLEAVAALGNK.light	705.4218	1183.668	36.44	22
ILPTLEAVAALGNK.light	705.4218	872.4836	36.44	28
ILPTLEAVAALGNK.light	705.4218	592.3377	36.44	16
ILPTLEAVAALGNK.light	705.4218	573.3355	36.44	28
ILPTLEAVAALGNK.light	705.4218	227.1754	36.44	16
ILVTGGSGLVGK.heavy	554.8444	882.5135	17.59	16
ILVTGGSGLVGK.heavy	554.8444	783.445	17.59	19
ILVTGGSGLVGK.heavy	554.8444	682.3974	17.59	16
ILVTGGSGLVGK.heavy	554.8444	326.2438	17.59	13
ILVTGGSGLVGK.heavy	554.8444	227.1754	17.59	16
ILVTGGSGLVGK.light	550.8373	874.4993	17.59	16
ILVTGGSGLVGK.light	550.8373	775.4308	17.59	19
ILVTGGSGLVGK.light	550.8373	674.3832	17.59	16
ILVTGGSGLVGK.light	550.8373	326.2438	17.59	13
ILVTGGSGLVGK.light	550.8373	227.1754	17.59	16
IRPECFELLR.heavy	429.2369	298.1813	26.8	7.1
IRPECFELLR.heavy	429.2369	411.2653	26.8	7.1
IRPECFELLR.heavy	429.2369	540.3079	26.8	10.1
IRPECFELLR.heavy	429.2369	599.267	26.8	10.1
IRPECFELLR.light	425.9008	288.193	26.8	7.1
IRPECFELLR.light	425.9008	401.2771	26.8	7.1
IRPECFELLR.light	425.9008	530.3297	26.8	10.1
IRPECFELLR.light	425.9008	599.297	26.8	10.1
IRPECFELLR.light	425.9008	746.3554	26.8	7.1
ISRPGDSDDSR.heavy	405.526	626.3257	1.75	13
ISRPGDSDDSR.heavy	405.526	589.2452	1.75	16
ISRPGDSDDSR.heavy	405.526	551.2434	1.75	10

Compound Name	Precursor Ion	Product Ion	RT (min)	Collision Energy
ISRPGDSDDSR.heavy	405.526	507.7274	1.75	7
ISRPGDSDDSR.heavy	405.526	272.1592	1.75	19
ISRPGDSDDSR.light	402.1899	626.3257	1.75	13
ISRPGDSDDSR.light	402.1899	579.2369	1.75	16
ISRPGDSDDSR.light	402.1899	546.2392	1.75	10
ISRPGDSDDSR.light	402.1899	502.7232	1.75	7
ISRPGDSDDSR.light	402.1899	262.151	1.75	19
IVIGYQSHADTATK.heavy	504.603	699.8588	9.88	13
IVIGYQSHADTATK.heavy	504.603	650.3246	9.88	10
IVIGYQSHADTATK.heavy	504.603	593.7826	9.88	13
IVIGYQSHADTATK.heavy	504.603	565.2718	9.88	16
IVIGYQSHADTATK.heavy	504.603	213.1598	9.88	10
IVIGYQSHADTATK.light	501.9316	695.8517	9.88	13
IVIGYQSHADTATK.light	501.9316	646.3175	9.88	10
IVIGYQSHADTATK.light	501.9316	589.7755	9.88	13
IVIGYQSHADTATK.light	501.9316	561.2647	9.88	16
IVIGYQSHADTATK.light	501.9316	213.1598	9.88	10
IVQAEGEAEAAK.heavy	612.3215	1011.483	4.69	19
IVQAEGEAEAAK.heavy	612.3215	883.4247	4.69	19
IVQAEGEAEAAK.heavy	612.3215	683.345	4.69	19
IVQAEGEAEAAK.heavy	612.3215	506.2453	4.69	16
IVQAEGEAEAAK.heavy	612.3215	341.2183	4.69	16
IVQAEGEAEAAK.light	608.3144	1003.469	4.69	19
IVQAEGEAEAAK.light	608.3144	875.4105	4.69	19
IVQAEGEAEAAK.light	608.3144	675.3308	4.69	19
IVQAEGEAEAAK.light	608.3144	502.2382	4.69	16
IVQAEGEAEAAK.light	608.3144	341.2183	4.69	16
LEQDEYALR.heavy	573.7869	904.4398	10.79	19
LEQDEYALR.heavy	573.7869	776.3813	10.79	19
LEQDEYALR.heavy	573.7869	532.3117	10.79	22
LEQDEYALR.heavy	573.7869	452.7236	10.79	13
LEQDEYALR.heavy	573.7869	243.1339	10.79	16
LEQDEYALR.light	568.7828	894.4316	10.79	19
LEQDEYALR.light	568.7828	766.373	10.79	19
LEQDEYALR.light	568.7828	522.3035	10.79	22
LEQDEYALR.light	568.7828	447.7194	10.79	13
LEQDEYALR.light	568.7828	243.1339	10.79	16

Compound Name	Precursor Ion	Product Ion	RT (min)	Collision Energy
LFDAPEAPLPSR.heavy	661.8526	376.1367	23.83	24.4
LFDAPEAPLPSR.heavy	661.8526	438.6943	23.83	18.4
LFDAPEAPLPSR.heavy	661.8526	579.2988	23.83	21.4
LFDAPEAPLPSR.heavy	661.8526	876.4313	23.83	21.4
LFDAPEAPLPSR.heavy	661.8526	1062.495	23.83	21.4
LFDAPEAPLPSR.light	656.8484	376.1967	23.83	24.4
LFDAPEAPLPSR.light	656.8484	433.7302	23.83	18.4
LFDAPEAPLPSR.light	656.8484	569.3406	23.83	21.4
LFDAPEAPLPSR.light	656.8484	866.473	23.83	21.4
LFDAPEAPLPSR.light	656.8484	1052.537	23.83	21.4
LFSGDVVLTAR.heavy	594.3365	927.5133	24.36	19
LFSGDVVLTAR.heavy	594.3365	840.4813	24.36	22
LFSGDVVLTAR.heavy	594.3365	569.3645	24.36	16
LFSGDVVLTAR.heavy	594.3365	470.2961	24.36	22
LFSGDVVLTAR.heavy	594.3365	261.1598	24.36	16
LFSGDVVLTAR.light	589.3324	917.5051	24.36	19
LFSGDVVLTAR.light	589.3324	830.473	24.36	22
LFSGDVVLTAR.light	589.3324	559.3562	24.36	16
LFSGDVVLTAR.light	589.3324	460.2878	24.36	22
LFSGDVVLTAR.light	589.3324	261.1598	24.36	16
LLIYWASTR.heavy	566.8231	906.4707	29.65	19
LLIYWASTR.heavy	566.8231	793.3867	29.65	16
LLIYWASTR.heavy	566.8231	630.3234	29.65	16
LLIYWASTR.heavy	566.8231	340.2595	29.65	13
LLIYWASTR.heavy	566.8231	227.1754	29.65	16
LLIYWASTR.light	561.8189	896.4625	29.65	19
LLIYWASTR.light	561.8189	783.3784	29.65	16
LLIYWASTR.light	561.8189	620.3151	29.65	16
LLIYWASTR.light	561.8189	340.2595	29.65	13
LLIYWASTR.light	561.8189	227.1754	29.65	16
LSVISVEDPPQR.heavy	675.3686	1050.545	19.41	22
LSVISVEDPPQR.heavy	675.3686	937.4613	19.41	22
LSVISVEDPPQR.heavy	675.3686	507.2913	19.41	31
LSVISVEDPPQR.heavy	675.3686	300.1918	19.41	19
LSVISVEDPPQR.heavy	675.3686	300.1918	19.41	19
LSVISVEDPPQR.light	670.3644	1040.537	19.41	22
LSVISVEDPPQR.light	670.3644	927.453	19.41	22

Compound Name	Precursor Ion	Product Ion	RT (min)	Collision Energy
LSVISVEDPPQR.light	670.3644	497.2831	19.41	31
LSVISVEDPPQR.light	670.3644	300.1918	19.41	19
LSVISVEDPPQR.light	670.3644	300.1918	19.41	19
LTIGSNLSIR.heavy	542.3234	869.5079	22.31	16
LTIGSNLSIR.heavy	542.3234	756.4238	22.31	22
LTIGSNLSIR.heavy	542.3234	699.4023	22.31	16
LTIGSNLSIR.heavy	542.3234	435.2576	22.31	13
LTIGSNLSIR.heavy	542.3234	215.139	22.31	16
LTIGSNLSIR.light	537.3193	859.4996	22.31	16
LTIGSNLSIR.light	537.3193	746.4155	22.31	22
LTIGSNLSIR.light	537.3193	689.3941	22.31	16
LTIGSNLSIR.light	537.3193	430.2534	22.31	13
LTIGSNLSIR.light	537.3193	215.139	22.31	16
LVNEVTEFAK.heavy	579.3182	945.4767	18.41	16
LVNEVTEFAK.heavy	579.3182	831.4338	18.41	16
LVNEVTEFAK.heavy	579.3182	702.3912	18.41	19
LVNEVTEFAK.heavy	579.3182	603.3228	18.41	16
LVNEVTEFAK.heavy	579.3182	213.1598	18.41	13
LVNEVTEFAK.light	575.3111	937.4625	18.41	16
LVNEVTEFAK.light	575.3111	823.4196	18.41	16
LVNEVTEFAK.light	575.3111	694.377	18.41	19
LVNEVTEFAK.light	575.3111	595.3086	18.41	16
LVNEVTEFAK.light	575.3111	213.1598	18.41	13
LVVVGAVGVGK.heavy	503.331	213.1098	19.64	13.5
LVVVGAVGVGK.heavy	503.331	312.1782	19.64	13.5
LVVVGAVGVGK.heavy	503.331	595.3153	19.64	13.5
LVVVGAVGVGK.heavy	503.331	694.3838	19.64	13.5
LVVVGAVGVGK.heavy	503.331	793.4522	19.64	13.5
LVVVGAVGVGK.light	499.3239	213.2098	19.64	13.5
LVVVGAVGVGK.light	499.3239	312.2782	19.64	13.5
LVVVGAVGVGK.light	499.3239	587.4011	19.64	13.5
LVVVGAVGVGK.light	499.3239	686.4696	19.64	13.5
LVVVGAVGVGK.light	499.3239	785.478	19.64	13.5
TGAAPIIDVVR.heavy	561.3313	821.5119	22.97	19
TGAAPIIDVVR.heavy	561.3313	411.2596	22.97	16
TGAAPIIDVVR.heavy	561.3313	306.1912	22.97	13
TGAAPIIDVVR.heavy	561.3313	230.1135	22.97	19

Compound Name	Precursor Ion	Product Ion	RT (min)	Collision Energy
TGAAPIIDVVR.light	556.3271	811.5036	22.97	19
TGAAPIIDVVR.light	556.3271	406.2554	22.97	16
TGAAPIIDVVR.light	556.3271	301.187	22.97	13
TGAAPIIDVVR.light	556.3271	230.1135	22.97	19
TIGTGLVTNTLAMTEEEK.heavy	639.3306	845.3801	31.69	13
TIGTGLVTNTLAMTEEEK.heavy	639.3306	774.3429	31.69	13
TIGTGLVTNTLAMTEEEK.heavy	639.3306	643.3025	31.69	13
TIGTGLVTNTLAMTEEEK.heavy	639.3306	479.7638	31.69	13
TIGTGLVTNTLAMTEEEK.heavy	639.3306	215.139	31.69	16
TIGTGLVTNTLAMTEEEK.light	636.6592	837.3659	31.69	13
TIGTGLVTNTLAMTEEEK.light	636.6592	766.3287	31.69	13
TIGTGLVTNTLAMTEEEK.light	636.6592	635.2883	31.69	13
TIGTGLVTNTLAMTEEEK.light	636.6592	479.7638	31.69	13
TIGTGLVTNTLAMTEEEK.light	636.6592	215.139	31.69	16
VLGLLGALDPYK.heavy	633.881	270.1312	39.98	20.5
VLGLLGALDPYK.heavy	633.881	383.2153	39.98	17.5
VLGLLGALDPYK.heavy	633.881	771.3627	39.98	17.5
VLGLLGALDPYK.heavy	633.881	884.4467	39.98	20.5
VLGLLGALDPYK.heavy	633.881	1054.552	39.98	20.5
VLGLLGALDPYK.light	629.8739	270.1812	39.98	20.5
VLGLLGALDPYK.light	629.8739	383.2553	39.98	17.5
VLGLLGALDPYK.light	629.8739	763.3885	39.98	17.5
VLGLLGALDPYK.light	629.8739	876.4825	39.98	20.5
VLGLLGALDPYK.light	629.8739	1046.588	39.98	20.5
VLIEGSINSVR.heavy	598.8473	984.5348	18.41	22
VLIEGSINSVR.heavy	598.8473	871.4507	18.41	25
VLIEGSINSVR.heavy	598.8473	742.4081	18.41	22
VLIEGSINSVR.heavy	598.8473	492.771	18.41	13
VLIEGSINSVR.heavy	598.8473	213.1598	18.41	19
VLIEGSINSVR.light	593.8431	974.5265	18.41	22
VLIEGSINSVR.light	593.8431	861.4425	18.41	25
VLIEGSINSVR.light	593.8431	732.3999	18.41	22
VLIEGSINSVR.light	593.8431	487.7669	18.41	13
VLIEGSINSVR.light	593.8431	213.1598	18.41	19
VLTLSDDLER.heavy	585.8156	958.4715	20.37	19
VLTLSDDLER.heavy	585.8156	857.4239	20.37	22
VLTLSDDLER.heavy	585.8156	744.3398	20.37	19

Compound Name	Precursor Ion	Product Ion	RT (min)	Collision Energy
VLTLSDDLER.heavy	585.8156	314.2074	20.37	16
VLTLSDDLER.heavy	585.8156	213.1598	20.37	13
VLTLSDDLER.light	580.8115	948.4633	20.37	19
VLTLSDDLER.light	580.8115	847.4156	20.37	22
VLTLSDDLER.light	580.8115	734.3315	20.37	19
VLTLSDDLER.light	580.8115	314.2074	20.37	16
VLTLSDDLER.light	580.8115	213.1598	20.37	13
VNIVPVIAK.heavy	480.8202	747.5218	22.57	13
VNIVPVIAK.heavy	480.8202	634.4378	22.57	13
VNIVPVIAK.heavy	480.8202	535.3694	22.57	13
VNIVPVIAK.heavy	480.8202	327.2027	22.57	10
VNIVPVIAK.heavy	480.8202	214.1186	22.57	13
VNIVPVIAK.light	476.8131	739.5076	22.57	13
VNIVPVIAK.light	476.8131	626.4236	22.57	13
VNIVPVIAK.light	476.8131	527.3552	22.57	13
VNIVPVIAK.light	476.8131	327.2027	22.57	10
VNIVPVIAK.light	476.8131	214.1186	22.57	13
VSLDVNHFAPDELTVK.heavy	597.9837	846.9378	28.95	16
VSLDVNHFAPDELTVK.heavy	597.9837	803.4218	28.95	16
VSLDVNHFAPDELTVK.heavy	597.9837	746.8797	28.95	16
VSLDVNHFAPDELTVK.heavy	597.9837	597.3698	28.95	13
VSLDVNHFAPDELTVK.heavy	597.9837	405.2284	28.95	13
VSLDVNHFAPDELTVK.light	595.3123	842.9307	28.95	16
VSLDVNHFAPDELTVK.light	595.3123	799.4147	28.95	16
VSLDVNHFAPDELTVK.light	595.3123	742.8726	28.95	16
VSLDVNHFAPDELTVK.light	595.3123	589.3556	28.95	13
VSLDVNHFAPDELTVK.light	595.3123	401.2213	28.95	13
VVDPFSK.heavy	400.2256	700.3756	13.34	10
VVDPFSK.heavy	400.2256	601.3072	13.34	10
VVDPFSK.heavy	400.2256	486.2802	13.34	16
VVDPFSK.heavy	400.2256	314.171	13.34	10
VVDPFSK.heavy	400.2256	242.159	13.34	22
VVDPFSK.light	396.2185	692.3614	13.34	10
VVDPFSK.light	396.2185	593.293	13.34	10
VVDPFSK.light	396.2185	478.266	13.34	16
VVDPFSK.light	396.2185	314.171	13.34	10
VVDPFSK.light	396.2185	234.1448	13.34	22

Compound Name	Precursor Ion	Product Ion	RT (min)	Collision Energy
VVNVSSIMSVR.heavy	600.8359	1002.528	25.75	22
VVNVSSIMSVR.heavy	600.8359	888.4847	25.75	19
VVNVSSIMSVR.heavy	600.8359	789.4163	25.75	19
VVNVSSIMSVR.heavy	600.8359	702.3842	25.75	16
VVNVSSIMSVR.heavy	600.8359	313.187	25.75	19
VVNVSSIMSVR.light	595.8317	992.5193	25.75	22
VVNVSSIMSVR.light	595.8317	878.4764	25.75	19
VVNVSSIMSVR.light	595.8317	779.408	25.75	19
VVNVSSIMSVR.light	595.8317	692.376	25.75	16
VVNVSSIMSVR.light	595.8317	313.187	25.75	19
VVTDTDETELAR.heavy	679.8373	1160.531	9.55	19
VVTDTDETELAR.heavy	679.8373	1059.483	9.55	25
VVTDTDETELAR.heavy	679.8373	944.4559	9.55	25
VVTDTDETELAR.heavy	679.8373	599.3387	9.55	34
VVTDTDETELAR.heavy	679.8373	580.7689	9.55	16
VVTDTDETELAR.light	674.8332	1150.522	9.55	19
VVTDTDETELAR.light	674.8332	1049.475	9.55	25
VVTDTDETELAR.light	674.8332	934.4476	9.55	25
VVTDTDETELAR.light	674.8332	589.3304	9.55	34
VVTDTDETELAR.light	674.8332	575.7648	9.55	16
VYPLINR.heavy	442.765	622.391	14.87	10
VYPLINR.heavy	442.765	525.3383	14.87	19
VYPLINR.heavy	442.765	412.2542	14.87	19
VYPLINR.heavy	442.765	311.6992	14.87	10
VYPLINR.heavy	442.765	263.139	14.87	7
VYPLINR.light	437.7609	612.3828	14.87	10
VYPLINR.light	437.7609	515.33	14.87	19
VYPLINR.light	437.7609	402.2459	14.87	19
VYPLINR.light	437.7609	306.695	14.87	10
VYPLINR.light	437.7609	263.139	14.87	7
VYTVDLGR.heavy	466.7574	833.4391	14.05	19
VYTVDLGR.heavy	466.7574	670.3758	14.05	13
VYTVDLGR.heavy	466.7574	569.3281	14.05	16
VYTVDLGR.heavy	466.7574	470.2597	14.05	16
VYTVDLGR.heavy	466.7574	263.139	14.05	10
VYTVDLGR.light	461.7533	823.4308	14.05	19
VYTVDLGR.light	461.7533	660.3675	14.05	13

Compound Name	Precursor Ion	Product Ion	RT (min)	Collision Energy
VYTVDLGR.light	461.7533	559.3198	14.05	16
VYTVDLGR.light	461.7533	460.2514	14.05	16
VYTVDLGR.light	461.7533	263.139	14.05	10
YDSLGLLELDQR.heavy	716.3713	279.0475	31.4	32.1
YDSLGLLELDQR.heavy	716.3713	313.1358	31.4	32.1
YDSLGLLELDQR.heavy	716.3713	670.2894	31.4	23.1
YDSLGLLELDQR.heavy	716.3713	783.3735	31.4	26.1
YDSLGLLELDQR.heavy	716.3713	953.479	31.4	23.1
YDSLGLLELDQR.light	711.3672	303.2075	31.4	32.1
YDSLGLLELDQR.light	711.3672	660.3311	31.4	23.1
YDSLGLLELDQR.light	711.3672	773.4252	31.4	26.1
YDSLGLLELDQR.light	711.3672	943.5207	31.4	23.1
YDSLGLLELDQR.light	711.3672	279.1275	31.4	32.1
YLTTAVITNK.heavy	566.3286	855.5026	15.5	13
YLTTAVITNK.heavy	566.3286	754.4549	15.5	19
YLTTAVITNK.heavy	566.3286	653.4072	15.5	19
YLTTAVITNK.heavy	566.3286	582.3701	15.5	16
YLTTAVITNK.heavy	566.3286	277.1547	15.5	13
YLTTAVITNK.light	562.3215	847.4884	15.5	13
YLTTAVITNK.light	562.3215	746.4407	15.5	19
YLTTAVITNK.light	562.3215	645.393	15.5	19
YLTTAVITNK.light	562.3215	574.3559	15.5	16
YLTTAVITNK.light	562.3215	277.1547	15.5	13

PRM-MS Inclusion

Peptide	RT	CE
AAEIASSDSANVSSR	9.6	22
AGSSEWLAVDGLVSPSNNSK	30.6	22
AINPINTFTK	22.1	26
DQIYDIFQK	29.5	30
EAGLDLR	13.8	26
EHIEIIAPSPQR	16	26
ELEEIVQPIISK	28.8	22
ELGIWEPLAVK	32.9	22
ELIFEETAR	22.1	26

Peptide	RT	CE
FDAGELITQR	23.9	26
FEISETSVNR	16.5	26
FFAGIVWQHVYEK	30	26
FIDTTSK	9.2	22
GDFIALDLGGSSFR	33.5	26
GLPAPIEK	14.3	26
GSTAPVGGGAFPTIVER	25.6	26
GTGIVSAPVPK	15.3	26
GTITVSAQELK	16.9	26
HGLLVPNNTTDQELQHIR	19.1	26
IADPEHDHTGFLTE(pY)VATR	22.2	26
IADPEHDHTGFLTEYVATR	22.8	26
IALDFQR	20.3	26
IFGVTTLDIVR	32.9	26
IFVNDDR	12	26
IGVLDEGK	14	26
IITLTGPTNAIFK	31	24
ILPTLEAVAALGNK	33.1	26
ILVTGGSGLVGK	19	22
ISRPGDSDDSR	5.4	26
IVIGYQSHADTATK	12.1	22
IVQAEGEAEAAK	8.3	26
LEQDEYALR	14	26
LFDAPEAPLPSR	24.8	26
LFSGDVVLTAR	25.3	26
LLIYWASTR	29.2	26
LSVISVEDPPQR	20.6	26
LTIGSNLSIR	23.7	26
LVNEVTEFAK	20.3	26
TGAAPIIDVVR	24	26
TIGTGLVTNTLAMTEEEK	30.7	22
VLGLLGALDPYK	35.7	26
VLIEGSINSVR	19.6	26
VLTLSDDLER	22.5	26
VNIVPVIAK	23.6	26
VSLDVNHFAPDELTVK	27.5	26

Peptide	RT	CE
VVDPFSK	16.3	26
VVNVSSIMSVR	26	26
VVTDTDETELAR	13.2	26
VYPLINR	17	26
VYTVDLGR	16.6	26
YDSLGLLELDQR	31.1	26
YLTTAVITNK	17.2	26

MRM Assay Linear Range

Gene name	Protein name	Peptide	Adjusted LLOQ 6495	Adjusted ULOQ 6495
PIK3CB	Phosphatidylinositol 4,5-bisphosphate 3-kinase catalytic subunit beta isoform	AAEIASSDSANVSSR	5.12	1,000
ATF4	Cyclic AMP-dependent transcription factor ATF-4	AGSSEWLAVDGLVSPSNNSK	91.6	1,145
ARHGAP1	Rho GTPase-activating protein 1	AINPINTFTK	5.48	2,675
EIF4A1	Eukaryotic initiation factor 4A-I	DQIYDIFQK	53.6	1,675
PIK3CB	Phosphatidylinositol 4,5-bisphosphate 3-kinase catalytic subunit beta isoform	EAGLDLR	12.8	1,000
EIF2AK3	Eukaryotic translation initiation factor 2-alpha kinase 3	EHIEIIAPSPQR	12.8	2,500
HSPA5	Endoplasmic reticulum chaperone BiP	ELEEIVQPIISK	128	1,603
CCT3	T-complex protein 1 subunit gamma	ELGIWEPLAVK	88.3	2,758
MAPK1	Mitogen-activated protein kinase 1	ELIFEETAR	14.9	1,163
PHB1	Prohibitin 1	FDAGELITQR	31.4	2,457
S6K1	Ribosomal protein S6 kinase beta-1	FEISETSVNR	32.0	2,500
AKT1 wt	RAC-alpha serine/threonine-protein kinase	FFAGIVWQHVYEK	80.0	2,500
RPL3	60S ribosomal protein L3	FIDTTSK	0.820	2,500
HK1	Hexokinase-1	GDFIALDLGGSSFR	106	1,324
IGHG2	Immunoglobulin heavy constant gamma 2	GLPAPIEK	0.846	1,031
PDIA6	Protein disulfide-isomerase A6	GSTAPVGGGAFPTIVER	26.8	2,091
RPS2	40S ribosomal protein S2	GTGIVSAPVPK	3.34	1,632
CPNE1	Copine-1	GTITVSAQELK	32.0	2,500
EIF6	Eukaryotic translation initiation factor 6	HGLLVPNNTTDQELQHIR	31.5	2,464
MAPK3	Mitogen-activated protein kinase 3	IADPEHDHTGFLTEp(Y)VATR	139	4,355
MAPK3	Mitogen-activated protein kinase 3	IADPEHDHTGFLTEYVATR	173	2,158
LGALS3	Galectin-3	IALDFQR	4.82	2,354
MDH2	Malate dehydrogenase, mitochondrial	IFGVTTLDIVR	42.7	1,335
ILF3	Interleukin enhancer-binding factor 3	IFVNDDR	1.13	3,450
RPS9	40S ribosomal protein S9	IGVLDEGK	2.00	2,500
PCBP1	Poly(rC)-binding protein 1	IITLTGPTNAIFK	61.3	1,914
ILF2	Interleukin enhancer-binding factor 2	ILPTLEAVAALGNK	48.7	609
TSTA3	GDP-L-fucose synthase	ILVTGGSGLVGK	5.12	2,500
HNRNPL	Heterogeneous nuclear ribonucleoprotein L	ISRPGDSDDSR	12.7	2,482
EIF4E	Eukaryotic translation initiation factor 4E	IVIGYQSHADTATK	5.24	1,024
PHB2	Prohibitin-2	IVQAEGEAEAAK	6.53	510

Gene name	Protein name	Peptide	Adjusted LLOQ 6495	Adjusted ULOQ 6495
HADHB	Trifunctional enzyme subunit beta, mitochondrial	LEQDEYALR	3.83	749
MTOR	Serine/threonine-protein kinase mTOR	LFDAPEAPLPSR	80.0	2,500
CBR1	Carbonyl reductase [NADPH] 1	LFSGDVVLTAR	201	2,509
IGKV4-1	Immunoglobulin kappa variable 4-1	LLIYWASTR	15.7	489
ETFB	Electron transfer flavoprotein subunit beta	LSVISVEDPPQR	25.6	1,998
XRCC5	X-ray repair cross-complementing protein 5	LTIGSNLSIR	200	2,500
ALB	serum albumin	LVNEVTEFAK	19.8	3,869
KRAS mut	GTPase Kras	LVVVGAVGVGK	32.0	2,500
RPL27A	60S ribosomal protein L27a	TGAAPIIDVVR	12.8	2,500
TUFM	Elongation factor Tu, mitochondrial	TIGTGLVTNTLAMTEEEK	200	2,500
MTOR	Serine/threonine-protein kinase mTOR	VLGLLGALDPYK	-	-
ARPC4	Actin-related protein 2/3 complex subunit 4	VLIEGSINSVR	33.1	2,584
EIF5	Eukaryotic translation initiation factor 5	VLTLSDDLER	17.6	1,372
SEPTIN2	Septin-2	VNIVPVIAK	5.12	2,500
HSPB1	Heat shock protein beta-1	VSLDVNHFAPDELTVK	118	1,469
RPS3A	40S ribosomal protein S3a	VVDPFSK	0.820	2,500
HSP90AB1	Heat shock protein HSP 90-beta	VVNVSSIMSVR	59.1	1,848
EIF2S1	Eukaryotic translation initiation factor 2 subunit 1	VVTDTDETELAR	25.7	2,008
MAP4K4	Mitogen-activated protein kinase kinase kinase kinase 4	VYPLINR	1.71	2,142
PIGR	Polymeric immunoglobulin receptor	VYTVDLGR	10.8	2,113
AKT2	RAC-beta serine/threonine-protein kinase	YDSLGLLELDQR	200	2,500
EIF3E	Eukaryotic translation initiation factor 3 subunit E	YLTTAVITNK	1.27	1,583

3. Methods: Dietary and Medical Questionnaire (DiMQu) & scoring

Dietary & Medication Questionnaire

QUESTIONNAIRE

		Insert check mark in the boxes which best represent your intake					
Food/Drink	**Serving Size**	**Never or Rarely**	**1-3 per month**	**1-3 per week**	**4-6 per week**	**1-2 times a day**	**3 or more times a day**
Coffee, regular	1 cup (250 mL)						
Coffee, decaffeinated	1 cup (250 mL)						
Tea, regular	1 cup (250 mL)						
Tea, decaffeinated	1 cup (250 mL)						
Carbonated Soda: e.g. Coke, Pepsi, 7UP, Sprite, Root Beer, Dr. Pepper	1 can (355 mL)						
Cruciferous Vegetables: e.g. Cauliflower, Broccoli, Cabbage, Bok Choy, Brussel Sprouts, Turnips, Radish	1 cup of vegetables						
Charbroiled, barbequed, or pan-fried meat: e.g. Chicken, Beef, Pork, Sausage, Lamb, Turkey	1 portion (3oz = about size of your palm)						
Red Wine	1 glass (5oz/ 150ml)						
Beer	1 bottle/can(12oz /355 ml)						
Spirits/Liquor	1 shot (1.5 oz/ 44ml)						
Garlic cloves	1 serving						
Grapefruit / Seville oranges	1 medium-sized orange						
Jufeng Grape Juice	1 cup (250 mL)						
Liquorice Candy	1 medium-sized pack of candy						
Indian food	1 serving						
Ground black pepper (for seasoning/taste in a meal)	-						

Smoking

Do you smoke (please circle one)? (Y / N)

How many cigarettes do you smoke in a day?

_____

Medical History:
Please list any current chronic medical problems or conditions that you have. If none, please write 'none.'

Complementary Natural Health Products:
Please list any complementary or natural health products that you take (example: curcumin, herbal products, vitamins, supplements, spices, etc.).

Name of Product	Amount of Product Taken	How Often Is It Taken

Current Medications:
Please list any medications you are currently taking, whether prescription or over the counter (Please remember to include any hormonal treatments, birth control, etc.).

Name of Medication	Dose of Medication	How Often Is It Taken?	How Do You Take it?

Time of first blood test: _____

Time of second blood test: _____

Height: _____

Weight: _____

Categorical Assignment of Inhibitors / Inducers from Dietary Exposures

Minor (*) inhibitors/inducers were assigned a strength score of 1. All others, strength = 2.

	CYP1A2		CYP3A4	
Item	Inducer	Inhibitor	Inducer	Inhibitor
Coffee	✓			
Tea	✓			
Red Wine*		✓		✓
Beer*		✓		✓
Spirits/Liquor*		✓		✓
Carbonated Soda	✓			
Grapefruit / Seville oranges				✓
Cruciferous Vegetables	✓			
Charbroiled, barbequed, or pan-fried meat	✓			
Jufeng Grape Juice	✓			
Indian food (curcuma)*		✓		✓
Liquorice Candy				
Ground black pepper				✓
Garlic			✓	

Note. Coffee and tea includes decaffeinated options. Meats include: chicken, beef, pork, sausage, lamb and turkey. Cruciferous vegetables include: cauliflower, broccoli, cabbage, bok choy, brussel sprouts, turnips, radish. * indicates minor inhibitor or inducer

Assignment of Inhibitors / Inducers from Patient-Reported Medications & Supplements

Minor inhibitors/inducers were assigned a strength score of 1. For all others, strength = 2.

	CYP1A2		CYP3A4	
	Inducer	Inhibitor	Inducer	Inhibitor
Modafinil	✓		✓	
Curcumin*		✓		✓
Omega 3 Fatty Acid		✓		
Melatonin		✓		
Loratidine			✓	
Oregano Oil				✓
Teva-venlafaxine XR				✓

*Note.** indicates minor inhibitor or inducer

4. Methods: Geneva cocktail MS method details

LC Settings

Parameter	Settings
System	Agilent 1290 Infinity system
Column	Zorbax Eclipse plus RRHD C18, 2.1x15mm, 1.8um (Column labeled "A")
Guard Column	none
Column temp. (°C)	50°C +/- 0.8°C
Mobile Phase A	H2O + 0.1% formic acid
Mobile Phase B	Acetonitrile + 0.1% formic acid
Flow Rate (ml/min)	0.6
Run Time (min)	5.2
Injection Volume (µl)	Default Injection volume in method: 5 uL Perform 2 injections of each sample: 2 uL for caffeine, paraxanthine; 18 uL for midazolam, OH-midazolam
Sample dispensing	0.0 mm needle draw position (Vial/Well bottom sensing on); 10 uL/min draw speed, 20 uL/min eject speed; 3 sec equilibration time, flush with 5.0 times injection volume
Needle Wash	Flush Port - 10 sec
AS Temperature (oC)	4
Max Pressure	1000 bar

LC Gradient

Step	Time (min)	% Mobile Phase B
Applying sample to column	0.00-0.50	2% → 20%
Pre-elution	0.50-1.00	2% → 20%
Elution	1.00-3.00	20 →25%
Post-elution	3.00-3.50	25 →98%
Wash	3.50-5.00	98 →100%
Reset	5.00-5.3	100 → 2%
Equilibration	5.3-5.8	2%
Post time	+0.2 min	2%

MS Transitions & Collision Energies

Analyte	Transition	CE
Hydroxymidazolam (IS)	346/328	22
Hydroxymidazolam (IS)	346/203	31
Hydroxymidazolam	342/324	22
Hydroxymidazolam	342/203	31
Midazolam (IS)	330/295	28
Midazolam (IS)	330/253	40
Midazolam	326/291	28
Midazolam	326/249	40
Caffeine (IS)	204/144	21
Caffeine (IS)	204/116	27
Caffeine	195/138	21
Caffeine	195/110	27
Paraxanthine (IS)	187/127	20
Paraxanthine	181/124	20

MS Settings

Parameter	Settings
System	Agilent 6495 MS/MS
Ion Source	AJS ESI
Method	MRM-MS
Delta EMV (+)	400
Source gas temp	150 C
Gas Flow	15 l/min
Nebulizer	30 psi
Sheath Gas Temp	250 C
Sheath Gas Flow	11 l/min
Polarity	positive
Capillary	3500V + / 3000 V neg
Nozzle voltage	300 V pos / 1500 V neg
Resolution (MS1 and MS2)	Unit Res
Fragmentor	380
Cell Accelerator Voltage	5
Cycle time	3.04 cycles/s, 329 ms/cycle (dwell 20/transition)
Time filtering	Peak width 0.03 min

Sample chromatograms

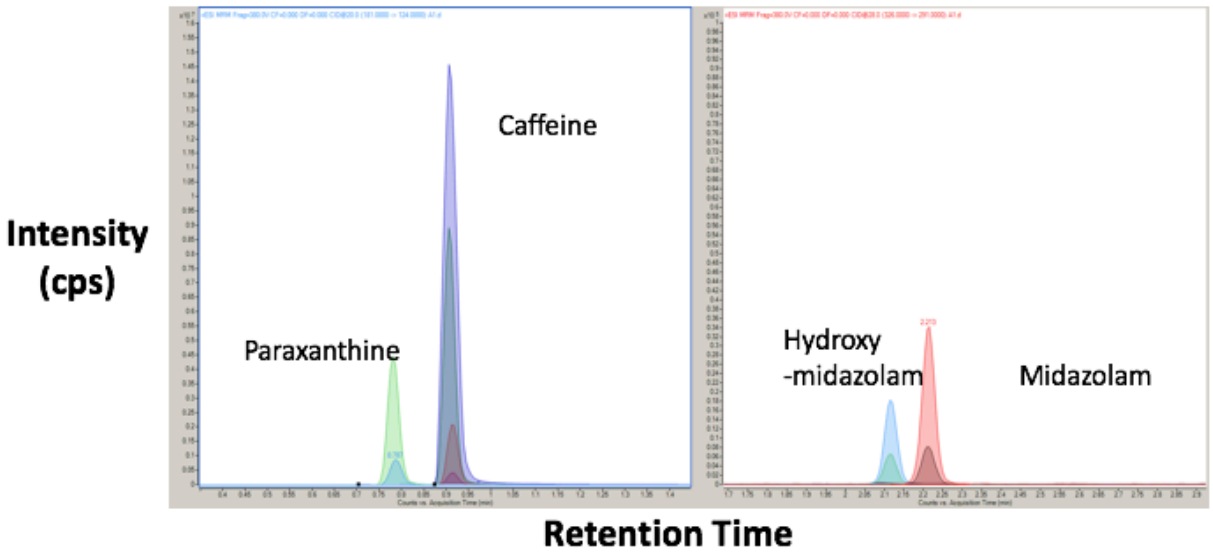

5. Results: Analysis of published AKT expression data in cancer cell lines

Source:

- Based on data published in Lapek, J., Greninger, P., Morris, R. et al. Detection of dysregulated protein-association networks by high-throughput proteomics predicts cancer vulnerabilities. Nat Biotechnol 35, 983–989 (2017). https://doi-org.proxy3.library.mcgill.ca/10.1038/nbt.3955

Methods:

- Published dataset includes publicly-deposited relative abundance data at protein level (RPPA) and transcriptomic level for 36 well-characterized breast cancer cell lines
- Categorized cell lines into commonly-used molecular subtypes (Luminal A, Luminal B, Basal, Her2-enriched)
- Extracted relative abundance data for Akt1, Akt2, Akt3 and analyzed using multi-variate statistics to assess protein-RNA concordance, subtype-specific differences in Aktexpression
- Coded cell lines according to published capivasertib sensitivity.
- Figures generated in MetaboAnalyst

Results:

- AKT1 and AKT2 protein expression appear higher in Luminal than in Basal subtypes (ANOVA $p<0.05$)
- AKT3 is elevated in Basal vs other subtypes
- Concordance varies by subtype and cell line
- No relationship between observed transcriptomic or protein expression and capivasertib sensitivity.

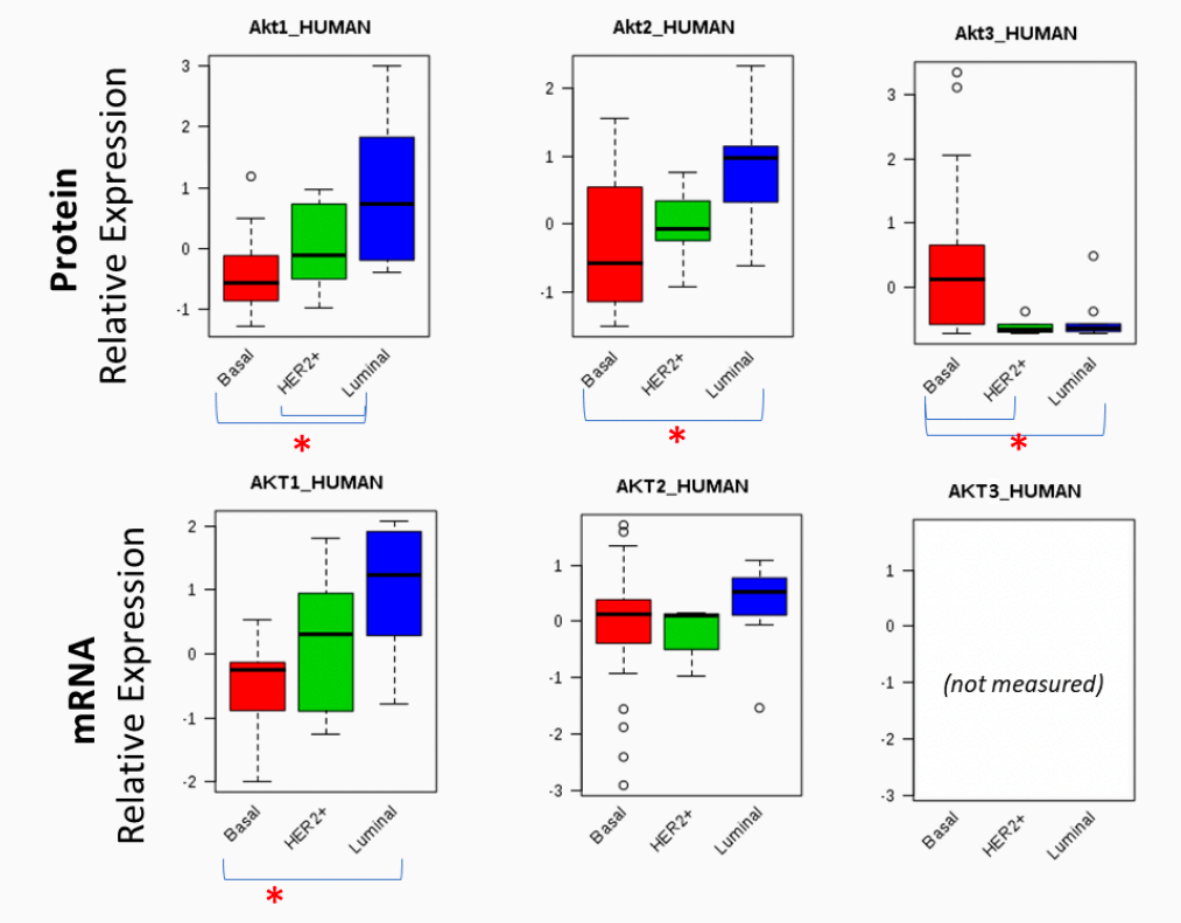

Protein & mRNA expression of AKT1, AKT2 & AKT3 in breast cancer cell lines by subtype

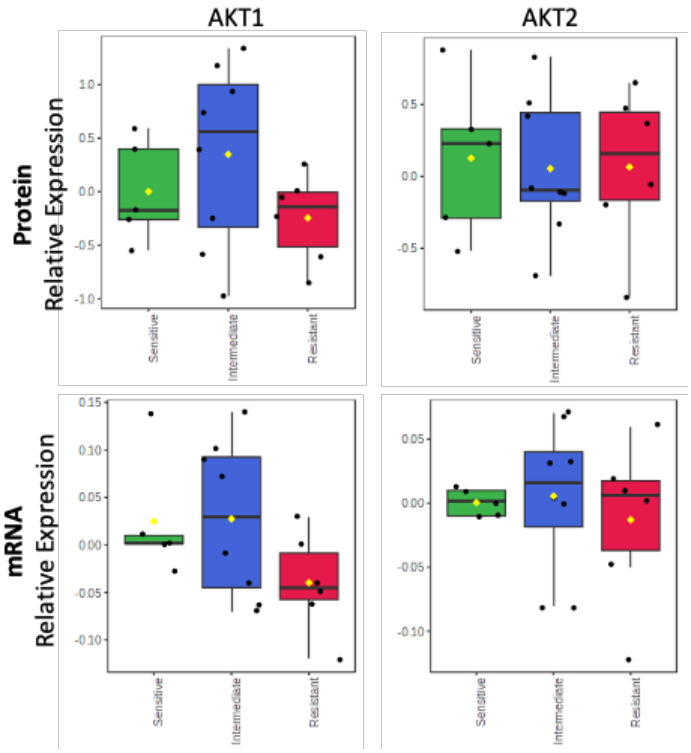

Protein and mRNA expression of AKT1 and AKT2 in cell lines by capivasertib sensitivity

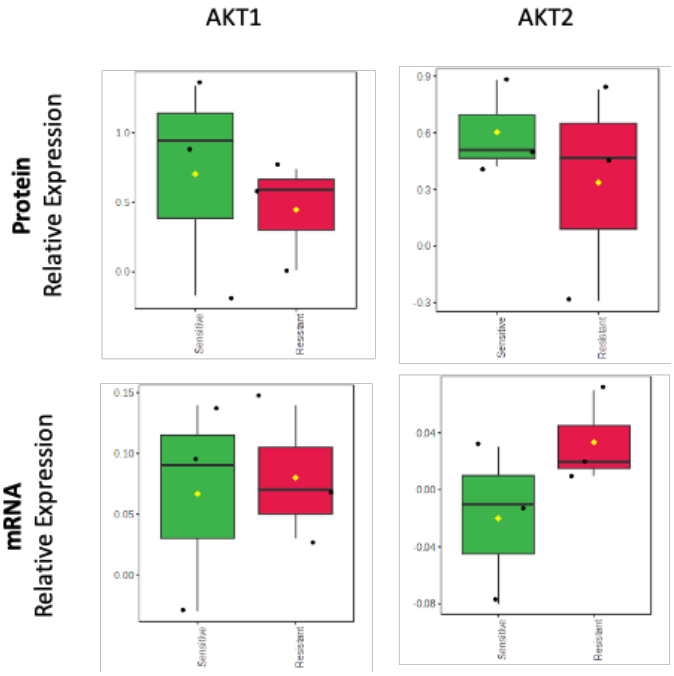

Protein and mRNA expression of AKT1 and AKT2 in luminal breast cancer cell lines by capivasertib sensitivity

6. Results: Review of additional published evidence related to proteins of interest

Relationship of proteins of interest to cancer and AKT activity

Black = role in cancer, prognostic / treatment response, Purple = relationship to AKT

PROTEIN ACCESSION	GENE NAME	Protein function	Observation	Evidence from Literature
P02768 Serum albumin	**ALB**	Serum protein - Osmotic pressure regulation, transporter	Higher in CB	• Albumin activates the AKT signaling pathway and promotes cell survival (241) • Albumin protects against chorambucil or radiation-induced apoptosis in CLL. TKIs targeting the PI3K pathway re-sensitize cells to these treatments.The protective action of albumin and AKT activation is compromised by lipid binding in blood. (241) • Hypoalbuminemia occurs in diabetes, with low insulin. Under higher insulin conditions, AKT is activated resulting in mTORC1-driven protein synthesis and lipogenesis. FOXO1 is inactivated. Akt is required for the effect of insulin on albumin production. FOXO1 represses albumin expression (435). • Low pretreatment serum albumin level associated with shorter PFS and OS for patients with non-small cell lung cancer treated with TKIs targeting EGFR (upstream from AKT) (436,437). Baseline serum albumin predicted OS better than tumour EGFR mutation, cancer stage or baseline ECOG PS (238). • Low pretreatment albumin in advanced thyroid cancer, together with other markers of nutritional status, strongly predicted PFS on TKI treatment (239) • Low serum albumin associated with increased pro-inflammatory cytokines, including TNF-alpha, which induces IL-6 and gluconeogenesis (239) **Possible interpretations:** • Upstream activation of AKT in CB group • Higher albumin is a positive prognostic marker in CB patients • Albumin has previously been associated with treatment response to TKIs • Nutritional status ties AKT activation • Since albumin is mainly found in blood, its higher level in CB could reflect better perfusion of the tested tissue

PROTEIN ACCESSION	GENE NAME	Protein function	Observation	Evidence from Literature
P01859 Immunoglobulin heavy constant gamma 2	**IGHG2**	Humoral immunity - immunoglobulin	Higher in CB	• IGHG2 has been linked to Phospholipase C signalling (245), which is an upstream activator of PI3K and AKT as well as the MEK-ERK pathway (244) • Similar protein, IGHG1, promotes proliferation, migration and chemo-resistance of gastric cancer to 3 common agents via the AKT/GSK-3/beta-catenin axis (438), increasing pAKT without affecting total expression of AKT • Higher IGHG2 was associated with improved paclitaxel sensitivity and relapse-free survival in TNBC (439) • Cancer-derived IgG is associated with activation of AKT in cisplatin resistance and MEK-ERK upregulation (440) **Possible interpretations:** • Increased upstream activation of AKT in CB group • Unclear relationship of IGHG to cancer aggressiveness and treatment sensitivity • Increased immune infiltration or surveillance of the tumours in CB group
P01834 Immunoglobulin kappa constant	**IGKC**	Humoral immunity - immunoglobulin	Higher in CB	• High IGKC is a positive prognostic marker for metastasis-free survival and response to chemotherapy, validated at the RNA- and protein-levels (441) • Another article reports that prognostic value is limited to specific breast cancer subtype and treatment combinations, particularly TNBC (248) • Though some data suggests limited prognostic utility for IGKC in HR+ breast cancers, this interpretation is likely confounded by the immuno-modulatory effects of endocrine therapies *(248)*, which does not apply to capivasertib. **Possible interpretations:** • Positive prognostic marker in CB group • Increased immune infiltration or surveillance of the tumours in CB group

PROTEIN ACCESSION	GENE NAME	Protein function	Observation	Evidence from Literature
P06312 Immunoglobulin kappa variable 4-1	**IGKV4-1**	Humoral immunity-immunoglobulin	Higher in CB	• High IGKV4-1 was associated with "low risk" in lung adenocarcinoma (442) • Fusions involving IGKV4 were observed in oral squamous cell carcinoma, in a model where Akt-mTOR/Akt-bad signaling was associated with metastasis and enhanced cell proliferation (443) • In an AKT2 knock-out model of human lung cancer, 14 of 20 downregulated mRNAs were associated with immunoglobulin genes, including IGKV (444) **Possible interpretations:** • Positive prognostic marker in CB group • Increased immune infiltration or surveillance of the tumours in CB group
P01833 Polymeric immunoglobulin receptor	**PIGR**	Immunity - Trans-cytosis of IgA / IgM across epithelial cells	Higher in CB	• pIgR activates PDK1/Akt/GSK3β/β-catenin and is associated with increased tumour aggressiveness that responds to AKT inhibitors (242) **Possible interpretations:** • Activation of AKT activity & sensitivity to AKT inhibitors in CB group • Increased immune infiltration or surveillance of the tumours in CB group
Q07960 Rho GTPase-activating protein 1	**ARHGAP1**	Negative regulator of Rho	Higher in NCB	• Associated with cell migration and invasion via negative regulation of Rho proteins (445)
P16152 Carbonyl reductase [NADPH] 1	**CBR1**	NADPH-dependent reductase	Higher in NCB	• Catalyzes the reduction of some antitumor drugs
Q99829 Copine-1	**CPNE1**	TNF-alpha signaling, membrane trafficking, endoprotease processing	Higher in NCB	• Involved in neuronal progenitor cell differentiation; induces neurite outgrowth via AKT-dependent signaling(446,447) **Possible interpretations:** • CB group with higher serum albumin may have decreased TNF alpha and gluconeogenesis, reduced B-catenin, which is a mechanism of resistance
Q7Z4W1 L-xylulose reductase	**DCXR**	NADPH-dependent reductase	Higher in NCB	• Involved in glucose metabolism

PROTEIN ACCESSION	GENE NAME	Protein function	Observation	Evidence from Literature
Q16698 2,4-dienoyl-CoA reductase, mitochondrial	**DECR1**	Mitochondrial - fatty acid beta-oxidation	Higher in NCB	• Uncoupling proteins (UCPs) oppose this phenotype by inducing futile mitochondrial respiration that is uncoupled from ATP synthesis, resulting in nutrient wasting. Mechanistic studies reveal that uncoupling increases fatty acid oxidation and membrane phospholipid catabolism, and impairs recruitment of Akt to the plasma membrane. These findings demonstrate that mitochondrial uncoupling is an effective strategy to limit proliferation and tumorigenesis through inhibition of Akt, and illuminate a novel mechanism of crosstalk between mitochondrial metabolism and growth signalling. Overexpression of Akt overcomes metabolic regulation by UCP3, rescuing carcinogenesis. (448) • PERK, upstream from EIF2 is an indispensable component of the unfolded protein response (UPR), which is induced by imbalances between the load of proteins entering the ER and ER's ability to process them (448)
P52597 Heterogeneous nuclear ribonucleoprotein F	**HNRNPF**	Translation - Ribosomal protein	Higher in NCB	• Additional proteins in this group such as Poly(rC)-binding proteins (PCBP1, PCBP2) and heterogeneous nuclear ribonucleoproteins (HNRNPL, HNRNPF), are involved in protein translation, localization, and degradation (253)
P14866 Heterogeneous nuclear ribonucleoprotein L	**HNRNPL**	Translation - Ribosomal protein	Higher in NCB	
Q12905 Interleukin enhancer-binding factor 2	**ILF2**	Transcription, innate immunity, cell growth, forms RNA-binding complex with IFL3	Higher in NCB	• High ILF-2 is associated with poor prognosis and with improved anthracycline/taxane response (257) • Interleukin enhancer-binding factors (ILF2, ILF3) are involved in DNA repair and RNA metabolism, and contribute to oncogenesis by regulating gene expression (257) • Negative regulators of tumour-suppressing microRNAs whose activity is known to be

PROTEIN ACCESSION	GENE NAME	Protein function	Observation	Evidence from Literature
Q12906 Interleukin enhancer-binding factor 3	**ILF3**	Transcription, innate immunity, cell growth, forms RNA-binding complex with IFL3	Higher in NCB	mediated by AKT-driven phosphorylation (449) • Depletion of ILF3 in HCC cells has been associated with decreased AKT phosphorylation in hepatocellular carcinoma, whereas expression of ILF2 and ILF3 has been linked to PI3K/AKT and MAPK signaling in esophageal squamous cell carcinoma (259,260) • Depletion of ILF3 in HCC cells has been associated with decreased AKT phosphorylation in hepatocellular carcinoma, whereas expression of ILF2 and ILF3 has been linked to PI3K/AKT and MAPK signaling in esophageal squamous cell carcinoma *(46,47)*.
P17931 Galectin-3	**LGALS3**	Pre-mRNA splicing factor. acute inflammatory response, recognizes membrane damage	Higher in NCB	• PI3K-AKT pathway activation induces Gal-3 expression in breast/prostate cancer (450) • Galectin-3 knockdown reduces AKT signaling (451) • Expression of galectin-3 (TSTA3) has been shown in gastric cancer cell lines to activate the PI3K pathway through increased AKT phosphorylation, resulting in a loss of responsiveness to IFN-γ, which is similarly observed in the context of PI3K mutations (264) **Possible interpretations:** • AKT activation in NCB group
P40926 Malate dehydrogenase, mitochondrial	**MDH2**	Mitochondrial – Glucose metabolism, citric acid cycle	Higher in NCB	• LncRNA AC020978 facilitates non–small cell lung cancer progression by interacting with malate dehydrogenase 2 and activating the AKT pathway (452) • MDH2 stimulated by estrogen-GPR30 pathway down-regulates PTEN expression and promotes proliferation and invasion in endometrial cancer. (453)
Q15365 Poly(rC)-binding protein 1	**PCBP1**	RNA – RNA binding, translational co-activator	Higher in NCB	• Additional proteins in this group such as Poly(rC)-binding proteins (PCBP1, PCBP2) and heterogeneous nuclear ribonucleoproteins (HNRNPL, HNRNPF), are involved in protein translation, localization, and degradation. (253)
Q15366 Poly(rC)-binding protein 2	**PCBP2**			

PROTEIN ACCESSION	GENE NAME	Protein function	Observation	Evidence from Literature
Q15084 Protein disulfide-isomerase A6	**PDIA6**	Translation - Chaperone for unfolded and misfolded proteins	Higher in NCB	• Negatively regulates the unfolded protein response (UPR) through binding to UPR sensors such as ERN1, which in turn inactivates ERN1 signaling (454) • May also regulate the UPR via the EIF2AK3 UPR sensor (454)
P35232 Prohibitin	**PHB1**		Higher in NCB	• Prohibitins (PHB1, PHB2) have specifically been associated directly with the activation of protein kinase c activity (455) • Both PHBs are directly phosphorylated by AKT, after which PHB forms a complex with RAF1 and activates the RAF1-MEK1-ERK pathway (455) • Phosphorylation of PHB in turn further increases AKT activity. (455)
Q99623 Prohibitin-2	**PHB2**		Higher in NCB	
Multiple	**RPLs**	Translation - Ribosomal protein	Higher in NCB	• Specific subsets of ribosomal proteins have previously been identified as regulatory factors in breast cancer as well as pediatric acute myeloid leukemia (456-458)
Multiple	**RPSs**		Higher in NCB	

7. Results: AKT E17K methods development

FASTA sequence of AKT1 showing location of E17K mutation

Due to many lysines and arginines in the surrounding sequence, trypsin would not produce targetable peptides. m/z shift associated with mutation is only +1 m/z. An alternative enzyme such as clostrapain is required to cleave a targetable peptide

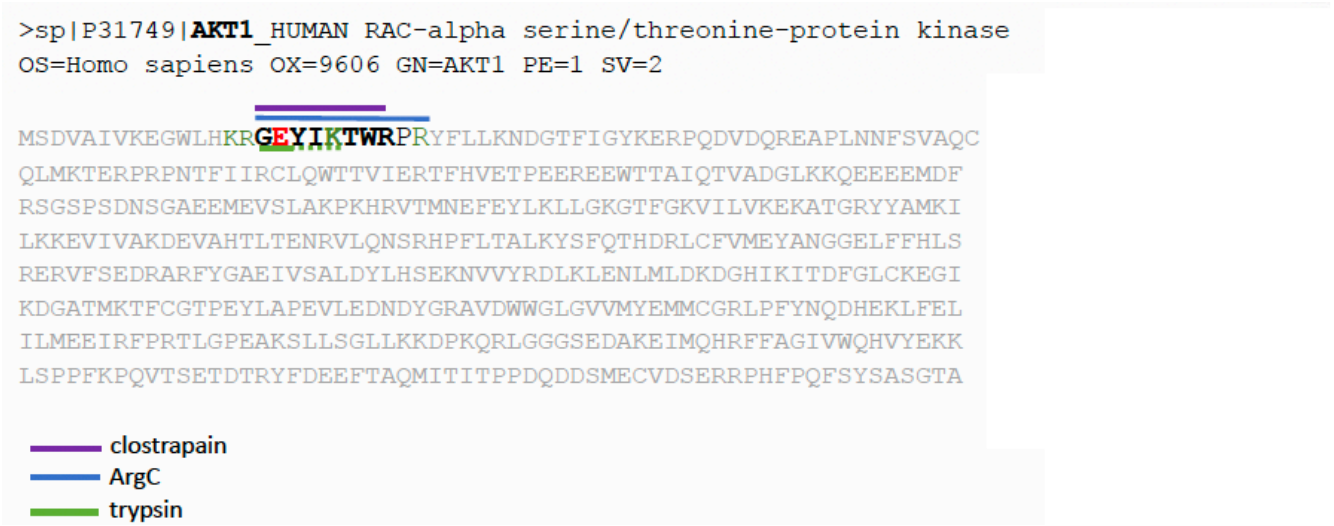

Scheduled optimized MRM-MS assay with 16-minute gradient

LC separation discriminates peptides even on a short gradient, and the transition ratio is distinctive for the mutant vs. wildtype peptides

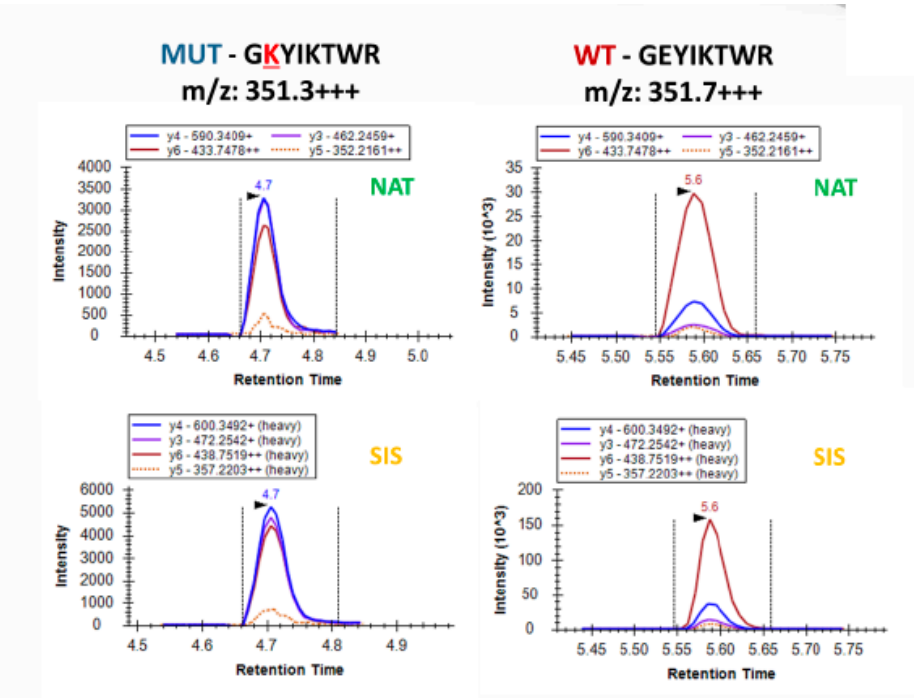

Immunoenrichment of AKT1 wt and AKT1 E17K peptides

A modified antibody-bead conjugation protocol and immunoenrichment procedure was developmed. We then assessed signal for the WT and MUT NAT and SIS peptides pull-down overnight in buffer by each of 2 antibodies (Signatope) using the developed immuno-LC-MRM-MS/MS method. Both polyclonal antibodies were found to enrich both the WT and MUT peptides, enabling analysis in a single run.

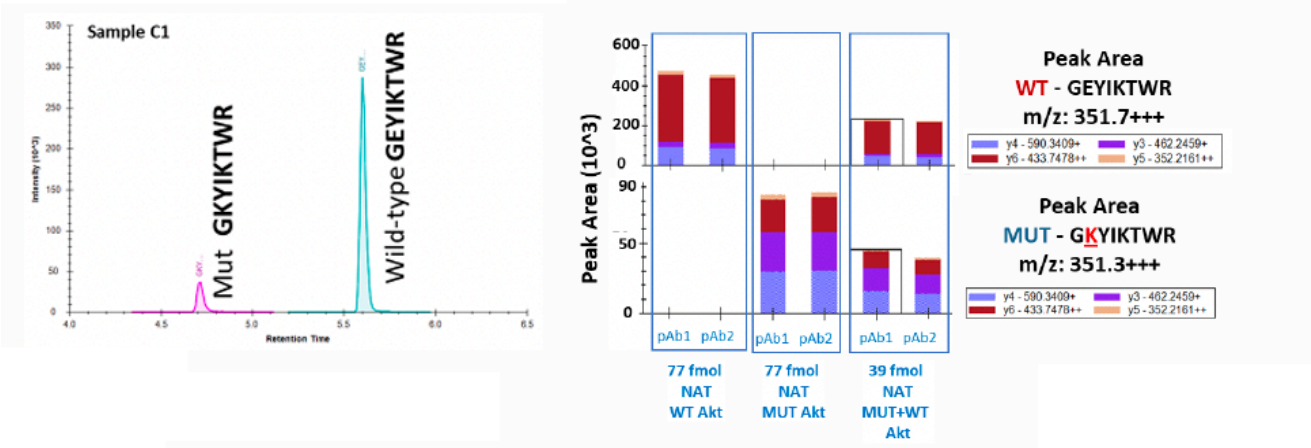

8. Results: Detection screening

Peptide	Protein	MCF-7 13 ug	MCF-7 25ug	MCF-7 26 ug	MCF-7 50ug	HT- 29 15ug	COLO-205 16ug	HCT-116 18ug	ZR- 75 40ug	MDA-MB-436 57ug
AGSSEWLAVDGLVSPSNNSK	ATF4	-	-	-	-	yes	-	-	-	-
AINPINTFTK	ARHGAP1	yes	yes	yes	yes	Yes	Yes	Yes	Yes	yes
DQIYDIFQK	Eif4a1	yes	yes	Yes	yes	Yes	Maybe	maybe	Yes	Yes
EHIEIIAPSPQR	EIF2AK3	-	-	-	-	-	-	-	Yes	-
ELEEIVQPIISK	HSPA5	yes	yes	yes	yes	yes	yes	yes	yes	yes
ELGIWEPLAVK	CCT3	yes	yes	yes	yes	yes	yes	yes	yes	yes
ELIFEETAR	MAPK1	yes	yes	yes	yes	yes	yes	yes	Yes	-
FDAGELITQR	PHB1	yes	yes	yes	yes	yes	yes	yes	yes	yes
FIDTTSK	RPL3	yes	yes	yes	yes	yes	yes	yes	yes	-
GDFIALDLGGSSFR	HK1	-	-	yes	yes	-	-	-	yes	yes
GLPAPIEK	IGHG2	yes	yes	yes	yes	yes	yes	yes	yes	yes
GSTAPVGGGAFPTIVER	PDIA6	Maybe	Maybe	Maybe	Maybe	yes	yes	-	yes	-
GTGIVSAPVPK	RPS2	yes	yes	yes	yes	yes	yes	yes	yes	maybe
GTITVSAQELK	CPNE1	Yes	Maybe	Yes	-	yes	yes	yes	yes	yes
HGLLVPNNTTDQELQHIR	Eif6	yes	yes	yes	yes	yes	yes	yes	yes	yes
IADPEHDHTGFLTEYVATR	MAPK3	yes	yes	yes	Yes	-	yes	yes	-	yes
IALDFQR	LGALS3	yes	yes	yes	yes	yes	yes	maybe	yes	yes
IFGVTTLDIVR	MDH2	yes	yes	yes	yes	yes	yes	yes	yes	yes
IFVNDDR	ILF3	yes	yes	yes	yes	yes	yes	yes	Yes	yes
IGVLDEGK	RPS9	yes	yes	yes	yes	yes	yes	yes	yes	yes
IITLTGPTNAIFK	PCBP1	yes	yes	yes	yes	yes	yes	yes	yes	yes
ILPTLEAVAALGNK	ILF2	yes	yes	yes	yes	yes	yes	yes	yes	yes
ILVTGGSGLVGK	TSTA3	yes	yes	yes	yes	yes	yes	yes	yes	Maybe
ISRPGDSDDSR	HNRNPL	yes	yes	yes	yes	yes	yes	yes	yes	Maybe
IVIGYQSHADTATK	EIF4E	yes	yes	yes	yes	yes	yes	yes	yes	yes
IVQAEGEAEAAK	PHB2	yes	Yes	yes	yes	yes	yes	yes	Yes	yes
LEQDEYALR	HADHB	yes	Yes	yes	yes	yes	yes	yes	yes	maybe
LFSGDVVLTAR	CBR1	yes	yes	yes	yes	yes	yes	yes	Yes	maybe
LLIYWASTR	IGKV4-1	-	-	-	-	yes	yes	yes	-	-
LSVISVEDPPQR	ETFB	yes	yes	yes	yes	yes	yes	yes	yes	yes
LTIGSNLSIR	XRCC5	yes	yes	yes	yes	yes	yes	yes	yes	yes
LVNEVTEFAK	ALB	yes	yes	yes	yes	yes	yes	yes	yes	yes
QTLPVIYVK	GSK3B	barely	barely	barely	barely	barely	barely	barely	barely	barely

Peptide	Protein	MCF-7 13 ug	MCF-7 25ug	MCF-7 26 ug	MCF-7 50ug	HT- 29 15ug	COLO-205 16ug	HCT-116 18ug	ZR- 75 40ug	MDA-MB-436 57ug
RPHFPQFSYSASGRE (missed 1)	AKT3	-	-	-	-	-	-	-	-	-
SPDLAPTPAPQSTPR	EIF2A	-	-	-	-	-	-	-	maybe	-
SPDLAPTPAPQSTPR	EIF2A	-	-	-	-	-	-	maybe	-	-
TGAAPIIDVVR	RPL27A	yes	yes	yes	yes	yes	yes	yes	Yes	yes
TIGTGLVTNTLAMTEEEK	TUFM	yes	yes	yes	yes	yes	yes	yes	yes	yes
TQADLDSLVR	DCXR	yes	yes	yes	yes	yes	yes	yes	yes	-
TVAAPSVFIFPPSDEQLK	IGKC	-	-	-	-	-	-	-	-	yes
VLIEGSINSVR	ARPC4	yes	yes	yes	yes	yes	yes	yes	yes	-
VLTLSDDLER	EIF5	yes	yes	yes	yes	yes	yes	yes	yes	yes
VNIVPVIAK	SEPTIN2	yes	yes	yes	yes	yes	yes	yes	yes	-
VSLDVNHFAPDELTVK	HSPB1	yes	yes	yes	yes	yes	yes	yes	Yes	yes
VVDPFSK	RPS3A	yes	yes	yes	yes	yes	yes	yes	yes	-
VVNVSSIMSVR	HSP90AB1	yes	yes	yes	yes	yes	yes	yes	yes	yes
VVTDTDETELAR	Eif2s1	yes	yes	yes	yes	yes	yes	yes	yes	yes
VYPLINR	MAP4K4	-	-	-	-	-	yes	maybe	-	-
VYTVDLGR	PIGR	yes	Yes	maybe	yes	maybe	maybe	maybe	maybe	yes
YLTTAVITNK	Eif3e	yes	yes	yes	yes	yes	yes	yes	yes	-

9. Ethics approval

The study described in Chapter 1 and Chapter 2 was conducted in accordance with the Declaration of Helsinki and approved by the Research Ethics Committee of the Jewish General Hospital (Project #2018-663 17-004, approved 03 Mar 2017) in Montreal, Quebec, Canada. Patient data and samples were originally obtained under site-specific Research Ethics Board approval as part of a registered international clinical trial (NCT01226316, posted 22 Oct 2010). Copies of required certificates are retained by Dr. Gerald Batist.

The study protocol for Chapter 3 was approved by the Ethics board at the Jewish General Hospital in Montreal, Canada (Study number: CODIM-MBM-16-235). Copies of certificates for this work will be maintained by Dr. R. Thomas Jagoe.